Mechanism behind clinical symptoms in cerebral small vessel disease:

a neuroimaging perspective

Hao Li (李浩)

DONDERS SERIES

RADBOUD UNIVERSITY PRESS

Radboud Dissertation Series

Mechanism behind clinical symptoms in cerebral small vessel disease: a neuroimaging perspective

Hao Li (李浩)

alzheimer nederland

Financial support by Alzheimer Nederland and Radboud Alzheimer Center for the publication of this thesis is gratefully acknowledged.

Mechanism behind clinical symptoms in cerebral small vessel disease: a neuroimaging perspective
Hao Li

Radboud Dissertation Series
ISSN: 2950-2772 (Online); 2950-2780 (Print)

Published by RADBOUD UNIVERSITY PRESS
Postbus 9100, 6500 HA Nijmegen, The Netherlands
www.radbouduniversitypress.nl

Design: Proefschrift AIO | Annelies Lips
Cover: Proefschrift AIO | Guntra Laivacuma
Printing: DPN Rikken/Pumbo

ISBN: 9789465152073
DOI: 10.54195/9789465152073
Free download at: https://doi.org/10.54195/9789465152073

RADBOUD UNIVERSITY PRESS

Mechanism behind clinical symptoms in cerebral small vessel disease: a neuroimaging perspective

Proefschrift ter verkrijging van de graad van doctor

aan de Radboud Universiteit Nijmegen

op gezag van de rector magnificus prof. dr. J.M. Sanders,

volgens besluit van het college voor promoties

in het openbaar te verdedigen op

maandag 15 december 2025

om 10.30 uur precies

door

Hao Li

geboren op 17 november 1995

te Hunan, China

Promotor:
Prof. dr. H.F. de Leeuw

Copromotor:
Dr. A.M. Tuladhar

Manuscriptcommissie:
Prof. dr. G.J.S. Litjens
Dr. M. Wiesmann
Prof. dr. G.J. Biessels (UMC Utrecht)

Mechanism behind clinical symptoms in cerebral small vessel disease: a neuroimaging perspective

Dissertation to obtain the degree of doctor

from Radboud University Nijmegen

on the authority of the Rector Magnificus prof. dr. J.M. Sanders,

according to the decision of the Doctorate Board

to be defended in public on

Monday, December 15, 2025

at 10:30 am

by

Hao Li

born on November 17, 1995

in Hunan, China

PhD supervisor:
Prof. dr. H.F. de Leeuw

PhD co-supervisor:
Dr. A.M. Tuladhar

Manuscript Committee:
Prof. dr. G.J.S. Litjens
Dr. M. Wiesmann
Prof. dr. G.J. Biessels (UMC Utrecht)

Table of Content

Part V General discussion

Part V Appendices

Part I.

Introduction and Thesis Outline

Chapter 1.

General introduction, aims, and outline of this thesis

Introduction

Background

Cerebral small vessel disease (SVD) is a common neurological condition in the aging population, characterized by a range of pathological abnormalities in the small perforating arterioles, capillaries and venules in brain (Figure 1).[1] It contributes up to 25% of ischemic strokes and is a leading cause of vascular cognitive impairment and dementia.[1] At present, detecting these small vessels *in vivo* remains unavailable with conventional MRI. Consequently, a spectrum of radiological manifestations of presumed vascular origin, including white matter hyperintensities (WMH), lacunes, enlarged perivascular spaces (PVS), cerebral microbleeds (CMBs) and cerebral cortical microinfarcts (CMIs) are currently used in the clinical practice to identify SVD (Figure 2).[2]

Clinically, patients with SVD present significant heterogeneity, ranging from asymptomatic individuals to those presenting with various cognitive, motor and neuropsychiatry symptoms.[1] Among these, cognitive impairment is one of the most common manifestations, characterized by the dysfunction in processing speed and executive function, which may eventually progress to deficits in all cognitive domains and dementia.[3] Gait disturbances increase the risk of falls and related injuries.[4] Neuropsychiatry symptoms, such as apathy, further complicate the clinical picture.[5] The cumulative effect of these symptoms places a substantial burden on patients, caregivers, and healthcare systems globally. Despite its high prevalence and substantial impact on public health, the mechanisms by which SVD leads to these diverse clinical symptoms remain incompletely understood. Clinicians often observe a remarkable heterogeneity in clinical symptoms among patients with a similar radiological degree of SVD. This could be explained that conventional MRI markers reveal only the tip of the iceberg of the total SVD-related brain damage, thus failing to capture the full extent of associations between radiology features and clinical deficits. Consequently, the perspectives and approaches beyond conventional SVD markers are warranted to advance our understandings on the mechanisms behind various symptoms of SVD.

Advanced neuroimaging assessment in SVD

Advances in quantitative MRI (qMRI) techniques, particularly diffusion imaging, have significantly enhanced the study of SVD (Figure 3).[6] These techniques provide significant advantages over traditional MRI markers of SVD by providing continuous rather than dichotomous measures and enabling a global assessment of brain abnormalities rather than a lesion-focused approach.[6,7] Furthermore,

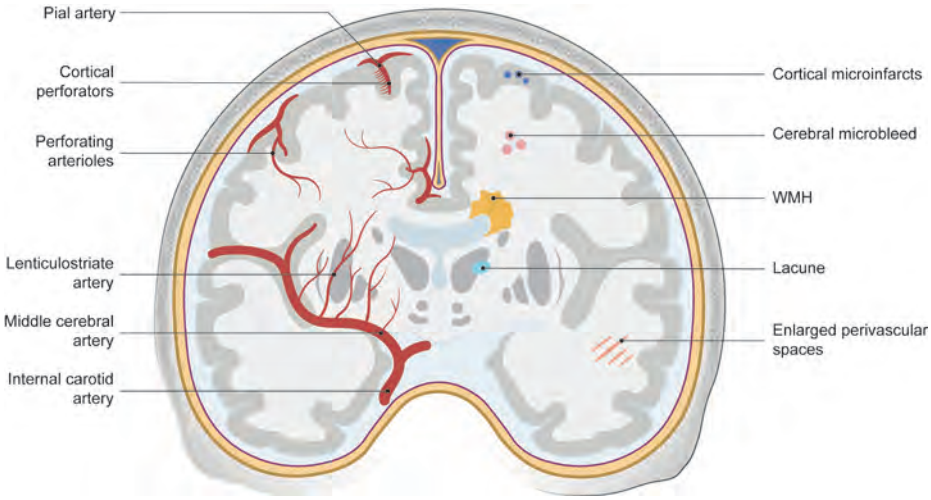

Figure 1. Schematic representation of the cerebral vasculature and associated neuroimaging markers in cerebral small vessel disease. Left side: the internal carotid artery supplies the brain, branching into the middle cerebral artery (MCA) and lenticulostriate arteries, which perfuse deep brain structures. Smaller vessels, including perforating arterioles and cortical perforators, extend to the white and grey matter, ensuring adequate perfusion; Right side: radiological manifestations that are presumed to originate from pathological abnormalities in small vessels are depicted, including white matter hyperintensities (WMH), lacunes, cerebral microbleeds (CMBs), enlarged perivascular spaces (EPVS), and cerebral cortical microinfarcts (CMIs). Created with *Biorender*.

qMRI provides quantitative measurements of specific physical properties of water molecules, which can serve as intrinsic probes of the surrounding tissue, thereby providing valuable insights into in vivo microstructure and tissue composition.[7] Specifically, diffusion MRI measures the random motion of water molecules within brain tissue. In the structured environment of brain's white matter, water molecules tend to diffuse more readily along the direction of nerve fibers rather than across them, due to barriers composed of axonal membranes and myelin sheaths.[8] By capturing this directional diffusion of water molecules, diffusion MRI indirectly informs the orientation of white matter fibbers, thereby enabling the mapping white matter tract (i.e., tractography).[9] When combined with specific mathematical models, diffusion MRI could assess white matter microstructural integrity through parameters derived from these models, such as fractional anisotropy (FA) and mean diffusivity (MD) values obtained from diffusion tensor imaging (DTI) model.[8]

In addition to diffusion MRI, other quantitative MRI techniques such as quantitative R1 and R2* mapping and quantitative susceptibility mapping (QSM) provide valuable insights into the brain's tissue composition.[7,10] Quantitative R1 mapping

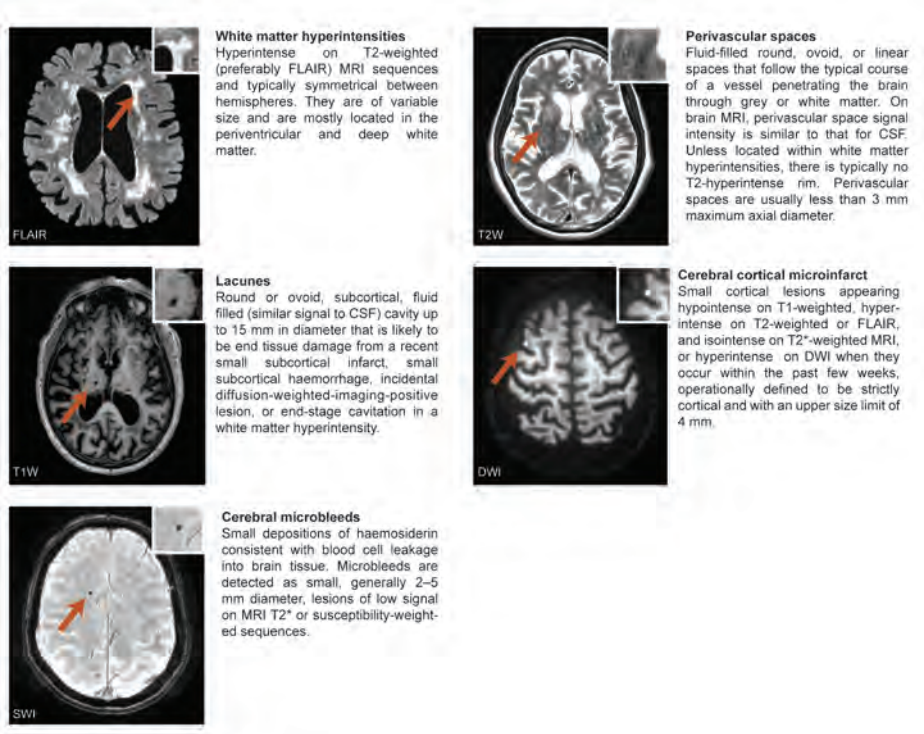

Figure 2. Neuroimaging markers in cerebral small vessel disease. This figure presents examples images of common neuroimaging markers of SVD. SVD, cerebral small vessel disease. CSF, cerebrospinal fluid; DWI, diffusion-weighted imaging; FLAIR, fluid-attenuated inversion recovery; SWI, susceptibility-weighted imaging.

measures the longitudinal relaxation rate of hydrogen protons in tissues, primarily influenced by the less-mobile myelin water compartment, thereby motivating the use of R1 as a surrogate of myelin.[7,11,12] Quantitative R2* mapping measures the effective transverse relaxation rate, which is affected by both myelin and iron levels.[7,11,13] QSM quantifies the magnetic susceptibility of tissues, offering information about the concentration of paramagnetic substances like iron (which increases susceptibility) and diamagnetic substances like myelin (which decreases susceptibility).[7,14] Combined histopathology-MRI studies have demonstrated that the R1 value is mainly positively correlated with myelin content;[15-17] the R2* value is positively correlated with both myelin and iron levels;[18,19] and the susceptibility value measured by QSM is primarily positively correlated with iron concentration and negatively correlated with myelin content.[20] These correlations make these imaging techniques valuable non-invasive tools for assessing tissue compositions, particularly myelin density and iron levels, in the living brain.

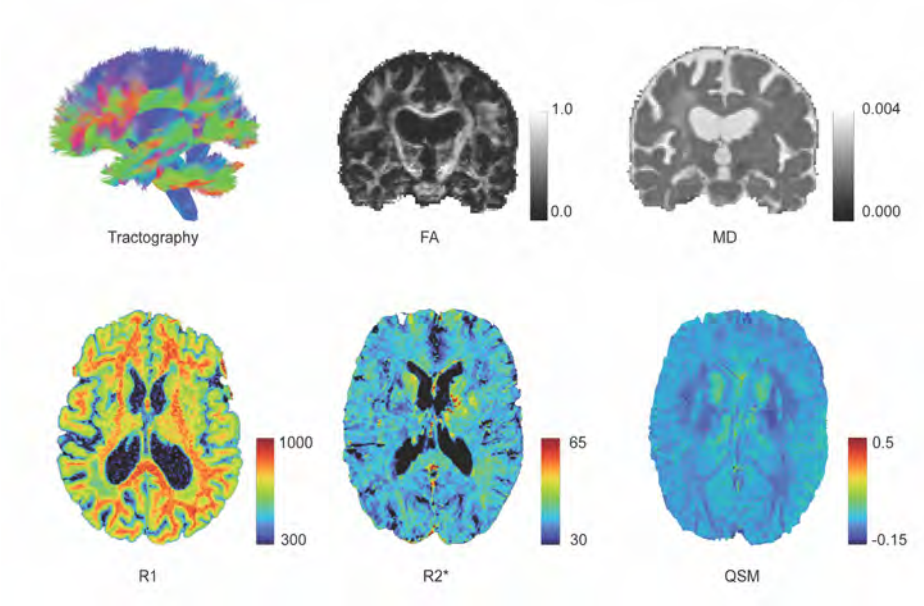

Figure 3. Advanced quantitative MRI in cerebral small vessel disease. First row: Parameters from diffusion MRI. Tractography represents white matter tract pathways reconstructed from diffusion data. FA measures the directionality of molecular displacement during diffusion, while MD quantifies the average magnitude of molecular displacement during diffusion. Second row: Parameters derived from quantitative R1, R2* and susceptibility mapping. R1 (1/T1 relaxation rate): Higher R1 values are associated with higher myelination or higher macromolecular content. R2* (1/T2* relaxation rate): R2* values are sensitive to magnetic field inhomogeneities and are associated with both iron and myelin levels. QSM measures magnetic susceptibility, which is mainly positively correlated with iron (paramagnetic substances that increase susceptibility) and negatively correlated with myelin (diamagnetic substances that decrease susceptibility). FA, fractional anisotropy; MD, mean diffusivity; QSM, quantitative susceptibility mapping.

Overall, by leveraging these advanced neuroimaging techniques, researchers can comprehensively assess SVD-related changes and may uncover new mechanistic insights, thereby elucidating the mechanisms behind clinical symptoms and for facilitating the development of targeted interventions in SVD.[7]

Potential mechanisms of clinical symptoms in small vessel disease

Strategic regions in small vessel disease

The lesion locations could be one key factor to understand the heterogeneity of clinical symptoms in SVD. Damage to specific strategic brain regions, even if localized, can have a greater impact more than widespread damage in less critical regions. Previous studies, particularly those using lesion-symptom mapping, have

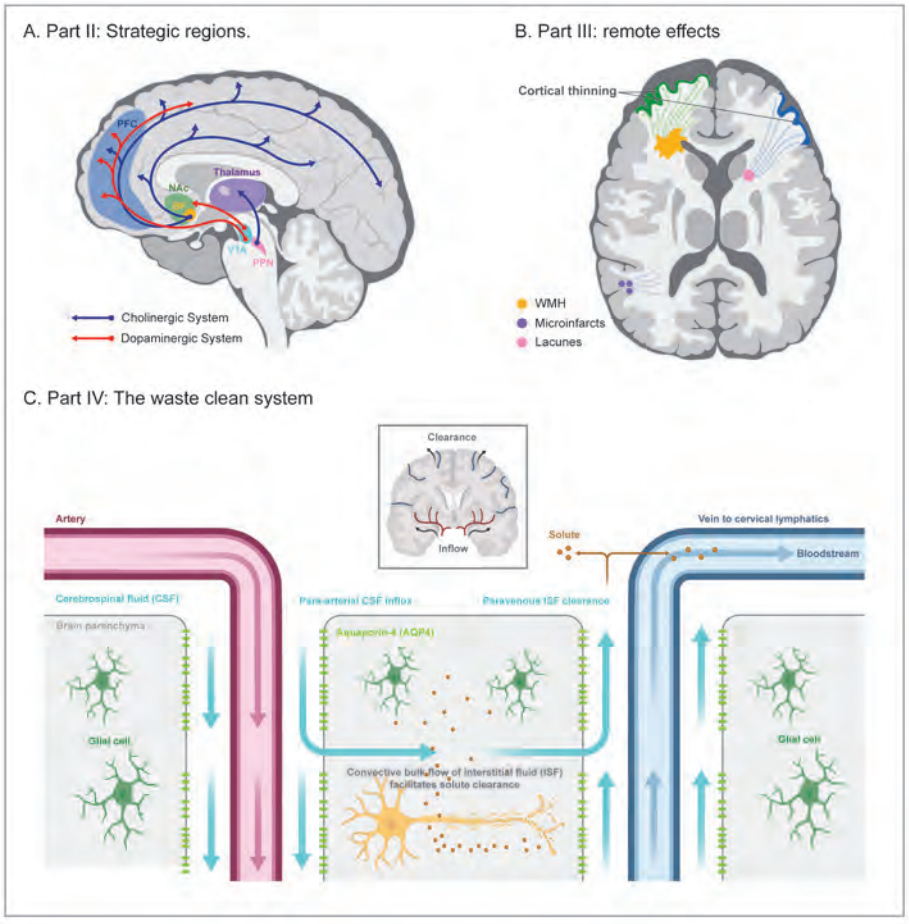

Figure 4. Potential mechanisms of clinical symptoms in cerebral small vessel disease. A, Damage to specific brain regions, such as the thalamus and white matter tracts within the dopaminergic and cholinergic systems, may strategically affect clinical symptoms in small vessel disease (SVD). B, Localized lesions, such as WMH, lacunes, and CMIs, may lead to structural changes remote from the initial lesions through secondary neurodegeneration of fibers passing through the lesion, thus contributing to clinical symptoms in SVD. C, The impaired waste clearance system, a dynamic waste clearance pathway in the CNS, may potentially drive the development and progression of SVD and its concomitant symptoms. Created with *Biorender*.

provided evidence supporting this concept. These studies found that lesions (i.e., WMH and lacunes) in specific white matter tracts, such as the anterior thalamic radiation (ATR) and forceps minor, were associated with cognitive deficits in SVD, especially in processing speed and executive function.[21-23] However, some regions with potential clinical significance remain not fully explored. For instance, the thalamus serves as the primary relay station in the cerebral communication system, ensuring efficient information transmission across brain networks.[24] Additionally, the thalamus is a complex structure with several subcomponents, each having distinct functions depending on their connections to specific cortical areas.[24,25] Therefore, examining damage to thalamic sub-regions, as well as their connectivity with the cortex, may provide a better understanding of their role in SVD-related symptoms. Moreover, the integrity of white matter tracts within the neurotransmitter system is fundamental to maintain their normal function and regulation in various brain physiological processes. Damage to these specific white matter pathways (e.g., dopamine and cholinergic circuits) can impair neurotransmitter release and transmission, resulting in dysfunction of corresponding neurotransmitter system and contributing to a range of symptoms. However, studies investigating these mechanisms in SVD are still limited.

Beyond focal lesion: the remote effects in small vessel disease

Another mechanism could be the remote effects caused by secondary neurodegeneration from local lesions. A growing body of evidence suggests that SVD is accompanied by structural changes both adjacent to and remote from initial MRI-detected lesions.[26] Studies using DTI-derived metrics, such as FA and MD, have demonstrated abnormal diffusion in regions surrounding WMH that appear normal on conventional MRI.[27,28] These surrounding regions are termed normal-appearing white matter (NAWM) or WMH penumbra. Moreover, diffusion abnormalities in penumbral areas tend to be more severe near the WMH and gradually decrease with distance.[27,28] These findings have been validated in post-mortem histopathological studies, which show inflammation, demyelination, and gliosis in the surrounding NAWM, with these pathologies decreasing in severity as the distance from the WMH increases.[29] Furthermore, these MRI-detected abnormalities in NAWM have related to cognitive impairment, independent of conventional SVD MRI markers, in several studies.[30-34] On the other hand, those subcortical lesions, particularly lacunes and incident infarcts, have been found to cause thinning in remote cortical regions connected to the initial subcortical lesion.[35,36] These observed focal cortical thinning was accompanied by microstructural damage in the white matter tracts connecting the subcortical lesion and the cortex, with greater damage in these tracts associated with more pronounced cortical thinning.[35,36] These findings

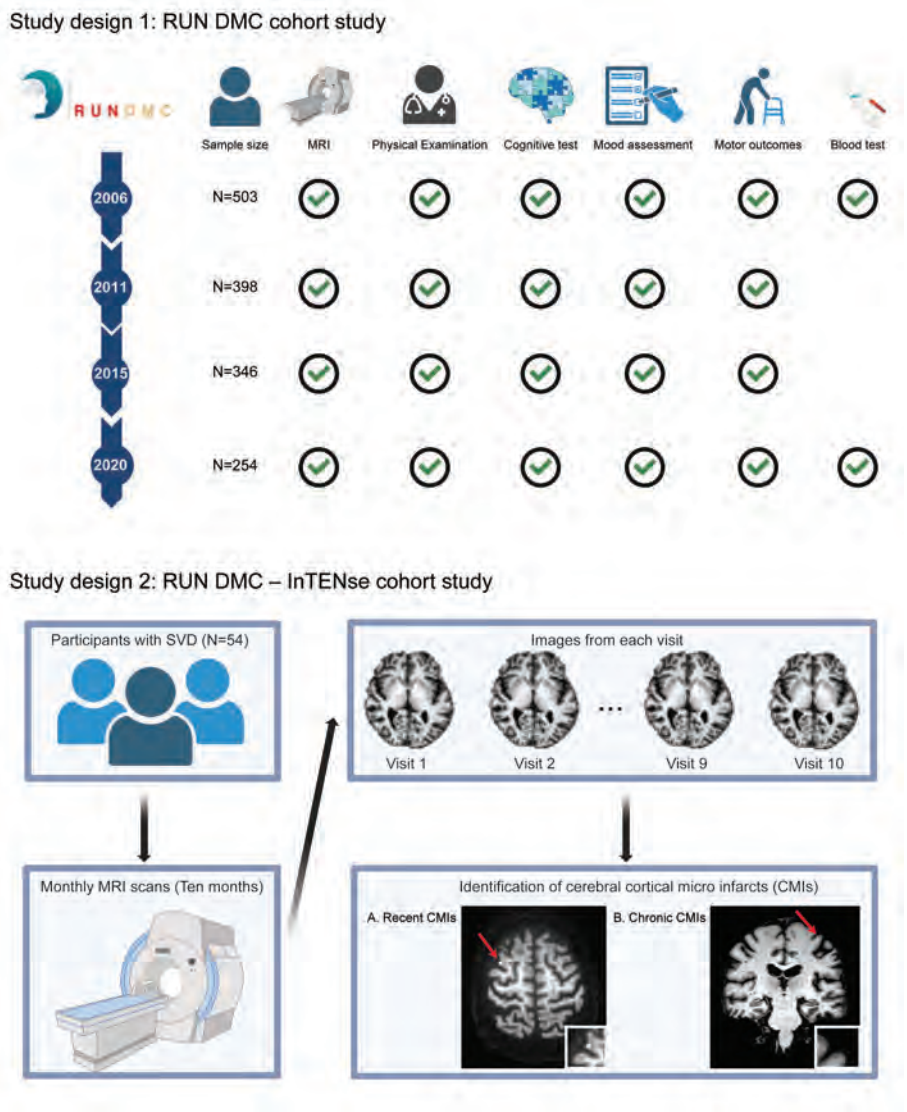

Figure 5. Study design of the thesis. Study design 1: Radboud University Nijmegen Diffusion tensor and Magnetic resonance imaging Cohort (RUN DMC) study is an ongoing prospective study that aims to investigate the causes and clinical consequences of sporadic SVD. This cohort was initiated in 2006, with follow-up assessments conducted in 2011, 2015, and 2020. Each evaluation included MRI scans, physical examinations, and assessments of cognition, mood, and motor functions for the participants. Study design 2: RUN DMC – Investigating The origin and EvolutioN of cerebral small vessel disease (RUN DMC-InTENse) study is a longitudinal observational study aiming to investigate the origin and short-term dynamical evolution of SVD. A total of 54 participants with SVD, but without other identifiable causes of cerebral ischemia, were recruited from the original RUN DMC cohort. Participants underwent 10 monthly MRI assessments, during which both chronic and acute CMIs were identified. Created with *Biorender*.

provided direct evidence of secondary degeneration-induced remote effects in SVD. In WMH, the most common and prominent SVD MRI marker, numerous studies have demonstrated the association between WMH and cortical thinning, which in turn contributed to cognitive impairment.[37,38] Nevertheless, a longitudinal study reported results inconsistent with this general finding, highlighting potential variability in the association over time or across populations.[39] Moreover, there is a lack of direct evidence showing that WMH leads to focal thinning in remote cortical regions through the degeneration of connecting white matter tracts in SVD population. In addition, CMIs, an emerging SVD markers in the cortex, have shown to be associated with cognitive impairment in the populations with cerebrovascular diseases and dementia.[40,41] This association could be partially attributed to cortical atrophy and the disruption of WM connectivity in the presence of CMIs, with underlying mechanisms speculated to involve remote effects caused by CMIs.[42,43] However, more evidence is required to validate this speculation.

The waste clearance system in small vessel disease

Lastly, dysfunction of the brain's waste clearance system may represent another crucial mechanism that link microvascular abnormalities and brain tissue damages at the early stage, thereby driving the development and progression in SVD. [1,44,45] This system comprises a network of perivascular channels through which cerebrospinal fluid (CSF) flows into brain parenchyma via the periarterial space and flow out along perivenous spaces. During CSF inflow and outflow, it exchanges with interstitial fluid (ISF), facilitating the removal of metabolic waste and neurotoxic substances, thus protecting neurons and supporting their function. Multiple imaging markers have recently been developed to study the role of this waste clearance system in various neurological disorders, including SVD.[46,47] These imaging markers included MRI-visible perivascular spaces (PVS), free water (FW), and diffusion tensor imaging along the PVS (DTI-ALPS).[46-48] DTI-ALPS was related to CSF outflow rates, as measured through invasive MRI with intrathecal gadolinium injection,[47] while the PVS volumes and FW values were suspected to be the consequence of blockage in CSF outflow.[48,49] Previous studies have suggested that individuals with SVD who have a higher SVD burden and worse cognitive performance exhibit lower DTI-ALPS values, higher PVS volumes, and higher FW values.[46,47,50-52] Nevertheless, the longitudinal trajectories and interrelations of these measures, as well as their associations with the radiological and clinical progression of SVD over time, remain unexplored. Additionally, small vessel's pathological abnormalities also involve small veins in SVD.[53,54] Deep medullary veins (DMVs), a type of cerebral small vein located adjacent to the lateral ventricle that supports

venous drainage of the surrounding white matter, may also be involved in waste clearance function in SVD, although evidence for this association remains unknown.

Aim of this thesis

The general aim of the thesis is to advance our understanding on the mechanisms behind the clinical symptoms, particular cognitive impairment, in SVD using advanced multimodal neuroimaging approaches. Particularly, this thesis focused on damages to several strategic regions, including thalamus, the white matter tracts within dopaminergic and cholinergic pathways, the remote effects of MRI-detected SVD lesions (i.e., WMH and CMIs), and the MRI markers of waste clearance system and their associations with DMV disruptions. By linking these novel imaging features with clinical symptoms, researchers may gain deeper insights into the mechanisms and pathophysiology of SVD, with the potential to inform novel management and intervention strategies.

Study design

Data used in this thesis were mostly derived from the Radboud University Nijmegen Diffusion tensor and Magnetic resonance imaging Cohort (RUN DMC) study, an ongoing hospital-based cohort study investigating the causes and clinical consequences of sporadic SVD.[55] The RUN DMC study was initiated in 2006 and included 503 non-demented individuals aged 50-85 years, all of whom presented SVD markers on MRI (i.e., WMH or lacunes), and had cognitive or motor symptoms attributable to SVD. After baseline data collection, three follow-up assessments were performed in 2011, 2015, and 2020. Each assessment included detailed clinical evaluations of cognition, motor function, and mood, along with multi-modal MRI scans. Notably, the 2020 follow-up implemented the most advanced quantitative MRI sequences, including multi-shell diffusion, quantitative R1, R2*, and QSM imaging. In addition, to examine the perilesional effects caused by CMIs and their temporal changes, data from the Radboud University Nijmegen Diffusion tensor and Magnetic resonance imaging Cohort - Investigating The origin and EvolutioN of cerebral small vessel disease (RUN DMC-InTENse) study were used.[56] The RUN DMC-InTENse study included 54 participants with SVD and without other identified causes of cerebral ischemia from the original RUN DMC study, with ten consecutive monthly MRI scans. The high-frequency serial imaging design of RUN DMC-InTENse study allowed us to capture incident acute events (i.e., recent CMIs) and investigate their changes in a short-term. Finally, to examine the associations between DMV disruptions and these MRI indices of glymphatic function in SVD, I

used the data from the Department of Neurology, First Affiliated Hospital of Sun Yat-sen University, Guangzhou, China. Participants with SVD MRI markers and without sever large artery stenosis were included. Clinical and MRI assessments were performed, particularly with available rating scores of DMV disruption on high quality SWI images.

Outline of the thesis

In **Part II**, I investigated the associations between the damage to several strategic regions and clinical symptoms in SVD. Specifically, in **Chapter 2**, I assessed the volumes and structural connectivity of each thalamic subregion, and their associations with cognitive impairment in each domain. In **Chapters 3** and **4**, I reconstructed the white matter tracts within the dopaminergic and cholinergic pathways, respectively, and examined the associations between damage to these tracts and cognitive impairment, apathy, and gait dysfunction in SVD. Furthermore, I related cognition, apathy, and gait dysfunction by showing close correlations among these symptom measurements and identified the common component underlying these conditions.

In **Part III**, I focused on the remote and perilesional effects in SVD. Specifically, in **Chapter 5**, I assessed the cortical abnormalities, including thinning, demyelination, and iron loss, in the remote regions connected to WMH. In **Chapter 6**, I examined the microstructural damages in CMIs adjacent regions within the cortex and subcortical regions along fibbers passing through CMIs. Additionally, I assessed whether these CMI-related damage persists over time in SVD.

In **Part IV**, I assessed the role of waste clearance system in SVD. Notably, in **Chapter 7**, I examined the temporal changes of waste clean function, as measured by several MRI measures, and the longitudinal interrelations among these measures. In **Chapter 8**, I examined a potential pathway in which disruption of DMVs contributes to radiological severity and cognitive deficits through impaired waste clearance function in SVD.

In **Part V**, I presented a summary and general discussion of our findings in **Chapter 9** and **10**, along with a Dutch summary in **Chapters 11**.

References

1. Wardlaw, J.M., C. Smith, and M. Dichgans, Small vessel disease: mechanisms and clinical implications. Lancet Neurol, 2019. 18(7): p. 684-696.
2. Duering, M., et al., Neuroimaging standards for research into small vessel disease-advances since 2013. Lancet Neurol, 2023. 22(7): p. 602-618.
3. Hamilton, O.K.L., et al., Cognitive impairment in sporadic cerebral small vessel disease: A systematic review and meta-analysis. Alzheimers Dement, 2021. 17(4): p. 665-685.
4. Sharma, B., et al., Gait and falls in cerebral small vessel disease: a systematic review and meta-analysis. Age Ageing, 2023. 52(3).
5. Clancy, U., et al., Neuropsychiatric symptoms associated with cerebral small vessel disease: a systematic review and meta-analysis. Lancet Psychiatry, 2021. 8(3): p. 225-236.
6. van den Brink, H., F.N. Doubal, and M. Duering, Advanced MRI in cerebral small vessel disease. Int J Stroke, 2023. 18(1): p. 28-35.
7. Weiskopf, N., et al., Quantitative magnetic resonance imaging of brain anatomy and in vivo histology. Nature Reviews Physics, 2021. 3(8): p. 570-588.
8. Sen, P.N. and P.J. Basser, A model for diffusion in white matter in the brain. Biophys J, 2005. 89(5): p. 2927-38.
9. Basser, P.J., et al., In vivo fiber tractography using DT-MRI data. Magn Reson Med, 2000. 44(4): p. 625-32.
10. Iordanishvili, E., et al., Quantitative MRI of cerebral white matter hyperintensities: A new approach towards understanding the underlying pathology. Neuroimage, 2019. 202: p. 116077.
11. Stüber, C., et al., Myelin and iron concentration in the human brain: a quantitative study of MRI contrast. Neuroimage, 2014. 93 Pt 1: p. 95-106.
12. Lutti, A., et al., Using high-resolution quantitative mapping of R1 as an index of cortical myelination. Neuroimage, 2014. 93 Pt 2: p. 176-88.
13. Fukunaga, M., et al., Layer-specific variation of iron content in cerebral cortex as a source of MRI contrast. Proc Natl Acad Sci U S A, 2010. 107(8): p. 3834-9.
14. Shmueli, K., et al., Magnetic susceptibility mapping of brain tissue in vivo using MRI phase data. Magn Reson Med, 2009. 62(6): p. 1510-22.
15. Schmierer, K., et al., Magnetization transfer ratio and myelin in postmortem multiple sclerosis brain. Annals of neurology, 2004. 56(3): p. 407-415.
16. Mottershead, J., et al., High field MRI correlates of myelin content and axonal density in multiple sclerosis: a post-mortem study of the spinal cord. Journal of neurology, 2003. 250: p. 1293-1301.
17. Schmierer, K., et al., Quantitative magnetic resonance of postmortem multiple sclerosis brain before and after fixation. Magnetic Resonance in Medicine: An Official Journal of the International Society for Magnetic Resonance in Medicine, 2008. 59(2): p. 268-277.
18. Langkammer, C., et al., Quantitative MR imaging of brain iron: a postmortem validation study. Radiology, 2010. 257(2): p. 455-62.
19. Wang, C., et al., Methods for quantitative susceptibility and R2* mapping in whole post-mortem brains at 7T applied to amyotrophic lateral sclerosis. Neuroimage, 2020. 222: p. 117216.
20. Langkammer, C., et al., Quantitative susceptibility mapping (QSM) as a means to measure brain iron? A post mortem validation study. Neuroimage, 2012. 62(3): p. 1593-9.
21. Duering, M., et al., Strategic white matter tracts for processing speed deficits in age-related small vessel disease. Neurology, 2014. 82(22): p. 1946-50.

22. Biesbroek, J.M., et al., Impact of Strategically Located White Matter Hyperintensities on Cognition in Memory Clinic Patients with Small Vessel Disease. PLoS One, 2016. 11(11): p. e0166261.
23. Benjamin, P., et al., Strategic lacunes and their relationship to cognitive impairment in cerebral small vessel disease. Neuroimage Clin, 2014. 4: p. 828-37.
24. Biesbroek, J.M., et al., When the central integrator disintegrates: A review of the role of the thalamus in cognition and dementia. Alzheimers Dement, 2024. 20(3): p. 2209-2222.
25. Behrens, T.E., et al., Non-invasive mapping of connections between human thalamus and cortex using diffusion imaging. Nat Neurosci, 2003. 6(7): p. 750-7.
26. Ter Telgte, A., et al., Cerebral small vessel disease: from a focal to a global perspective. Nat Rev Neurol, 2018. 14(7): p. 387-398.
27. Maillard, P., et al., White matter hyperintensity penumbra. Stroke, 2011. 42(7): p. 1917-22.
28. Maniega, S.M., et al., White matter hyperintensities and normal-appearing white matter integrity in the aging brain. Neurobiol Aging, 2015. 36(2): p. 909-18.
29. Silbert, L.C., et al., White matter hyperintensities and the surrounding normal appearing white matter are associated with water channel disruption in the oldest old. Alzheimers Dement, 2024. 20(6): p. 3839-3851.
30. van Norden, A.G., et al., Diffusion tensor imaging and cognition in cerebral small vessel disease: the RUN DMC study. Biochim Biophys Acta, 2012. 1822(3): p. 401-7.
31. Jokinen, H., et al., Diffusion changes predict cognitive and functional outcome: the LADIS study. Ann Neurol, 2013. 73(5): p. 576-83.
32. Tuladhar, A.M., et al., White matter integrity in small vessel disease is related to cognition. Neuroimage Clin, 2015. 7: p. 518-24.
33. Brandhofe, A., et al., T(2) relaxation time of the normal-appearing white matter is related to the cognitive status in cerebral small vessel disease. J Cereb Blood Flow Metab, 2021. 41(7): p. 1767-1777.
34. Dao, E., et al., Exploring the Contribution of Myelin Content in Normal Appearing White Matter to Cognitive Outcomes in Cerebral Small Vessel Disease. J Alzheimers Dis, 2021. 80(1): p. 91-101.
35. Duering, M., et al., Incident subcortical infarcts induce focal thinning in connected cortical regions. Neurology, 2012. 79(20): p. 2025-8.
36. Duering, M., et al., Acute infarcts cause focal thinning in remote cortex via degeneration of connecting fiber tracts. Neurology, 2015. 84(16): p. 1685-92.
37. Tuladhar, A.M., et al., Relationship between white matter hyperintensities, cortical thickness, and cognition. Stroke, 2015. 46(2): p. 425-32.
38. Lambert, C., et al., Characterising the grey matter correlates of leukoaraiosis in cerebral small vessel disease. Neuroimage Clin, 2015. 9: p. 194-205.
39. Dickie, D.A., et al., Progression of White Matter Disease and Cortical Thinning Are Not Related in Older Community-Dwelling Subjects. Stroke, 2016. 47(2): p. 410-6.
40. van Veluw, S.J., et al., Detection, risk factors, and functional consequences of cerebral microinfarcts. Lancet Neurol, 2017. 16(9): p. 730-740.
41. Hilal, S., et al., Cortical cerebral microinfarcts predict cognitive decline in memory clinic patients. J Cereb Blood Flow Metab, 2020. 40(1): p. 44-53.
42. Ferro, D.A., et al., Association Between Cerebral Cortical Microinfarcts and Perilesional Cortical Atrophy on 3T MRI. Neurology, 2022. 98(6): p. e612-e622.

43. Huang, J., et al., Loss of white matter integrity mediates the association between cortical cerebral microinfarcts and cognitive dysfunction: A longitudinal study. J Cereb Blood Flow Metab, 2024: p. 271678x241258563.
44. Mestre, H., Y. Mori, and M. Nedergaard, The Brain's Glymphatic System: Current Controversies. Trends Neurosci, 2020. 43(7): p. 458-466.
45. Xu, J., et al., Glymphatic pathway in sporadic cerebral small vessel diseases: From bench to bedside. Ageing Res Rev, 2023. 86: p. 101885.
46. Tian, Y., et al., Impaired glymphatic system as evidenced by low diffusivity along perivascular spaces is associated with cerebral small vessel disease: a population-based study. Stroke Vasc Neurol, 2023. 8(5): p. 413-423.
47. Zhang, W., et al., Glymphatic clearance function in patients with cerebral small vessel disease. Neuroimage, 2021. 238: p. 118257.
48. Kamagata, K., et al., Association of MRI Indices of Glymphatic System With Amyloid Deposition and Cognition in Mild Cognitive Impairment and Alzheimer Disease. Neurology, 2022. 99(24): p. e2648-e2660.
49. Wardlaw, J.M., et al., Perivascular spaces in the brain: anatomy, physiology and pathology. Nat Rev Neurol, 2020. 16(3): p. 137-153.
50. Ding, J., et al., Large Perivascular Spaces Visible on Magnetic Resonance Imaging, Cerebral Small Vessel Disease Progression, and Risk of Dementia: The Age, Gene/Environment Susceptibility-Reykjavik Study. JAMA Neurol, 2017. 74(9): p. 1105-1112.
51. Evans, T.E., et al., Determinants of Perivascular Spaces in the General Population: A Pooled Cohort Analysis of Individual Participant Data. Neurology, 2023. 100(2): p. e107-e122.
52. Duering, M., et al., Free water determines diffusion alterations and clinical status in cerebral small vessel disease. Alzheimers Dement, 2018. 14(6): p. 764-774.
53. Keith, J., et al., Collagenosis of the Deep Medullary Veins: An Underrecognized Pathologic Correlate of White Matter Hyperintensities and Periventricular Infarction? J Neuropathol Exp Neurol, 2017. 76(4): p. 299-312.
54. Lahna, D., et al., Venous Collagenosis as Pathogenesis of White Matter Hyperintensity. Ann Neurol, 2022. 92(6): p. 992-1000.
55. van Norden, A.G., et al., Causes and consequences of cerebral small vessel disease. The RUN DMC study: a prospective cohort study. Study rationale and protocol. BMC Neurol, 2011. 11: p. 29.
56. Ter Telgte, A., et al., Investigating the origin and evolution of cerebral small vessel disease: The RUN DMC - InTENse study. Eur Stroke J, 2018. 3(4): p. 369-378.

Part II.

Strategic regions in cerebral small vessel disease

Chapter 2.

Dissociable contributions of thalamic subregions to cognitive impairment in small vessel disease

Published as:
Hao Li, Mengfei Cai, Mina A Jacob, David G Norris, José P Marques, Maxime Chamberland, Marco Duering, Roy PC Kessels, Frank-Erik de Leeuw, Anil M Tuladhar. Dissociable contributions of thalamic-subregions to cognitive impairment in small vessel disease. Stroke, 54(5): 1367-1376, 2023.

Abstract

Background: Structural network damage is a potentially important mechanism by which cerebral small vessel disease (SVD) can cause cognitive impairment. As a central hub of the structural network, the role of thalamus in SVD-related cognitive impairments remains unclear. We aimed to determine the associations between the structural alterations of thalamic subregions and cognitive impairments in SVD.

Methods: In this cross-sectional study, 205 SVD participants without thalamic lacunes from the third follow-up (2020) of the prospective Radboud University Nijmegen Diffusion Tensor and Magnetic resonance Cohort (RUN DMC) study, which was initiated in 2006, Nijmegen, were included. Cognitive functions included processing speed, executive function, and memory. Probabilistic tractography was performed from thalamus to six cortical regions, followed by connectivity-based thalamic segmentation to assess each thalamic subregion volume and connectivity (measured by mean diffusivity [MD] of the connecting white matter tracts) with the cortex. LASSO regression analysis was conducted to identify the volumes or connectivity of the total thalamus and six thalamic subregions that have the strongest association with cognitive performance. Linear regression and mediation analyses were performed to test the association of LASSO-selected thalamic subregion volume or MD with cognitive performance, while adjusting for age and education.

Results: We found that higher MD of the thalamic-motor tract was associated with worse processing speed (β=-0.27, p<0.001); higher MD of the thalamic-frontal tract was associated with worse executive function (β=-0.24, p=0.001) and memory (β=-0.28, p<0.001), respectively. The mediation analysis showed that MD of thalamocortical tracts mediated the association between corresponding thalamic subregion volumes and the cognitive performances in three domains.

Conclusions: Our results suggest that the structural alterations of thalamus are linked to cognitive impairment in SVD, largely depending on the damage pattern of the white matter tracts connecting specific thalamic subregions and cortical regions.

Introduction

Cerebral small vessel disease (SVD) is the leading vascular cause of cognitive impairment and dementia.[1] MRI features of SVD include white matter hyperintensities (WMH), lacunes, and cerebral microbleeds (CMBs).[2] Although these MRI markers are associated with cognitive impairment, studies have shown that their dose-response relation with cognitive impairment is modest.[3] Recent studies highlighted that SVD can be considered a diffuse brain disease causing global brain dysfunction.[4] Cognitive decline in SVD patients is probably a result of widespread white matter network disruption,[5] especially between the highly connected hubs. In this regard, structural alterations of the thalamus, being one of the central hubs, might be important contributors to cognitive impairment in SVD.

Several studies, especially in multiple sclerosis (MS), have shown that thalamic atrophy and thalamocortical disconnections were associated with impairments in processing speed, executive function and memory.[6-9] In SVD, studies have reported that lacunes in the thalamus and WMH accumulation in the tracts connecting thalamus and prefrontal cortex were associated with lower processing speed and worse executive functions.[10-13] However, studies on the relation between the thalamus structural changes and cognitive impairment in SVD patients without thalamic lacunes are lacking. The thalamus is a complex structure with several subcomponents, each having different functions depending on their connections to specific cortex.[14] Studies considering the different thalamic subregions and specific cognitive domains are crucial to characterize the role of thalamus in SVD.

Therefore, we hypothesized that the volumes and connectivity of each thalamic subregion may display specific associations with different cognitive domains in SVD patients without thalamic lacunes. In addition, considering the white matter damage is the predominant feature of SVD, we further hypothesized that the effect of thalamic atrophy on cognitive performances is mediated by the disrupted thalamic connectivity. To test our hypothesis, we assessed the volume and connectivity of thalamic subregions and their association with each cognitive domain (processing speed, executive function, and memory) in 205 SVD participants without thalamic lacunes.

Materials and methods

The data that of this study are available from the corresponding author, depending on reasonable request from qualified investigators after permission of appropriate regulatory bodies.

Study population

The study is a part of Radboud University Nijmegen Diffusion tensor and Magnetic resonance imaging Cohort (RUN DMC). We included participants meeting the following criteria: (1) age between 50 and 85 years, (2) WMHs or lacunes on MRI, (3) cognitive and/or motor symptoms that could be attributed to SVD. Baseline data was collected in 2006, with three follow-up assessments in 2011, 2015 and 2020. At baseline 503 participants were included, however, due to the change of MRI scanners, we only used the data from the third follow-up assessment to perform cross-sectional analyses in the present study. Out of 230 participants in the third follow-up, 25 participants were excluded due to thalamic lacunes (n = 21), uncompleted MRI scans (n = 2), low-quality of MRI images (n = 1) and image processing failure (n = 1), resulting in 205 participants included in the present study (Figure s1). The study was approved by the Medical Review Ethics Committee Region Arnhem-Nijmegen, and written informed consent was obtained from all participants. Detailed information of the RUN DMC has been described in previous studies.[15,16]

Neuropsychological assessment

All participants underwent a detailed cognitive assessment in three domains: processing speed, executive function, and memory. Processing speed was assessed using the Trail Making Test A (TMT-A) and Symbol-Digit Modalities Test (SDMT); executive function was assessed using the TMT-A, TMT-B, and Verbal Fluency test; memory was assessed using the forward and backward of Digit Span test, the immediate and delayed recall of the Rey Auditory Verbal Learning Test (RAVLT) and the immediate and delayed recall of Rey-Osterrieth Complex Figure Test (RCFT). The raw test scores were scaled as Z-scores. Next, compound scores were computed per cognitive domain (Table s1).

MRI acquisition

Participants were scanned on a 3T MRI scanner (MAGNETOM Prisma, Siemens) with a 32-channel head coil, including the following sequences: 3D T1-weighted Magnetization Prepared 2 Rapid Acquisition Gradient Echoes (MP2RAGE), multi-shell diffusion weighted imaging (DWI), 3D fluid-attenuated inversion recovery

(FLAIR) images, susceptibility-weighted images (SWI). Details were provided in supplementary materials and previous study.[17]

MRI markers for SVD

MRI markers of SVD (WMH, lacunes, CMBs) and brain atrophy were assessed according to the Standards for Reporting Vascular changes on neuroimaging (STRIVE).[2] WMH was segmented using a previously validated convolutional network algorithm.[16] WMH volumes were calculate and normalized for the intracranial volume (ICV). A visual rating of WMH was performed according to the modified Fazekas scale (mild: 0–1 score, moderate: 2 score, severe: 3 score).[16,18] Grey matter (GM), white matter (WM) and cerebrospinal fluid (CSF) volumes were calculated based on T1-weighted images. Due to the similar intensities between WMH and GM, WMH mask was employed to correct the GM/WM segmentation. The total brain volume was calculated as the sum of GM and WM volumes. Brain parenchymal fraction (BPF) was determined as the ratio of total brain volume and ICV and employed to assess brain atrophy. Lastly, a simple total SVD score consisting of WMH, lacunes, and CMBs was generated to assess the total SVD burden.[19] Since our cohort lacked information regarding perivascular spaces (PVS) and the PVS counts showed no association with cognitive impairment in previous study,[20] we did not include the PVS in the simple SVD score. In this simple SVD score without PVS, one point was respectively assigned for WMH Fazekas score ≥ 2, lacunes number ≥3, the presence of CMBs.[19]

Segmentation of thalamus and cortical regions

The thalamus was segmented using Freesurfer 7.2.0.[21] The thalamus segmentation was manually corrected. The total thalamic volume was calculated. The six cortical regions connected to the thalamus were derived based on the Harvard-Oxford cortical atlas and included: frontal cortex, motor cortex, temporal cortex, sensory cortex, posterior parietal cortex, and occipital cortex (Table s2). Afterwards, the thalamus and six cortical regions in the native T1-space were registered to diffusion space through the linear and nonlinear transforms using FMRIB Software Library (FSL; v6.0.1, Figure 1). All segmented and transformed images were visually inspected. Details in supplementary materials.

Diffusion MRI processing

Diffusion MRI data were preprocessed for denoising, removal of Gibbs artifacts, correction of head motion, eddy currents-induced distortion, susceptibility-induced distortion, and intensity bias.[22-26] Next, multi-fiber directions within each voxel were estimated using the ball-and-two-sticks model. Fractional anisotropy (FA) and mean diffusivity (MD) images for each participant were obtained from the processed images (only $b = 0$ and $b = 1000$ s/mm^2).

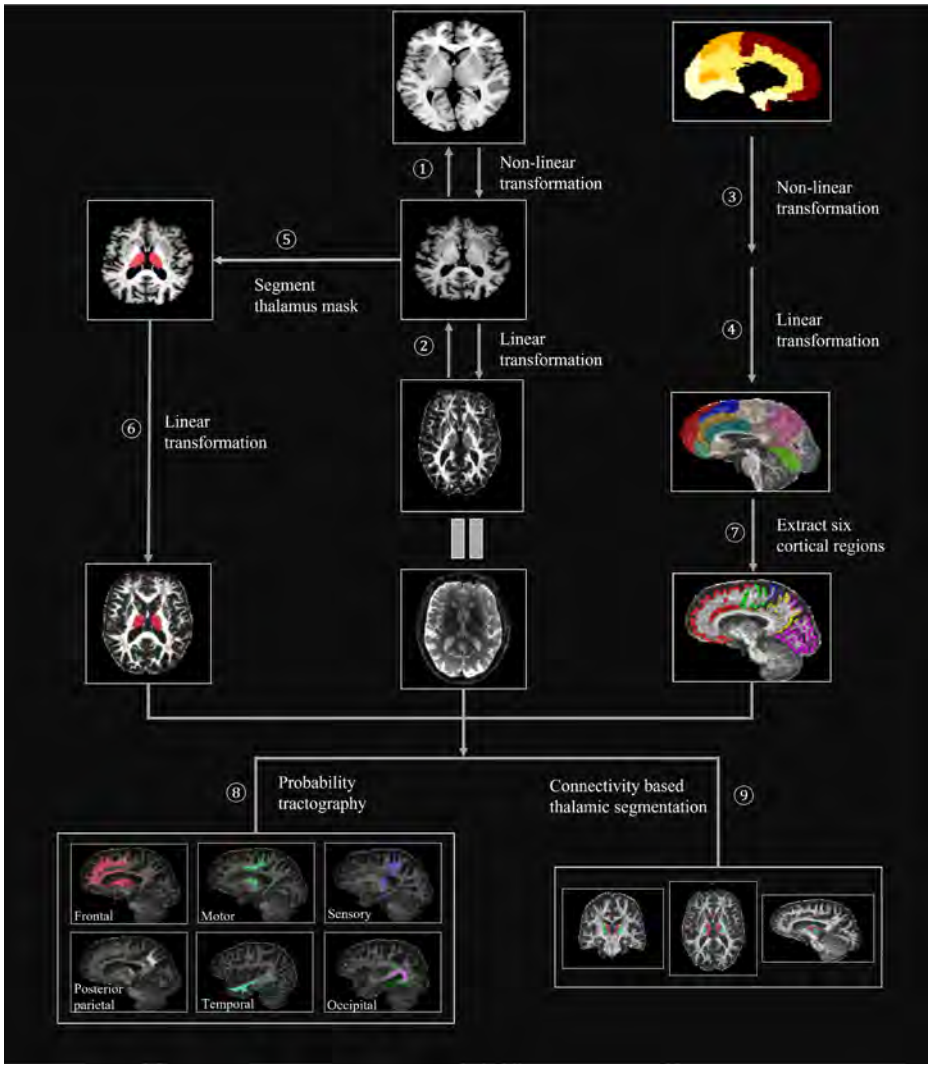

Figure 1. Flowchart of the performed neuroimaging analysis. ①, non-linear transformation between individual's T1-weighted image and MNI152 standard space; ②, linear transformation between individual's T1-weighted image and individual's DTI space; ③ and ④, the transformation matrix from step ① and ② were used to transform Harvard-Oxford cortical atlas from standard MNI space to individual's DTI space; ⑤, extract thalamic mask in individual's T1-weighted images; ⑥, the transformation matrix from step ② were used to transform thalamic mask from individual's T1 space to individual's DWI space; ⑦, six cortical regions were extracted in Harvard-Oxford cortical atlas in individual's DWI space: frontal cortex(red), motor cortex(green), sensory cortex(blue), posterior parietal cortex(yellow), temporal cortex(light blue), and occipital cortex(pink); ⑧, probability tractography from thalamus to six cortical regions; ⑨, thalamic segmentation based on the thalamic-cortex connectivity pattern.

Probabilistic tractography and connectivity-based thalamic segmentation

Probabilistic tractography were performed from thalamus to six cortical regions, respectively. The resulting connectivity maps were normalized by dividing the total streamlines number and then thresholded at 0.01 to generate tract masks[27]. The mean MD values of each tract mask were calculated to measure the white matter integrity of the tract as a proxy of thalamocortical structural connectivity of each thalamic subregion. The six tracts were also combined to form a total thalamocortical tract mask and applied to extract mean MD values as the total thalamocortical structural connectivity. The MD index was preferentially selected over the FA index because MD is less affected by the crossing fibers and has showed stronger association with cognitive impairments in SVD.[3,28] The total thalamus was segmented into six subregions based on the thalamic-cortical connectivity pattern.[14] The resulting segmentations were thresholded at 50 samples (5000 samples were initiated per seed voxel) and used to calculate each thalamic subregion volume (Figure 1). Details in supplementary materials.

Statistical analysis

Continuous variables were described by mean (standard deviation, SD) or median (interquartile ranges, IQRs), according to their distribution. When non-normally distributed data were used as response variables, we used the 'bestnormalized' package in R to perform the normalizing transformations. The volumes of total thalamus and thalamic subregions were normalized by dividing ICV.

To assess the effects of total SVD burden and each SVD marker on the total thalamic volume and thalamocortical connectivity, we divided all participants into two groups according to the total SVD score (splitting at score 1), normalized WMH volumes (splitting at the median volume), lacunes (splitting by the presence), CMBs (splitting by the presence) and BPF (splitting at the median value), respectively. Two-sample t-tests were used to examine the group differences of normalized total thalamic volume and thalamocortical MD. Next, using the Kendall rank correlation, we assessed the inter-correlation among normalized total thalamic volumes, thalamocortical MD and each SVD MRI marker and BPF across the total sample.

Then, we examined the associations between the total thalamic volume and thalamocortical connectivity, and cognitive function. Linear regression analyses were performed between each cognitive domain (i.e., processing speed, executive function, and memory) and normalized total thalamic volumes and thalamocortical MD. Different adjustments were included in the models: model 1:

age and education; model 2: model 1 plus SVD MRI markers (i.e., normalized WMH volumes, the presence of lacunes, the presence of CMBs) and BPF; model 3: model 2 plus vascular risk factors (i.e., hypertension, diabetes, hypercholesterolemia, and smoking). These regression models were checked for multicollinearity using the variance of inflation factors (VIFs).

In addition, to test if the relation between thalamic volume and each cognitive domain was mediated by the disrupted thalamic connectivity, we performed mediation analyses while controlling for age and education. We also tested an alternative mediation model in which thalamic volume mediated the relationship between thalamic connectivity and cognition.

To identify the volumes or connectivity of total thalamus and six thalamic subregions that have the strongest association with each cognitive domain, we employed the least absolute shrinkage and selection operator (LASSO) regression analysis while adjusting for age and education. Next, the association of LASSO selected volumes/connectivity of the thalamic subregion with each cognitive domain were tested in three linear regression models (model 1, model 2 and model 3). This was then followed by mediation analyses as described above to assess the relation between volume and connectivity of each thalamic subregion, and each cognitive domain.

All statistical analyses were completed using R software (version 4.1.0). The significant level was set at a two-tailed P value < 0.05. Details in supplementary materials.

There were no missing data for outcome variables in this study, except for 1–6% (Table s3) of participants, who were missing one or more cognitive tests. The missing data were imputed by the mean of the available participants to fully utilize available information.

Results

A total of 205 SVD participants without thalamic lacunes were included in this study. The median age was 73.0 (IQRs, 69.0 – 79.0) years and 89 (43.4%) were women. The raw and normalized volume of WMH were 3.8 (IQRs 1.8-8.7) ml and 0.3 (IQRs, 0.1-0.6) % respectively. 44 (21.5%) participants had lacunes, 70 (34.1%) participants had CMBs, and the median simple SVD score was 1.0 (IQRs 0.0 - 1.0) (Table 1 and Table s3). The raw and normalized mean volume of total thalamus was 11.1 (SD 1.1)

ml and 0.8 (SD 0.1) %, respectively. The mean MD value of the thalamocortical tract was 7.9 (SD 0.7) × 10^{-4}mm^2/s. The mean volumes of the six thalamic-subregions and mean MD values of the six tracts connecting thalamic-subregions and cortical regions were shown in Table s4.

Table 1. Demographic, clinical and imaging characteristics of the study cohort

	N=205
Demographic	
Age, y, median (IQR)	73.0 (69.0 – 79.0)
Female, n (%)	89 (43.4%)
Education, y, median (IQR)	10.0 (10.0 – 15.0)
Vascular risk factors	
Hypertension, n (%)	133 (64.9%)
Diabetes, n (%)	28 (13.7%)
hypercholesterolemia, n (%)	108 (52.7%)
Smoking history, n (%)	130 (63.4%)
Cognition function	
MMSE score, median (IQRs)	29.0 (27.0 – 30.0)
Processing speed, Z score, median (IQRs)	0.3 (-0.8 – 1.2)
Executive function, Z score, median (IQRs)	0.1 (-0.3 – 0.4)
Memory, Z score, mean (SD)	0.0 (1.9)
SVD markers	
Raw WMH volumes, ml, median (IQRs)	3.8 (1.8-8.7)
Normalized WMH volumes, %, median (IQRs)	0.3 (0.1 – 0.6)
WMH Fazekas score ≥ 2, n (%)	89 (43.4%)
Lacunes, n (%)	44 (21.5%)
CMBs, n (%)	70 (34.1%)
Simple SVD score, median (IQRs)	1.0 (0.0 – 1.0)
Brain volume, ml, mean (SD)	1085.5 (115.8)

IQRs, interquartile ranges; SD, standard deviation; WMH, white matter hyperintensities; CMBs, cerebral microbleeds; SVD, small vessel disease.

Thalamic volume, thalamocortical MD and SVD burden

The group with high SVD burden, which assessed by the presence of lacunes or lower BPF showed smaller normalized thalamic volume than the group with low SVD burden. The group with high SVD burden assessed by the simple SVD score ≥ 1, higher normalized WMH volumes, the presence of lacune, the presence of CMBs or lower BPF showed higher thalamocortical MD than the group with lower SVD burden

(*P-uncorrected* < 0.05, Figure 2.A, Figure s2). Higher normalized thalamic volume was significantly correlated with higher BPF (*r*=0.42), lower thalamocortical MD (*r*=-0.18) and the presence of lacunes (*r*=-0.12). Higher thalamocortical MD was significantly associated with lower BPF (*r*=-0.36), higher normalized WMH volumes (*r*=0.52), the presence of lacunes (*r*=0.32) and the presence of CMBs (*r*=0.18) (Figure 2.B).

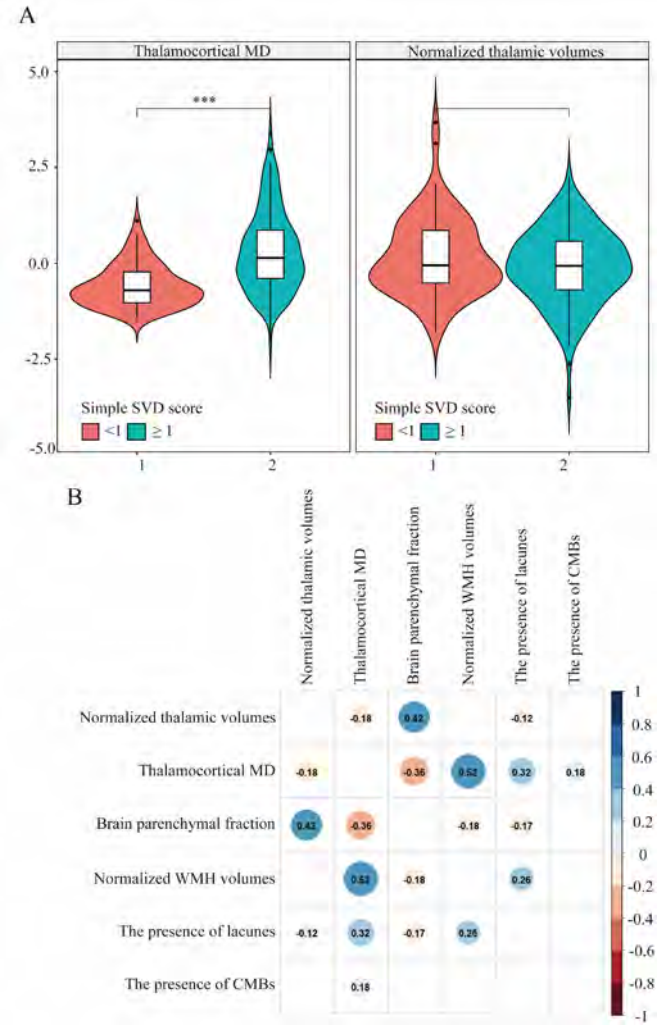

Figure 2. A, Intergroup differences of total thalamic volume, thalamocortical MD based on the simple SVD score; B, Inter-correlation among total thalamic volume, thalamocortical MD, MRI markers of SVD and brain atrophy. *, P-uncorrected <0.05; **, P-uncorrected <0.01, ***, P-uncorrected <0.001. MD, mean diffusivity, SVD, small vessel disease, WMH, white matter hyperintensities, CMBs, cerebral microbleeds. All numbers in Figure B represent correlation coefficients (P-uncorrected < 0.05), blank means no statistically significant results (P-uncorrected > 0.05)

Table 2. Association between cognitive function, total thalamic volume, and thalamocortical MD

	Processing speed		Executive function		Memory	
	β	P-value	β	P-value	β	P-value
Normalized thalamic volume						
Model 1	-0.049	0.446	0.062	0.350	0.121	0.067
Model 2	-0.064	0.383	-0.024	0.760	0.114	0.114
Model 3	-0.039	0.605	-0.018	0.817	0.129	0.099
Thalamocortical MD						
Model 1	-0.248	<0.001	-0.235	0.001	-0.301	<0.001
Model 2	-0.156	0.145	-0.170	0.129	-0.332	0.003
Model 3	-0.159	0.142	-0.216	0.054	-0.346	0.002

Adjustments in model 1: age and education; in model 2: model 1 plus MRI markers of SVD (i.e., normalized WMH volumes, the presence of lacunes, the presence of CMBs) and BPF; in model 3: model 2 plus vascular risk factors (i.e., hypertension, diabetes, hypercholesterolemia, and smoking). MD, mean diffusivity; SVD, small vessel disease; WMH, white matter hyperintensities; CMBs, cerebral microbleeds; BPF, brain parenchymal fraction.

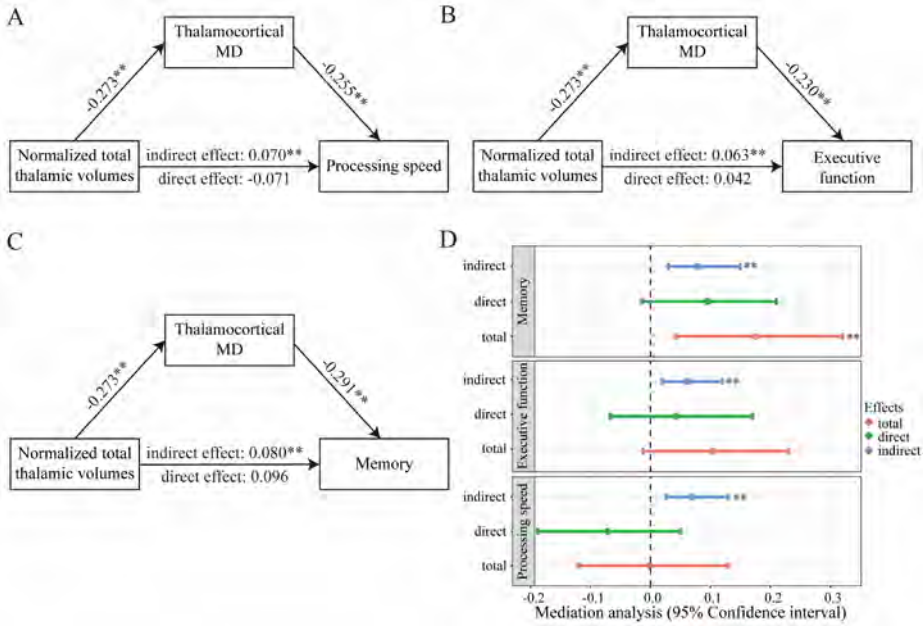

Figure 3. Mediation analysis of thalamocortical connectivity in the relation between thalamic volume and cognitive function. *, $P < 0.05$; **, $P < 0.01$. A-C, the path diagrams of three mediation models; D, the 95% confidence intervals for indirect effects, direct effects and total effects using bootstrapping (n = 1000 samples).

Thalamic volume, thalamocortical MD and cognitive function

Normalized thalamic volume was not related to processing speed, executive function, and memory (Table 2). Higher thalamocortical MD was related to worse cognitive functions while adjusting for age and education (model 1): processing speed (β=-0.248, p<0.001), executive function (β=-0.235, p=0.001) and memory (β=-0.301, p<0.001). The relation between thalamocortical MD and memory remained significant after additionally adjusted SVD MRI markers, BPF and vascular risk factors (model 2: β=-0.332, p=0.003; model 3: β=-0.346, p=0.002), but not for processing speed and executive function (Table 2).

The mediation analyses showed thalamocortical MD mediated the relations between normalized thalamic volume and three cognitive domains (Figure 3), while normalized thalamic volume showed no mediating effects in the relations between the thalamocortical MD and each cognitive domain (Figure s3).

Thalamic subregions and cognitive domain

LASSO regression analyses showed that MD of the thalamic-motor tract was associated with processing speed, and MD of the thalamic-frontal tract with executive function and memory (Table s5). Linear regression models confirmed the results showing that higher MD of the thalamic-motor tract was associated with lower processing speed (model 1: β=-0.27, p<0.001), higher MD of the thalamic-frontal tract was associated with worse executive function (model 1: β = -0.24, p=0.001) and memory (model 1: β = -0.28, p<0.001), respectively (Figure 4). Further adjustments for SVD MRI markers, BPF (model 2) and vascular risk factors (model 3) had little effects on these relations (Table s6, s7).

Mediation analyses showed that: MD of the thalamic-motor tract mediated the relation between the normalized volume of thalamic-motor subregion and processing speed; MD of the thalamic-frontal tract mediated the relations between the normalized volume of thalamic-frontal subregion and executive function and memory, respectively; while the normalized volume of these thalamic subregions showed no mediating effect in the relations between MD of the thalamic-cortex tracts and each cognitive domain (Figure 4).

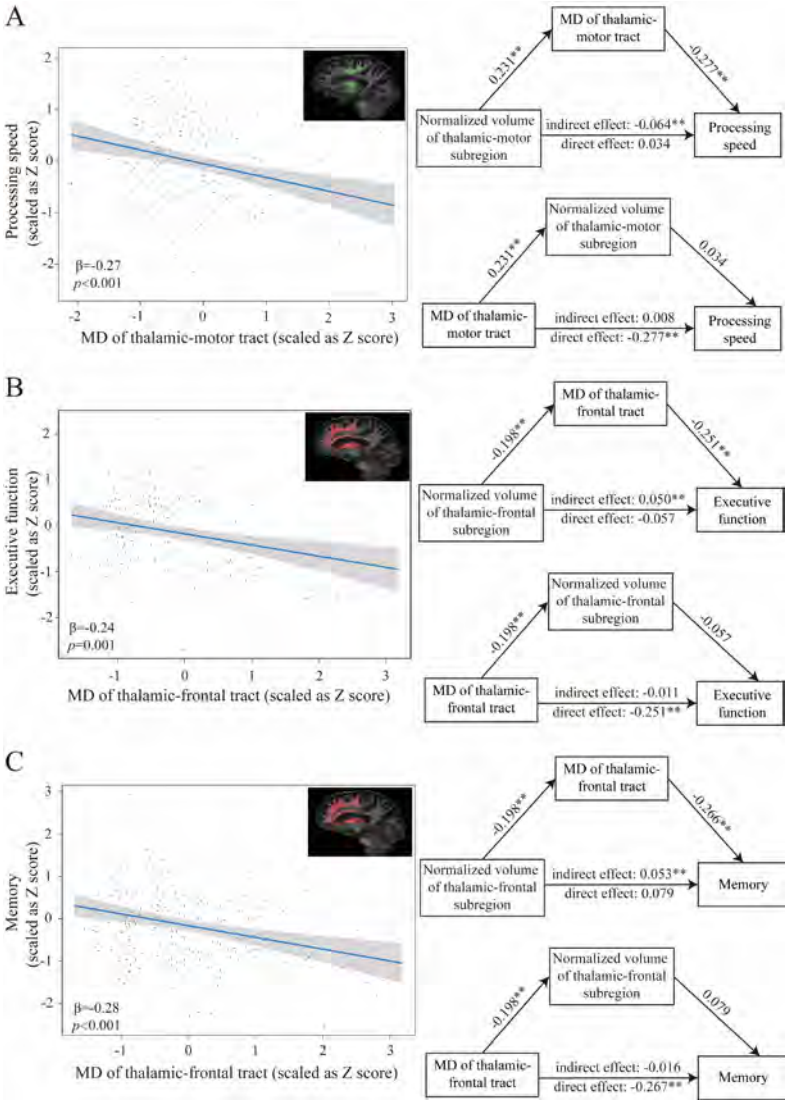

Figure 4. The relation between least absolute shrinkage and selection operator (LASSO) selected thalamic subregion and three cognitive domains. A. Left, linear regression between MD of thalamic-motor tract and processing speed while adjusting for age and education and the visualization of thalamic-motor tract (green); Right, the mediation analysis of corresponding thalamic-subregion volumes, connectivity, and processing speed; B. Left, linear regression between MD of thalamic-frontal tract and executive function while adjusting for age and education and the visualization of thalamic-frontal tract (red); Right, the mediation analysis of corresponding thalamic-subregion volumes, connectivity, and executive function; C. Left, linear regression between MD of thalamic-frontal tract and memory while adjusting for age and education and the visualization of thalamic-frontal tract (red); Right, the mediation analysis of corresponding thalamic-subregion volumes, connectivity, and memory. MD, mean diffusivity, *, P < 0.05; **, P < 0.01.

Discussion

In the present study, we found that 1) thalamic volume and thalamocortical MD (as a proxy for thalamocortical connectivity) were correlated with SVD burden; 2) thalamocortical connectivity was associated with processing speed, executive function, and memory, while the total thalamic volume was not; and 3) damage to specific white matter tracts projecting from the thalamus to the cortex was related to specific cognitive deficit. Executive function and memory were related to thalamic-frontal connections and processing speed to thalamic-motor connections. Our results suggest that the thalamic volume and the thalamocortical connections are affected in SVD patients without thalamic lacunes and that these thalamic alterations are linked to the cognitive impairment, largely depending on the damage patterns of the white matter tracts connecting thalamic subregions and cortical regions.

The number of studies on the role of thalamus in SVD is limited.[2] Here, we found that the participants with high SVD burden showed lower thalamic volume and thalamocortical connections compared to those with low SVD burden. This is consistent with previous findings showing that SVD patients with more severe WMH have smaller thalamic volumes.[29] This association could be explained by the shrinkage of thalamic dendrites and cell bodies due to the loss of synaptic input,[30] and the accumulation of microvascular damage in the thalamus.[31]

We found that total thalamocortical connectivity was associated with the three cognitive domains (i.e., processing speed, executive function, and memory). This finding is in line with previous studies showing the associations between WMH accumulation in the thalamic-cortical tract and processing speed.[12,13] However, in our study, the total thalamic volume showed no association with cognition. In the mediation analyses, thalamocortical connectivity mediated the relations between thalamic volumes and the performances in three cognitive domains, while thalamic volume showed no mediating effects in the relations between thalamocortical connectivity and cognition. These findings suggest that the effects of thalamic structural abnormalities on cognitive impairments in SVD are mainly linked to the damage of the cortical-subcortical pathways, which may disrupt the complex network underpinning cognitive functions.[32]

Next, we used LASSO and linear regression analyses to identify the volumes and connectivity of thalamic subregions that have the strongest association with each cognitive domain. The connectivity of thalamic-motor tract was related to processing

speed in our study, which has been reported in MS.[33] This could be explained by the effects of motor impairment on the processing speed task. However, the lack of association between the connectivity of thalamic-frontal tract and processing speed is inconsistent with previous studies.[12,34] This inconsistency may originate from the differences in the approach used to assess processing speed. Most previous studies employed TMT-B, instead of SDMT, to assess processing speed, which may account for the different results. In addition, we found that the thalamic-frontal tract was related to executive function. This is in line with a study showing that WMH located in the anterior thalamic radiations played a strategic role in executive dysfunction in sporadic SVD.[35] Also, we found that the connectivity of thalamic-frontal tract was related to memory. Few studies have examined the role of thalamus in SVD-related memory impairment. The memory impairment following thalamic infarcts has been reported in several cases.[36,37] Studies in Alzheimer's disease and MS also proved a role of the thalamus in memory decline.[9,38] The prefrontal cortex and its connections with the mediodorsal thalamus are thought to be crucial for working memory,[39] which is the major impaired part in SVD-related memory damage.[40]

Besides, we found that higher volume of the thalamic-motor subregion was associated with higher MD of the thalamic-motor tract, which was not expected. This finding should be treated with some caution, as we would expect to see facilitation of water diffusion (e.g., higher MD) in case of neurodegeneration. Several possible explanations may account for this. First, compensatory enlargement of grey matter in thalamic-motor subregion may occur in case of disrupted thalamic-motor connections. Second, there may be small registration errors in the image transformations, which will be more obvious in the small-size segmentation (i.e., thalamic-motor subregion). Considering this possibility, we combined the subregions connected to the frontal and motor cortex to calculate the volume and then tested the association between volume and connectivity in thalamic frontal/motor subregion. This result, however, showed that the volume of thalamic-frontal/motor subregion was not associated with the MD of thalamic-frontal/motor tracts (Figure s4).

The main strengths of this study are the quantitative measurement of thalamic volume, thalamocortical connectivity and the connectivity-based thalamic segmentations. Considering the higher rate of crossing fibers within one voxel in sub-cortical regions, we used the probabilistic tractography, which can better resolve this problem. In addition, using MP2RAGE sequence and manually adjusting the thalamic mask provided the accuracy of thalamic segmentation. The comprehensive cognitive data in this cohort provided us to better understand the role of thalamus in SVD-related cognitive impairment.

Several limitations should be acknowledged. First, we only used the data of third follow-up of RUN DMC study. RUN DMC study is a long-term longitudinal study. However, due to the change of MRI scanners, we could not use previous MRI data for longitudinal analysis. We were therefore only able to conduct cross-sectional analyses, which limited us to make causal inferences. Future longitudinal studies are needed to test the direction of the observed associations. Second, our cohort does not include the age-matched healthy controls. This limitation makes it difficult to distinguish the observed effects from those of normal aging. To minimize this confounding effect, we adjusted for age and education in the regression models, and we performed group-analyses based on the severity of SVD burden. Third, we have missing data (1-6%) in some cognitive tests for which we have performed imputation. Also, about a half of the original RUN DMC participants did not participate in the third follow-up due to various reasons, who have more severe SVD burden and/or are more cognitively impaired. This missing data may cause bias, however, if any, this may lead to an underestimation of the effects of the thalamic volume and connectivity measures. Fourth, we excluded patients with thalamic lacunes. This enabled us to discard the influence of thalamic lacunes and therefore provide solid proof that the thalamic structural alterations, independent of the thalamic lacunes, are related to cognitive impairment, but may also lead to an underestimation of the findings.

In conclusion, our study showed that thalamic volume and thalamocortical connections are lower in participants with high SVD burden compared to participants with low SVD burden and, more importantly, we demonstrated that damage to specific white matter tracts projecting from the thalamus to the cortex are linked to specific cognitive deficit. Our study highlights the importance of studying specific white matter tracts originating from the thalamus in relation to cognitive function and provides additional evidence of the role of the damage of the cortical-subcortical pathways in processing speed, executive function, and memory deficits in SVD patients independent of thalamic lacunes. Further studies preferably with multiple timepoints are necessary to further elucidate the pathophysiology of thalamus alterations and their exact role of cognitive impairments in SVD.

Supplementary materials

Materials and methods

Study population

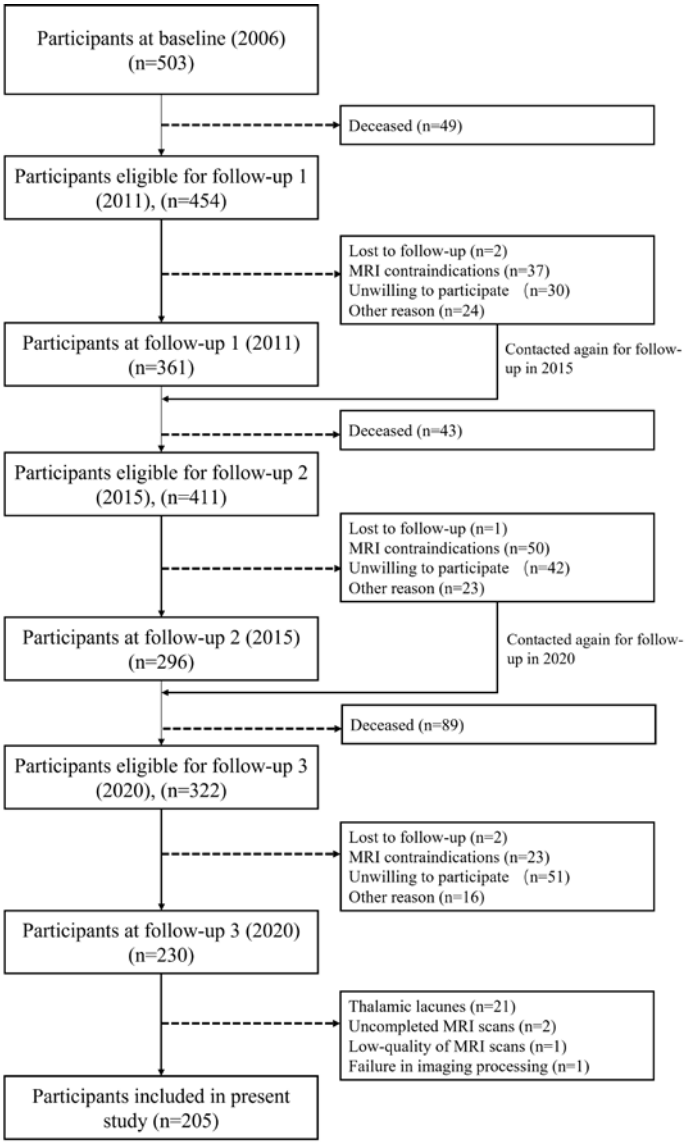

Figure s1. Flow chart of included participants. Note: in this study, we only included SVD participants without thalamic lacunes in the third follow-up.

Neuropsychological assessment

Processing speed was calculated by the sum of (1) the inverse Z score of the Trail Making Test (TMT) part A; (2) the Z score of Symbol-Digit Modalities Test (SDMT). Executive function was calculated by the sum of (1) the inverse Z score of the TMT ratio (TMT-B/TMT-A); (2) the average Z score of Verbal Fluency Test animal naming and job naming. Memory was calculated as the sum of (1) the Z score of Digit span test (DST); (2) the average Z score of Rey's Auditory Verbal learning test (RAVLT) immediate recall and delayed recall; (3) the average Z score of Rey–Osterie Complex Figure Test (ROCF) immediate recall and delayed recall.

Table s1. Calculation of each cognitive domain

Cognitive domain	Cognitive test	Calculation of compound score
Processing speed	Trail Making Test A	$Z_{TMT\text{-}A} \times -1 + Z_{SDMT}$
	Symbol-Digit Modalities Test	
Executive function	Trail Making Test A	$Z_{(TMT\text{-}B/TMT\text{-}A)} \times -1 + (Z_{VFT\text{-}A} + Z_{VFT\text{-}J})/2$
	Trail Making Test B	
	Verbal Fluency Test (Animals and jobs)	
Memory	Digit span test (Forward and backward)	$Z_{(DST\text{-}f + DST\text{-}b)} + (Z_{RAVLT\text{-}I} + Z_{RAVLT\text{-}D})/2 + (Z_{ROCF\text{-}I} + Z_{ROCF\text{-}D})/2$
	Rey's Auditory Verbal learning test (Immediate recall and delayed recall)	
	Rey–Osterie Complex Figure Test (Immediate recall and delayed recall)	

Note: Z, the Z transformed score; DST-f, Digit span forward test; DST-b, Digit span backward test; RAVLT-I, the Immediate recall of Rey's Auditory Verbal learning test; RAVLT-D, the delayed recall of Rey's Auditory Verbal learning test; ROCF-I, the Immediate recall of Rey–Osterrieth Complex Figure Test; ROCF -I, the Immediate recall of Rey–Osterrieth Complex Figure Test; ROCF -D, the delayed recall of Rey–Osterrieth Complex Figure Test; TMT, Trail Making Test; SDMT, Symbol-Digit Modalities Test, VFT-A, Verbal Fluency Test (animals); VFT-A, Verbal Fluency Test (jobs)

MRI acquisition

3D T1-weighted Magnetization Prepared 2 Rapid Acquisition Gradient Echoes (MP2RAGE) with following the parameters: 0.85mm isotropic voxels, and repetition time (TR) = 5500 ms, inversion time (TI1 and TI2) = 700 and 2500 ms; Multi-shell DWI using multi-band accelerated echo planar imaging (EPI) with the following parameters: 99 diffusion-weighted directions (3 × b = 200, 6 × b = 500, 30 × b = 1,000, and 60 × b = 3,000s/mm2), 10 × b = 0 images, 1.7mm isotropic voxels, and TR = 3220ms, TE = 74 ms; one b=0 image with acquisition parameters equal to the previous b=0 images, but acquired in opposite phase-encoding

direction; 3D fluid-attenuated inversion recovery (FLAIR) with 0.85mm isotropic voxels, and TR = 5000ms, TE = 394 ms, TI = 1800ms; 3D multi-echo fast low-angle shot providing magnitude and phase images (9 echoes; TR = 35ms, ΔTE = 4.92ms) to create susceptibility-weighted images with 0.8 × 0.8 × 2.0 mm3 voxels.

Segmentation of thalamus and cortical regions

Using the Functional Magnetic Resonance Imaging of the Brain Software Library (FSL; v6.0.1) software, the T1-weighted images were non-linearly registered to the Montreal Neurological Institute (MNI) 152 template using Functional MRI of the Brain nonlinear registration tool (FNIRT). We then used the transformation matrix and deformation fields to register the atlas to the native T1-space to define the six cortical regions. Finally, the thalamus and the six cortical regions in the native T1-space were linearly registered to the diffusion space using Functional MRI of the brain linear image registration tool (FLIRT). All segmented and transformed brain regions were visually inspected and corrected if necessary.

Table s2. Six cortical regions derived from the Harvard-Oxford cortical atlas

Cortical regions	Harvard-Oxford cortical labels
Frontal cortex	Frontal Pole
	Insular Cortex
	Superior Frontal Gyrus
	Middle Frontal Gyrus
	Inferior Frontal Gyrus, pars triangularis
	Inferior Frontal Gyrus, pars opercularis
	Frontal Medial Cortex
	Subcallosal Cortex
	Paracingulate Gyrus
	Cingulate Gyrus, anterior division
	Frontal Orbital Cortex
Motor cortex	Precentral Gyrus,
	Supplementary Motor Cortex
Sensory cortex	Postcentral Gyrus
Posterior parietal cortex	Superior Parietal Lobule
	Supramarginal Gyrus, anterior division
	Supramarginal Gyrus, posterior division
	Angular Gyrus
	Cingulate Gyrus, posterior division
	Precuneous Cortex
	Parietal Operculum Cortex

Cortical regions	Harvard-Oxford cortical labels
Temporal cortex	Temporal Pole
	Superior Temporal Gyrus, anterior division
	Superior Temporal Gyrus, posterior division
	Middle Temporal Gyrus, anterior division
	Middle Temporal Gyrus, posterior division
	Middle Temporal Gyrus, temporooccipital part
	Inferior Temporal Gyrus, anterior division
	Inferior Temporal Gyrus, posterior division
	Inferior Temporal Gyrus, temporooccipital part
	Parahippocampal Gyrus, anterior division
	Parahippocampal Gyrus, posterior division
	Temporal Fusiform Cortex, anterior division
	Temporal Fusiform Cortex, posterior division
	Temporal Occipital Fusiform Cortex
	Central Opercular Cortex
	Planum Polare
	Heschl's Gyrus
	Planum Temporale
Occipital cortex	Lateral Occipital Cortex, superior division
	Lateral Occipital Cortex, inferior division
	Intracalcarine Cortex
	Angular Gyrus
	Cingulate Gyrus, posterior division
	Cuneal Cortex
	Lingual Gyrus
	Occipital Fusiform Gyrus
	Supracalcarine Cortex
	Occipital Pole

Diffusion MRI processing

Denoising and removing of Gibbs artifacts were completed using tools from MRtrix (v3.0, http://www.mrtrix.org). Eddy and topup functions within the FSL were used to corrected for head motion, eddy-induced and susceptibility-induced distortions, motion. Intensity bias correction was performed with N4 bias correction as implemented in Advanced Normalization Tools, version 2.1.0. The 'bedpostx' tool from FSL was used to estimate the multi-fiber directions within each voxel of the brain using the multi-shell ball-and-two-sticks model. The diffusion tensor fit of each voxel was achieved using 'dtifit' function in FSL to create fractional anisotropy (FA) and MD images for each participant.

Probabilistic tractography and connectivity-based thalamic segmentation

The probtractx2 function from FSL was used to perform probabilistic tractography with default parameters: number of samples = 5000, number of steps per sample = 2000, step length in mm = 0.5, curvature threshold = 0.2.

The hard segmentation of thalamus based on the pattern of the thalamic-cortical connectivity was performed using the 'find the biggest' function within FSL.

Statistical analysis

The multicollinearity was checked using variance of inflation factors (VIFs) in the regression analyses. All regression models showed low VIFs (VIF<5), indicating no substantial multicollinearity between the variables.

Mediation analyses were performed using the 'mediation' package in R. 1000 bias-corrected bootstrapping samples and the 95% confidence interval were used to estimate the statistical significance of the mediation analyses.

In the LASSO regression models, the parameter α was set at 1 and the optimal λ of was determined using 10 cross-validation.

Table s3. Results on each cognitive task

Cognitive task	Raw score
DST	
Forward, median (IQR)	9.0 (7.0 – 10.0)
backward, median (IQR)	5.0 (4.0 – 7.0)
RAVLT	
Immediate recall, median (IQR)	22.0 (19.0 – 25.0)
Delayed recall, median (IQR)	6.0 (4.0 – 8.0)
ROCF	
Immediate recall, median (IQR)	21.0 (16.0 – 25.0)
Delayed recall, median (IQR)	20.0(15.0 – 24.0)
TMT-A, median (IQR)	47.1 (37.8 – 65.5)
TMT-B, median (IQR)	108.7 (82.8 – 154.0)
SDMT, median (IQR)	40.0 (32.0 – 47.0)
VFT, median (IQR)	
Animals	20.0 (16.0 – 23.0)
Jobs	15.0 (11.0 – 17.0)

Note: DST, Digit span forward test; RAVLT, Rey's Auditory Verbal learning test; ROCF, Rey–Osterrieth Complex Figure Test; TMT, Trail Making Test; SDMT, Symbol-Digit Modalities Test; VFT, Verbal Fluency Test.

Table s4. Volume and MD values of six thalamic subregions

Subregions	Raw volume (ml, mean, SD)	Normalized volume (10^{-3}, mean, SD)	MD ($10^{-4}mm^2/s$, mean, SD)
Frontal	4.9 (0.8)	3.4 (0.6)	7.5 (0.7)
Motor	1.5 (0.6)	1.1 (0.3)	7.3 (0.5)
Sensory	1.3 (0.5)	0.9 (0.3)	7.4 (0.5)
Posterior parietal	1.2 (0.6)	0.8 (0.3)	8.1 (0.8)
Temporal	0.5 (0.3)	0.4 (0.1)	8.8 (0.6)
Occipital	1.2 (0.8)	0.9 (0.4)	8.3 (0.8)

MD, mean diffusivity; SD, standard deviation.

Table s5. Regression coefficients from LASSO analysis

	Processing Speed	Executive function	Memory
Volume			
Total thalamus	-	-	-
Thalamic-frontal subregion	-	-	-
Thalamic-motor subregion	-	-	-
Thalamic-occipital subregion	-	-	-
Thalamic-parietal subregion	-	-	-
Thalamic-sensory subregion	-	-	-
Thalamic-temporal subregion	-	-	-
MD			
Thalamocortical tract	-	-	-
Thalamic-frontal tract	-	-6.5×10^{-2}	-7.0×10^{-2}
Thalamic-motor tract	-14.1×10^{-2}	-	-
Thalamic-occipital tract	-	-	-
Thalamic-parietal tract	-	-	-
Thalamic-sensory tract	-	-	-
Thalamic-temporal tract	-	-	-

LASSO, least absolute shrinkage, and selection operator

Table s2. Continued

Table s6. Association between LASSO selected volume/connectivity of thalamic subregion and each cognitive domain in linear regression (model 2)

	Processing speed		Executive function		Memory	
	β	***P***	***β***	***P***	***β***	***P***
MD of thalamic-motor tract	-0.22	**0.022**	-	-	-	-
MD of thalamic-frontal tract	-	-	-0.18	0.078	-0.24	**0.017**

Model: adjusted for age and education, MRI markers of SVD (i.e., normalized WMH volumes, the presence of lacunes, the presence of CMBs) and BPF. MD, mean diffusivity; SVD, small vessel disease; WMH, white matter hyperintensities; CMBs, cerebral microbleeds; BPF, brain parenchymal fraction.

Table s7. Association between LASSO selected volume/connectivity of thalamic subregion and each cognitive domain in linear regression (model 3)

	Processing speed		Executive function		Memory	
	β	***P***	***β***	***P***	***β***	***P***
MD of thalamic-motor tract	-0.25	**0.013**	-	-	-	-
MD of thalamic-frontal tract	-	-	-0.24	**0.018**	-0.26	**0.011**

Model: adjusted for age, education, MRI markers of SVD (i.e., normalized WMH volumes, the presence of lacunes, the presence of CMBs), BPF, vascular risk factors (i.e., hypertension, diabetes, hypercholesterolemia, and smoking). MD, mean diffusivity; SVD, small vessel disease; WMH, white matter hyperintensities; CMBs, cerebral microbleeds; BPF, brain parenchymal fraction.

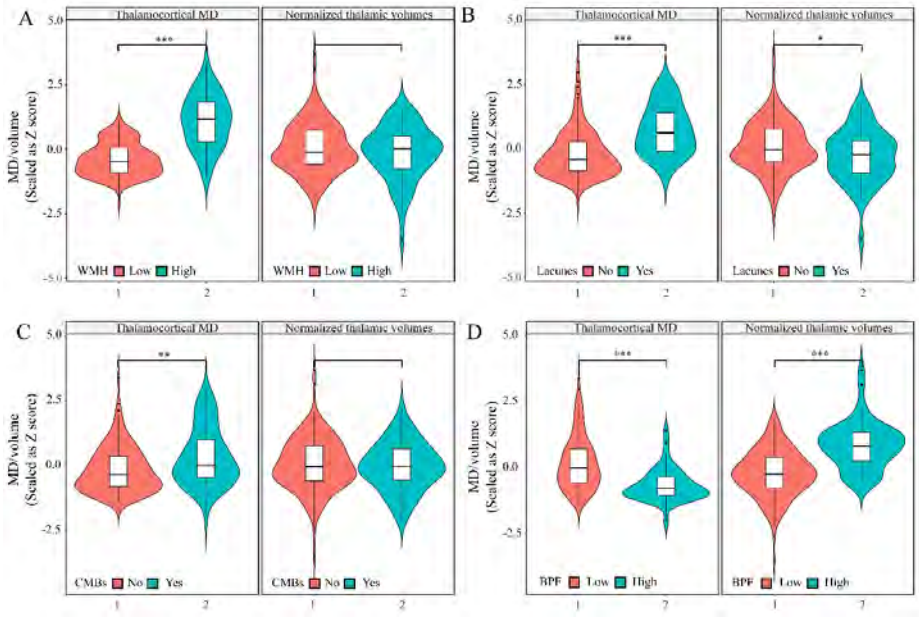

Figure s2. Intergroup differences of total thalamic volume, thalamocortical MD based on the normalized WMH volumes, the presences of lacunes, the presences of CMBs, and the BPF, respectively. *, p-uncorrected < 0.05; **, p-uncorrected < 0.01, ***, p-uncorrected <0.001, WMH, white matter hyperintensities, CMBs, cerebral microbleeds, BPF, Brain parenchymal fraction.

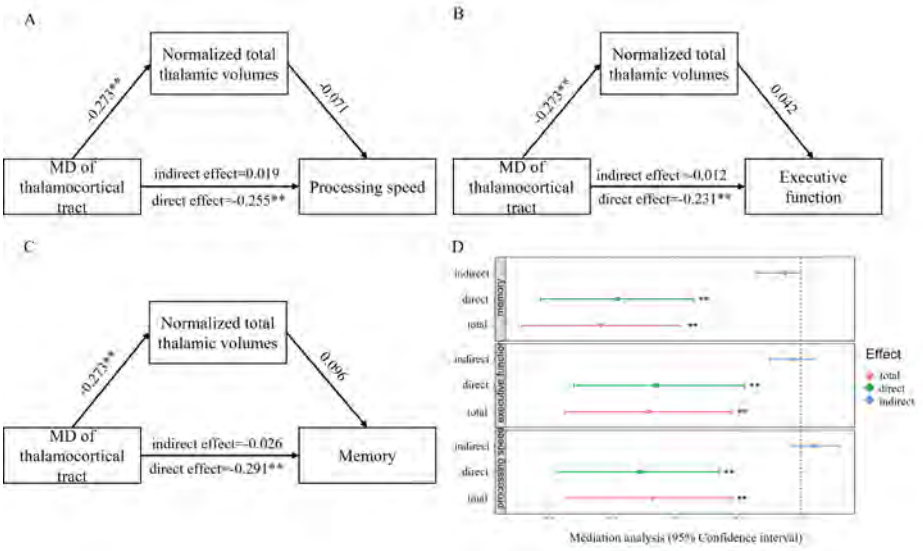

Figure s3. Mediation analysis of thalamic volume in the relation between thalamocortical connectivity and cognitive function. *, $P < 0.05$; **, $P < 0.01$. A-C, the path diagrams of three mediation models; D, the 95% confidence intervals for indirect effects, direct effects and total effects using the bootstrapping (n = 1000 samples) method. The mediation analyses showed no significant statistical mediation between thalamocortical connectivity and cognitive function by thalamic volume in small vessel disease.

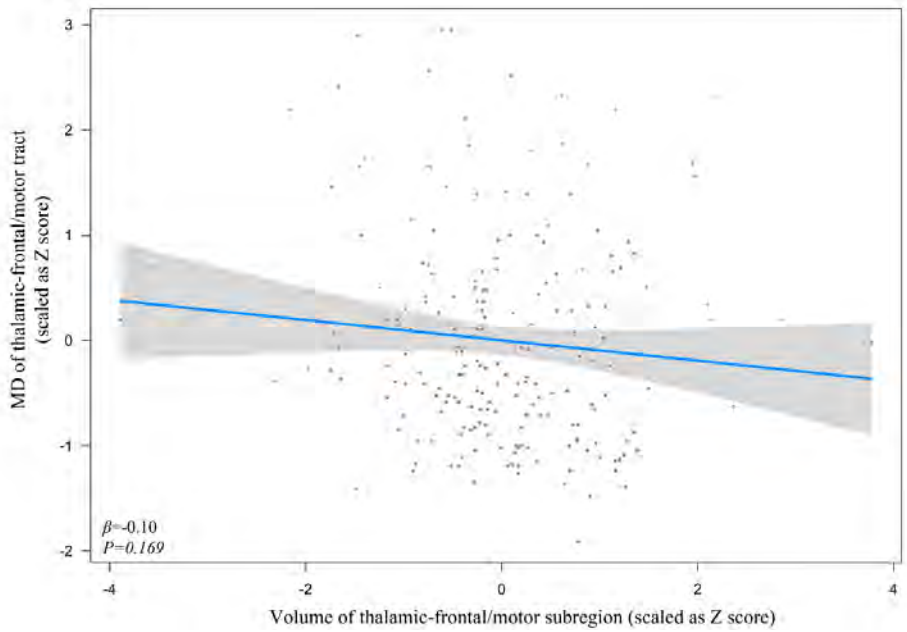

Figure s4. Linear regression analysis between volume and connectivity in thalamic frontal/motor subregion.

Reference

1. Hamilton OKL, Backhouse EV, Janssen E, Jochems ACC, Maher C, Ritakari TE, Stevenson AJ, Xia L, Deary IJ, Wardlaw JM. Cognitive impairment in sporadic cerebral small vessel disease: A systematic review and meta-analysis. Alzheimers Dement. Apr 2021;17(4):665-685. doi:10.1002/alz.12221
2. Wardlaw JM, et al. Neuroimaging standards for research into small vessel disease and its contribution to ageing and neurodegeneration. Lancet Neurol. Aug 2013;12(8):822-38. doi:10.1016/s1474-4422(13)70124-8
3. van Norden AG, van Uden IW, de Laat KF, van Dijk EJ, de Leeuw FE. Cognitive function in small vessel disease: the additional value of diffusion tensor imaging to conventional magnetic resonance imaging: the RUN DMC study. Journal of Alzheimer's disease : JAD. 2012;32(3):667-76. doi:10.3233/jad-2012-120784
4. Ter Telgte A, van Leijsen EMC, Wiegertjes K, Klijn CJM, Tuladhar AM, de Leeuw FE. Cerebral small vessel disease: from a focal to a global perspective. Nat Rev Neurol. Jul 2018;14(7):387-398. doi:10.1038/s41582-018-0014-y
5. Tuladhar AM, van Dijk E, Zwiers MP, van Norden AG, de Laat KF, Shumskaya E, Norris DG, de Leeuw FE. Structural network connectivity and cognition in cerebral small vessel disease. Human brain mapping. Jan 2016;37(1):300-10. doi:10.1002/hbm.23032
6. Bergsland N, Zivadinov R, Dwyer MG, Weinstock-Guttman B, Benedict RH. Localized atrophy of the thalamus and slowed cognitive processing speed in MS patients. Multiple sclerosis (Houndmills, Basingstoke, England). Sep 2016;22(10):1327-36. doi:10.1177/1352458515616204
7. Bernabéu-Sanz Á, Morales S, Naranjo V, Sempere Á P. Contribution of Gray Matter Atrophy and White Matter Damage to Cognitive Impairment in Mildly Disabled Relapsing-Remitting Multiple Sclerosis Patients. Diagnostics (Basel, Switzerland). Mar 23 2021;11(3)doi:10.3390/diagnostics11030578
8. Philp DJ, Korgaonkar MS, Grieve SM. Thalamic volume and thalamo-cortical white matter tracts correlate with motor and verbal memory performance. NeuroImage. May 1 2014;91:77-83. doi:10.1016/j.neuroimage.2013.12.057
9. van de Mortel LA, Thomas RM, van Wingen GA. Grey Matter Loss at Different Stages of Cognitive Decline: A Role for the Thalamus in Developing Alzheimer's Disease. Journal of Alzheimer's disease : JAD. 2021;83(2):705-720. doi:10.3233/jad-210173
10. Benjamin P, Lawrence AJ, Lambert C, Patel B, Chung AW, MacKinnon AD, Morris RG, Barrick TR, Markus HS. Strategic lacunes and their relationship to cognitive impairment in cerebral small vessel disease. Neuroimage Clin. 2014;4:828-37. doi:10.1016/j.nicl.2014.05.009
11. Benisty S, Gouw AA, Porcher R, Madureira S, Hernandez K, Poggesi A, van der Flier WM, Van Straaten EC, Verdelho A, Ferro J, Pantoni L, Inzitari D, Barkhof F, Fazekas F, Chabriat H. Location of lacunar infarcts correlates with cognition in a sample of non-disabled subjects with age-related white-matter changes: the LADIS study. Journal of neurology, neurosurgery, and psychiatry. May 2009;80(5):478-83. doi:10.1136/jnnp.2008.160440
12. Duering M, Gesierich B, Seiler S, Pirpamer L, Gonik M, Hofer E, Jouvent E, Duchesnay E, Chabriat H, Ropele S, Schmidt R, Dichgans M. Strategic white matter tracts for processing speed deficits in age-related small vessel disease. Neurology. Jun 3 2014;82(22):1946-50. doi:10.1212/wnl.0000000000000475
13. Duering M, Zieren N, Hervé D, Jouvent E, Reyes S, Peters N, Pachai C, Opherk C, Chabriat H, Dichgans M. Strategic role of frontal white matter tracts in vascular cognitive impairment: a

voxel-based lesion-symptom mapping study in CADASIL. Brain. Aug 2011;134(Pt 8):2366-75. doi:10.1093/brain/awr169

14. Behrens TE, Johansen-Berg H, Woolrich MW, Smith SM, Wheeler-Kingshott CA, Boulby PA, Barker GJ, Sillery EL, Sheehan K, Ciccarelli O, Thompson AJ, Brady JM, Matthews PM. Non-invasive mapping of connections between human thalamus and cortex using diffusion imaging. Nat Neurosci. Jul 2003;6(7):750-7. doi:10.1038/nn1075
15. van Norden AG, de Laat KF, Gons RA, van Uden IW, van Dijk EJ, van Oudheusden LJ, Esselink RA, Bloem BR, van Engelen BG, Zwarts MJ, Tendolkar I, Olde-Rikkert MG, van der Vlugt MJ, Zwiers MP, Norris DG, de Leeuw FE. Causes and consequences of cerebral small vessel disease. The RUN DMC study: a prospective cohort study. Study rationale and protocol. BMC Neurol. Feb 28 2011;11:29. doi:10.1186/1471-2377-11-29
16. Cai M, Jacob MA, van Loenen MR, Bergkamp M, Marques J, Norris DG, Duering M, Tuladhar AM, de Leeuw FE. Determinants and Temporal Dynamics of Cerebral Small Vessel Disease: 14-Year Follow-Up. Stroke. May 4 2022:101161strokeaha121038099. doi:10.1161/strokeaha.121.038099
17. Dewenter A, Gesierich B, Ter Telgte A, Wiegertjes K, Cai M, Jacob MA, Marques JP, Norris DG, Franzmeier N, de Leeuw FE, Tuladhar AM, Duering M. Systematic validation of structural brain networks in cerebral small vessel disease. Journal of cerebral blood flow and metabolism : official journal of the International Society of Cerebral Blood Flow and Metabolism. Dec 20 2021:271678x211069228. doi:10.1177/0271678x211069228
18. Fazekas F, Chawluk JB, Alavi A, Hurtig HI, Zimmerman RA. MR signal abnormalities at 1.5 T in Alzheimer's dementia and normal aging. AJR Am J Roentgenol. Aug 1987;149(2):351-6. doi:10.2214/ajr.149.2.351
19. Amin Al Olama A, Wason JMS, Tuladhar AM, van Leijsen EMC, Koini M, Hofer E, Morris RG, Schmidt R, de Leeuw FE, Markus HS. Simple MRI score aids prediction of dementia in cerebral small vessel disease. Neurology. Mar 24 2020;94(12):e1294-e1302. doi:10.1212/wnl.0000000000009141
20. Benjamin P, Trippier S, Lawrence AJ, Lambert C, Zeestraten E, Williams OA, Patel B, Morris RG, Barrick TR, MacKinnon AD, Markus HS. Lacunar Infarcts, but Not Perivascular Spaces, Are Predictors of Cognitive Decline in Cerebral Small-Vessel Disease. Stroke. Mar 2018;49(3):586-593. doi:10.1161/strokeaha.117.017526
21. Puonti O, Iglesias JE, Van Leemput K. Fast and sequence-adaptive whole-brain segmentation using parametric Bayesian modeling. Neuroimage. Dec 2016;143:235-249. doi:10.1016/j.neuroimage.2016.09.011
22. Kellner E, Dhital B, Kiselev VG, Reisert M. Gibbs-ringing artifact removal based on local subvoxel-shifts. Magn Reson Med. Nov 2016;76(5):1574-1581. doi:10.1002/mrm.26054
23. Veraart J, Novikov DS, Christiaens D, Ades-Aron B, Sijbers J, Fieremans E. Denoising of diffusion MRI using random matrix theory. Neuroimage. Nov 15 2016;142:394-406. doi:10.1016/j.neuroimage.2016.08.016
24. Andersson JLR, Sotiropoulos SN. An integrated approach to correction for off-resonance effects and subject movement in diffusion MR imaging. Neuroimage. Jan 15 2016;125:1063-1078. doi:10.1016/j.neuroimage.2015.10.019
25. Smith SM, Jenkinson M, Woolrich MW, Beckmann CF, Behrens TE, Johansen-Berg H, Bannister PR, De Luca M, Drobnjak I, Flitney DE, Niazy RK, Saunders J, Vickers J, Zhang Y, De Stefano N, Brady JM, Matthews PM. Advances in functional and structural MR image analysis and implementation as FSL. NeuroImage. 2004;23 Suppl 1:S208-19. doi:10.1016/j.neuroimage.2004.07.051
26. Tustison NJ, Avants BB, Cook PA, Zheng Y, Egan A, Yushkevich PA, Gee JC. N4ITK: improved N3 bias correction. IEEE Trans Med Imaging. Jun 2010;29(6):1310-20. doi:10.1109/tmi.2010.2046908

27. Tsai SY. Reproducibility of structural brain connectivity and network metrics using probabilistic diffusion tractography. Scientific reports. Aug 1 2018;8(1):11562. doi:10.1038/s41598-018-29943-0
28. Dauguet J, Peled S, Berezovskii V, Delzescaux T, Warfield SK, Born R, Westin CF. Comparison of fiber tracts derived from in-vivo DTI tractography with 3D histological neural tract tracer reconstruction on a macaque brain. Neuroimage. Aug 15 2007;37(2):530-8. doi:10.1016/j.neuroimage.2007.04.067
29. Wang Y, Yang Y, Wang T, Nie S, Yin H, Liu J. Correlation between White Matter Hyperintensities Related Gray Matter Volume and Cognition in Cerebral Small Vessel Disease. Journal of stroke and cerebrovascular diseases : the official journal of National Stroke Association. Dec 2020;29(12):105275. doi:10.1016/j.jstrokecerebrovasdis.2020.105275
30. Duering M, Schmidt R. Remote changes after ischaemic infarcts: a distant target for therapy? Brain : a journal of neurology. 2017;140(7):1818-1820. doi:10.1093/brain/awx135 %J Brain
31. Gao Y, Li D, Lin J, Thomas AM, Miao J, Chen D, Li S, Chu C. Cerebral small vessel disease: Pathological mechanisms and potential therapeutic targets. Frontiers in aging neuroscience. 2022;14:961661. doi:10.3389/fnagi.2022.961661
32. Menegaux A, Meng C, Bäuml JG, Berndt MT, Hedderich DM, Schmitz-Koep B, Schneider S, Nuttall R, Zimmermann J, Daamen M, Zimmer C, Boecker H, Bartmann P, Wolke D, Sorg C. Aberrant cortico-thalamic structural connectivity in premature-born adults. Cortex; a journal devoted to the study of the nervous system and behavior. Aug 2021;141:347-362. doi:10.1016/j.cortex.2021.04.009
33. Bisecco A, Capuano R, Caiazzo G, d'Ambrosio A, Docimo R, Cirillo M, Russo A, Altieri M, Bonavita S, Rocca MA, Filippi M, Tedeschi G, Gallo A. Regional changes in thalamic shape and volume are related to cognitive performance in multiple sclerosis. Multiple sclerosis (Houndmills, Basingstoke, England). Jan 2021;27(1):134-138. doi:10.1177/1352458519892552
34. Duering M, Gonik M, Malik R, Zieren N, Reyes S, Jouvent E, Hervé D, Gschwendtner A, Opherk C, Chabriat H, Dichgans M. Identification of a strategic brain network underlying processing speed deficits in vascular cognitive impairment. Neuroimage. Feb 1 2013;66:177-83. doi:10.1016/j.neuroimage.2012.10.084
35. Biesbroek JM, Weaver NA, Hilal S, Kuijf HJ, Ikram MK, Xu X, Tan BY, Venketasubramanian N, Postma A, Biessels GJ, Chen CP. Impact of Strategically Located White Matter Hyperintensities on Cognition in Memory Clinic Patients with Small Vessel Disease. PLoS One. 2016;11(11):e0166261. doi:10.1371/journal.pone.0166261
36. Winocur G, Oxbury S, Roberts R, Agnetti V, Davis C. Amnesia in a patient with bilateral lesions to the thalamus. Neuropsychologia. 1984;22(2):123-43. doi:10.1016/0028-3932(84)90056-3
37. Swartz RH, Stuss DT, Gao F, Black SE. Independent cognitive effects of atrophy and diffuse subcortical and thalamico-cortical cerebrovascular disease in dementia. Stroke. Mar 2008;39(3):822-30. doi:10.1161/strokeaha.107.491936
38. Amin M, Ontaneda D. Thalamic Injury and Cognition in Multiple Sclerosis. Frontiers in neurology. 2020;11:623914. doi:10.3389/fneur.2020.623914
39. Fuster J. The prefrontal cortex. Academic press; 2015.
40. Metoki A, Brookes RL, Zeestraten E, Lawrence AJ, Morris RG, Barrick TR, Markus HS, Charlton RA. Mnemonic function in small vessel disease and associations with white matter tract microstructure. Neuropsychologia. Sep 2017;104:1-7. doi:10.1016/j.neuropsychologia.2017.07.027

Chapter 3.

Meso-cortical pathway damage in cognition, apathy and gait in cerebral small vessel disease

Published as:
Hao Li, Mina A Jacob, Mengfei Cai, Roy PC Kessels, David G Norris, Marco Duering, Frank-Erik de Leeuw, Anil M Tuladhar. Meso-cortical pathway damage in cognition, apathy and gait in cerebral small vessel disease. Brain, awa145, 2024.

Abstract

Cerebral small vessel disease (SVD) is known to contribute to cognitive impairment, apathy, and gait dysfunction. Although associations between cognitive impairment and either apathy or gait dysfunction have been shown in SVD, the inter-relations among these three clinical features and their potential common neural basis remains unexplored. The dopaminergic meso-cortical and meso-limbic pathways have been known as the important brain circuits for both cognitive control, emotion regulation and motor function. Here, we investigated the potential inter-relations between cognitive impairment, apathy, and gait dysfunction, with a specific focus on determining whether these clinical features are associated with damage to the meso-cortical and meso-limbic pathways in SVD.

In this cross-sectional study, we included 213 participants with SVD in whom MRI scans and comprehensive neurobehavioral assessments were administered. These assessments comprised of six clinical measures: processing speed, executive function, memory, apathy (based on the Apathy Evaluation Scale), and gait function (based on the time and steps in Timed Up and Go test). We reconstructed five tracts connecting ventral tegmental area (VTA) and the dorsolateral prefrontal cortex (dlPFC), ventral lateral PFC (vlPFC), medial orbitofrontal cortex (mOFC), anterior cingulate cortex (ACC) and nucleus accumbens (NAc) within meso-cortical and meso-limbic pathways using diffusion weighted imaging. The damage along the five tracts was quantified using the free water (FW) and FW-corrected mean diffusivity (MD-t) indices. Furthermore, we explored the inter-correlations among the six clinical measures and identified their common components using principal component analysis (PCA).

Linear regression analyses showed that higher FW values of tracts within meso-cortical pathways were related to these clinical measures in cognition, apathy, and gait (all P-corrected values < 0.05). PCA showed strong inter-associations among these clinical measures and identified a common component wherein all six clinical measures loaded on. Higher FW values of tracts within meso-cortical pathways were related to the PCA-derived common component (all P-corrected values < 0.05). Moreover, FW values of VTA-ACC tract showed the strongest contribution to the PCA-derived common component over all other neuroimaging features.

In conclusion, our study showed that the three clinical features (cognitive impairment, apathy, and gait dysfunction) of SVD are strongly inter-related and that the damage in meso-cortical pathway could be the common neural basis

underlying the three features in SVD. These findings advance our understanding of the mechanisms behind these clinical features of SVD and have the potential to inform novel management and intervention strategies for SVD.

Introduction

Cerebral small vessel disease (SVD) is a complex brain disease that encompasses a diverse range of pathological changes of small vessels in the brain.[1,2] These changes manifest as various abnormalities on MRI, including white matter hyperintensities (WMH), lacunes, and cerebral microbleeds (CMBs).[1] The primary neurobehavioral symptoms associated with SVD are cognitive impairment, apathy, and gait dysfunction.[2-4] However, these symptoms are often studied in isolation, without considering their interrelations. A recent study in older adults tentatively identified a vascular triad that includes apathy, executive dysfunction, and gait disorder, highlighting the inter-connected nature of these conditions.[5] In SVD, the association between cognitive impairment and apathy has been established.[6-8] Furthermore, gait dysfunction was related with cognitive impairment in individuals with SVD, as well as with apathy in those suffering from subcortical vascular dementia.[9-11] These findings indicated that the three neurobehavioral symptoms in SVD may share some common components, potentially arising from a single neurological basis. Identification of the common component and the shared neural basis of cognitive impairment, apathy, and gait dysfunction may contribute to novel approaches for intervention and treatment in SVD. However, the inter-associations among the three symptoms and their potentially shared neural basis remains largely unknown in SVD.

The meso-cortical and meso-limbic pathways, wherein dopaminergic neurons from the ventral tegmental area (VTA) project to the prefrontal cortex (PFC), anterior cingulate cortex (ACC) and nucleus accumbens (NAc) respectively,[12] have been regarded as the important brain circuits for cognitive control, emotion regulation, as well as motor function.[13] Multiple studies have reported that apathy might be associated with structural disconnections within the cerebral dopaminergic reward network in SVD.[14-16] In addition, our previous study found an association between striatal atrophy and apathy, which was also independently associated with cognitive impairment in SVD.[6] Moreover, another study on cerebral autosomal dominant arteriopathy with subcortical infarcts and leukoencephalopathy (CADASIL), a rare monogenetic form of SVD, further demonstrated that dysfunctional effort-based decision-making might be a cognitive basis for apathy and that the reduced white matter integrity of orbitofrontal-anterior cingulate white matter was associated with both apathy and this specific cognitive dysfunction.[17] Regarding gait performance, as far as we are aware, no studies have specifically explored its association with dopaminergic pathway damage in SVD. However, evidence from Parkinson's disease (PD) has demonstrated that abnormalities in the meso-cortical and meso-limbic pathways, in addition to the nigrostriatal pathway, were related to gait

dysfunction.[18-20] Additionally, the dopaminergic white matter (WM) pathways, with long-range fiber connections, may be vulnerable to SVD-related pathology.[21,22] Hence, it can be hypothesized that the disruption of meso-cortical and meso-limbic WM pathways may contribute to cognitive impairment, apathy, and gait dysfunction. However, to the best of our knowledge, no study has specifically assessed the disruption of the meso-cortical and meso-limbic WM pathways and their relations to composite performances in cognitive function, apathy, and gait in SVD.

The goal of this study was 1) to *in-vivo* reconstruct the meso-cortical and meso-limbic WM pathways and assess the damage in these pathways in patients with sporadic SVD, using advanced neuroimaging approaches; 2) to determine the inter-relations between the three clinical features (i.e., cognitive impairment, apathy, and gait dysfunction); and 3) to relate the extent of damages of the meso-cortical and meso-limbic WM pathways to these clinical features in SVD. We hypothesized that cognitive impairment, apathy, and gait dysfunction are inter-related and that their dysfunction might be due to disruption in the meso-cortical and meso-limbic WM pathways.

Materials and methods

Study population

Data were derived from the Radboud University Nijmegen Diffusion tensor and Magnetic resonance imaging Cohort (RUN DMC) study, an ongoing cohort study investigating the causes and clinical consequences of sporadic SVD. Detailed information has been described previously.[23] In brief, participants meeting the following criteria were included: 1) age between 50 and 85 years; 2) presence of SVD MRI markers (identified as WMH or lacunes); 3) cognitive or motor symptoms that could be attributed to SVD. After the baseline data collection in 2006, participants underwent three follow-up assessments in 2011, 2015, and 2020 respectively. However, due to the change of MRI-scanners, we only used the data from the third follow-up assessment in 2020 (Figure e-1). Additionally, all participants underwent a thorough and detailed clinical work-up, during which extensive standardized motor and neuropsychological screening tests were performed to identify participants with concomitant dementia or Parkinsonism. A detailed description of the diagnostic work-up has been provided previously.[24,25] Participants diagnosed with non-vascular dementia or Parkinson's disease were excluded (n=14) from the present study, resulting in a final sample of 213 participants (Figure e-1).

Neuropsychological and gait assessment

Three cognitive domains (processing speed, executive function, and memory) were assessed using a standardized cognitive assessment battery, including the Trail Making Test, Symbol-Digit Modalities Test, Verbal Fluency Test, Digit Span Test, Rey Auditory Verbal Learning Test, and Rey-Osterrieth Complex Figure Test. The raw scores from each cognitive test were standardized to z-scores, which were subsequently used to compute a compound score for each cognitive domain (Table e-1).

Apathy was measured by the clinician-rated version of the Apathy Evaluation Scale (AES-C),[26] an instrument validated across various neurological conditions, including SVD.[15] The AES-C encompasses 18 items, each scored from 1 to 4 points. Higher scores indicate more severe apathy. We consider participants with an AES score ≥ 34 as apathy.[15] Depression was measured using the modified 18-item Centre for Epidemiologic Studies Depression Scale (CESD), excluding two items related to motivation to ensure a more pure measure of depressive symptoms (termed as modified CSED score), as described in the previous study.[7] The internal consistency (α=0.87) of the modified 18-item CESD is comparable with the original 20-item CESD (α=0.88).[7] The inclusion of depression assessment was justified by its significant overlap with apathy symptoms and its potential impact on cognitive functions and gait performance.[27,28] Due to the lack of a validated cut-off score specifically for modified 18-item CESD, we considered participants with an original 20-item CESD ≥ 16 as depression.[15]

Gait performance was assessed by employing the Timed Up and Go (TUG) test,[29] whereby both the mean time (in seconds) and the number of steps derived from three repetitive TUG tests were used in the analyses.[9]

MRI acquisition

All participants underwent scanning on a 3T MRI scanner (MAGNETOM Prisma; Siemens Healthineers, Erlangen, Germany) with a 32-channel head coil. The following sequences were collected: Magnetization Prepared 2 Rapid Acquisition Gradient Echoes (MP2RAGE) sequence with sparse sampling for creating T1-weighted (T1W) image, a 3D fluid-attenuated inversion recovery (FLAIR) sequence, a 3D multi-echo gradient echo (GRE) sequence for susceptibility weighted image (SWI), and multi-shell multi-directional diffusion-weighted imaging (DWI). Full acquisition details were provided in the supplementary materials and have been previously described.[30]

SVD MRI markers

MRI markers of SVD (i.e., WMH, lacunes, CMBs) and brain atrophy were assessed according to version 2 of the Standards for Reporting Vascular Changes on

Neuroimaging criteria (STRIVE-2).[1] WMH was semi-automatically segmented based on FLAIR and T1 images using a validated 3D U-net deep learning algorithm.[31] All segmented WMH masks were visually inspected and manually corrected when necessary. The lacunes were identified on T1 and FLAIR images, while the CMBs were identified on SWI images; both were manually counted by two well-trained raters who were blind to the clinical data, with subsequent consensus meetings. Grey matter (GM), WM, and cerebrospinal fluid (CSF) were segmented on T1 images using SPM12 software. To avoid misclassification of WMH as GM, these segmented images of GM, WM, and CSF were corrected using the WMH mask. Brain volumes were determined by the ratio between the sum of GM and WM volumes and the sum of GM, WM and CSF volumes [i.e. intracranial volumes (ICV)] and served as a proxy of brain atrophy. WMH volumes were normalized to the ICV.

Diffusion MRI processing and free water mapping

Diffusion MRI data were pre-processed for denoising and removal of Gibbs artifacts, correction of head motion, eddy currents-induced distortion, susceptibility-induced distortion (top-up), and intensity bias.[32-36] Next, multi-fibre directions within each voxel of the brain were estimated based on the multi-shell ball-and-two-sticks model.[37] Subsequently, with the processed images (only b=0 and b=1000 s/mm^2), fractional anisotropy (FA) and mean diffusivity (MD) images for each participant were obtained by using the 'dtifit' function within FSL. Additionally, free water (FW) and FW-corrected MD (MD-t) were acquired using a nonlinear regularised minimization process implemented in Matlab.[38] The FW image model is a two-compartment model that enhances traditional diffusion tensor imaging (DTI) models by modelling both a FW component and a FW-corrected tissue compartment (Figure e-2). The FW component signifies the unrestricted and undirected extracellular water fraction and was associated with multiple pathological processes, including the disruption of blood-brain barrier, neuroinflammation, and vasogenic oedema in SVD.[39] The tissue compartment is estimated from the remaining signal after removing FW contribution, thus allowing for a more precise assessment of white matter fibre organization.

Regions of interest and probabilistic tractography

Probabilistic tractography was performed to capture two WM pathways originating from VTA, with one projecting to PFC and ACC (meso-cortical pathway) and the other projecting to NAc (meso-limbic pathway).[40,41] Additionally, the nigrostriatal WM pathway originating from the substantia nigra (SN) and projecting to the striatum was identified.[42] Note that our analyses focused on the meso-cortical and meso-limbic pathways, with the nigrostriatal WM pathway serving as a control in the sensitivity analyses.

First, a list of regions of interest (ROI) masks was extracted. VTA and SN were identified based on a previously validated human sub-cortical atlas.[43] NAc, putamen and globus pallidus were extracted from the structural segmentation of each participant's T1w image using 'samseg' function within Freesurfer (version 7.3.2).[44] In addition, considering the substantial size of the prefrontal cortex, this region was subdivided into three discrete regions: dorsolateral prefrontal cortex (dlPFC), ventral lateral PFC (vlPFC), and medial orbitofrontal cortex (mOFC), to enhance the accuracy and specificity of tractography. Three subregions of PFC and ACC were defined based on previous studies using Anatomical Automatic Labelling (AAL) atlas:[45] dlPFC (3,4, 7,8), mOFC (27, 28, 5, 6, 25, 26), vlPFC (9, 10, 15, 16), and ACC (35, 36).[46,47] These numbers correspond to the brain parcellation in the AAL atlas. Next, a cortex mask for each participant was obtained from 'Sequence Adaptive Multimodal SEGmentation (SAMSEG)'-based structural segmentation.[44] Only the cortical part of each participant's AAL-derived dlPFC, mOFC, vlPFC, and ACC regions were retained through the cortical mask and then employed as the ROIs in subsequent analyses. According to previous studies, prior anatomical knowledge and visual inspection, multiple tailored ROIs were extracted as the exclusion masks for the WM pathway reconstruction based on the AAL atlas, [45] Johns Hopkins University WM atlas,[48] Harvard-Oxford cortical atlas and structural segmentation of T1w image (Table e-2),[49].[40] Subsequently, these ROIs in their corresponding native spaces were registered to diffusion space using the non-linear SyN registration algorithm in Advanced Normalization Tools (ANTs, http://stnava.github.io/ANTs/).[50] All segmented and transformed ROIs were visually inspected.

Afterwards, probabilistic tractography was performed by repeating 5000 random samples from each voxel within the seed ROI, generating streamlines using 'probtractx2' function from FSL.[51] For the meso-cortical pathway, VTA was employed as the seed mask, each of the three PFC subregions and the ACC were respectively employed as target mask, resulting in four different bundles of meso-cortical pathway: VTA-dlPFC, VTA-mOFC, VTA- vlPFC and VTA-ACC.[40] For the meso-limbic pathway, the NAc was selected as the seeded mask, while the VTA was set as the target masks, aligning with a previous study.[41] Regarding the nigrostriatal WM pathway, the SN was employed as the seeded mask, with the combination mask of putamen and globus pallidus designated as the target mask, consistent with a prior study.[42]

Common pathway and features extraction

To minimize the effects of individual anatomical variations, we formulated a common representative template for each tract, following similar methodology in previous studies.[52,53] Briefly, an unbiased template was created based on FA images from all

participants using the ANTs (http://stnava.github.io/ANTs/). Next, the individually tracked pathway was brought to this unbiased group template space using SyN registration algorithm within ANTs.[50] Subsequently, the binary masks of common representative tracts were created by considering all individually warped tracts and retaining only the voxels present in a minimum of 60% of all participants.[52] The selection of a 60% group threshold was guided by visual inspection, ensuring both the extent and specificity of the resultant group common pathways. Afterwards, six group-template tracts (i.e., VTA-dlPFC, VTA-mOFC, VTA-vlPFC, VTA-ACC, VTA-NAc and SN-putamen) were transformed back to each participant's diffusion space. An ROI of the residual WM, designated as the WM reference region, was created by excluding the six group common tracts from the total WM mask in individual's diffusion space. Finally, the mean values of MD-t and FW of six tracts were calculated. Additionally, we extracted the mean values of MD-t and FW of the residual WM mask as a reference. We prioritized the MD-t and FW indices over other diffusion indices since the MD index is less affected by crossing fibres, and FW determines diffusion alterations in SVD, as reported in previous studies.[39,54]

Statistical analysis

Continuous variables were presented by either mean (standard deviation, SD) or median (interquartile ranges, IQRs), based on their distribution.

To examine the effects of SVD burden on the disruption of five specified tracts (i.e., VTA-dlPFC, VTA-mOFC, VTA-vlPFC, VTA-ACC and VTA-NAc) within meso-cortical and meso-limbic pathways, the inter-correlations between mean MD-t or FW values of these tracts and WM reference regions, and SVD MRI markers, in addition to normalized brain volumes, were assessed across the total sample using Kendall rank correlation coefficient.

To test the associations between the disruption of five specified tracts and the three clinical features (i.e., cognitive function, apathy, and gait performance), we performed linear regression analyses. Six clinical measures (processing speed, executive function, memory, apathy, TUG time and TUG steps) for three features were used as dependent variables in separate models, with mean MD-t or FW values across the five tracts serving as independent variables. Adjustments were made for age, sex, education, modified CESD score, the corresponding diffusion index from the WM reference mask, SVD MRI markers and normalized brain volumes. The diffusion index of WM reference mask was included as a control representing the global white matter damages, which is essential to test the specificity of any effects for the meso-cortical and meso-limbic pathways.[52]

To determine the potential common factors underlying cognitive function, apathy, and gait performance, we performed principal component analysis (PCA) on all clinical measures using 'psych' package in R.[55,56] First, Pearson's correlation analyses were performed among all pairs of the six clinical measures to explore their potential inter-correlations. Next, PCA was applied to the six clinical measures without rotation. The Kaiser–Meyer–Olkin (KMO) test examined the sampling adequacy, and Bartlett's test of sphericity assessed whether the correlations among the six measures were sufficiently large in the PCA.[57] A KMO values greater than 0.6 indicate the sampling is adequate for PCA.[57] Kaiser's criterion (greater than one) was used to define the number of components that were retained in the subsequent analysis.[58] The clinical measures with a factor loading ≥0.30 on a given component were considered as relevant.[59] Finally, each participant's factor values of preserved PCA components were computed and used as dependent variables in the linear regression model. The independent variables and adjustments were the same as in the above linear regression models.

To identify the relative importance of meso-cortical and meso-limbic tracts, SVD burden and brain atrophy on clinical outcomes, we included mean MD-t and FW of the five tracts into separate random forest analysis models. SVD MRI markers, normalized brain volumes, the corresponding diffusion measure from WM reference mask were also included as predictors in these random forest models. The preserved PCA components and six clinical outcome measures were respectively assigned as outcome variables in these models. Subsequently, relative importance of each predictor was assessed using the percentage increase in mean squared error (%IncMSE) index through 'randomForest' package in R,[60,61] as described in previous studies.[52] This %IncMSE index was determined through a perturbation approach, where the predictors' values are permuted to assess their impact on model accuracy.[61] The selection of random forest approach over other regression models was justified by its ability to handle multicollinearity and complex non-linear relations within these models.[60]

For the linear regression models, multicollinearity was assessed using variance inflation factors (VIFs) and the correlation matrix of independent variables, with a VIF value ≥5 or a correlation coefficient between any pair of independent variables ≥ 0.7 indicating strong multicollinearity.[62] When non-normally distributed data were used as response variables, the Yeo-Johnson approach was employed to approximate a normal distribution in R.[63]

All statistical analyses were performed using R software (version 4.1.1) and alpha was set at 0.05 (two-tailed). The Bonferroni method was employed to correct for multiple comparisons.

Sensitivity analyses

First, to confirm the specificity of these associations between tracts within meso-cortical and meso-limbic pathways and the three clinical features, additional analyses were conducted. We assessed the associations between the diffusion features values of SN-putamen tract within nigrostriatal pathway and the six clinical measures, as well as the association with the diffusion features values of SN-putamen tract and the PCA-derived common component (i.e., PC1). The SN-putamen tract was selected as a control due to its primary association with motor function, as opposed to cognitive or mood function, and its anatomical proximity to the caudal part of meso-cortical pathways.

Furthermore, given the established effects of frontal WM on cognitive function, apathy, and gait performance,[15,64,65] we employed another more specific frontal WM reference mask as the reference region. This frontal WM reference region was obtained by segregating the frontal area (derived from AAL atlas) from the whole white matter mask after omitting the five meso-cortical and meso-limbic tracts. Next, we calculated the mean MD-t and FW values within this delineated region. Subsequently, we re-assessed the associations between diffusion measures of the five tracts within meso-cortical and meso-limbic pathways and the six clinical measures, as well as PC1 (i.e. the PCA-derived first principal component), while adjusting for the corresponding diffusion measures of the frontal white matter reference region, along with other covariates in the primary analysis.

Second, to ensure comprehensive exploration beyond PC1 and reduce the risk of overlooking potentially interesting components in our PCA methodology, we employed an alternative principal component selection approach. That is, selecting the number of components that generate a cumulative sum of explained variance over 80%.[66] We further assessed the associations between the preserved PCA components and the diffusion measures of five specified tracts within meso-cortical and meso-limbic pathways.

Data availability

The data that support the findings of this study are available from the corresponding author, depending on reasonable request from qualified investigators after permission of the appropriate regulatory bodies.

Results

A total of 213 participants were included in the present study, with a median age of 73.0 years (IQR, 69.0–79.0); 96 were women (45.1%). Detailed information on demographic data, cognitive function and neuroimaging characteristics was provided in Table 1 and Table e-3. The five common representative tracts of meso-cortical and meso-limbic white matter pathways, along with their mean MD-t and FW values, were shown in Figure 1 and Table e-4.

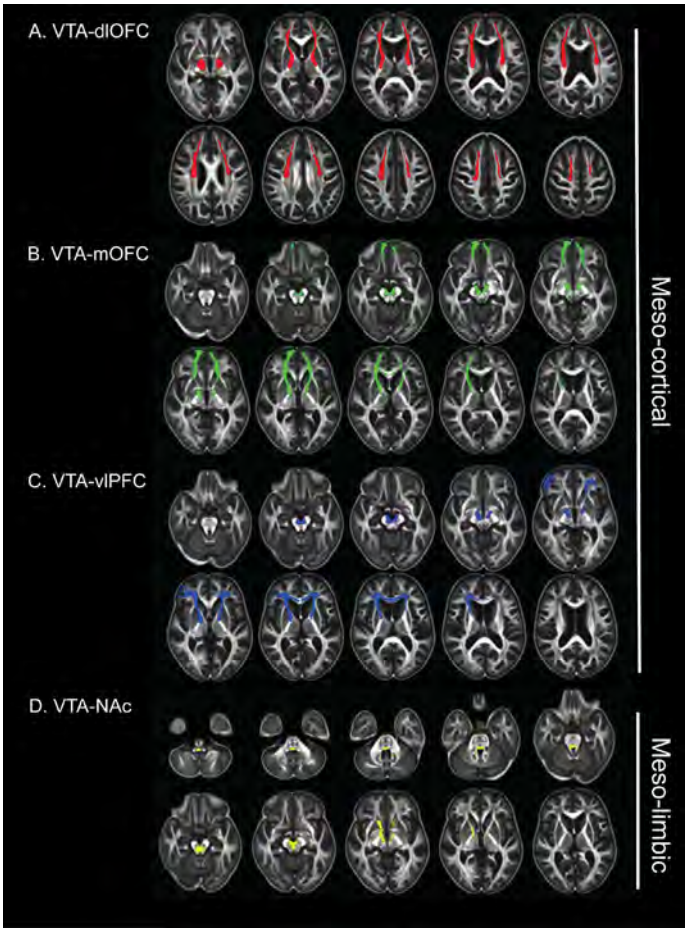

Figure 1. Meso-cortical and meso-limbic white matter pathways. Red for VTA-dlPFC tract (first row); Green for VTA-mOFC tract (second row); Dark blue for VTA-vlPFC tract (third row); Light blue for VTA-ACC tract (fourth row); Yellow for VTA-NAc tract (fifth row). Meso-cortical pathways included the VTA-dlPFC, VTA-mOFC, VTA-vlPFC and VTA-ACC tracts; meso-limbic pathway referred to the VTA-NAc tract. VTA: ventral tegmental area, dlPFC: dorsolateral prefrontal cortex, vlPFC: ventral lateral prefrontal cortex, mOFC: medial orbitofrontal cortex, ACC: anterior cingulate cortex

SVD burden and meso-cortical and meso-limbic pathways

In the correlation analysis, SVD MRI markers (i.e., WMH volumes, the presence of lacunes and CMBs) and normalized brain volumes showed significant correlations with FW values across five specific tracts within the meso-cortical and meso-limbic pathways (i.e., VTA-dlPFC, VTA-mOFC, VTA-vlPFC, VTA-ACC, VTA-NAc tracts), and the WM reference regions. The only exception was the lack of correlation between the presence of CMBs and FW values of VTA-dlPFC tract. In contrast, the correlations between SVD burden and MD-t values of these tracts and WM reference regions were markedly weaker (Figure 2).

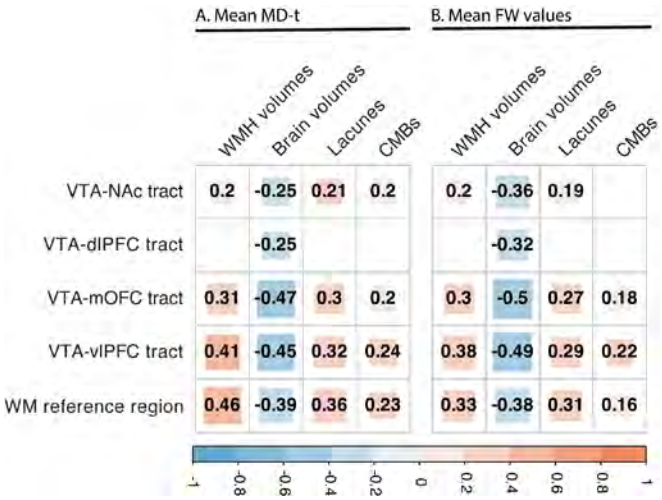

Figure 2. Inter-correlation analyses among mean MD-t and FW values of five tracts of interest and WM reference regions, SVD MRI markers and brain atrophy. A. Correlation coefficients of MD-t values. B. Correlation coefficients of FW values; MD-t, FW-corrected MD values, FW, free water, WMH, white matter hyperintensities, CMBs, cerebral microbleeds; WMH and brain volumes were normalized to intracranial volumes; all numbers within squares represent correlation coefficients (P-corrected <0.05), blank means no statistically significant results (P-corrected >0.05).

Relation between disruption of meso-cortical, meso-limbic pathways and clinical outcomes

MD-t values of these tracts showed no associations with clinical measures. By contrast, higher FW values of the VTA-dlPFC tract were related to worse memory performance, higher AES scores and higher step number of TUG test; higher FW values of the VTA-mOFC tract were related to worse executive function; higher FW values of the VTA-vlPFC and VTA-ACC tract were both related to slower processing speed, worse executive function and worse memory performance; higher FW values of the VTA-ACC tract were additionally related to higher AES scores (all P-corrected values < 0.05, Table 2).

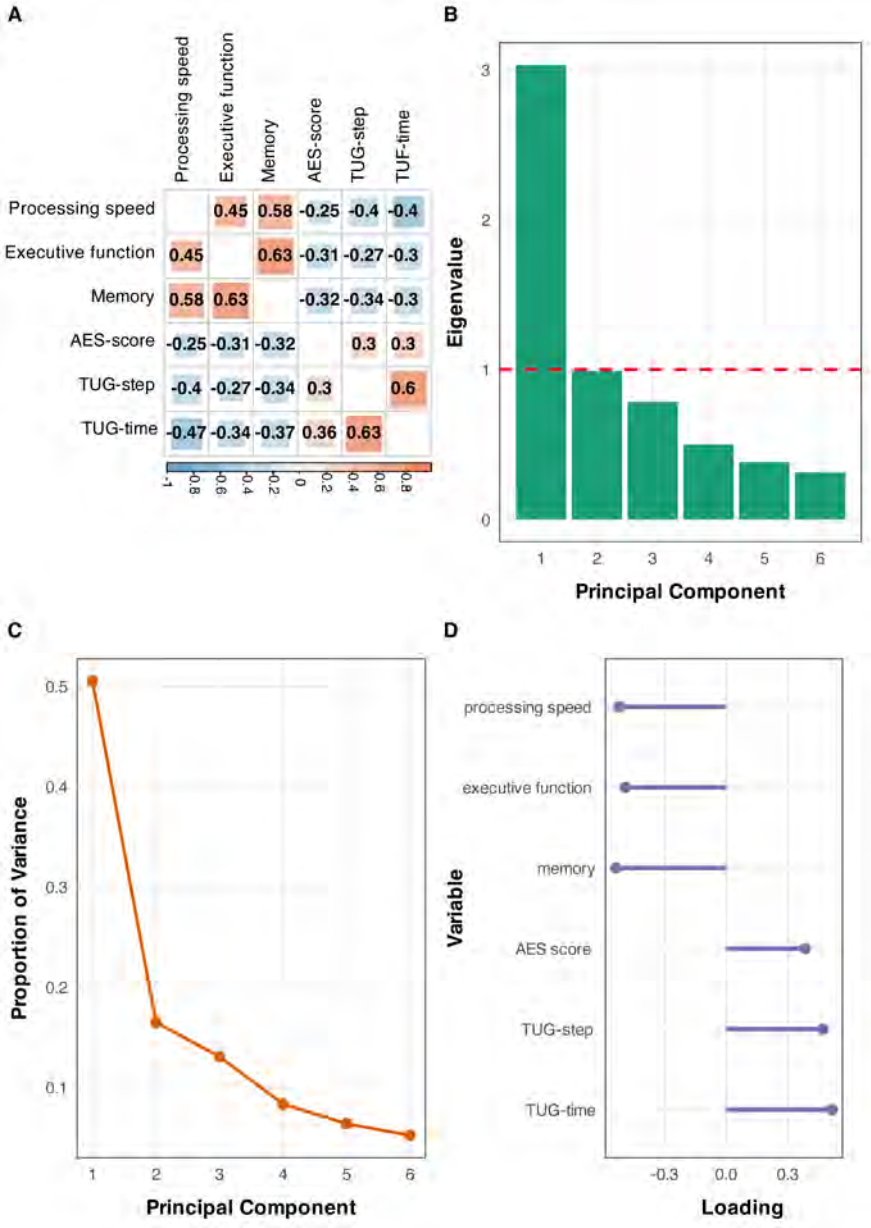

Figure 3. Principal components analysis (PCA) in the six clinical measures of cognition, apathy, and gait. A. Inter-correlation analyses among six clinical measures. Number within square represent correlation coefficients with a P-corrected value <0.05). P values were corrected using Bonferroni method. B. Eigenvalue of each PCA-derived principal component. The principal component with an eigenvalue value greater than 1 (red line) was preserved. C. The proportion of variance explained by any given principal component. D. The factor loading of each original clinical measures to the preserved principal component (i.e., the first principal component [PC1]).

Common factors underlying cognition, apathy, and gait

Pearson's correlation analyses showed significant associations between each pair among the six clinical outcome measures (all P-corrected values < 0.05, Figure 3A). This result suggests the existence of shared factors underlying the three clinical features (i.e., cognition, apathy, and gait), thus justifying subsequent PCA to identify the common components.

The Kaiser–Meyer–Olkin test showed a value of 0.772 and Bartlett's test of sphericity was significant (P<0.001). This result confirmed the appropriateness of conducting a factor analysis. Therefore, PCA was performed and identified a total of six components in the data. The first component (PC1) had eigenvalues above Kaiser's criterion of 1 and explained 50.52% of the total variance (Figure 3B and 3C). All six clinical outcome measures showed meaningful loadings on the first component (all factor loadings > 0.3; Figure 3.D). The direction of associations between each clinical outcome measure and PC1 provided excellent clinical interpretability, that is, higher PC1 values suggesting worse performances in the common factors of cognition, apathy, and gait.

Linear regression analyses showed that higher FW values of VTA-dlPFC, VTA-mOFC, VTA-vlPFC and VTA-ACC tracts were related to higher PC1 values (all P-corrected values <0.05, Table 3).

Relative importance of each neuroimaging markers on clinical outcomes

In the analyses for PC1, FW values of VTA-ACC tract showed the highest contribution compared to all other imaging features, including the FW values of VTA-dlPFC, VTA-mOFC, VTA-vlPFC, VTA-NAc tracts and WM reference regions, SVD MRI markers and normalized brain volumes (Figure 4). Similar findings were found for each clinical measurement (i.e., processing speed, executive function, memory, AES-score, TUG-step, TUG-time. Figure e-4 and e-5).

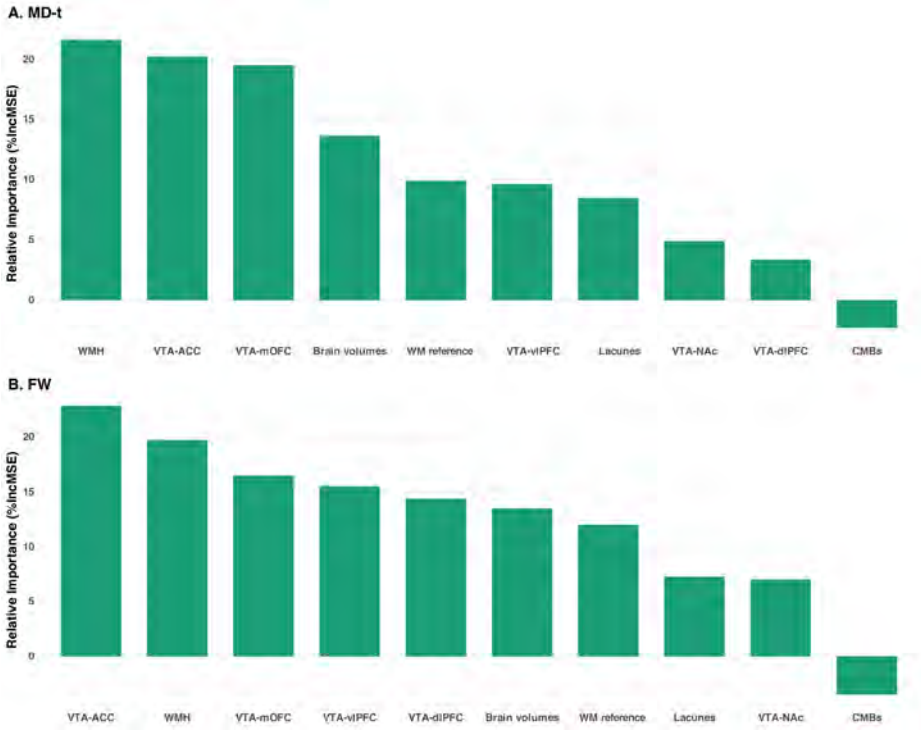

Figure 4. Relative importance of imaging markers on PC1. A. MD-t values of VTA-ACC showed a high contribution to PC1; B. FW values of VTA-ACC contributed most to PC1 among all imaging markers. PC1: first principal component, VTA: ventral tegmental area, dlPFC: dorsolateral prefrontal cortex, vlPFC: ventral lateral prefrontal cortex, mOFC: medial orbitofrontal cortex, ACC, anterior cingulate cortex, NAc: nucleus accumbens, FW: free water, MD-t: FW corrected MD values, WMH: white matter hyperintensities, CMBs: cerebral microbleeds; %IncMSE, the percentage increase in mean squared error, it is calculated through a perturbation approach, where the predictors' values are permuted to assess its impact on model accuracy.

Sensitivity analyses

In the analyses for nigrostriatal pathway, only an association between increased FW in the SN-putamen tract and worse executive function (β=0.26, P-corrected = 0.023) was found (Table e-5).

Associations between the diffusion features of the five tracts within the meso-cortical and meso-limbic pathways and the six clinical measures, alongside PC1, were consistent with our initial findings while adjusting for the corresponding diffusion measures of the frontal white matter reference region (Table e-6). Notably, the FW values of the VTA-ACC tract consistently showed the greatest contribution to PC1 across all examined imaging features (Figure e-6).

Using a different approach for component selection, the combination of first three components (PC1, PC2 and PC3) explained 80.06% of the total variance (Table e-7). PC2 was mainly loaded by executive function, memory, TUG step, and TUG time; PC3 was mainly loaded by processing speed and AES score (Table e-7). Furthermore, we found no significant associations between PC2 or PC3 and the diffusion measures of the five specific tracts within the meso-cortical and meso-limbic pathways (Table e-8).

Discussion

In the present study, we found that: 1) higher MD-t and FW values of the meso-cortical and meso-limbic WM pathways were correlated with higher SVD burden, with FW showing notably stronger correlations; 2) higher FW values of four tracts within meso-cortical pathway showed associations with clinical measures both in cognitive function, apathy, and gait, whereas MD-t values of these tracts were not associated with these clinical measures; 3) the six clinical measures (encompassing cognitive function, apathy, and gait function) were strongly related to each other and collectively informed a PCA-derived common and meaningful component, which is hereafter termed as composite performances in cognition, apathy and gait; 4) the FW values of four tracts within meso-cortical pathway demonstrated significant associations with the composite performances in cognition, apathy and gait, with FW values of VTA-ACC tract identified as the strongest contributor. Taken together, our results suggested that cognitive impairment, apathy, and gait dysfunction shared some common pathophysiological substrates and that the white matter damage of the meso-cortical pathway in SVD, potentially serves as their common neural basis.

We found varied correlations between SVD MRI markers and the diffusion measures across meso-cortical and meso-limbic pathways, as well as the WM reference regions. Notably, the FW index showed remarkable stronger correlations compared to the MD-t index. Furthermore, the FW values of these tracts were related to clinical measures, whereas the MD-t index showed no such relations. This result is not surprising since the previous study has reported that SVD-related DTI changes (i.e., decrease in FA and increase in MD) were predominantly attributed to the increased FW, rather than the tissue compartment changes (i.e. FA-t and MD-t).[39] In addition, they also reported that FW showed stronger associations with clinical deficits than MD-t.[39] These findings suggested that FW measures have the potential to serve as a better marker for assessing the progression in SVD burden and clinical deficits than conventional diffusional measures.

We found significant associations between FW values of meso-cortical pathway and the clinical measures in both cognition, apathy, and gait. This finding suggested that damage to the meso-cortical pathways may serve as the common neural foundation for cognitive impairment, apathy, and gait dysfunction in SVD. So far, to the best of our knowledge, no study has investigated the role of dopaminergic meso-cortical or meso-limbic pathways in SVD. Despite the lack of pre-existing evidence in SVD, studies in other brain disorders, notably Alzheimer's disease (AD) and PD, have shown that crucial regions within the meso-cortical and meso-limbic pathways (mainly VTA, NAc, and PFC) undergo a range of alterations. These alterations include volume loss, altered inter-connectivity both functionally and structurally, changes in dopaminergic function of presynaptic terminals, and post-synaptic dopamine receptor levels.[67,68] Such abnormalities have been associated, to varying degrees, with cognitive function, neuropsychiatric symptoms, and motor symptoms in AD and PD.[67,68]

Interestingly, our findings suggested that apathy was associated with deficits in the meso-cortical pathway, as opposed to the mesolimbic pathway that traditionally linked with reward and emotion regulation. A previous study demonstrated that apathy in SVD was associated with deficits in effort-based decision making,[69] a process that is regarded as determined by the meso-cortical pathway.[70] These findings indicated that apathy in SVD is more aligned with cognitive deficits than solely with emotional regulation dysfunction. In addition, we found that higher FW values of SN-putamen tract were related to executive function, but not to memory performance and PC1. This could be explained by the effects of motor impairment on the executive function task.

Another crucial finding in this study is the PCA-derived common component (PC1) underlying cognitive impairment, apathy, and gait dysfunction in SVD. Note that the direction of associations between each clinical measure and PC1 provided excellent clinical interpretability. By contrast, the second and third principal components derived from PCA (PC2 and PC3) presented ambiguous associations with the clinical outcome measures. Although further validation is required in another independent dataset, our findings suggested that PC1 successfully captured the predominant common components underlying cognitive impairment, apathy, and gait dysfunction in this present SVD population. The presence of this PCA-derived common component, along with the high inter-correlations among these measures for the three clinical features, strongly suggest that the three clinical features of SVD were inter-related and shared some common mechanisms. This finding is in line with previous studies that showed that cognitive impairment is associated

with either apathy or gait dysfunction,[7,8,71] while also offering a deeper exploration on the inter-relations of the three clinical features in SVD. Furthermore, this PCA-derived common component represents the composite performances in cognition, apathy, and gait, and could potentially be employed as a comprehensive metric for clinical status assessment in SVD. However, further validations in independent cohorts are required.

Furthermore, we found that deficits in meso-cortical pathways were associated with composite impairments in cognition, apathy, and gait. Moreover, damage to VTA-ACC tract showed the highest contribution to the composite performance in cognitive impairment, apathy, and gait, exceeding the effects of other neuroimaging features. This result supported that the damage in meso-cortical pathways could be the shared underlying neural foundation for cognitive impairment, apathy, and gait dysfunction in SVD. In addition, this result remained consistent when we employed the frontal WM reference mask, instead of the whole WM reference mask, as the reference region. This finding reinforced the specificity of the effects of meso-cortical pathway deficits on clinical outcomes and our confidence in the interpretation of our results.

The strengths of this study lay in the comprehensive assessment of cognitive function, apathy, and gait performance in a substantial sample of SVD population (n=213), combined with state-of-the-art neuroimaging approaches that identify five tracts of the meso-cortical and meso-limbic pathways and quantify the damage along these tracts. With the detailed clinical data of cognitive function, apathy, and gait performances, we were able to capture the common component underlying the three clinical features of SVD through a bottom-up analysis approach (i.e., PCA).

Several limitations should be acknowledged. First, due to the change of MRI scanners, we could only use the data from the third follow-up of our cohort. While this provided access to the advanced and high-quality MRI scans, it limited us to performing only cross-sectional analyses. The temporal and causal relations between the observed meso-cortical and meso-limbic damages and clinical outcomes need further examination in longitudinal studies. Second, we lacked the age-matched healthy controls as a reference, making it difficult to distinguish our findings from the effects of normal ageing and the concurrent neurodegenerative pathologies. Although excluding participants diagnosed with non-vascular dementia and/or Parkinsonism has minimized the effects from concurrent neurodegenerative pathologies, studies including healthy controls are still essential to more accurately elucidate the effects of SVD burden on damages to meso-cortical and meso-limbic

pathways and subsequently on clinical outcomes. Third, the identification of these tracts within the meso-cortical and meso-limbic pathways was based solely on diffusion imaging. While the two pathways are predominantly innervated by dopaminergic neurons, other neurotransmitters, such as glutamatergic, are also involved. Hence, caution is required to interpret the identified meso-cortical and meso-limbic pathways in this study strictly as dopaminergic. Subsequent studies employing dopamine-specific PET imaging could facilitate identifying these dopaminergic-specific tracts within meso-cortical and meso-limbic system, thereby validating our findings. Fourth, given the strong correlations among the six clinical measures and the multicollinearity observed among certain tracts, it is possible that the observed associations between FW values of these tracts within the meso-cortical pathway and clinical measures are driven by statistical correlations rather than clinically meaningful relationships. Although our results are supported by not only statistical analyses but also neurobiological evidence from prior studies, further investigation into the temporal or causal associations between changes in specific tracts and clinical outcomes is necessary to validate our findings. Fifth, the specificity of the observed effects of the meso-cortical pathway was mainly examined by adjusting for diffusion index of (frontal) WM reference region. It is still possible that other tracts, such as the cholinergic pathways or thalamus-cortex projections, might also constitute a shared neural basis for the three clinical features of SVD. Notably, disruption in the cholinergic system has been associated with cognitive impairment, apathy, and gait dysfunction in PD.[72-74] Further research is needed to investigate the impact of cholinergic pathway disconnections on these symptoms in SVD. In addition, studies employing a non-hypothesis-driven approach, such as lesion-symptom mapping, could also provide further insights into this question.

Conclusion

In conclusion, these findings of our study suggested that the three neurobehavioral symptoms (cognitive impairment, apathy, and gait dysfunction) of SVD are strongly related to each other and that the damage in the meso-cortical pathway could be the common neural basis underlying these three clinical features. These findings advance our understanding of the mechanisms of the primary clinical features in SVD and have the potential to inform novel management and intervention strategies for SVD.

Supplementary material

Materials and methods

Neuropsychological assessment

Processing speed was assessed using the Trail Making Test A (TMT-A) and Symbol-Digit Modalities Test (SDMT); executive function was assessed using the TMT ratio score, the Verbal Fluency test (animal and profession naming); memory was assessed using the forward and backward scores of the Digit Span test, the immediate and delayed recall scores of the Rey Auditory Verbal Learning Test (RAVLT) and the delayed recall score of Rey-Osterrieth Complex Figure Test (RCFT). The raw test scores were standardized as z-scores. Next, compound scores were computed per cognitive domain: processing speed was calculated by the sum of (1) the inverse Z score of the TMT-A, (2) the Z score of SDMT; executive function was calculated by the sum of (1) the inverse Z score of the TMT ratio (TMT-B/TMT-A), (2) the average Z score of Verbal Fluency Test of animal naming and job naming; memory was calculated as the sum of (1) the Z score of DST, (2) the average Z score of RAVLT of immediate recall and delayed recall; (3) the average Z score of ROCF of immediate recall and delayed recall. (Table e-1).

MRI acquisition

Parameters for each sequence: 3D T1-weighted Magnetization Prepared 2 Rapid Acquisition Gradient Echoes (MP2RAGE): 0.85mm isotropic voxels, repetition time (TR) = 5500 ms, inversion time (TI1 and TI2) = 700 and 2500 ms, field of view (FOV) = 218×272mm^2, Flip Angle = 4; 3D multi-echo fast low-angle shot images (9 echoes): 0.85mm isotropic voxels, TR = 44ms, ΔTE = 4ms, FOV = 197×245mm^2, Flip angle = 20; 3D fluid-attenuated inversion recovery (FLAIR) image: 0.85mm isotropic voxels, TR = 5000ms, TE = 394 ms, TI = 1800ms, FOV = 163×272mm^2, Flip angle = 120; Multi-shell DWI using multi-band accelerated echo planar imaging (EPI): 99 diffusion-weighted directions (3 × b = 200, 6 × b = 500, 30 × b = 1,000, and 60 × b = 3,000s/mm2), 10 × b = 0 images, 1.7mm isotropic voxels, TR = 3220ms, TE = 74 ms, FOV = 221×221mm^2 , Flip angle = 90; one b=0 image with acquisition parameters equal to the previous b=0 images, but acquired in opposite phase-encoding direction.

Table e-1. Calculation of each cognitive domain

Cognitive domain	Cognitive test	Version	Calculation of compound score
Processing speed	Trail Making Test	Part A[75]	$Z_{TMT\text{-}A} \times -1 + Z_{SDMT}$
	Symbol-Digit Modalities Test	Written version[76]	
Executive function	Trail Making Test	Part B (B/A ratio)[77]	$Z_{(TMT\text{-}B/TMT\text{-}A)} \times -1 + (Z_{VFT\text{-}A} + Z_{VFT\text{-}J})/2$
	Verbal Fluency Test	Animal and profession naming[78]	
Memory	Digit Span test (Forward and backward)	Wechsler Adult Intelligence Scale – 3rd ed.[79]	$Z_{(DST\text{-}f + DST\text{-}b)} + (Z_{RAVLT\text{-}I} + Z_{RAVLT\text{-}D})/2 + (Z_{ROCF\text{-}I} + Z_{ROCF\text{-}D})/2$
	Rey's Auditory Verbal Learning Test (Immediate and delayed recall) [5]	3-trial version[80]	
	Complex Figure Test (Immediate and delayed recall) [6]	MCG Figure 3[81]	

Z, the Z transformed score; DST-f, Digit Span forward test; DST-b, Digit Span backward test; RAVLT-I, Immediate recall of Rey's Auditory Verbal Learning Test; RAVLT-D, the delayed recall of Rey's Auditory Verbal Learning Test; ROCF-I, Immediate recall of Rey–Osterrieth Complex Figure Test; ROCF-D, delayed recall of Rey–Osterrieth Complex Figure Test; TMT, Trail Making Test; SDMT, Symbol-Digit Modalities Test, VFT-A, Verbal Fluency Test (animals); VFT-A, Verbal Fluency Test (professions)

Table e-2. Tailored exclusion masks employed in probabilistic tractography for each tract.

Tracts of interest	Exclusion criteria	Mask resources
VTA-dlPFC	vlPFC, mOFC, ACC	AAL atlas
	corpus callosum,	JHU white matter tractography atlas
	temporal lobe, parietal lobe	Harvard-Oxford cortical atlas
	thalamus	'samseg' on T1 image
VTA-mOFC	dlPFC, vlPFC, ACC	AAL atlas
	temporal lobe, parietal lobe	Harvard-Oxford cortical atlas
	thalamus, NAc	'samseg' on T1 image
VTA-vlPFC	dlPFC, vlPFC	AAL atlas
	temporal lobe, parietal lobes	Harvard-Oxford cortical atlas
	thalamus, NAc	'samseg' on T1 image
VTA-ACC	dlPFC, mOFCvlPFC	AAL atlas
	temporal lobe, parietal lobe	Harvard-Oxford cortical atlas
VTA-NAc	fornix	JHU white matter tractography atlas
SN-putamen	internal and external capsule	JHU white matter tractography atlas

VTA: ventral tegmental area, dlPFC: dorsolateral prefrontal cortex, vlPFC: ventral lateral prefrontal cortex, mOFC: medial orbitofrontal cortex, ACC: anterior cingulate cortex, NAc: nucleus accumbens, AAL: Automated Anatomical Labeling. JHU: Johns Hopkins University.

Table e-3. Results on each cognitive task

Cognitive task	Raw score
Trail Making Test	
Part A, median (IQR)	48.7 (38.0 – 66.2)
Part-B, median (IQR)	110.9 (83.0 – 154.0)
Symbol-Digit Modalities Test, median (IQR)	39.0 (30.0 – 47.0)
Verbal Fluency Test	
Animal naming, median (IQR)	20.0 (16.0 – 23.0)
Profession naming, median (IQR)	15.0 (11.0 – 17.0)
Digit Span Test	
Forward, median (IQR)	8.0 (7.0 – 10.0)
Backward, median (IQR)	5.0 (4.0 – 7.0)
Rey Auditory Verbal Learning Test	
Immediate recall, median (IQR)	22.0 (19.0 – 25.0)
Delayed recall, median (IQR)	6.0 (4.0 – 8.0)
Rey-Osterrieth Complex Figure Test	
Immediate recall, median (IQR)	21.0 (16.0 – 25.0)
Delayed recall, median (IQR)	20.0(15.5 – 25.0)

Table e-4. MD-t, FW and MD of five tracts within meso-cortical and meso-limbic pathways, and WM reference regions.

Regions of interest	Mean MD (10-4 mm2/s, mean, SD)	Mean FW (mean, SD)	Mean MD-t (10-4 mm2/s, mean, SD)
VTA-dlPFC	9.71 (0.88)	0.26 (0.05)	5.59 (0.25)
VTA-mOFC	8.77 (0.81)	0.23 (0.05)	5.86 (0.12)
VTA- vlPFC	8.57 (0.90)	0.22 (0.06)	5.88 (0.11)
VTA-ACC	8.08 (0.86)	0.19 (0.05)	5.91 (0.11)
VTA-NAc	8.27 (0.10)	0.19 (0.05)	5.81 (0.14)
WM reference regions	8.05 (0.14)	0.18 (0.07)	5.99 (0.27)

Meso-cortical pathways included the VTA-dlPFC, VTA-mOFC, VTA-vlPFC and VTA-ACC tracts; meso-limbic pathways referred to the VTA-NAc tract; MD, mean diffusivity, FW: free water, MD-t: FW corrected MD values, VTA: ventral tegmental area, dlPFC: dorsolateral prefrontal cortex, vlPFC: ventral lateral prefrontal cortex, mOFC: medial orbitofrontal cortex, ACC, anterior cingulate cortex, NAc: nucleus accumbens, WM: white matter.

Table e-5. Relation between MD-t and FW values of nigrostriatal pathway and cognitive function, apathy, and gait performances.

	MD-t		FW	
	β (SE)	p-corrected	β (SE)	p-corrected
Processing speed	-0.10 (0.06)	0.505	-0.15 (0.09)	0.542
Executive function	-0.03 (0.06)	1.000	-0.26 (0.09)	0.023
Memory	0.01 (0.06)	1.000	-0.03 (0.06)	1.000
AES-score	0.04 (0.06)	1.000	0.08 (0.06)	1.000
TUG-step	0.05 (0.06)	1.000	-0.08 (0.06)	1.000
TUG-time	0.02 (0.06)	1.000	0.05 (0.06)	1.000
PC1	0.10 (0.09)	1.000	0.08 (0.13)	1.000

Nigrostriatal pathway referred to the SN-putamen tract. All models were adjusted for age, sex, education years, modified CESD score, the corresponding diffusion measures of white matter reference regions, SVD MRI markers and normalized brain volumes. FW: free water, MD-t: FW corrected MD values, SN: Substantia nigra, AES: Apathy Evaluation Scale, TUG: time up and go test; PC1: principal component 1. β were reported as the standardized b values, P values were corrected using Bonferroni method for multiple comparisons (number=6); P-corrected values in Bold represent < 0.05.

Table e-6. Relation between MD-t and FW values of meso-cortical and meso-limbic pathways and cognitive function, apathy and gait performances with using frontal WM reference region as the reference region.

	VTA-dlPFC		VTA-mOFC		VTA-vlPFC		VTA-ACC		VTA-NAc	
	β (SE)	p-corrected	β (SE)	p-corrected	β (SE)	p-corrected	β (SE)	p-corrected	β (SE)	p-corrected
Models for MD-t										
Processing speed	0.00 (0.06)	1.000	-0.01 (0.06)	1.000	-0.11 (0.07)	0.840	-0.10 (0.08)	1.000	-0.05 (0.06)	1.000
Executive function	-0.04 (0.06)	1.000	-0.02 (0.07)	1.000	-0.02 (0.07)	1.000	0.03 (0.08)	1.000	-0.07 (0.07)	1.000
Memory	0.05 (0.06)	1.000	-0.04 (0.06)	1.000	-0.03 (0.06)	1.000	-0.06 (0.07)	1.000	-0.04 (0.05)	1.000
AES-score	-0.08 (0.06)	1.000	0.00 (0.07)	1.000	0.03 (0.07)	1.000	0.05 (0.08)	1.000	0.14 (0.07)	0.347
TUG-step	-0.12 (0.060	0.213	-0.10 (0.07)	0.959	0.00 (0.06)	1.000	0.01 (0.06)	1.000	0.08 (0.05)	0.952
TUG-time	-0.11 (0.06)	0.379	-0.03 (0.06)	1.000	-0.01 (0.06)	1.000	-0.02 (0.06)	1.000	0.03 (0.05)	1.000
PC1	-0.12 (0.09)	1.000	-0.02 (0.09)	1.000	0.05 (0.10)	1.000	0.03 (0.09)	1.000	0.12 (0.09)	1.000
Models for FW										
Processing speed	-0.16 (0.07)	0.120	-0.28 (0.10)	0.039	-0.33 (0.10)	0.009	-0.41 (0.11)	0.002	-0.14 (0.07)	0.236
Executive function	-0.12 (0.07)	0.571	-0.33 (0.10)	0.010	-0.44 (0.10)	<0.001	-0.33 (0.10)	0.004	-0.16 (0.08)	0.209
Memory	-0.18 (0.07)	0.033	-0.32 (0.10)	0.011	-0.44 (0.10)	<0.001	-0.48 (0.10)	<0.001	-0.11 (0.06)	0.540
AES-score	0.25 (0.07)	0.005	0.23 (0.12)	0.266	0.20 (0.10)	0.290	0.24 (0.11)	0.145	0.08 (0.15)	1.000
TUG-step	0.21 (0.08)	0.042	0.10 (0.11)	1.000	0.00 (0.10)	1.000	0.00 (0.10)	1.000	-0.05 (0.06)	1.000
TUG-time	0.15 (0.07)	0.152	0.09 (0.08)	1.000	0.12 (0.09)	1.000	0.15 (0.08)	0.414	0.04 (0.05)	1.000
PC1	0.37 (0.09)	0.001	0.44 (0.14)	0.015	0.67 (0.14)	<0.001	0.66 (0.15)	<0.001	0.14 (0.10)	1.000

Meso-cortical pathways included the VTA-dlPFC, VTA-mOFC, VTA-vlPFC and VTA-ACC tracts; meso-limbic pathways referred to the VTA-NAc tract. All models were adjusted for age, sex, education years, modified CESD score, the corresponding diffusion measures of frontal white matter reference regions, SVD MRI markers and normalized brain volumes. MD-t: FW-corrected MD values, FW: free water, VTA: ventral tegmental area, dlPFC: dorsolateral prefrontal cortex, vlPFC: ventral lateral prefrontal cortex, mOFC: medial orbitofrontal cortex, ACC: anterior cingulate cortex, NAc: nucleus accumbens, AES: Apathy Evaluation Scale; TUG: time up and go test; PC1: first principal component, b were reported as the standardized b values and standard error (SE), P values were corrected for multiple comparisons (number=6) using Bonferroni method; P-corrected values in Bold represent < 0.05.

Table e-7. Preserved principal components based on the cumulative sum of explained variance in principal component analysis.

	PC1	PC2	PC3
Explained total variance	50.52%	16.49%	13.06%
Factor loading			
Processing speed	-0.44	-0.16	0.34
Executive function	-0.41	-0.49	-0.07
Memory	-0.45	-0.43	0.06
AES-score	0.32	-0.14	0.90
TUG-step	0.39	-0.55	-0.21
TUG-time	0.43	-0.47	-0.13

Note that: a factor loading ≥ 0.30 on a given component was considered as relevant; higher PC1 values suggested worse performance in cognitive function, apathy and gait; higher PC2 values suggested worse performance in the cognitive domains of executive function and memory, yet better performance in gait measures; higher PC3 values suggested worse performance in the cognitive domains of processing speed, yet better performance in apathy measures. AES: Apathy Evaluation Scale, TUG: time up and go test; PC1: first principal component; PC2: second principal component; PC3: third principal component.

Table e-8. Relation between MD-t and FW values of meso-cortical and meso-limbic pathways and PC2 and PC3

	PC2		PC3	
	β (SE)	p-corrected	β (SE)	p-corrected
MD-t				
VTA-dlPFC	0.05 (0.06)	1.000	-0.08 (0.06)	1.000
VTA-mOFC	0.14 (0.07)	0.379	-0.02 (0.06)	1.000
VTA-vlPFC	0.04 (0.07)	1.000	0.02 (0.06)	1.000
VTA-ACC	-0.01 (0. 09)	1.000	0.00 (0.08)	1.000
VTA-NAc	-0.04 (0.06)	1.000	0.04 (0.07)	1.000
FW				
VTA-dlPFC	-0.11 (0.09)	1.000	0.11 (0.07)	0.769
VTA-mOFC	0.04 (0.09)	1.000	0.10 (0.06)	1.000
VTA-vlPFC	0.13 (0.10)	1.000	0.07 (0.09)	1.000
VTA-ACC	0.13 (0.09)	0.842	0.02 (0.13)	1.000
VTA-NAc	0.15 (0.07)	0.178	-0.16 (0.12)	0.943

Meso-cortical pathways included the VTA-dlPFC, VTA-mOFC, and VTA-vlPFC tracts; meso-limbic pathways referred to the VTA-NAc tract. All models were adjusted for age, sex, education years, modified CESD score, the corresponding diffusion measures of white matter reference regions, SVD MRI markers and normalized brain volumes. MD-t: FW-corrected MD values, FW: free water, VTA: ventral tegmental area, dlPFC: dorsolateral prefrontal cortex, vlPFC: ventral lateral prefrontal cortex, mOFC: medial orbitofrontal cortex, NAc: nucleus accumbens; PC2: the second principal component; PC3: the third principal component. β were reported as the standardized β values and standard error (SE), P values were corrected for multiple comparisons (number=6) using Bonferroni method; P-corrected values in Bold represent < 0.05.

Reference

1. Duering M, et al. Neuroimaging standards for research into small vessel disease-advances since 2013. Lancet Neurol. Jul 2023;22(7):602-618. doi:10.1016/s1474-4422(23)00131-x
2. Wardlaw JM, Smith C, Dichgans M. Small vessel disease: mechanisms and clinical implications. Lancet Neurol. Jul 2019;18(7):684-696. doi:10.1016/s1474-4422(19)30079-1
3. Clancy U, Gilmartin D, Jochems ACC, Knox L, Doubal FN, Wardlaw JM. Neuropsychiatric symptoms associated with cerebral small vessel disease: a systematic review and meta-analysis. Lancet Psychiatry. Mar 2021;8(3):225-236. doi:10.1016/s2215-0366(20)30431-4
4. Sharma B, Wang M, McCreary CR, Camicioli R, Smith EE. Gait and falls in cerebral small vessel disease: a systematic review and meta-analysis. Age Ageing. Mar 1 2023;52(3)doi:10.1093/ageing/afad011
5. Hachinski V, Finger E, Pieruccini-Faria F, Montero-Odasso M. The apathy, gait impairment, and executive dysfunction (AGED) triad vascular variant. Alzheimers Dement. Sep 2022;18(9):1662-1666. doi:10.1002/alz.12637
6. Li H, Cui L, Wang M, Liao M, Li JB, Ouyang F, Mei T, Zen H, Fan Y. Apathy is associated with striatal atrophy and cognitive impairment in cerebral small vessel disease. J Affect Disord. May 1 2023;328:39-46. doi:10.1016/j.jad.2023.02.004
7. Tay J, Morris RG, Tuladhar AM, Husain M, de Leeuw FE, Markus HS. Apathy, but not depression, predicts all-cause dementia in cerebral small vessel disease. J Neurol Neurosurg Psychiatry. Sep 2020;91(9):953-959. doi:10.1136/jnnp-2020-323092
8. Lohner V, Brookes RL, Hollocks MJ, Morris RG, Markus HS. Apathy, but not depression, is associated with executive dysfunction in cerebral small vessel disease. PLoS One. 2017;12(5):e0176943. doi:10.1371/journal.pone.0176943
9. Cai M, Jacob MA, Norris DG, de Leeuw FE, Tuladhar AM. Longitudinal Relation Between Structural Network Efficiency, Cognition, and Gait in Cerebral Small Vessel Disease. J Gerontol A Biol Sci Med Sci. Mar 3 2022;77(3):554-560. doi:10.1093/gerona/glab247
10. Cai M, Jacob MA, Norris DG, Duering M, de Leeuw FE, Tuladhar AM. Cognition mediates the relation between structural network efficiency and gait in small vessel disease. Neuroimage Clin. 2021;30:102667. doi:10.1016/j.nicl.2021.102667
11. Moretti R, Cavressi M, Tomietto P. Gait and apathy as relevant symptoms of subcortical vascular dementia. Am J Alzheimers Dis Other Demen. Jun 2015;30(4):390-9. doi:10.1177/1533317514550329
12. Russo SJ, Nestler EJ. The brain reward circuitry in mood disorders. Nat Rev Neurosci. Sep 2013;14(9):609-25. doi:10.1038/nrn3381
13. Weinstein AM. Reward, motivation and brain imaging in human healthy participants - A narrative review. Front Behav Neurosci. 2023;17:1123733. doi:10.3389/fnbeh.2023.1123733
14. Lisiecka-Ford DM, Tozer DJ, Morris RG, Lawrence AJ, Barrick TR, Markus HS. Involvement of the reward network is associated with apathy in cerebral small vessel disease. J Affect Disord. May 2018;232:116-121. doi:10.1016/j.jad.2018.02.006
15. Tay J, Tuladhar AM, Hollocks MJ, Brookes RL, Tozer DJ, Barrick TR, Husain M, de Leeuw FE, Markus HS. Apathy is associated with large-scale white matter network disruption in small vessel disease. Neurology. Mar 12 2019;92(11):e1157-e1167. doi:10.1212/wnl.0000000000007095
16. Chokesuwattanaskul A, Zanon Zotin MC, Schoemaker D, Sveikata L, Gurol ME, Greenberg SM, Viswanathan A. Apathy in Patients With Cerebral Amyloid Angiopathy: A Multimodal Neuroimaging Study. Neurology. May 9 2023;100(19):e2007-e2016. doi:10.1212/wnl.0000000000207200

17. Le Heron C, Manohar S, Plant O, Muhammed K, Griffanti L, Nemeth A, Douaud G, Markus HS, Husain M. Dysfunctional effort-based decision-making underlies apathy in genetic cerebral small vessel disease. Brain. Nov 1 2018;141(11):3193-3210. doi:10.1093/brain/awy257

18. Yang Z, Xie Y, Dou K, Yang L, Xie A. Associations of striatal dopamine transporter binding with motor and non-motor symptoms in early Parkinson's disease. Clin Transl Sci. Jun 2023;16(6):1021-1038. doi:10.1111/cts.13508

19. Chung SJ, Yoo HS, Oh JS, Kim JS, Ye BS, Sohn YH, Lee PH. Effect of striatal dopamine depletion on cognition in de novo Parkinson's disease. Parkinsonism Relat Disord. Jun 2018;51:43-48. doi:10.1016/j.parkreldis.2018.02.048

20. Costello H, Yamamori Y, Reeves S, Schrag AE, Howard R, Roiser JP. Longitudinal decline in striatal dopamine transporter binding in Parkinson's disease: associations with apathy and anhedonia. J Neurol Neurosurg Psychiatry. Oct 2023;94(10):863-870. doi:10.1136/jnnp-2022-330790

21. Wilmskoetter J, Marebwa B, Basilakos A, Fridriksson J, Rorden C, Stark BC, Johnson L, Hickok G, Hillis AE, Bonilha L. Long-range fibre damage in small vessel brain disease affects aphasia severity. Brain. Oct 1 2019;142(10):3190-3201. doi:10.1093/brain/awz251

22. Lambert C, Benjamin P, Zeestraten E, Lawrence AJ, Barrick TR, Markus HS. Longitudinal patterns of leukoaraiosis and brain atrophy in symptomatic small vessel disease. Brain. Apr 2016;139(Pt 4):1136-51. doi:10.1093/brain/aww009

23. van Norden AG, de Laat KF, Gons RA, van Uden IW, van Dijk EJ, van Oudheusden LJ, Esselink RA, Bloem BR, van Engelen BG, Zwarts MJ, Tendolkar I, Olde-Rikkert MG, van der Vlugt MJ, Zwiers MP, Norris DG, de Leeuw FE. Causes and consequences of cerebral small vessel disease. The RUN DMC study: a prospective cohort study. Study rationale and protocol. BMC Neurol. Feb 28 2011;11:29. doi:10.1186/1471-2377-11-29

24. Jacob MA, Cai M, Bergkamp M, Darweesh SKL, Gelissen LMY, Marques J, Norris DG, Duering M, Esselink RAJ, Tuladhar AM, de Leeuw FE. Cerebral Small Vessel Disease Progression Increases Risk of Incident Parkinsonism. Ann Neurol. Jun 2023;93(6):1130-1141. doi:10.1002/ana.26615

25. Jacob MA, Cai M, van de Donk V, Bergkamp M, Marques J, Norris DG, Kessels RPC, Claassen J, Duering M, Tuladhar AM, Leeuw FE. Cerebral Small Vessel Disease Progression and the Risk of Dementia: A 14-Year Follow-Up Study. Am J Psychiatry. Jul 1 2023;180(7):508-518. doi:10.1176/appi.ajp.20220380

26. Marin RS, Biedrzycki RC, Firinciogullari S. Reliability and validity of the Apathy Evaluation Scale. Psychiatry Res. Aug 1991;38(2):143-62. doi:10.1016/0165-1781(91)90040-v

27. Lanctôt KL, Ismail Z, Bawa KK, Cummings JL, Husain M, Mortby ME, Robert P. Distinguishing apathy from depression: A review differentiating the behavioral, neuroanatomic, and treatment-related aspects of apathy from depression in neurocognitive disorders. Int J Geriatr Psychiatry. Feb 2023;38(2):e5882. doi:10.1002/gps.5882

28. Rodakowski J. Relationship among Depression, Gait Disturbance, Disability, and Neurobiological Abnormalities. Am J Geriatr Psychiatry. Jan 2018;26(1):87-88. doi:10.1016/j.jagp.2017.09.016

29. Podsiadlo D, Richardson S. The timed "Up & Go": a test of basic functional mobility for frail elderly persons. J Am Geriatr Soc. Feb 1991;39(2):142-8. doi:10.1111/j.1532-5415.1991.tb01616.x

30. Li H, Jacob MA, Cai M, Duering M, Chamberland M, Norris DG, Kessels RPC, de Leeuw FE, Marques JP, Tuladhar AM. Regional cortical thinning, demyelination, and iron loss in cerebral small vessel disease. Brain. Jun 27 2023;doi:10.1093/brain/awad220

31. Shelhamer E, Long J, Darrell T. Fully Convolutional Networks for Semantic Segmentation. IEEE Trans Pattern Anal Mach Intell. Apr 2017;39(4):640-651. doi:10.1109/tpami.2016.2572683

32. Kellner E, Dhital B, Kiselev VG, Reisert M. Gibbs-ringing artifact removal based on local subvoxel-shifts. Magn Reson Med. Nov 2016;76(5):1574-1581. doi:10.1002/mrm.26054

33. Veraart J, Novikov DS, Christiaens D, Ades-Aron B, Sijbers J, Fieremans E. Denoising of diffusion MRI using random matrix theory. Neuroimage. Nov 15 2016;142:394-406. doi:10.1016/j.neuroimage.2016.08.016

34. Andersson JLR, Sotiropoulos SN. An integrated approach to correction for off-resonance effects and subject movement in diffusion MR imaging. Neuroimage. Jan 15 2016;125:1063-1078. doi:10.1016/j.neuroimage.2015.10.019

35. Smith SM, Jenkinson M, Woolrich MW, Beckmann CF, Behrens TE, Johansen-Berg H, Bannister PR, De Luca M, Drobnjak I, Flitney DE, Niazy RK, Saunders J, Vickers J, Zhang Y, De Stefano N, Brady JM, Matthews PM. Advances in functional and structural MR image analysis and implementation as FSL. Neuroimage. 2004;23 Suppl 1:S208-19. doi:10.1016/j.neuroimage.2004.07.051

36. Tustison NJ, Avants BB, Cook PA, Zheng Y, Egan A, Yushkevich PA, Gee JC. N4ITK: improved N3 bias correction. IEEE Trans Med Imaging. Jun 2010;29(6):1310-20. doi:10.1109/tmi.2010.2046908

37. Jbabdi S, Sotiropoulos SN, Savio AM, Graña M, Behrens TE. Model-based analysis of multishell diffusion MR data for tractography: how to get over fitting problems. Magn Reson Med. Dec 2012;68(6):1846-55. doi:10.1002/mrm.24204

38. Pasternak O, Sochen N, Gur Y, Intrator N, Assaf Y. Free water elimination and mapping from diffusion MRI. Magn Reson Med. Sep 2009;62(3):717-30. doi:10.1002/mrm.22055

39. Duering M, Finsterwalder S, Baykara E, Tuladhar AM, Gesierich B, Konieczny MJ, Malik R, Franzmeier N, Ewers M, Jouvent E, Biessels GJ, Schmidt R, de Leeuw FE, Pasternak O, Dichgans M. Free water determines diffusion alterations and clinical status in cerebral small vessel disease. Alzheimers Dement. Jun 2018;14(6):764-774. doi:10.1016/j.jalz.2017.12.007

40. Carandini T, Mancini M, Bogdan I, Rae CL, Barritt AW, Sethi A, Harrison N, Rashid W, Scarpini E, Galimberti D, Bozzali M, Cercignani M. Disruption of brainstem monoaminergic fibre tracts in multiple sclerosis as a putative mechanism for cognitive fatigue: a fixel-based analysis. Neuroimage Clin. 2021;30:102587. doi:10.1016/j.nicl.2021.102587

41. Supekar K, Kochalka J, Schaer M, Wakeman H, Qin S, Padmanabhan A, Menon V. Deficits in mesolimbic reward pathway underlie social interaction impairments in children with autism. Brain. Sep 1 2018;141(9):2795-2805. doi:10.1093/brain/awy191

42. Zhang Y, Wu IW, Buckley S, Coffey CS, Foster E, Mendick S, Seibyl J, Schuff N. Diffusion tensor imaging of the nigrostriatal fibers in Parkinson's disease. Mov Disord. Aug 2015;30(9):1229-36. doi:10.1002/mds.26251

43. Pauli WM, Nili AN, Tyszka JM. A high-resolution probabilistic in vivo atlas of human subcortical brain nuclei. Sci Data. Apr 17 2018;5:180063. doi:10.1038/sdata.2018.63

44. Puonti O, Iglesias JE, Van Leemput K. Fast and sequence-adaptive whole-brain segmentation using parametric Bayesian modeling. Neuroimage. Dec 2016;143:235-249. doi:10.1016/j.neuroimage.2016.09.011

45. Tzourio-Mazoyer N, Landeau B, Papathanassiou D, Crivello F, Etard O, Delcroix N, Mazoyer B, Joliot M. Automated anatomical labeling of activations in SPM using a macroscopic anatomical parcellation of the MNI MRI single-subject brain. Neuroimage. Jan 2002;15(1):273-89. doi:10.1006/nimg.2001.0978

46. van den Bos W, Rodriguez CA, Schweitzer JB, McClure SM. Adolescent impatience decreases with increased frontostriatal connectivity. Proc Natl Acad Sci U S A. Jul 21 2015;112(29):E3765-74. doi:10.1073/pnas.1423095112

47. Yuan K, Zhao M, Yu D, Manza P, Volkow ND, Wang GJ, Tian J. Striato-cortical tracts predict 12-h abstinence-induced lapse in smokers. Neuropsychopharmacology. Nov 2018;43(12):2452-2458. doi:10.1038/s41386-018-0182-x

48. Wakana S, Caprihan A, Panzenboeck MM, Fallon JH, Perry M, Gollub RL, Hua K, Zhang J, Jiang H, Dubey P, Blitz A, van Zijl P, Mori S. Reproducibility of quantitative tractography methods applied to cerebral white matter. Neuroimage. Jul 1 2007;36(3):630-44. doi:10.1016/j.neuroimage.2007.02.049

49. Desikan RS, Ségonne F, Fischl B, Quinn BT, Dickerson BC, Blacker D, Buckner RL, Dale AM, Maguire RP, Hyman BT, Albert MS, Killiany RJ. An automated labeling system for subdividing the human cerebral cortex on MRI scans into gyral based regions of interest. Neuroimage. Jul 1 2006;31(3):968-80. doi:10.1016/j.neuroimage.2006.01.021

50. Avants BB, Epstein CL, Grossman M, Gee JC. Symmetric diffeomorphic image registration with cross-correlation: evaluating automated labeling of elderly and neurodegenerative brain. Med Image Anal. Feb 2008;12(1):26-41. doi:10.1016/j.media.2007.06.004

51. Behrens TE, Berg HJ, Jbabdi S, Rushworth MF, Woolrich MW. Probabilistic diffusion tractography with multiple fibre orientations: What can we gain? Neuroimage. Jan 1 2007;34(1):144-55. doi:10.1016/j.neuroimage.2006.09.018

52. Nemy M, et al. Cholinergic white matter pathways along the Alzheimer's disease continuum. Brain. May 2 2023;146(5):2075-2088. doi:10.1093/brain/awac385

53. Nemy M, Cedres N, Grothe MJ, Muehlboeck JS, Lindberg O, Nedelska Z, Stepankova O, Vyslouzilova L, Eriksdotter M, Barroso J, Teipel S, Westman E, Ferreira D. Cholinergic white matter pathways make a stronger contribution to attention and memory in normal aging than cerebrovascular health and nucleus basalis of Meynert. Neuroimage. May 1 2020;211:116607. doi:10.1016/j.neuroimage.2020.116607

54. Dauguet J, Peled S, Berezovskii V, Delzescaux T, Warfield SK, Born R, Westin CF. Comparison of fiber tracts derived from in-vivo DTI tractography with 3D histological neural tract tracer reconstruction on a macaque brain. Neuroimage. Aug 15 2007;37(2):530-8. doi:10.1016/j.neuroimage.2007.04.067

55. Revelle WR. psych: Procedures for personality and psychological research. 2017;

56. Kaufmann BC, Cazzoli D, Pastore-Wapp M, Vanbellingen T, Pflugshaupt T, Bauer D, Müri RM, Nef T, Bartolomeo P, Nyffeler T. Joint impact on attention, alertness and inhibition of lesions at a frontal white matter crossroad. Brain. Apr 19 2023;146(4):1467-1482. doi:10.1093/brain/awac359

57. Dziuban CD, Shirkey EC. When is a correlation matrix appropriate for factor analysis? Some decision rules. Psychological bulletin. 1974;81(6):358.

58. Braeken J, Van Assen MA. An empirical Kaiser criterion. Psychological methods. 2017;22(3):450.

59. Hair Jr J, Anderson R, Tatham R, Black W. Multivariate data analysis 5th ed Prentice Hall Upper Saddle River. NJ Retrieved from https://www scirp org/(S (351jmbntvnsjt1aadkpo szje))/reference/ReferencesPapers aspx. 1998;

60. Breiman L. Random Forests. Machine Learning. 2001/10/01 2001;45(1):5-32. doi:10.1023/A:1010933404324

61. Strobl C, Boulesteix AL, Zeileis A, Hothorn T. Bias in random forest variable importance measures: illustrations, sources and a solution. BMC Bioinformatics. Jan 25 2007;8:25. doi:10.1186/1471-2105-8-25

62. Witten D, James G. An introduction to statistical learning with applications in R. springer publication; 2013.

63. Yeo IK, Johnson RA. A new family of power transformations to improve normality or symmetry. Biometrika. 2000;87(4):954-959.

64. Brugulat-Serrat A, Salvadó G, Sudre CH, Grau-Rivera O, Suárez-Calvet M, Falcon C, Sánchez-Benavides G, Gramunt N, Fauria K, Cardoso MJ, Barkhof F, Molinuevo JL, Gispert JD. Patterns of

white matter hyperintensities associated with cognition in middle-aged cognitively healthy individuals. Brain Imaging Behav. Oct 2020;14(5):2012-2023. doi:10.1007/s11682-019-00151-2

65. de Laat KF, Tuladhar AM, van Norden AG, Norris DG, Zwiers MP, de Leeuw FE. Loss of white matter integrity is associated with gait disorders in cerebral small vessel disease. Brain. Jan 2011;134(Pt 1):73-83. doi:10.1093/brain/awq343
66. Jolliffe I. Principal Component Analysis. In: Lovric M, ed. International Encyclopedia of Statistical Science. Springer Berlin Heidelberg; 2011:1094-1096.
67. Krashia P, Spoleti E, D'Amelio M. The VTA dopaminergic system as diagnostic and therapeutical target for Alzheimer's disease. Front Psychiatry. 2022;13:1039725. doi:10.3389/fpsyt.2022.1039725
68. Hirano S. Clinical implications for dopaminergic and functional neuroimage research in cognitive symptoms of Parkinson's disease. Mol Med. Apr 15 2021;27(1):40. doi:10.1186/s10020-021-00301-7
69. Saleh Y, Le Heron C, Petitet P, Veldsman M, Drew D, Plant O, Schulz U, Sen A, Rothwell PM, Manohar S, Husain M. Apathy in small vessel cerebrovascular disease is associated with deficits in effort-based decision making. Brain. May 7 2021;144(4):1247-1262. doi:10.1093/brain/awab013
70. Hauser TU, Eldar E, Dolan RJ. Separate mesocortical and mesolimbic pathways encode effort and reward learning signals. Proc Natl Acad Sci U S A. Aug 29 2017;114(35):E7395-e7404. doi:10.1073/pnas.1705643114
71. Blumen HM, Jayakody O, Verghese J. Gait in cerebral small vessel disease, pre-dementia, and dementia: A systematic review. Int J Stroke. Jan 2023;18(1):53-61. doi:10.1177/17474930221114562
72. Ray NJ, Lawson RA, Martin SL, Sigurdsson HP, Wilson J, Galna B, Lord S, Alcock L, Duncan GW, Khoo TK, O'Brien JT, Burn DJ, Taylor JP, Rea RC, Bergamino M, Rochester L, Yarnall AJ. Free-water imaging of the cholinergic basal forebrain and pedunculopontine nucleus in Parkinson's disease. Brain. Mar 1 2023;146(3):1053-1064. doi:10.1093/brain/awac127
73. Sperling SA, Druzgal J, Blair JC, Flanigan JL, Stohlman SL, Barrett MJ. Cholinergic nucleus 4 grey matter density is associated with apathy in Parkinson's disease. Clin Neuropsychol. Apr 2023;37(3):676-694. doi:10.1080/13854046.2022.2065362
74. Morris R, Martini DN, Madhyastha T, Kelly VE, Grabowski TJ, Nutt J, Horak F. Overview of the cholinergic contribution to gait, balance and falls in Parkinson's disease. Parkinsonism Relat Disord. Jun 2019;63:20-30. doi:10.1016/j.parkreldis.2019.02.017
75. Bowie CR, Harvey PD. Administration and interpretation of the Trail Making Test. Nat Protoc. 2006;1(5):2277-81. doi:10.1038/nprot.2006.390
76. Smith A. Symbol digit modalities test. Los Angeles, CA. 2013;
77. Oosterman JM, Vogels RL, van Harten B, Gouw AA, Poggesi A, Scheltens P, Kessels RP, Scherder EJ. Assessing mental flexibility: neuroanatomical and neuropsychological correlates of the Trail Making Test in elderly people. Clin Neuropsychol. Feb 2010;24(2):203-19. doi:10.1080/13854040903482848
78. Van der Elst W, Van Boxtel MP, Van Breukelen GJ, Jolles J. Normative data for the Animal, Profession and Letter M Naming verbal fluency tests for Dutch speaking participants and the effects of age, education, and sex. J Int Neuropsychol Soc. Jan 2006;12(1):80-9. doi:10.1017/s1355617706060115
79. Wechsler D. Wechsler adult intelligence scale. Archives of Clinical Neuropsychology. 1955;
80. Van der Elst W, van Boxtel MP, van Breukelen GJ, Jolles J. Rey's verbal learning test: normative data for 1855 healthy participants aged 24-81 years and the influence of age, sex, education, and mode of presentation. J Int Neuropsychol Soc. May 2005;11(3):290-302. doi:10.1017/s1355617705050344
81. Loring D, Meador K. The Medical College of Georgia (MCG) complex figures: four forms for follow-up. Rey-Osterrieth handbook Psychological Assessment Resources. 2003;

Chapter 4.

Cholinergic system disruption contributes to motoric cognitive dysfunction in cerebral small vessel disease

Submitted as:
Hao Li*, Mengfei Cai *, Milan Nemy, Mina A. Jacob, David G. Norris, Marco Duering, Yuhu Zhang, Roy P. C. Kessels, Stefan J Teipel, Daniel Ferreira, Frank-Erik de Leeuw, Anil M. Tuladhar. Cholinergic system disruption contributes to motoric cognitive dysfunction in cerebral small vessel disease.

Abstract

Cerebral small vessel disease (SVD) is a key vascular contributor to both cognitive and motor dysfunction, consequently leading to an increased risk of dementia, parkinsonism, and loss of functional independence. Cognitive decline and gait disturbance are often observed simultaneously in SVD patients, also known as motoric cognitive dysfunction, but its shared underlying neural basis remains not fully understood.

In this cross-sectional study, we included 213 SVD patients with multi-modality MRI scans, motor, and cognitive assessments (i.e., processing speed, executive function, and memory) available. Cholinergic cortical and thalamic pathways were reconstructed using probabilistic tractography on diffusion images, followed by the quantification of the disruption in these tracts with diffusion metrics derived from neurite orientation dispersion and density imaging (NODDI) model. Conventional MRI markers for SVD were assessed. Our results showed that (i) SVD markers are differentially associated with disrupted cholinergic pathways, as indicated by a higher isotropic volume fraction and a lower neurite density index, with white matter hyperintensities being the dominant contributor; (ii) Diffusion metrics in cholinergic cortical pathways mediated the relationship between SVD and both cognitive and gait dysfunction. In contrast, cholinergic thalamic pathways mediate only the relationship between SVD and cognition; (iii) Microstructural abnormalities in cholinergic cortical pathways are central to the pathophysiology underlying the combined performance of cognition and gait, i.e., motoric cognitive dysfunction. Taken together, our findings suggest that disruption in cholinergic cortical pathways attributable to SVD, rather than cholinergic thalamic pathways, contributed to the combined dysfunction of cognition and gait in patients with SVD.

Introduction

Cerebral small vessel disease (SVD), radiologically characterized by white matter hyperintensities (WMH), microbleeds, and lacunes, is a key vascular contributor to cognitive and motor dysfunction, consequently leading to an increased risk of dementia, parkinsonism and loss of functional independence.[1,2] Gait serves as a strong predictor of cognitive decline and requires cognitive control, highlighting the bi-directional relationship between gait and cognition. This interplay is mediated by shared mechanisms, such as densely connected white matter networks.[3-5] Cognitive decline and gait disturbance are often observed simultaneously in older people, also known as motoric cognitive dysfunction.[3,4,6] However, gait and cognitive dysfunction in SVD patients are often investigated as isolated outcomes rather than as co-occurring conditions. This limits our understanding of the shared neural basis underlying the combined performance in motor and cognition in SVD patients. Two primary sources of cholinergic projections have been identified in the brain.[7,8] First, the nucleus basalis of Meynert (NBM) in the basal forebrain serves as the primary source of cholinergic input to the entire cortex via white matter tracts. Second, the pedunculopontine nucleus (PPN), located in the brainstem, provides cholinergic innervation mainly to the thalamus, thereby modulating thalamocortical activity.[9,10] Cholinergic projections are impaired in neurodegenerative disorders such as Alzheimer's disease and Parkinson's disease, contributing to deficits in both cognitive and motor functions.[11-14] This cholinergic dysfunction may represent a potential shared neural mechanism underlying these conditions. However, the role of cholinergic projections in the combined performance of cognitive and gait in patients with SVD remains to be elucidated, especially considering these tracts are partly located in areas vulnerable for SVD. High SVD burden (i.e., WMH) is associated with lower integrity of the cholinergic system and is a stronger contributor to the degeneration of the cholinergic projections as compared to amyloid and tau levels in cerebrospinal fluid in older adults.[8] Despite these findings, several important knowledge gaps remain. First, the neurodegeneration of cholinergic tracts in response to brain pathology is heterogeneous, while the relative contributions of other SVD markers (i.e., lacunes, microbleeds) to the disruption of cholinergic system are unknown. Second, the thalamus functions as a strategic hub with extensive connections that are susceptible to SVD lesions.[15,16] However, previous studies have predominantly examined cholinergic projections to the cortex, with limited investigation into cholinergic projections from the pedunculopontine nucleus (PPN) to the thalamus, specifically the PPN-thalamus pathway.[10] Third, the cholinergic system was characterized using conventional diffusion tensor imaging (DTI) previously. However, the DTI model may oversimplify tissue diffusivity.[17]

Therefore, more advanced diffusion models, such as Neurite Orientation Dispersion and Density Imaging (NODDI) with multi-shell diffusion scans, are warranted to probe the microstructural abnormalities of the cholinergic system more accurately.

Our first aim of the present study was to investigate the relative contributions of SVD markers to microstructural abnormalities in cholinergic pathways projected to the cortex and thalamus in SVD patients. Second, we examined the contribution of a disrupted cholinergic system to cognitive and motor dysfunction in SVD patients. We hypothesized that SVD markers differentially contribute to deficits in cholinergic cortical and thalamic pathways, which in turn contribute to worse performance both in cognition and gait, the two prominent clinical symptoms in patients with SVD

Methods

Study population

The data used in the present study were from the Radboud University Nijmegen Diffusion tensor and Magnetic resonance imaging Cohort (RUN DMC), an ongoing prospective cohort study investigating the causes and clinical consequences of sporadic SVD. Detailed information has been described previously.[18] In brief, the selection criteria included: 1) age between 50 and 85 years; 2) presence of SVD as demonstrated on MRI markers (identified as WMH or lacunes); 3) cognitive or motor symptoms that could be attributed to SVD. Baseline data collection was carried out in 2006 among 503 participants who underwent three follow-up assessments in 2011, 2015, and 2020. Clinical information was available for 499 patients (response rate 99.2%) during the 2020 follow-up. Data were not available for 4 participants: 3 due to emigration and 1 being a non-responder. Due to the multi-shell diffusion data only being available at the third follow-up, the present study used the data from the third follow-up assessment in 2020. In addition, to minimize the influence of non-SVD pathologies (e.g., Aβ, tau, α-synuclein) on the disruption of cholinergic pathways in the present study, participants with dementia due to causes other than vascular, e.g., Alzheimer's dementia, dementia with Lewy bodies, or Parkinson's disease, were excluded (n=14), resulting in a final sample of 213 participants (Supplementary Figure 1)

MRI acquisition

All participants underwent neuroimaging scans on a 3T MRI scanner (MAGNETOM Prisma; Siemens) with a 32-channel head coil. The following sequences were

acquired: the Magnetization Prepared 2 Rapid Acquisition Gradient Echoes (MP2RAGE) sequence for creating T1-weighted (T1W) image, a 3D fluid-attenuated inversion recovery (FLAIR) sequence, a 3D multi-echo gradient echo (GRE) sequence for creating susceptibility weighted image (SWI), and multi-shell diffusion weighted imaging (DWI). Full acquisition details have been described previously and are provided in the supplementary materials.[16,19]

MRI markers of SVD and brain volumes

SVD MRI markers (i.e., WMH, lacunes, Cerebral microbleeds) and brain atrophy were assessed according to version 2 of the Standards for Reporting Vascular Changes on Neuroimaging criteria (STRIVE2).[1] WMH was semi-automatically segmented based on FLAIR and T1 images using a validated 3D U-net deep learning algorithm.[19] All segmented WMH masks were visually inspected and manually corrected when necessary. Lacunes were identified on T1 and FLAIR images, while the microbleeds were identified on SWI scans. Both lacunes and microbleeds were manually counted by two well-trained raters who were blind to the clinical data, with subsequent consensus meetings (M.C, M.A.J). Gray matter (GM), white matter (WM), and cerebrospinal fluid (CSF) were segmented on T1 images using SPM12 software. To avoid the misclassification of WMH as GM, these segmented images of GM, WM, and CSF were corrected using the WMH mask. Total brain volumes (TBV) were determined by the sum of GM and WM volumes. To increase clinical generalizability, WMH volumes were also rated semi-quantitatively according to the Fazekas visual rating scale (mild: Fazekas 1; moderate: Fazekas 2; severe: Fazekas 3)(H.L).[20]

Diffusion MRI processing and NODDI mappings

Diffusion MRI data were pre-processed, including denoising and removal of Gibbs artifacts, correction of head motion, eddy currents-induced distortion, susceptibility-induced distortion (top-up), and intensity bias,[21-23] as described previously.[24] The processed multi-shell diffusion images were fed into the NODDI toolbox (http://mig.cs.ucl.ac.uk/index.php?n=Download.NODDI) implemented in Matlab to obtain NODDI mappings, including neurite density index (NDI), orientation dispersion index (ODI), and CSF isotropic volume fraction (ISOVF).[25]

The NODDI model estimates three microstructural compartments within one voxel: the intra-cellular, extra-cellular, and CSF compartments. As a result, this model could provide a more detailed and specific characterization of neural microstructure over the DTI model.[26] The NODDI model can estimate the NDI, which serves as a proxy for axonal density, the ODI, which reflects the degree of axonal alignment,

and the ISOVF, which represents the fraction of water that diffuses freely without encountering cellular membranes.[27]

Additionally, fractional anisotropy (FA) images for each participant were obtained from pre-processed diffusion images (b=0 and b=1000 s/mm^2) using the 'dtifit' function in FSL. These FA images were used for image registration and the creation of a group template in subsequent analyses.

Identification of cholinergic pathways

Probabilistic tractography based on the multi-shell ball-and-two-sticks model[28] was conducted to delineate two white matter (WM) pathways originating from the nucleus basalis of Meynert (NBM) in the basal forebrain (BF) connecting to the cortex; one traversing the cingulum and the other the external capsule.[29] In addition, the WM pathway connecting the pedunculopontine nucleus (PPN) and the thalamus was identified.[30] To reconstruct these pathways, we conducted the following steps.

First, regions of interest (ROI) masks were extracted as follows: the NBM ROI was identified from a cytoarchitectonic map of BF cholinergic nuclei in Montreal Neurological Institute (MNI) space, derived from combined histology and in cranio MRI of a post-mortem brain[31].[31] The cingulum and external capsule masks were extracted from the Johns Hopkins University (JHU) WM atlas, available as part of the FSL package. The PPN was extracted using a recently developed PPN-specific atlas, which achieved optimal spatial resolution and precise localization of the PPN.[32] This was accomplished by integrating the MuSus-100 QSM atlas in MNI space with a super-resolution technique, guided by a myelin-stained histological human brain atlas.[32] The thalamus was directly segmented from each participant's T1w image using 'Sequence Adaptive Multimodal SEGmentation (SAMSEG)' tool in Freesurfer (version 7.3.2).[33] These ROIs in their corresponding native spaces were registered to diffusion space with a non-linear registration in Advanced Normalization Tools (ANTs, http://stnava.github.io/ANTs/).[34] All segmented and transformed ROIs were visually inspected.

Next, probabilistic tractography was performed by repeating 5,000 random samples from each voxel within the seed ROI, generating streamlines using 'probtractx2' function from FSL.[35] First, the NBM ROI served as the seeding mask, while the cingulum or external capsule ROIs were respectively designated as waypoint masks to identify the two WM tracts originating from the NBM, that is, cholinergic cortical projections: the NBM-cingulum (NBM-CG) and NBM-external capsule (NBM-EC)

tracts.[7,12] Furthermore, the PPN was used as the seeding mask, with the thalamus as the target mask to delineate the cholinergic thalamic projections, i.e., PPN-thalamus tract.[10]

To minimize the effects of individual anatomical variations, we constructed a common representative template for each tract, following a similar methodology as in previous studies.[7,12] Briefly, an unbiased template was created based on FA images from all participants using the ANTs (http://stnava.github.io/ANTs/). Next, the individually tracked pathways were brought into this unbiased group template space using the SyN registration algorithm within ANTs.[34] Subsequently, binary masks of group-template tracts were created by considering all individual warped tracts.[7] NBM-cingulum (NBM-CG) and NBM-external capsule (NBM-EC) group-template tracts were created by selecting all voxels that were included in at least 60% of the individual tracts.[7] The threshold for the PPN-thalamus group-template tract was set at 90%. Here, we have utilized a different threshold which differs from for that used in cholinergic cortical projections (NBM-EC, NBM-CG), since we performed careful and robust visual inspection according to the consensus from neurologists (H.L, M.C, A.M.T) to ensure the anatomical accuracy and specificity of the resultant group-based common pathways. Afterwards, the three group-template tracts (i.e., NBM-CG, NBM-EC and PPN-thalamus) were transformed back to individual's diffusion space. The representative cholinergic pathways are shown in Supplementary Figure 2.

An ROI of the residual WM, designated as the WM reference region (i.e., WM control mask), was created by excluding the three group-template tracts from the total WM mask in individual's diffusion space. Finally, the mean values of NDI, ODI and ISOVF of the three cholinergic tracts and WM control mask were calculated.

Cognitive assessment

Three cognitive domains (processing speed, executive function, and memory) were assessed using a standardized cognitive assessment battery using validated tests such as the Trail Making Test, Symbol-Digit Modalities Test (written version), Verbal Fluency Test, Digit Span Test, Rey Auditory Verbal Learning Test, and the Complex Figure Test. The raw scores from each cognitive test were converted to z-scores based on the whole-sample mean and standard deviation (with higher Z scores indicating a better performance), which were subsequently used to compute a composite score for each cognitive domain. More details can be found in the Supplementary materials (Table e-1).

Gait assessment

Gait speed was assessed by employing the 6-meter walk test, which is a reliable and valid assessment for measuring walking speed over a distance of 6 meters.[36] In this test, participants are instructed to walk a 6-meter distance at their usual gait speed, starting from a stationary position. The time taken to walk the distance is recorded, then the average time from three attempts is used for analysis. The walking speed is calculated by dividing the 6-meter distance by the average time taken to complete it.

Statistical analyses

Demographic characteristics were presented as mean±SD (standard deviation) for normally distributed data and median with interquartile ranges (IQR) for the skewed parameters.

Relative contribution of SVD markers to the cholinergic system disruption

Given that SVD markers contribute differently to microstructural changes in white matter tracts,[37] and considering the stronger correlation of higher SVD with NDI and ISOVF in cholinergic pathways (as shown in results), we further analyzed the relative contribution of SVD markers to the diffusion metrics in cholinergic pathways. This analysis was conducted using random forest regression with the 'randomForest' package in R, employing 1,000 conditional inference trees. Here, to account for potential confounding effects of age and sex on NDI and ISOVF, the extracted residuals from linear regression models (NDI and ISOVF in the cholinergic pathways as dependent variables and age and sex as independent variables) were taken as the outcome variables in random forest regression. The percent increase in mean squared error (%IncMSE) was determined and taken as a proxy for relative importance. The advantage of the random forest approach over other regression models is its ability to handle multicollinearity and complex non-linear relationships among variables.[38]

The relationship between NODDI metrics, cognition, and gait

To evaluate the relationship between NODDI metrics and cognition, linear regression was performed with adjustments for various covariates. Two models were used: Model 1 adjusted for age, sex, years of education, and NODDI metrics in the WM control mask; Model 2 was additionally adjusted for SVD markers to further account for potential confounding effects from SVD burden.

To assess the relation between NODDI metrics and gait speed, linear regression was performed with adjustments for various covariates. Two models were used: Model 1

adjusted for age, sex, and height, and NODDI metrics in the WM control mask, while Model 2 further included adjustments for SVD markers.

Mediation of NODDI metrics between SVD markers and cognition as well as gait

Given the fact that SVD markers were found to be correlated with NODDI metrics, and NODDI metrics were related to cognition and gait, we further tested whether NODDI metrics mediated the relationships between SVD markers and cognition as well as gait speed. Here, we performed a mediation analysis using 'lavaan' package in R and estimated the direct effect of SVD markers on outcomes (cognition and gait) and the indirect effect of SVD markers on cognition and gait via NODDI metrics, adjusted for the aforementioned covariates.

Relative contributions of neuroimaging metrics to the combined performance of cognition and gait

To examine the relative contribution of NODDI metrics, in addition to SVD markers to the combined performance in cognition and gait, we used principal component analysis (PCA) for the cognitive scores (processing speed, memory, executive function) and gait speed with the 'psych' package in R. First, Spearman correlations were computed among all pairs of the 4 clinical outcomes to assess their potential inter-correlations. Next, PCA was performed for the 4 clinical measures without rotation. The Kaiser-Meyer-Olkin (KMO) test was used to assess sampling adequacy,[39] while Bartlett's test of sphericity evaluated whether the correlations among the 4 measures were sufficiently large for PCA. A KMO value greater than 0.6 indicates that the sampling is adequate for PCA. Kaiser's criterion (eigenvalues greater than 1) was used to determine the number of components retained for subsequent analyses.[40] Clinical measures with factor loadings of 0.30 or higher on a given component were considered relevant. Finally, each participant's loading values for the retained PCA components were calculated and used as dependent variables. Finally, random forest regression was used to examine the relative contribution of NODDI metrics in cholinergic pathways and WM control mask, and SVD markers to motoric cognitive dysfunction (i.e., the common component identified by PCA).

Correction for multiple comparisons in the present study was performed using the Benjamini–Hochberg method. Two-tailed P values of <0.05 were considered statistically significant. Unless otherwise specified, all statistical analyses were performed in R, version 4.1.1.

Results

A total of 213 SVD patients were included in the present study, with a mean (SD) age of 74.6 (6.8) years, of whom 96 (45.1%) were women (Table 1).

Table 1. Baseline characteristics of the study population

n	213
Demographics	
Age (mean (SD))	74.55 (6.76)
Sex, female (%)	96 (45.1)
Education years (mean (SD))	11.62 (3.24)
Vascular risk factors	
Hypertension, n (%)	140 (66.0)
Diabetes, n (%)	31 (14.6)
Hypercholesterolemia, n 1 (%)	115 (54.2)
Smoking history, n (%)	136 (63.8)
SVD markers	
Lacune presence, n (%)	59 (27.6)
Microbleeds presence, n (%)	78 (36.4)
WMH volume (median [IQR])	4.39 [1.80, 12.32]
Cognition and gait	
Processing speed, z-score	0.19 [-0.52, 0.68]
Executive function, z-score	0.08 [-0.39, 0.59]
Memory, z-score (median [IQR])	0.00 [-0.67, 0.70]
Gait speed (mean (SD))	1.19 (0.24)

WMH, white matter hyperintensities; Cognitive scores were reported as z-score.

SVD markers are associated with the disruption of cholinergic pathways

ODI in NBM-EC and NBM-CG cholinergic pathways did not differ between the subgroups of SVD markers (Supplementary Figure 3A). Participants with presence of lacunes, microbleeds, and high Fazekas scores had lower NDI and higher ISOVF in NBM-EC and NBM-CG pathways (Supplementary Figure 3B, 3C). In addition, participants with SVD markers did not show any difference in ODI and NDI, but had higher ISOVF in the PPN-thalamus pathway (Supplementary figure 4).

Higher WMH volume was associated with lower NDI and ISOVF in both NBM-EC and NBM-CG pathways, while these associations were not found for ODI in NBM-EC, NBM-CG pathways (Figure 2A, 2B). Also, WMH burden was associated with higher ISOVF in PPN-thalamus pathway, but not with ODI and NDI (Figure 2C). In light of these findings, we focused on NDI and ISOVF metrics in cholinergic pathways in the subsequent analyses.

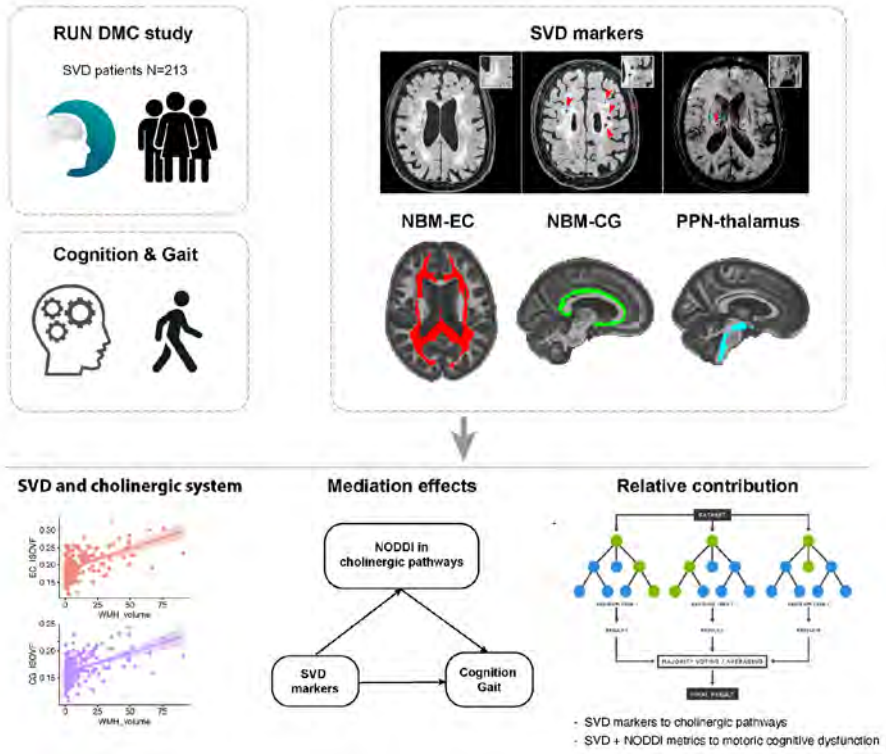

Figure 1. Outline of the study. The included SVD patients with data on cognition, gait, and MRI scans available. SVD markers and NODDI metrics in cholinergic system (NBM-EC, NBM-CG, PPN-thalamus pathway) were assessed. The role of SVD makers in the disruption of cholinergic system and the relative contribution of neuroimaging metrics (SVD and NODDI metircs) to motoric cognitive dysfunction were examined. NBM-EC, NBM-external capsule cholinergic tract; NBM-CG; NBM cingulum cholinergic tract; PPN-thalamus, PPN- thalamus cholinergic tract; NOODDI, Neurite Orientation Dispersion and Density imaging; NDI, neurite density index; ODI, orientation dispersion index; ISOVF, CSF isotropic volume fraction; NBM, nucleus basalis of Meynert; PPN, pedunculopontine nucleus; SVD, Small vessel disease; WMH, white matter hyperintensities.

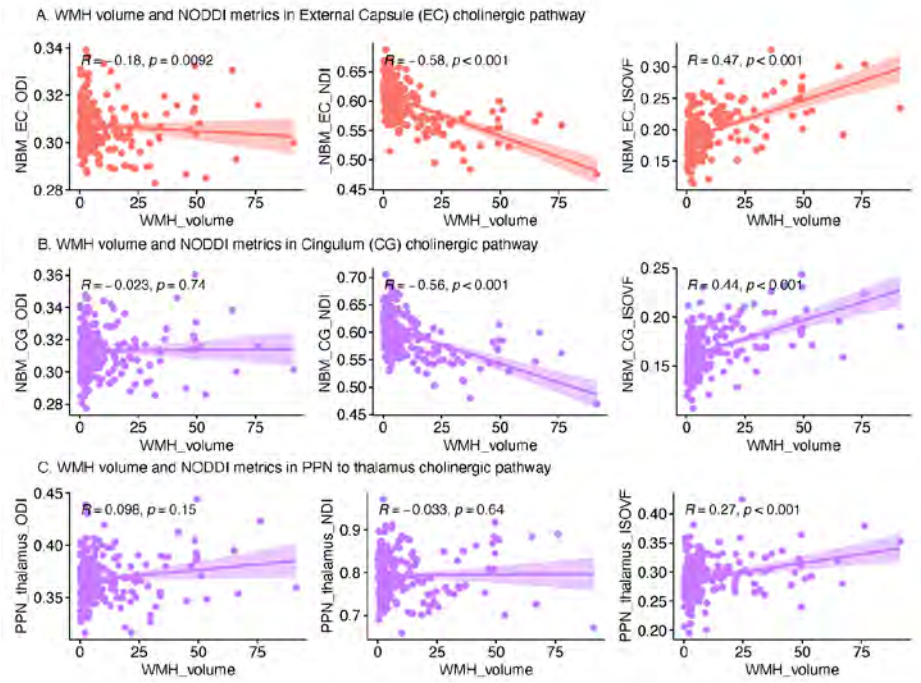

Figure 2. Correlations between WMH volumes and NODDI metrics in cholinergic pathways. (A-B) Higher WMH volume was significantly associated with lower NDI and ISOVF in both NBM-EC and NBM-CG pathways, while these associations were not found for ODI in NBM-EC, NBM-CG. (C) WMH burden was associated with higher ISOVF in PPN-thalamus pathway, but was not with ODI and NDI. NBM-EC, NBM-external capsule cholinergic tract; NBM-CG; NBM cingulum cholinergic tract; PPN-thalamus, PPN-thalamus cholinergic tract; NOODDI, Neurite Orientation Dispersion and Density imaging; NDI, neurite density index; ODI, orientation dispersion index; ISOVF, CSF isotropic volume fraction; NBM, nucleus basalis of Meynert; PPN, pedunculopontine nucleus; SVD, Small vessel disease; WMH, white matter hyperintensities.

Relative contribution of SVD markers to the disruption of cholinergic pathways

WMH volume was consistently the most significant contributor to both NDI and ISOVF in the NBM-EC and NBM-CG pathways (Figure 3A, 3B, 3D, 3E), followed by lacune count. In contrast, for PPN-thalamus pathway, total brain volume emerged as the dominant contributor to NDI, while the microbleeds count was the most significant contributor to ISOVF in this tract (Figure 3C, 3F).

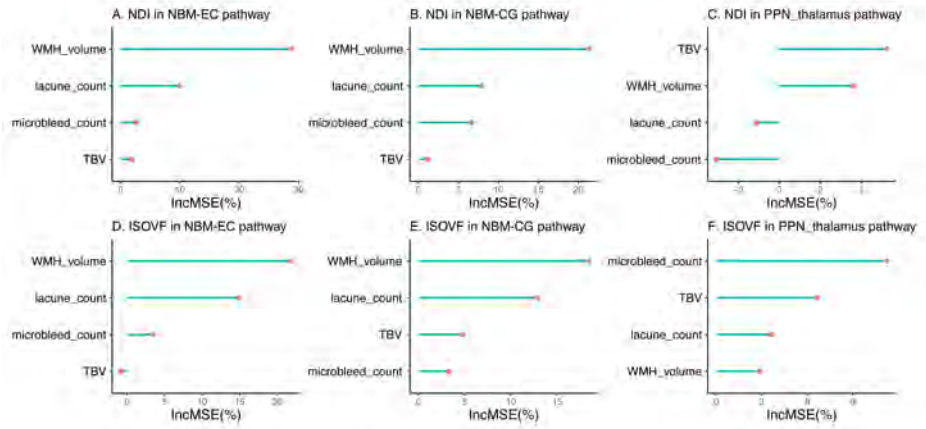

Figure 3. Relative contribution of SVD markers to NODDI metrics in cholinergic pathway. Random forest regressions to estimate the importance of SVD markers to the disruption of each cholinergic pathway. The final importance (%IncMSE) of each predictor denotes its contribution to the model. Importance values below or equal to zero denote no contribution. NBM-EC, NBM-external capsule cholinergic tract; NBM-CG; NBM cingulum cholinergic tract; PPN-thalamus, PPN- thalamus cholinergic tract; NOODDI, Neurite Orientation Dispersion and Density imaging; NDI, neurite density index; ODI, orientation dispersion index; ISOVF, CSF isotropic volume fraction; NBM, nucleus basalis of Meynert; PPN, pedunculopontine nucleus; SVD, Small vessel disease; WMH, white matter hyperintensities.

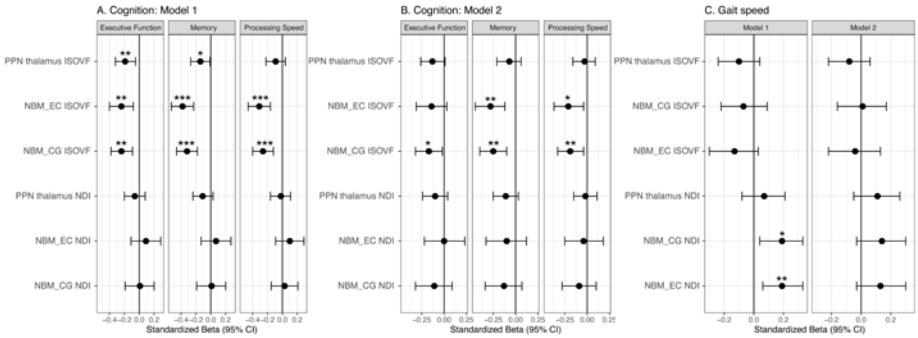

Figure 4. Relation between NODDI metrics and cognition as well as gait speed. (A) NODDI metrics in cholinergic pathways and cognition, adjusted for age, sex and education years, NODDI metrics in white matter control mask (model 1); (B) model 2, additionally adjusted for SVD markers; (C) NODDI metrics in cholinergic pathways and gait speed, Model 1 adjusted for age, sex, and height, and NODDI metrics in the WM control mask. To examine whether SVD markers could influence the relation between NODDI metrics and gait speed, SVD markers were additionally adjusted in Model 2; * $p<0.05$; **$p<0.01$. NBM-EC, NBM-external capsule cholinergic tract; NBM-CG; NBM cingulum, cholinergic tract; PPN-thalamus, PPN- thalamus cholinergic tract; NOODDI, Neurite Orientation Dispersion and Density imaging; NDI, neurite density index; ODI, orientation dispersion index; ISOVF, CSF isotropic volume fraction; NBM, nucleus basalis of Meynert; PPN, pedunculopontine nucleus; SVD, Small vessel disease; WMH, white matter hyperintensities.

Disruption in cholinergic pathways is associated with dysfunction in cognition and gait

Higher ISOVF in NBM-EC and NBM-CG pathways was associated with worse executive function, memory, and processing speed (Model 1, Figure 4A). When additionally adjusted for SVD markers, the results remained mostly similar, although the relation with ISOVF in NBM-EC cholinergic pathway was no longer significant (Model 2, Figure 4B). Regarding the PPN-thalamus pathway, higher ISOVF in this tract was associated with worse performance in executive function and memory, but this relation was not significant anymore after adjusting for SVD markers (Figure 4A, 4B).

Similarly, we found that higher NDI in NBM-EC and NBM-CG was associated with faster gait speed (Model 1, Figure 4C). However, these associations were not observed in Model 2 with additional adjustment for SVD markers (Model 2, Figure 4C)

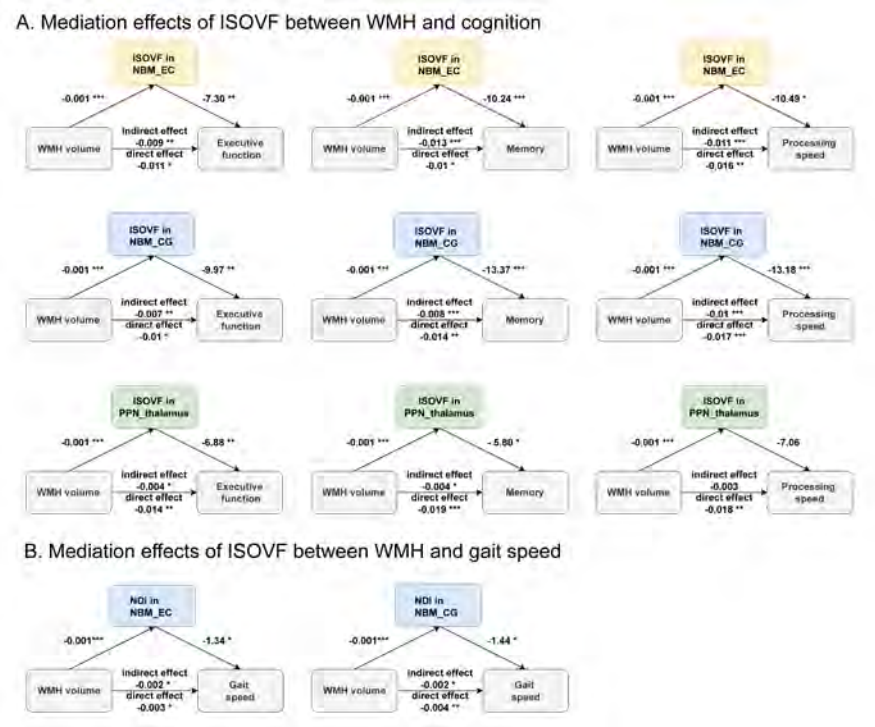

Figure 5. Mediation effects of NODDI metrics between WMH and cognition, gait. (A) NODDI metrics in cholinergic pathways mediates the relation between WMH volume and cognition; (B) NODDI metrics in cholinergic pathways mediates the relation between WMH volume and gait. NBM-EC, NBM-external capsule cholinergic tract; NBM-CG; NBM cingulum cholinergic tract; PPN-thalamus, PPN- thalamus cholinergic tract; NOODDI, Neurite Orientation Dispersion and Density imaging; NDI, neurite density index; ODI, orientation dispersion index; ISOVF, CSF isotropic volume fraction; NBM, nucleus basalis of Meynert; PPN, pedunculopontine nucleus; SVD, Small vessel disease; WMH, white matter hyperintensities.

Mediation effects of NODDI metrics between SVD and both cognition and gait

ISOVF in NBM-EC and NBM-CG pathways mediated the relation between WMH volume and cognition (processing speed, executive function, memory) (Figure 5A). In addition, ISOVF in the PPN-thalamus cholinergic pathway mediated the relation between WMH volume and executive function and memory (Figure 5A).

With gait speed as the dependent variable, NDI in NBM-EC and NBM-CG cholinergic pathways mediated the relation between WMH volume and gait speed. (Figure 5B). However, NODDI metrics did not exhibit any mediating effects between the presence of lacunes, microbleeds, and cognitive domains, nor with gait speed.

Cholinergic disruption contributes to combined performance of cognition and gait

Cognitive performance and gait speed were inter-correlated (Figure 6A), suggesting the existence of shared factors underlying cognition and gait. This serves as the prerequisite for performing subsequent PCA to identify the shared components. The Kaiser–Meyer–Olkin test showed a value of 0.72 and Bartlett's test of sphericity was significant ($P<0.001$), confirming the appropriateness of conducting a factor analysis. PCA identified a total of 4 components (Figure 6B). The first component (PC1) had eigenvalues above Kaiser's criterion of 1 and explained 61.6% of the total variance, while PC2, PC3, PC4 accounted for 19.8%, 11.3% and 7.3% of total variance across the included cognitive domains and gait speed, respectively (Figure 6B)

All 4 clinical outcome measures showed meaningful loadings on the first component (all loadings coefficient > 0.3, Figure 6C). The direction of associations between each clinical outcome measure and PC1 provided excellent clinical interpretability, that is, higher PC1 values suggesting better performance in the common factors of cognition and gait. Therefore, PC1 was used as a latent variable to capture the relative better combined performance in cognition and gait speed (Figure 6C). The relationships between NODDI metrics and PC1 were shown in Supplementary table 2.

Using random forest regression with PC1 as the dependent variable, we found IOSVF in NBM-EC cholinergic pathway was the most important contributor to PC1 (Figure 6D), after controlling for the WM control mask. For each clinical outcome, the relative contribution of neuroimaging metrics is shown in Supplementary Figure 5.

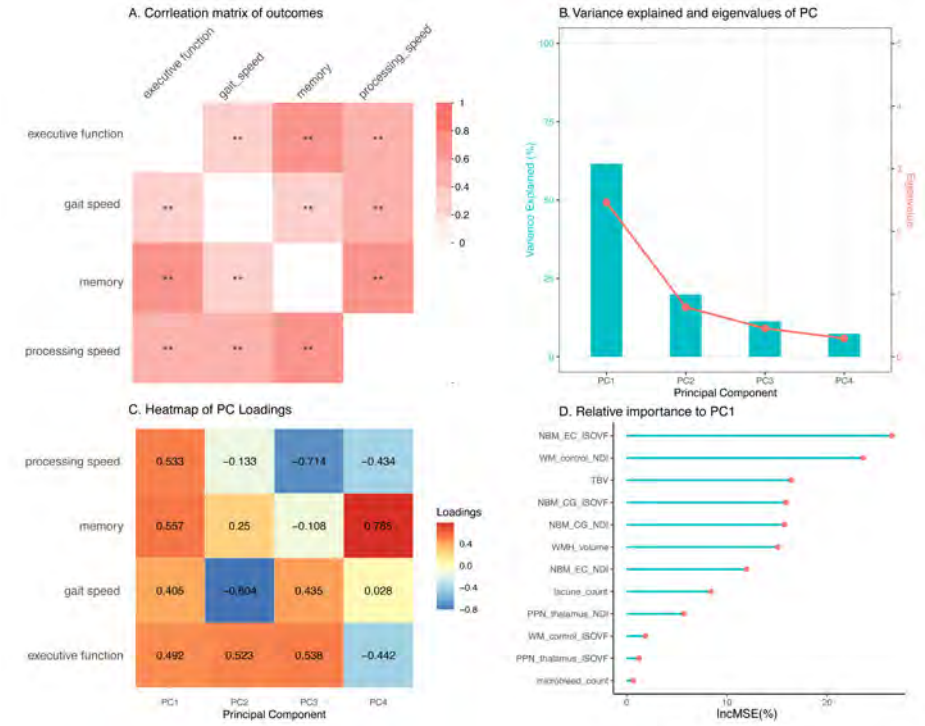

Figure 6. relative contribution of SVD markers and NDI metrics to PC1 of cognition and gait. (A) Correlation matrix of among cognitive domains and gait speed, ** correlation coefficient P<0.01; (B) Variance explained and eigenvalues of each principal component; (C) The factor loadings coefficient of each original clinical measures to the preserved principal component; (D) Relative importance of SVD marker and NODDI metrics in cholinergic pathways to PC1 derived PCA. NBM-EC, NBM-external capsule cholinergic tract; NBM-CG; NBM cingulum cholinergic tract; PPN-thalamus, PPN- thalamus cholinergic tract; NDI, neurite density index; ODI, orientation dispersion index; ISOVF, CSF isotropic volume fraction; NBM, nucleus basalis of Meynert; PPN, pedunculopontine nucleus; SVD, Small vessel disease; WMH, white matter hyperintensities; PC, principal component. TBV, total brain volume.

Discussion

In this study, we found that: (i) SVD markers are differentially associated with disruptions in cholinergic pathways with WMH being the dominant contributor; (ii) Disruption of cholinergic cortical pathways mediated the relationship between WMH and both cognition and gait dysfunction. In contrast, cholinergic thalamic pathways mediated only the relationship between WMH and cognition; (iii) Disruption in cholinergic cortical pathways was associated with combined performance of cognition and gait, suggesting that disruption in these pathways may be important in the pathophysiology of motoric cognitive dysfunction. In

summary, our findings suggest that disruptions in cholinergic cortical pathways due to SVD, rather than cholinergic thalamic pathways, could serve as the neural basis for motoric cognitive dysfunction of cognition and gait in patients with SVD.

Although SVD markers are known to be key contributors of impaired integrity in the white matter microstructure, it should be noted that the integrity of white matter tracts was differentially influenced by these SVD lesions.[41] White matter pathways at strategic locations such as the nucleus basalis of Meynert have a high connectivity with other key regions, playing a pivotal role in complex cognitive processes.[42] Because of their broad and long-distance connectivity, they are vulnerable to pathological alterations (e.g., SVD markers) in the brain, probably leading to more widespread effects on network functioning compared with the damage to peripheral connections.[43,44] The cholinergic cortical and thalamic pathways are such tracts that are clinically relevant in cognitive and motoric dysfunction.[11] With NODDI diffusion metrics derived from multi-shell MRI scans to decipher the intra- and extracellular microscopic features in cholinergic pathways, we found that patients with lacunes, microbleeds, and a high WMH burden had a lower neurite density and higher isotropic volume fraction in cholinergic cortical pathways, as well as higher isotropic volume fraction in the cholinergic thalamic pathway, with no difference in neurite density index. In addition, regarding the relative contributions of SVD markers to the deficits of cholinergic cortical and thalamic pathways, we observed that WMH volume was the dominant contributor to the disruption in the cholinergic cortical projections followed by lacunes count, while WMH was not a significant contributor to the disruption in the cholinergic thalamic pathway. Our prior study indicated that the regions or fibers intersected to WMH could be more easily disrupted compared with WMH-unconnected regions, reflected by lower microstructural integrity.[45] As shown in the WMH lesion probability mappings (Supplementary Figure 6), WMH was located in supratentorial areas, rather than infratentorial regions. The WMH and cholinergic cortical projection tracts are both distributed in supratentorial regions with extensive spatial overlap in our cohort. Therefore, the overall integrity of cholinergic cortical tracts intersected by WMH was likely to be disrupted. In contrast, the PPN-thalamus cholinergic pathway is dominantly located in the infratentorial region, that is, the brain stem. It is therefore less likely that predominantly supratentorial WMH would intersect with this tract.[10] This could explain why the burden of WMH did not emerge as the most significant contributor to abnormalities in the pedunculopontine nucleus to the thalamus cholinergic pathway.

To the best of our knowledge, this is the first study to comprehensively investigate the role of abnormalities in cholinergic pathways in the SVD population in relation

to cognition and gait. We have identified a mediation framework, in which the effect of SVD markers on cognition and gait is mainly driven by the disrupted cholinergic system. This mediation framework involved WMH, isotropic volume fraction in the cholinergic system and cognitive performance. The probable mechanism could be that increased SVD burden predisposes the cholinergic system to the structural disconnection with cortical and subcortical regions (i.e., the thalamus), which are crucial for cognitive functioning.[15,16] It is in line with the observed associations between magnitude of cholinergic deficits and the severity of cognitive impairments in prior studies, where cholinergic deficits preferentially affected memory, executive function, as well as processing speed.[7,13,45] However, it should be noted that neurite density index in cholinergic cortical pathways, rather than in cholinergic thalamic pathways, mediated the relation between WMH burden and gait speed, indicating that in SVD patients deficits in the cholinergic cortical pathways could be one of the key neural mechanisms underlying gait disturbance. This finding is pivotal, as it highlights the need to consider the involvement of different cholinergic tracts and their corresponding clinical manifestations. For instance, a recent study demonstrated that while both cholinergic cortical and thalamic tracts are implicated in dementia, including dementia with Lewy bodies and Alzheimer's dementia, the NBM-cortical projections are similarly affected in both conditions. In contrast, the PPN-thalamus system appears to be more selectively impaired in DLB.[10] The intricate architecture of the cholinergic system indicates that projections from the nucleus basalis of Meynert to the cortex may represent a clinically relevant and promising target for interventions aimed at alleviating cognitive and gait dysfunction in patients with SVD. This is particularly significant considering that both the NBM and the pedunculopontine nucleus have been explored as targets for deep brain stimulation.[46]

Cognitive decline and gait disturbances frequently co-occur in patients with SVD, a condition often referred to as motoric cognitive dysfunction.[3,4,6] However, the underlying neural mechanisms remain poorly understood. We found a strong correlation between cognitive performance and gait speed, with both sharing a common component that reflects performance of cognition and gait jointly, as identified through principal component analysis. This aligns with our previous findings that in SVD patients, cognitive functioning has a reciprocal relationship with gait performance, suggesting that gait can be considered a cognitive process to some extent.[3] In addition, when assessing the relative contributions of NODDI metrics to the shared component, in addition to SVD markers, we found the isotropic volume fraction in NBM-EC pathway had dominant contribution to the PCA-derived component of cognition and gait, compared with other neuroimaging metrics. These results support

the conclusion that deficits in cholinergic cortical pathways, as a potential neural basis, are the contributor to worse combined performance in cognition and gait.

The main strength of our study is that we have included a well-phenotyped SVD cohort with comprehensive cognitive data, using a multimodal neuroimaging approach to reconstruct cholinergic tracts. In addition, we have employed multi-shell diffusion metrics derived from NODDI pipeline, which could explicitly be accounted for the potential CSF contamination common in DWI studies. This approach by quantifying the microstructural changes of these tracts could contribute to a more precise characterization of microstructural alterations in white matter attributable to SVD, relative to the conventional DTI metrics.[47]

Some limitations should be acknowledged. First, despite the advanced MRI sequences, multi-shell diffusion data were only available as part of the third follow-up assessment in the RUN DMC study. Future longitudinal studies should therefore be carried out to disentangle the temporal relationships between cholinergic deficits and motoric cognitive dysfunction. Second, we have excluded participants with non-vascular dementia (Alzheimer's dementia, dementia with Lewy bodies) or Parkinson's disease to attempt to minimize the influence of non-SVD pathologies (Aβ, tau, α-synuclein) on the disruption of cholinergic pathways. However, these markers, often accumulate with age, cannot be fully taken into account in this study due to the lack of specific biomarkers. However, their potential influence may be limited, since one study suggested that SVD markers, rather than Aβ and tau pathology, are the key contributors to the degeneration of cholinergic WM[8].[8] Third, we should be cautious to interpret the cholinergic tracts disruption as a proxy of cholinergic dysfunction. The identification of these tracts was accomplished through tractography using diffusion MRI, incorporating constraints from various anatomical regions within the cholinergic circuits. Although this reconstruction method is recognized as reliable and valid,[7,8,12] it is important to acknowledge that these tracts are primarily innervated by cholinergic neurons, yet some spatial overlap with fibers innervated by other neurotransmitters may exist. Further studies using PET tracers specifically designed for the cholinergic system are necessary to validate our findings. Finally, the principal component analysis was used with three cognitive variables and only one gait variable. The inclusion of additional gait variables, such as gait length and variability, particularly those that are correlated could enhance the capacity to capture shared variance between cognition and gait, facilitating more accurate interpretations of the findings. Therefore, incorporating spatiotemporal gait parameters in future studies could significantly deepen our understanding of the interplay between these domains.

In conclusion, our findings show that microstructural alterations in cholinergic cortical pathways that are attributable to SVD markers, rather than cholinergic thalamic pathways, are related to motor and cognitive dysfunction in patients with SVD. These findings suggest a shared neural mechanism underlying the combined performance of cognition and gait, therefore advancing current understanding on pathophysiological mechanism behind these clinical symptoms in SVD. Given the role of cholinergic vulnerability in both worse cognitive and motor performance in SVD patients, the cholinergic system has the potential to be a potential target in the treatment and rehabilitation approaches.

Supplementary materials

Materials and methods

Cognitive assessment

Processing speed was assessed using the Trail Making Test A (TMT-A) and Symbol-Digit Modalities Test (SDMT); executive function was assessed using the TMT B/A ratio score and the Verbal Fluency test (animal and profession naming); memory was assessed using the forward and backward scores of the Digit Span test, the immediate and delayed recall scores of the Rey Auditory Verbal Learning Test (RAVLT) and the immediate and delayed recall score of Complex Figure Test (CFT). The raw test scores were standardized as z-scores. Next, compound scores were computed per cognitive domain: processing speed was calculated by the sum of (1) the inverse Z score of the TMT-A, (2) the Z score of SDMT; executive function was calculated by the sum of (1) the inverse Z score of the TMT ratio (TMT-B/TMT-A), (2) the average Z score of Verbal Fluency Test of animal naming and job naming; memory was calculated as the sum of (1) the Z score of DST, (2) the average Z score of RAVLT of immediate recall and delayed recall; (3) the average Z score of CFT of immediate recall and delayed recall. (Table e-1).

MRI acquisition

Parameters for each sequence: 3D T1-weighted Magnetization Prepared 2 Rapid Acquisition Gradient Echoes (MP2RAGE): 0.85mm isotropic voxels, repetition time (TR) = 5500 ms, inversion time (TI1 and TI2) = 700 and 2500 ms, field of view (FOV) = 218×272mm^2, Flip Angle = 4°; 3D multi- echo fast low-angle shot images (9 echoes): 0.85mm isotropic voxels, TR = 44ms, ΔTE = 4ms, FOV = 197×245mm^2, Flip angle = 20°; 3D fluid-attenuated inversion recovery (FLAIR) image: 0.85mm isotropic voxels, TR = 5000ms, TE = 394 ms, TI = 1800ms, FOV = 163×272mm^2, Flip angle = 120; Multi-shell DWI using multi-band accelerated echo planar imaging (EPI): 99 diffusion-weighted directions (3 × b = 200, 6 × b = 500, 30 × b = 1,000, and 60 × b = 3,000s/mm^2), 10 × b = 0 images, 1.7mm isotropic voxels, TR = 3220ms, TE = 74 ms, FOV = 221×221mm^2 , Flip angle = 90°; one b=0 image with acquisition parameters equal to the previous b=0 images, but acquired in opposite phase-encoding direction.

Table e-1. Calculation of each cognitive domain

Cognitive domain	Cognitive test	Version	Calculation of compound score
Processing speed	Trail Making Test	Part A[48]	$Z_{TMT\text{-}A} \times -1 + Z_{SDMT}$
	Symbol-Digit Modalities Test	Written version[49]	
Executive function	Trail Making Test	Part B (B/A ratio)[50]	$Z_{(TMT\text{-}B/TMT\text{-}A)} \times -1 + (Z_{VFT\text{-}A} + Z_{VFT\text{-}J})/2$
	Verbal Fluency Test	Animal and profession naming[51]	
Memory	Digit Span test (Forward and backward)	Wechsler Adult Intelligence Scale – 3rd ed.[52]	$Z_{(DST\text{-}f + DST\text{-}b)} + (Z_{RAVLT\text{-}I} + Z_{RAVLT\text{-}D})/2 + (Z_{ROCF\text{-}I} + Z_{ROCF\text{-}D})/2$
	Rey's Auditory Verbal Learning Test (Immediate and delayed recall) [5]	3-trial version[53]	
	Complex Figure Test (Immediate and delayed recall) [6]	MCG Figure 3[54]	

Z, the Z transformed score; DST-f, Digit Span forward test; DST-b, Digit Span backward test; RAVLT-I, Immediate recall of Rey's Auditory Verbal Learning Test; RAVLT-D, the delayed recall of Rey's Auditory Verbal Learning Test; ROCF-I, Immediate recall of Rey–Osterrieth Complex Figure Test; ROCF-D, delayed recall of Rey–Osterrieth Complex Figure Test; TMT, Trail Making Test; SDMT, Symbol-Digit Modalities Test, VFT-A, Verbal Fluency Test (animals); VFT-A, Verbal Fluency Test (professions)

Table e-2. Relations between NODDI metrics of cholinergic pathways and PC1

	Model 1			Model 2		
Predictors	**Std.beta**	**CI**	**p**	**Std.beta**	**CI**	**p**
NBM-EC NDI	12.85	6.88 – 18.81	<0.001	6.59	-0.37 – 13.56	0.063
NBM-CG NDI	11.26	5.39 – 17.13	<0.001	5.15	-1.34 – 11.63	0.119
PPN thalamus NDI	0.40	-4.21 – 5.00	0.866	-0.02	-4.54 – 4.50	0.994
NBM-EC ISOVF	-16.70	-23.15 – -10.25	<0.001	-10.77	-18.05 – -3.49	0.004
NBM-CG ISOVF	-20.39	-30.07 – -10.71	<0.001	-13.38	-23.68 – -3.09	0.011
PPN-thalamus ISOV	-9.74	-16.22 – -3.26	0.003	-6.07	-12.39 – 0.26	0.060

Model 1 adjusted for age, sex, and height, education years, and NODDI metrics in the WM control mask. Model 2 were additionally adjusted for SVD markers. Bold p-values denote the statistical significance. NBM-EC, NBM external capsule cholinergic tract; NBM-CG; NBM_cingulum, cholinergic tract; PPN-thalamus, PPN- thalamus cholinergic tract; NOODDI, Neurite Orientation Dispersion and Density maging; NDI, neurite density index; ODI, orientation dispersion index; ISOVF, CSF isotropic volume fraction; NBM, nucleus basalis of Meynert; PPN, pedunculopontine nucleus;

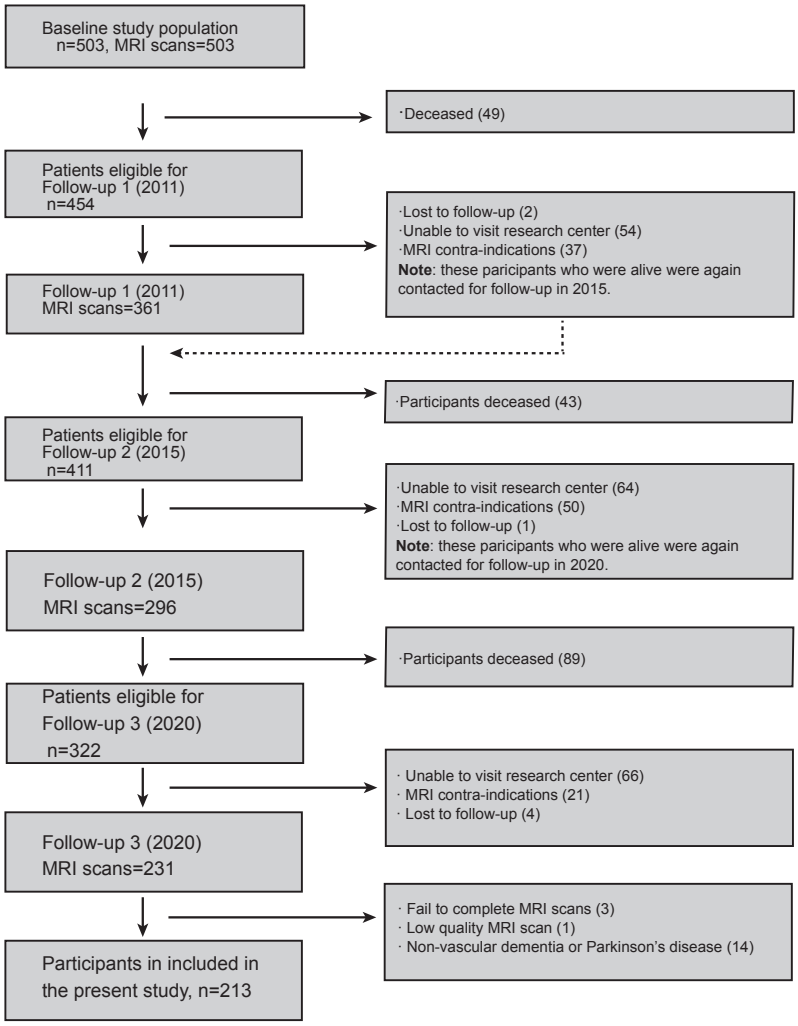

Supplementary Figure 1. Flow chart of the study population.

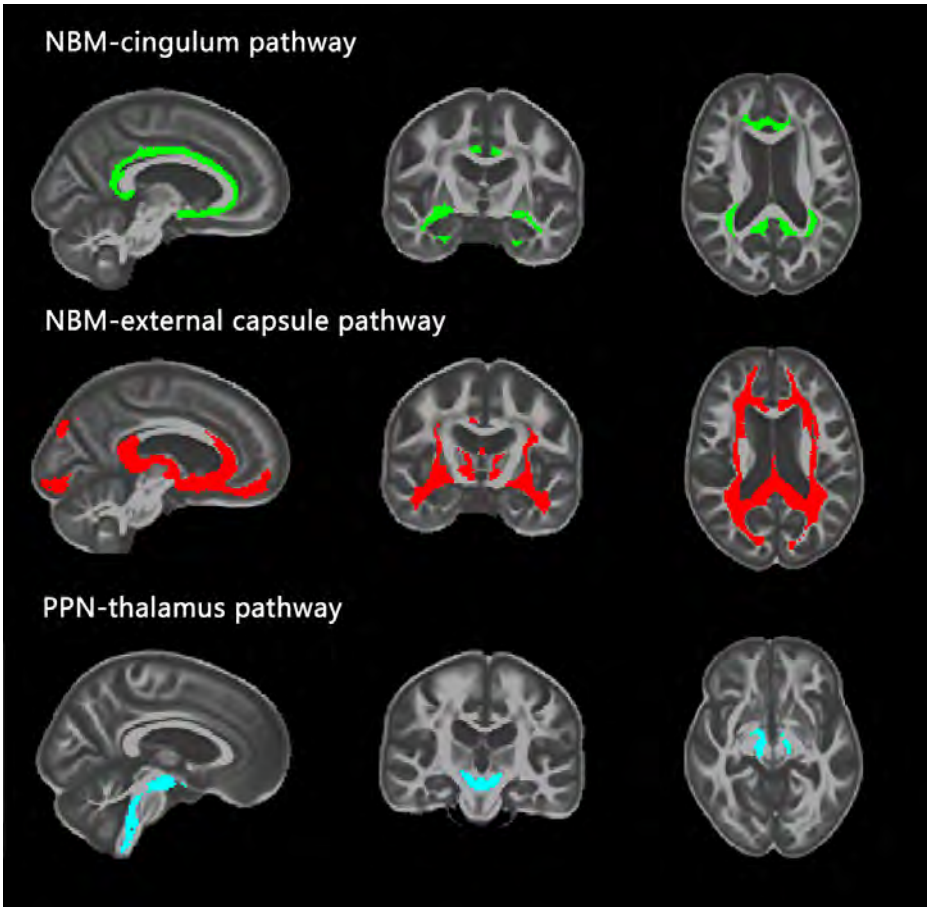

Supplementary Figure 2. Representative images of cholinergic pathways. NBM-EC, NBM-external capsule cholinergic tract (red); NBM-CG; NBM_cingulum, cholinergic tract (green); PPN- thalamus, PPN-thalamus cholinergic tract (cyan).

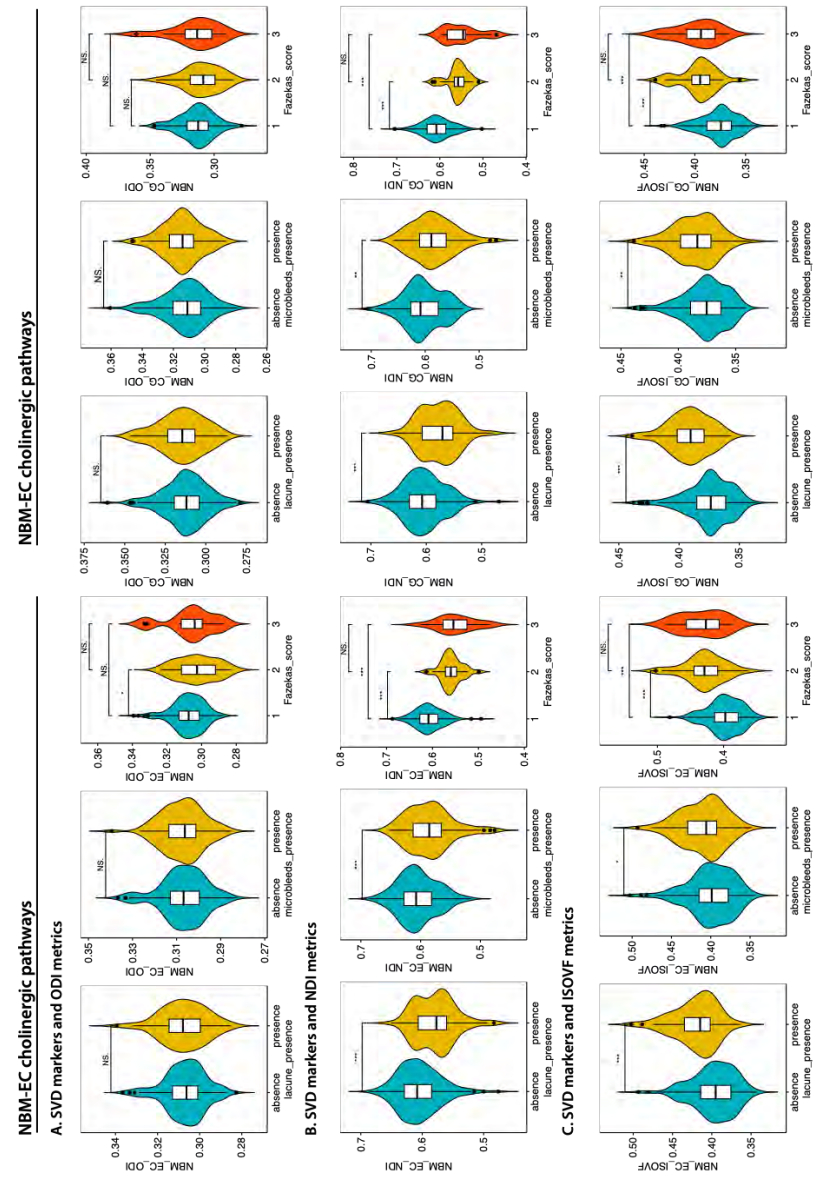

Supplementary Figure 3. SVD markers and NODDI metrics in cholinergic pathways.

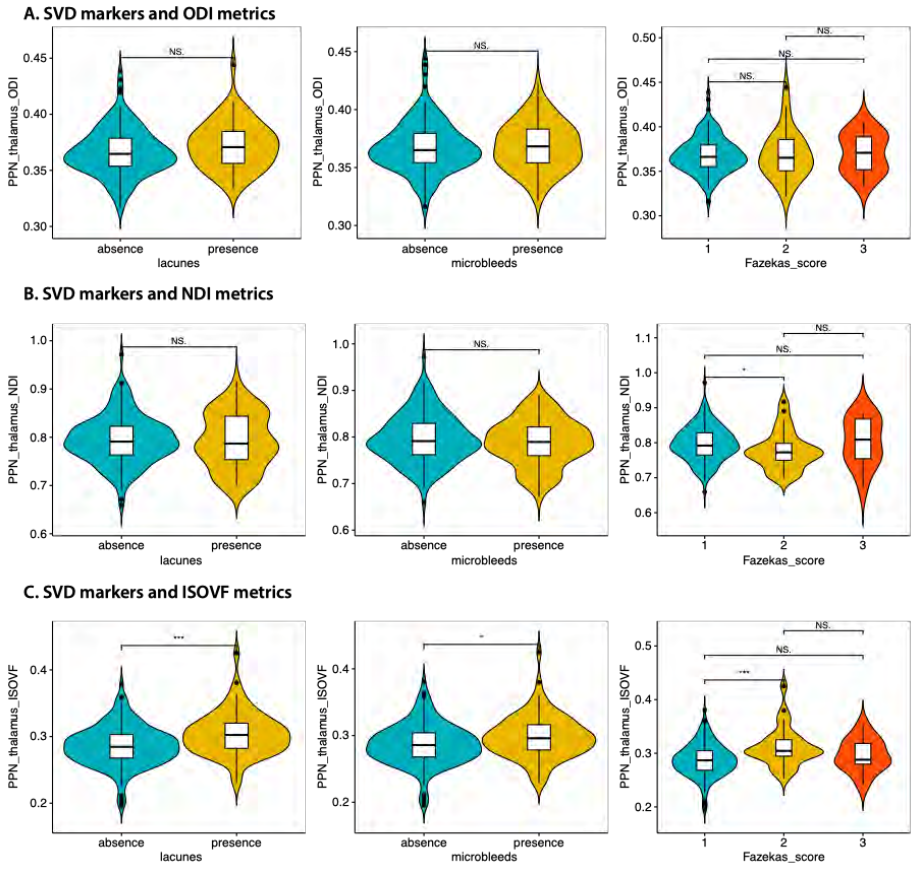

Supplementary figure 4. SVD markers and NODDI metrics in PPN to thalamus cholinergic pathway.

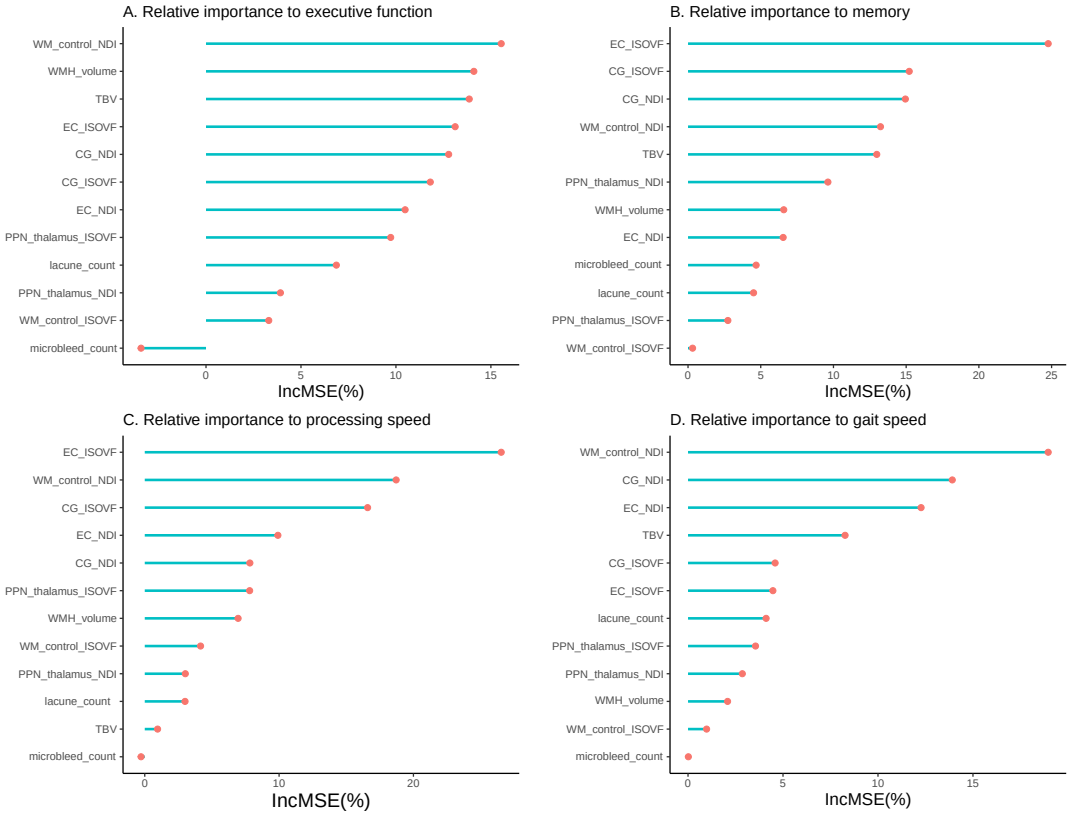

Supplementary Figure 5. Relation importance of imaging markers to cognition and gait. The final importance (%IncMSE) of each predictor denotes its contribution to the model. Importance values below or equal to zero denote no contribution.

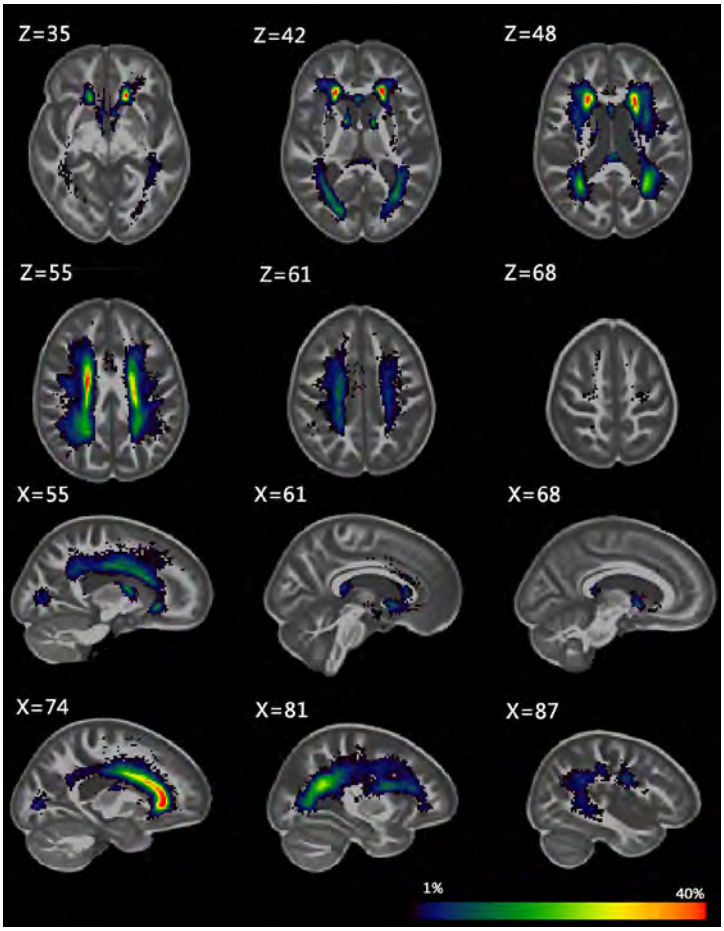

Supplementary Figure 6. WMH lesion probability mappings. To capture the spatial pattern of WMH lesion, we generated the probabilistic lesion mapping, which is a widely used approach to visualize lesion distribution and frequency of lesion occurrence in a given brain location. Probabilistic lesion mapping was generated by first merging and then averaging all the lesion masks onto group template, and it indicated the percentage of patients who had lesions localized in a certain brain region. The registration results were visually inspected, and manual adjustments were made in case of minor displacements. Color bar represents the probability of WMH lesion voxels located in a given area.

Reference

1. Duering M, et al. Neuroimaging standards for research into small vessel disease-advances since 2013. Lancet Neurol. Jul 2023;22(7):602-618. doi:10.1016/s1474-4422(23)00131-x
2. Jacob MA, Cai M, Bergkamp M, Darweesh SKL, Gelissen LMY, Marques J, Norris DG, Duering M, Esselink RAJ, Tuladhar AM, de Leeuw FE. Cerebral Small Vessel Disease Progression Increases Risk of Incident Parkinsonism. Ann Neurol. Jun 2023;93(6):1130-1141. doi:10.1002/ana.26615
3. Cai M, Jacob MA, Norris DG, Duering M, de Leeuw FE, Tuladhar AM. Cognition mediates the relation between structural network efficiency and gait in small vessel disease. Neuroimage Clin. 2021;30:102667. doi:10.1016/j.nicl.2021.102667
4. Morris R, Lord S, Bunce J, Burn D, Rochester L. Gait and cognition: Mapping the global and discrete relationships in ageing and neurodegenerative disease. Neurosci Biobehav Rev. May 2016;64:326-45. doi:10.1016/j.neubiorev.2016.02.012
5. Cai M, Jacob MA, Norris DG, de Leeuw FE, Tuladhar AM. Longitudinal Relation Between Structural Network Efficiency, Cognition, and Gait in Cerebral Small Vessel Disease. J Gerontol A Biol Sci Med Sci. Mar 3 2022;77(3):554-560. doi:10.1093/gerona/glab247
6. Verghese J, Ayers E, Barzilai N, Bennett DA, Buchman AS, Holtzer R, Katz MJ, Lipton RB, Wang C. Motoric cognitive risk syndrome: Multicenter incidence study. Neurology. Dec 9 2014;83(24):2278-84. doi:10.1212/wnl.0000000000001084
7. Nemy M, Cedres N, Grothe MJ, Muehlboeck JS, Lindberg O, Nedelska Z, Stepankova O, Vyslouzilova L, Eriksdotter M, Barroso J, Teipel S, Westman E, Ferreira D. Cholinergic white matter pathways make a stronger contribution to attention and memory in normal aging than cerebrovascular health and nucleus basalis of Meynert. Neuroimage. May 1 2020;211:116607. doi:10.1016/j.neuroimage.2020.116607
8. Cedres N, Ferreira D, Nemy M, Machado A, Pereira JB, Shams S, Wahlund LO, Zettergren A, Stepankova O, Vyslouzilova L, Eriksdotter M, Teipel S, Grothe MJ, Blennow K, Zetterberg H, Schöll M, Kern S, Skoog I, Westman E. Association of Cerebrovascular and Alzheimer Disease Biomarkers With Cholinergic White Matter Degeneration in Cognitively Unimpaired Individuals. Neurology. Oct 11 2022;99(15):e1619-e1629. doi:10.1212/wnl.0000000000200930
9. Schumacher J, Ray N, Teipel S, Storch A. Associations of cholinergic system integrity with cognitive decline in GBA1 and LRRK2 mutation carriers. NPJ Parkinsons Dis. Jun 29 2024;10(1):127. doi:10.1038/s41531-024-00743-w
10. Schumacher J, Ray NJ, Hamilton CA, Bergamino M, Donaghy PC, Firbank M, Watson R, Roberts G, Allan L, Barnett N, O'Brien JT, Thomas AJ, Taylor JP. Free water imaging of the cholinergic system in dementia with Lewy bodies and Alzheimer's disease. Alzheimers Dement. Oct 2023;19(10):4549-4563. doi:10.1002/alz.13034
11. Bohnen NI, Yarnall AJ, Weil RS, Moro E, Moehle MS, Borghammer P, Bedard MA, Albin RL. Cholinergic system changes in Parkinson's disease: emerging therapeutic approaches. Lancet Neurol. Apr 2022;21(4):381-392. doi:10.1016/s1474-4422(21)00377-x
12. Nemy M, et al. Cholinergic white matter pathways along the Alzheimer's disease continuum. Brain. May 2 2023;146(5):2075-2088. doi:10.1093/brain/awac385
13. Schumacher J, Ray NJ, Hamilton CA, Donaghy PC, Firbank M, Roberts G, Allan L, Durcan R, Barnett N, O'Brien JT, Taylor JP, Thomas AJ. Cholinergic white matter pathways in dementia with Lewy bodies and Alzheimer's disease. Brain. Jun 3 2022;145(5):1773-1784. doi:10.1093/brain/awab372

14. Crowley SJ, Kanel P, Roytman S, Bohnen NI, Hampstead BM. Basal forebrain integrity, cholinergic innervation and cognition in idiopathic Parkinson's disease. Brain. May 3 2024;147(5):1799-1808. doi:10.1093/brain/awad420

15. Biesbroek JM, Verhagen MG, van der Stigchel S, Biessels GJ. When the central integrator disintegrates: A review of the role of the thalamus in cognition and dementia. Alzheimers Dement. Mar 2024;20(3):2209-2222. doi:10.1002/alz.13563

16. Li H, Cai M, Jacob MA, Norris DG, Marques JP, Chamberland M, Duering M, Kessels RPC, de Leeuw FE, Tuladhar AM. Dissociable Contributions of Thalamic-Subregions to Cognitive Impairment in Small Vessel Disease. Stroke. May 2023;54(5):1367-1376. doi:10.1161/strokeaha.122.041687

17. Konieczny MJ, Dewenter A, Ter Telgte A, Gesierich B, Wiegertjes K, Finsterwalder S, Kopczak A, Hübner M, Malik R, Tuladhar AM, Marques JP, Norris DG, Koch A, Dietrich O, Ewers M, Schmidt R, de Leeuw FE, Duering M. Multi-shell Diffusion MRI Models for White Matter Characterization in Cerebral Small Vessel Disease. Neurology. Feb 2 2021;96(5):e698-e708. doi:10.1212/wnl.0000000000011213

18. van Norden AG, de Laat KF, Gons RA, van Uden IW, van Dijk EJ, van Oudheusden LJ, Esselink RA, Bloem BR, van Engelen BG, Zwarts MJ, Tendolkar I, Olde-Rikkert MG, van der Vlugt MJ, Zwiers MP, Norris DG, de Leeuw FE. Causes and consequences of cerebral small vessel disease. The RUN DMC study: a prospective cohort study. Study rationale and protocol. BMC Neurol. Feb 28 2011;11:29. doi:10.1186/1471-2377-11-29

19. Cai M, Jacob MA, van Loenen MR, Bergkamp M, Marques J, Norris DG, Duering M, Tuladhar AM, de Leeuw FE. Determinants and Temporal Dynamics of Cerebral Small Vessel Disease: 14-Year Follow-Up. Stroke. Sep 2022;53(9):2789-2798. doi:10.1161/strokeaha.121.038099

20. Fazekas F, Chawluk JB, Alavi A, Hurtig HI, Zimmerman RA. MR signal abnormalities at 1.5 T in Alzheimer's dementia and normal aging. AJR Am J Roentgenol. Aug 1987;149(2):351-6. doi:10.2214/ajr.149.2.351

21. Andersson JLR, Sotiropoulos SN. An integrated approach to correction for off-resonance effects and subject movement in diffusion MR imaging. Neuroimage. Jan 15 2016;125:1063-1078. doi:10.1016/j.neuroimage.2015.10.019

22. Veraart J, Novikov DS, Christiaens D, Ades-Aron B, Sijbers J, Fieremans E. Denoising of diffusion MRI using random matrix theory. Neuroimage. Nov 15 2016;142:394-406. doi:10.1016/j.neuroimage.2016.08.016

23. Kellner E, Dhital B, Kiselev VG, Reisert M. Gibbs-ringing artifact removal based on local subvoxel-shifts. Magn Reson Med. Nov 2016;76(5):1574-1581. doi:10.1002/mrm.26054

24. Li H, Jacob MA, Cai M, Kessels RPC, Norris DG, Duering M, de Leeuw FE, Tuladhar AM. Meso-cortical pathway damage in cognition, apathy and gait in cerebral small vessel disease. Brain. Nov 4 2024;147(11):3804-3816. doi:10.1093/brain/awae145

25. Zhang H, Schneider T, Wheeler-Kingshott CA, Alexander DC. NODDI: practical in vivo neurite orientation dispersion and density imaging of the human brain. Neuroimage. Jul 16 2012;61(4):1000-16. doi:10.1016/j.neuroimage.2012.03.072

26. Raghavan S, Reid RI, Przybelski SA, Lesnick TG, Graff-Radford J, Schwarz CG, Knopman DS, Mielke MM, Machulda MM, Petersen RC, Jack CR, Jr., Vemuri P. Diffusion models reveal white matter microstructural changes with ageing, pathology and cognition. Brain Commun. 2021;3(2):fcab106. doi:10.1093/braincomms/fcab106

27. Raghavan S, Przybelski SA, Reid RI, Lesnick TG, Ramanan VK, Botha H, Matchett BJ, Murray ME, Reichard RR, Knopman DS, Graff-Radford J, Jones DT, Lowe VJ, Mielke MM, Machulda MM, Petersen RC, Kantarci K, Whitwell JL, Josephs KA, Jack CR, Jr., Vemuri P. White matter damage due to vascular, tau, and TDP-43 pathologies and its relevance to cognition. Acta Neuropathol Commun. Feb 5 2022;10(1):16. doi:10.1186/s40478-022-01319-6

28. Jbabdi S, Sotiropoulos SN, Savio AM, Graña M, Behrens TE. Model-based analysis of multishell diffusion MR data for tractography: how to get over fitting problems. Magn Reson Med. Dec 2012;68(6):1846-55. doi:10.1002/mrm.24204

29. Selden NR, Gitelman DR, Salamon-Murayama N, Parrish TB, Mesulam MM. Trajectories of cholinergic pathways within the cerebral hemispheres of the human brain. Brain. Dec 1998;121 (Pt 12):2249-57. doi:10.1093/brain/121.12.2249

30. Aravamuthan BR, Muthusamy KA, Stein JF, Aziz TZ, Johansen-Berg H. Topography of cortical and subcortical connections of the human pedunculopontine and subthalamic nuclei. Neuroimage. Sep 1 2007;37(3):694-705. doi:10.1016/j.neuroimage.2007.05.050

31. Kilimann I, Grothe M, Heinsen H, Alho EJ, Grinberg L, Amaro E, Jr., Dos Santos GA, da Silva RE, Mitchell AJ, Frisoni GB, Bokde AL, Fellgiebel A, Filippi M, Hampel H, Klöppel S, Teipel SJ. Subregional basal forebrain atrophy in Alzheimer's disease: a multicenter study. J Alzheimers Dis. 2014;40(3):687-700. doi:10.3233/jad-132345

32. Li J, Guan X, Wu Q, He C, Zhang W, Lin X, Liu C, Wei H, Xu X, Zhang Y. Direct localization and delineation of human pedunculopontine nucleus based on a self-supervised magnetic resonance image super-resolution method. Hum Brain Mapp. Jun 15 2023;44(9):3781-3794. doi:10.1002/hbm.26311

33. Puonti O, Iglesias JE, Van Leemput K. Fast and sequence-adaptive whole-brain segmentation using parametric Bayesian modeling. Neuroimage. Dec 2016;143:235-249. doi:10.1016/j.neuroimage.2016.09.011

34. Avants BB, Epstein CL, Grossman M, Gee JC. Symmetric diffeomorphic image registration with cross-correlation: evaluating automated labeling of elderly and neurodegenerative brain. Med Image Anal. Feb 2008;12(1):26-41. doi:10.1016/j.media.2007.06.004

35. Behrens TE, Berg HJ, Jbabdi S, Rushworth MF, Woolrich MW. Probabilistic diffusion tractography with multiple fibre orientations: What can we gain? Neuroimage. Jan 1 2007;34(1):144-55. doi:10.1016/j.neuroimage.2006.09.018

36. Lyons JG, Heeren T, Stuver SO, Fredman L. Assessing the agreement between 3-meter and 6-meter walk tests in 136 community-dwelling older adults. J Aging Health. Jun 2015;27(4):594-605. doi:10.1177/0898264314556987

37. Duering M, Finsterwalder S, Baykara E, Tuladhar AM, Gesierich B, Konieczny MJ, Malik R, Franzmeier N, Ewers M, Jouvent E, Biessels GJ, Schmidt R, de Leeuw FE, Pasternak O, Dichgans M. Free water determines diffusion alterations and clinical status in cerebral small vessel disease. Alzheimers Dement. Jun 2018;14(6):764-774. doi:10.1016/j.jalz.2017.12.007

38. Machado A, Barroso J, Molina Y, Nieto A, Díaz-Flores L, Westman E, Ferreira D. Proposal for a hierarchical, multidimensional, and multivariate approach to investigate cognitive aging. Neurobiol Aging. Nov 2018;71:179-188. doi:10.1016/j.neurobiolaging.2018.07.017

39. Braeken J, Van Assen MA. An empirical Kaiser criterion. Psychological methods. 2017;22(3):450.

40. Dziuban CD, Shirkey EC. When is a correlation matrix appropriate for factor analysis? Some decision rules. Psychological bulletin. 1974;81(6):358.

41. Dewenter A, Jacob MA, Cai M, Gesierich B, Hager P, Kopczak A, Biel D, Ewers M, Tuladhar AM, de Leeuw FE, Dichgans M, Franzmeier N, Duering M. Disentangling the effects of Alzheimer's and small vessel disease on white matter fibre tracts. Brain. Feb 13 2023;146(2):678-689. doi:10.1093/brain/awac265

42. van den Heuvel MP, Sporns O. Rich-club organization of the human connectome. J Neurosci. Nov 2 2011;31(44):15775-86. doi:10.1523/jneurosci.3539-11.2011

43. Duering M, Zieren N, Hervé D, Jouvent E, Reyes S, Peters N, Pachai C, Opherk C, Chabriat H, Dichgans M. Strategic role of frontal white matter tracts in vascular cognitive impairment: a voxel-based lesion-symptom mapping study in CADASIL. Brain. Aug 2011;134(Pt 8):2366-75. doi:10.1093/brain/awr169

44. van Leijsen EMC, van Uden IWM, Bergkamp MI, van der Holst HM, Norris DG, Claassen J, Kessels RPC, de Leeuw FE, Tuladhar AM. Longitudinal changes in rich club organization and cognition in cerebral small vessel disease. Neuroimage Clin. 2019;24:102048. doi:10.1016/j.nicl.2019.102048

45. Li H, Jacob MA, Cai M, Duering M, Chamberland M, Norris DG, Kessels RPC, de Leeuw FE, Marques JP, Tuladhar AM. Regional cortical thinning, demyelination and iron loss in cerebral small vessel disease. Brain. Nov 2 2023;146(11):4659-4673. doi:10.1093/brain/awad220

46. Taylor JP, McKeith IG, Burn DJ, Boeve BF, Weintraub D, Bamford C, Allan LM, Thomas AJ, O'Brien JT. New evidence on the management of Lewy body dementia. Lancet Neurol. Feb 2020;19(2):157-169. doi:10.1016/s1474-4422(19)30153-x

47. Kraguljac NV, Guerreri M, Strickland MJ, Zhang H. Neurite Orientation Dispersion and Density Imaging in Psychiatric Disorders: A Systematic Literature Review and a Technical Note. Biol Psychiatry Glob Open Sci. Jan 2023;3(1):10-21. doi:10.1016/j.bpsgos.2021.12.012

48. Bowie CR, Harvey PD. Administration and interpretation of the Trail Making Test. Nat Protoc. 2006;1(5):2277-81. doi:10.1038/nprot.2006.390

49. Smith A. Symbol digit modalities test. Los Angeles, CA. 2013;

50. Oosterman JM, Vogels RL, van Harten B, Gouw AA, Poggesi A, Scheltens P, Kessels RP, Scherder EJ. Assessing mental flexibility: neuroanatomical and neuropsychological correlates of the Trail Making Test in elderly people. Clin Neuropsychol. Feb 2010;24(2):203-19. doi:10.1080/13854040903482848

51. Van der Elst W, Van Boxtel MP, Van Breukelen GJ, Jolles J. Normative data for the Animal, Profession and Letter M Naming verbal fluency tests for Dutch speaking participants and the effects of age, education, and sex. J Int Neuropsychol Soc. Jan 2006;12(1):80-9. doi:10.1017/s1355617706060115

52. Wechsler D. Wechsler adult intelligence scale. Archives of Clinical Neuropsychology. 1955;

53. Van der Elst W, van Boxtel MP, van Breukelen GJ, Jolles J. Rey's verbal learning test: normative data for 1855 healthy participants aged 24-81 years and the influence of age, sex, education, and mode of presentation. J Int Neuropsychol Soc. May 2005;11(3):290-302. doi:10.1017/s1355617705050344

54. Loring D, Meador K. The Medical College of Georgia (MCG) complex figures: four forms for follow-up. Rey-Osterrieth handbook Psychological Assessment Resources. 2003;

Part III.

Beyond focal lesion: the remote effects in cerebral small vessel disease

Chapter 5.

Regional cortical thinning, demyelination and iron loss in cerebral small vessel disease

Published as:
Hao Li, Mina A Jacob, Mengfei Cai, Marco Duering, Maxime Chamberland, David G Norris, Roy PC Kessels, Frank-Erik de Leeuw, José P Marques, Anil M Tuladhar. Regional cortical thinning, demyelination and iron loss in cerebral small vessel disease. Brain, 146(11): 4659-4673, 2023.

Abstract

The link between white matter hyperintensities (WMH) and cortical thinning is thought to be an important pathway by which WMH contributes to cognitive deficits in cerebral small vessel disease (SVD). However, the mechanism behind this association and the underlying tissue composition abnormalities are unclear. The objective of this study is to determine the association between WMH and cortical thickness, and the in-vivo tissue composition abnormalities in the WMH-connected cortical regions.

In this cross-sectional study, we included 213 participants with SVD who underwent standardized protocol including multimodal neuroimaging scans and cognitive assessment (i.e., processing speed, executive function, and memory). We identified the cortex connected to WMH using probabilistic tractography starting from the WMH and defined the WMH-connected regions at three connectivity levels (low, medium, and high connectivity level). We calculated the cortical thickness, myelin and iron of the cortex based on T1-weighted, quantitative R1, R2*, and susceptibility maps. We used diffusion-weighted imaging to estimate the mean diffusivity (MD) of the connecting white matter tracts.

We found that cortical thickness, R1, R2*, and susceptibility values in the WMH-connected regions were significantly lower than in the WMH-unconnected regions (all $p\text{-corrected}<0.001$). Linear regression analyses showed that higher MD of the connecting white matter tracts were related to lower thickness ($\beta=-0.30$, $p\text{-corrected}<0.001$), R1 ($\beta=-0.26$, $p\text{-corrected}=0.001$), R2* ($\beta=-0.32$, $p\text{-corrected}<0.001$) and susceptibility values ($\beta=-0.39$, $p\text{-corrected}<0.001$) of WMH-connected cortical regions at high connectivity level. In addition, lower scores on processing speed were significantly related to lower cortical thickness ($\beta=0.20$, $p\text{-corrected}=0.030$), lower R1 values ($\beta=0.20$, $p\text{-corrected}=0.006$), lower R2* values ($\beta=0.29$, $p\text{-corrected}=0.006$), and lower susceptibility values ($\beta=0.19$, $p\text{-corrected}=0.024$) of the WMH-connected regions at high connectivity level, independent of WMH volumes and the cortical measures of WMH-unconnected regions.

Together, our study demonstrated that the microstructural integrity of white matter tracts passing through WMH is related to the regional cortical abnormalities as measured by thickness, R1, R2* and susceptibility values in the connected cortical regions. These findings are indicative of cortical thinning, demyelination and iron loss in the cortex, which is most likely through the disruption of the connecting white matter tracts and may contribute to processing speed impairment in SVD,

a key clinical feature of SVD. These findings may have implications for finding intervention targets for the treatment of cognitive impairment in SVD by preventing secondary degeneration.

Introduction

Cerebral small vessel disease (SVD) is a disease that affects small vessels of the brain and is the leading cause of vascular cognitive impairment and dementia.[1,2] The features of SVD seen on MRI include white matter hyperintensities (WMH), lacunes of presumed vascular origin, and cerebral microbleeds (CMBs), with WMH being the most common and prominent MRI marker.[1] Many studies have shown an association between WMH and cortical thinning.[3-5] However, the mechanism behind this association, as well as the tissue composition changes underpinning the decreased cortical thickness, are complex and poorly understood.

Secondary neurodegeneration has been proposed as a potential mechanism through which WMH may contribute to thinning of the regional cortex connected to WMH, thereby influencing the clinical status of SVD.[2] Studies in other subcortical ischemic lesions, such as incident lacunes and subcortical infarcts, have shown that regional cortical thinning occurred in areas connected to the initial lesion as a result of degeneration of the connecting white matter tracts, providing evidence for secondary neurodegeneration.[6,7] In WMH, this mechanism was also partly supported by Mayer C *et al.*[8] study, which examined the association between WMH connectivity and cortical thickness. Specifically, the probabilities that WMH and the cortex are connected through white matter tracts, defined as WMH connectivity, showed a negative association with cortical thickness in their study. However, this study was conducted on a community-based population and did not assess the link between reduced cortical thickness and the microstructural damage of the white matter tracts connecting WMH and cortex. These limitations constrain the generalizability of their findings in the SVD population and weaken the evidence supporting the proposed mechanism.

In addition to cortical thinning, other tissue changes in the WMH-connected cortex may occur, including changes in the myelin density and iron deposition. Quantitative MRI (qMRI), such as quantitative R1 (1/T1) maps, quantitative R2* (1/T2*) maps and quantitative susceptibility maps (QSM), could provide specific indices of in-vivo tissue composition.[9] Previous combined histopathology-MRI studies have demonstrated that the R1 value is mainly positively correlated with myelin;[10] R2* value is positively correlated with both myelin and iron;[11] and the susceptibility value is mainly positively correlated with iron and negatively correlated with myelin.[12] Therefore, the combination of R1, R2* and susceptibility indexes allows us to accurately probe the myelin density and iron deposition in the cortical tissue. So far, to the best of our knowledge, no study has in-vivo measured

cortical myelin and iron in regions connected to WMH using the combination of quantitative R1, R2* maps and QSM in SVD.

The goal of this study is to employ a multimodal neuroimaging approach to systematically assess the cortical abnormalities in the WMH-connected regional cortex, as well as their associations with microstructural damage of the connecting white matter tracts in SVD patients. We hypothesized that measures of thickness, myelin and iron in the cortical regions connected to WMH are related to the microstructural integrity of the white matter tracts connecting the WMH and the cortex. To test our hypothesis, we utilized a range of advanced MRI methodologies, including high-resolution T1-maps, quantitative R1, R2*, susceptibility maps, and diffusion-weighted images (DWI) for probabilistic tractography, to specifically measure the cortical thickness, myelin content, and iron deposition in the WMH-connected regional cortex. We tested the relations between these measures in the WMH-connected cortical regions and the mean diffusivity (MD) values of the connecting white matter tracts, and related the effects of these measures in the WMH-connected cortical regions to cognitive performance.

Materials and methods

Study population

Data were derived from the Radboud University Nijmegen Diffusion tensor and Magnetic resonance imaging Cohort (RUN DMC) study, which is an ongoing prospective study that aims to investigate the causes and clinical consequences of sporadic SVD. Detailed information on the RUN DMC study has been described previously.[13] In brief, the participants were included in 2006 based on the following criteria: (1) age between 50 and 85 years, (2) cerebral SVD on MRI (defined as WMH or lacunes) and cognitive or motor symptoms that could be attributed to SVD. After the baseline data collection, follow-ups were conducted in 2011, 2015, and 2020. We included 230 participants who participated in the third follow-up assessment (2020), based on the availability of Magnetization Prepared 2 Rapid Acquisition Gradient Echoes (MP2RAGE), multi-echo gradient echo (GRE) and multi-shell DWI sequences to perform a cross-sectional analysis. Of the 230 participants, 17 participants were excluded due to the lack of required MRI scans (n=7), low quality of MRI images (n=2), and obvious head movements (n=8) (Figure e-1). The study was approved by the Medical Review Ethics Committee Region Arnhem-Nijmegen, and written informed consent was obtained from all participants.

Neuropsychological assessment

All participants underwent a detailed cognitive assessment. For this study, we used cognitive data covering three cognitive domains: processing speed, executive function, and memory. The raw scores of each cognitive test were standardized as z-scores and then used to compute a compound score for each cognitive domain. Details of these cognitive tests and the calculation of compound scores per cognitive domain were provided in Supplementary (Table e-1).

MRI acquisition

Participants underwent MRI scanning on a 3T MRI scanner (MAGNETOM Prisma; Siemens Healthineers, Erlangen, Germany) with a 32-channel head coil, including the following sequences: MP2RAGE to construct robust T1-weighted (T1W) image and quantitative R1 maps, 3D multi-echo GRE providing magnitude and phase images to create susceptibility weighted image (SWI), R2* (1/T2*) maps and QSM, 3D fluid-attenuated inversion recovery (FLAIR) image and multi-shell DWI. Detailed parameters for each sequence were provided in the Supplementary Data and described previously.[13]

WMH segmentation

We used a validated 3-dimensional U-net deep learning algorithm to automatically segment WMH on registered and bias-corrected T1 and FLAIR images.[14] All segmented WMH masks were visually inspected. The lacunes located within or at the edge of WMH were excluded from the WMH mask. T1W images were segmented into grey matter (GM), white matter (WM), and cerebrospinal fluid (CSF) using unified segmentation from the SPM12 toolbox. To avoid misclassifying WMH as GM, these segmented GM, WM, and CSF images were corrected using the WMH mask. The intracranial volume (ICV) was calculated as the sum of the GM, WM, and CSF volumes. WMH volumes were corrected for the ICV.

We performed visual assessments of SVD markers (WMH, lacunes and cerebral microbleeds) on MRI in accordance with the Standards for Reporting Vascular changes on neuroimaging (STRIVE).[1] Given the absence of perivascular space (PVS) information in our cohort, we did not include PVS in the SVD assessment. WMH was scored using a modified Fazekas scale (mild WMH: Fazekas score 0–1, moderate WMH: Fazekas score 2, severe WMH: Fazekas score 3).[15] Subsequently, a simple SVD score consisting of WMH, lacunes, and CMBs was generated to assess the total SVD burden.[16] In this simple SVD score, one point was respectively assigned for the WMH Fazekas score ≥ 2, the number of lacunes ≥ 3, the presence of CMBs, as described in previous study.[16,17]

Diffusion MRI processing

Multi-shell diffusion MRI data were preprocessed for denoising and Gibbs artefact removal using tools from MRtrix 3.0 (http://www.mrtrix.org) and subsequently corrected for head motion, eddy currents-induced distortions, susceptibility-induced distortions (topup), intensity bias using the Functional Magnetic Resonance Imaging of the Brain Software Library (FSL; v6.0.1) and the Advanced Normalization Tools (ANTs, v 2.1.0).[18-22] Next, we used the Bedpostx function within FSL to estimate the voxel-wise multi-fiber directions based on the ball-and-two-sticks model.[23] Subsequently, tensor fit for the processed diffusion image (only $b = 0$ and $b = 1000$ s/mm^2 image) was executed using the dtifit function within FSL to produce the fractional anisotropy (FA) and MD images for each participant.

Identification of connected cortex

Probabilistic tractography was performed using the probtractx2 function within FSL software with the default parameters. WMH mask was employed as the seed mask and the WM/GM matter boundary derived from Freesurfer (version 7.1.0) as the target mask, producing the "fdt_path" images. In the cortical part of the "fdt_path" image, each voxel value represents the numbers of streamlines connecting cortex and WMH. Subsequently, voxel values in cortical part of the "fdt_path" image were normalized by dividing the total number of streamlines sent out from the seed masks (5000 times per voxel), resulting a probability map of the cortex connected to WMH. This map was further thresholded at three levels (low, medium, and high), as described in the supplementary materials and previous studies.[6,7] Lower connectivity levels are more susceptible to noise and may lead to false-positive tracts, whereas higher levels are more specific but might eliminate subordinate connectivity. It is crucial to emphasize that the term "connectivity level" in our study refers solely to the connectivity profile of the cortex (i.e., the connectivity probability to WMH), and does not function as a surrogate marker for white matter microstructural integrity. The cortical regions connected by the tracts were identified as WMH-connected regions. Cortex outside the connected region was defined as WMH-unconnected regions and employed as a control representing the global tissue composition abnormalities unrelated to the WMH (Figure 1A).[6,7] Details were provided in the Supplementary Data.

Cortical surface reconstruction and cortical thickness analysis

MP2RAGE images were processed to create the robust T1W image, using a home-made MATLAB (R2016b; MathWorks, Natick, MA) script,[24] which has the advantage of combining the unbiased tissue contrast, while enabling robust and reproducible tissue segmentation[25]. The robust T1W image was fed into the standard 'recon-

all' processing pipeline within Freesurfer to reconstruct the cortical surface and estimate cortical thickness. The resulting CSF/GM boundary (pial surface) and GM/WM boundary (white matter surface) were visually inspected to avoid obvious reconstruction errors. Cortical thickness was measured as the distance between the pial surface and the white matter surface. Notably, given the nonuniform distribution of cortical thickness across the brain regions and the certain connectivity patterns of the WMH to the cortex,[8,26] it will be hard to attribute any potential thinner cortical thickness detected in the WMH-connected regions to the remote effects of WMH or the inter-regional differences of cortical thickness. To minimize this effect, we calculated the mean cortical thickness of each brain region using the *Desikan-Killiany* atlas, which parcellates the cortex into 68 regions based on the morphologic features.[27] We then normalized the inter-regional differences by dividing the value of each vertex in the cortical thickness map by the average cortical thickness of the corresponding cortical region of the study population (Figure 1C, Figure e-2). The normalized cortical thickness map was subsequently smoothed to improve the signal-to-noise ratio. The smooth size was set at a 10 mm full-width at half maximum (FWMH) Gaussian Kernel,[28] as larger smoothing levels reduce the spatial resolution of surface-based cortical measurements.[29] Finally, the mean cortical thickness in the WMH-connected and WMH-unconnected regions was calculated from the normalized-smoothed cortical thickness map.

Surface-based R1 mapping analysis

MP2RAGE images were processed to obtain the quantitative T1 map using an in-house MATLAB script.[30] The quantitative R1 map was created by taking the reciprocal of the T1 map and scaling that in mHz (ms^{-1}). The R1 map and the robust T1 image are intrinsically aligned since they are from the same data (i.e., MP2RAGE image). Next, the R1 map was registered to the '*fsaverage*' surface template and sampled along the cortex at the 50% depth from the pial surface to the white matter surface. Resampled cortical R1 maps were visually checked. Given that myelination is known to differ across brain regions,[31] similar steps to the cortical thickness described above were performed to normalize the inter-regional differences of R1 (Figure 1C). The normalized R1 map was then smoothed using a 10mm FWMH Gaussian Kernel and subsequently used to calculate the mean R1 values in the WMH-connected and WMH-unconnected regions.

Surface-based R2* mapping analysis

R2* map was obtained from the multi-echo GRE images, by approximating the integration of the magnitude decay using a closed-form solution based on the trapezoidal rule. This step was achieved using an in-house MATLAB toolbox

(https://github.com/kschan0214/r2starmapping).[32] R2* map was registered to the corresponding robust T1W image using '*bbregister*' function within Freesurfer.[33] Given that previous studies have shown that the values of R2* are typically 15 s^{-1} for GM,[34] exceedingly low for CSF and approximate 30 s^{-1} for white matter,[11] a threshold range from 5 s^{-1} to 30 s^{-1} was therefore applied in the R2* map to reduce the partial volume effects from WM and CSF, as described in the previously study.[35] Then, following the similar processing steps described in the above R1 mapping analysis, the R2* map was then registered to the '*fsaverage*' surface template, sampled along the cortex, normalized for the inter-regional differences, smoothed using a 10mm FWMH Gaussian Kernel and finally used to calculate the mean R2* values in the WMH-connected and WMH-unconnected regions.

Surface-based susceptibility mapping analysis

QSM was reconstructed from the multi-echo GRE images using the SEPIA toolbox.[36] The reconstruction process included: removing non-brain tissue, the combination of multi-echo phases, phase unwrapping, the background magnetic field removal and the calculation of susceptibility values using CSF as a reference region.[37-40] QSM was then registered to the corresponding robust T1W image, and then to the '*fsaverage*' surface template, sampled along the cortex, as described in the above R2* map analysis. Of note, the cortical susceptibility included both positive and negative values. We, therefore, took the exponentials of the value of each vertex in the cortical susceptibility map and the exponentials of the average susceptibility of the 68 cortical regions of the study population to keep all values greater than 0, which we termed 'converted susceptibility' (. Next, the value of each vertex in the converted cortical susceptibility map was divided by the average converted susceptibility values of the corresponding cortical region to normalize for the inter-regional differences (Figure 1C) resulting in a region-normalized QSM map. Lastly, the normalized QSM map was smoothed using a 10mm FWMH Gaussian Kernel and then used to calculate the mean susceptibility values in the WMH-connected and WMH-unconnected regions.

Microstructural integrity of the connecting white matter tracts

The connectivity map obtained from the probability tractography above was normalized by dividing the total number of streamlined samples and then thresholded at 2×10^{-4} to achieve the best balance between removing potentially noisy fiber tracts and minimizing any false negative pathways.[41] The thresholded tracts were visually inspected to ensure their accuracy and specificity. Then, mean MD values for the tracts connecting WMH and the cortex were extracted, and were used as a proxy of white matter microstructural integrity. The MD index was chosen

over other diffusion metrics because it is less affected by the crossing fibers and has shown the strongest association with cognitive impairments in SVD.[42,43]

Statistical analyses

Continuous variables were tested for normality distribution using the Anderson-Darling method and described by mean (standard deviation, SD) or median (interquartile ranges, IQRs), according to their distribution.

To evaluate cortical abnormalities in the WMH-connected regional cortex, we first compared the four cortical metrics (i.e., cortical thickness, R1, R2*, and susceptibility values) of WMH-connected regions with those of their corresponding WMH-unconnected regions at three connectivity levels using paired t-tests. Next, we compared the four cortical metrics of WMH-connected regions across three connectivity levels (i.e., low level *vs*. medium level, low level *vs*. high level, medium level *vs*. high level) using three times paired t-tests. We employed three separate paired t-tests instead of analysis of covariance (ANCOVA), because our focus was on pairwise comparisons between cortical metrics at different connectivity levels rather than determining if there is an overall difference among the three connectivity levels.

To investigate the relations between microstructural damage of the connecting white matter tract and the cortical abnormalities of the WMH-connected regions, we employed linear regression analyses. Linear regression models were established using the mean MD values of the connecting white matter tracts as the main independent variables and all cortical metrics (i.e., cortical thickness, R1, R2*, and susceptibility values) of WMH-connected regions in three connectivity levels as the dependent variables. Adjustments were made for age, sex, and the areas of WMH-connected regions. The inclusion of the areas of WMH-connected regions in the model was essential due to its variability among participants, which may subsequently impact the calculation of the mean values of the cortical metrics. In addition, given that previous studies have demonstrated an association between WMH volumes and cortical thickness,[3-5] we also performed linear regression analyses to test the relation between WMH volumes and the cortical metrics of the WMH-connected regions, using the same covariates.

To link the cortical abnormalities of WMH-connected region with the cognitive performance, we employed linear regression models. Each cortical metric of the WMH-connected regions at each connectivity level was employed as the independent variable and cognitive score in each domain (i.e., processing speed,

executive function, and memory) as the dependent variable. To minimize potential confounding effects on cognitive function, we employed two models with different adjustments. Model 1 included age, years of education, areas of WMH-connected regions, WMH volumes, and corresponding cortical metrics of WMH-unconnected regions. Model 2 included the mean MD values of the connecting white matter tracts as an additional adjustment based on Model 1. In these linear regression models, WMH volumes and the mean MD values of the connecting white matter tracts were included as covariates due to their potential effects on cognitive function in SVD.[44,45] The cortical metrics of WMH-unconnected regions were included as control for the global tissue composition abnormalities unrelated to WMH, such as normal ageing and comorbid Alzheimer's disease pathologies, as included in previous studies.[6,7]

Furthermore, to test if the abnormalities of WMH-connected regions mediated the effects of microstructural damage of the connecting white matter tract on cognitive performance, we employed structural equation model (SEM) using the "lavaan" package in R. Specifically, we firstly assessed two latent variables, separately representing global cortical abnormalities of WMH-connected and WMH-unconnected regions, using confirmatory factor analysis (CFA). Following this, we performed mediation analysis with the mean MD values of the connecting white matter tract as the initial variable, the latent variable representing the global cortical abnormalities of the WMH-connected regions as the mediator, and processing speed as the outcome variable. We adjusted for age, years of education, areas of WMH-connected regions, WMH volumes, and global cortical abnormalities in WMH-unconnected region in the mediation analysis. 10.000 bootstrapping samples were used to estimate the 95% confidence interval and determine statistical significance. Note that the CFA and mediation analyses were only performed at the high connectivity level, as the cortical abnormalities of the WMH-connected regions at this level were the most representative. Processing speed was selected as the only outcome variable based on the results of linear regression analyses between cortical abnormalities in WMH-connected regions and cognitive performance described earlier.

For group comparisons, outliers were identified as values out of the 1.5 times IQRs and removed. For all linear regression models, the dependent variables that did not meet a normal distribution were transformed using the Yeo-Johnson approach to approximate a normal distribution,[46] and the outliers with a Cook's distance four times greater than the group mean were discarded to prevent outlier bias.[47] Multicollinearity was also assessed in all linear regression models using variance

inflation factors (VIFs), with values of VIFs greater than 10 indicating strong multicollinearity.[48] For CFA model, the Comparative Fit Index (CFI), Root Mean Square Error of Approximation (RMSEA), and Standardized Root Mean Residual (SRMR) were employed as the indicators of model fit.[49] An acceptable model fit was determined by CFI values greater than 0.90, RMSEA values less than 0.08, and SRMR values less than 0.08.[49]

All statistical analyses were performed using R software (version 4.1.1) and the significance level was set at a two-tailed p-value < 0.05. The *Hommel-Hochberg* method was employed to perform the correction for multiple comparisons.[50]

Sensitivity analyses

First, to confirm specific relations between the cortical measures of WMH-connected regions and the microstructural damage of the connecting white matter tracts or the WMH volumes, we performed linear regression analyses between the mean MD values of the connecting white matter tracts and the four cortical metrics of WMH-unconnected regions, as well as between WMH volumes and the four cortical metrics of WMH-unconnected regions.

Second, to address the potential partial volume effects for R1, R2* and susceptibility values in cortical regions with cortical thinning, we re-tested the group differences of R1, R2* and susceptibility values between the WMH-connected and WMH-unconnected regions at three connectivity levels and the group differences of R1, R2* and susceptibility values of the WMH-connected regions across three connectivity levels using analysis of covariance (ANCOVA), while adjusting for cortical thickness. We also re-tested the relations between the WMH volumes/mean MD values of the connecting tracts and the R1, R2*, and susceptibility values of WMH-connected regions, while additionally adjusting for the cortical thickness of WMH-connected regions.

Data availability

The data that support the findings of this study are available from the corresponding author, depending on reasonable request from qualified investigators after permission of the appropriate regulatory bodies.

Results

A total of 213 participants were included in the present study, with a median age of 73 years (IQR, 69-79), and 95 were women (44.6%). Detailed information on demographic data, cognitive function and neuroimaging characteristics were provided in Table 1 and Supplementary Table e-2.

Identification of connected cortex

The cortical regions connected to WMH as determined by probabilistic tractography at three connectivity levels were averaged across all participants and visualized on the '*fsaverage*' surface. As shown in Figure 1B, higher connectivity probabilities with WMH were observed in the frontal and occipital regions at all three connectivity levels. The *Desikan-Killiany* atlas was applied to the probability map to identify the connectivity probabilities of each brain region at three connectivity levels. For the high connectivity level, the top-five ranking of cortical regions with higher connectivity probabilities to WMH were frontal-pole, pars-triangularis, pars-opercularis, superior-frontal and pericalcarine (Supplementary Table e-3).

Cortical thickness, R1, R2* and susceptibility in the connected regions

Compared with the WMH-unconnected regions, the cortical thickness, R1, R2*, and susceptibility of WMH-connected regions showed significantly lower values at all connectivity levels (*p-corrected* < 0.001, Figure 2-5). The comparisons between the three connectivity levels showed that the WMH-connected regions with higher connectivity levels had more pronounced lower cortical thickness, R1, R2*, and susceptibility values (*p-corrected* < 0.001, Figure 2-5).

Higher WMH volumes were related to lower cortical thickness of the WMH-connected regions at the low (β = -0.25, *p-corrected* = 0.006) and medium (β = -0.23, *p-corrected* = 0.046) connectivity levels (Supplementary Table e-4); higher MD values of the connecting white matter tracts were significantly related to lower cortical thickness, lower R1 and R2* values of the WMH-connected regions at three connectivity levels and related to lower susceptibility values of the WMH-connected regions at high connectivity level (β = [-0.389, -0.143], *p-corrected* values < 0.05, Figure 6).

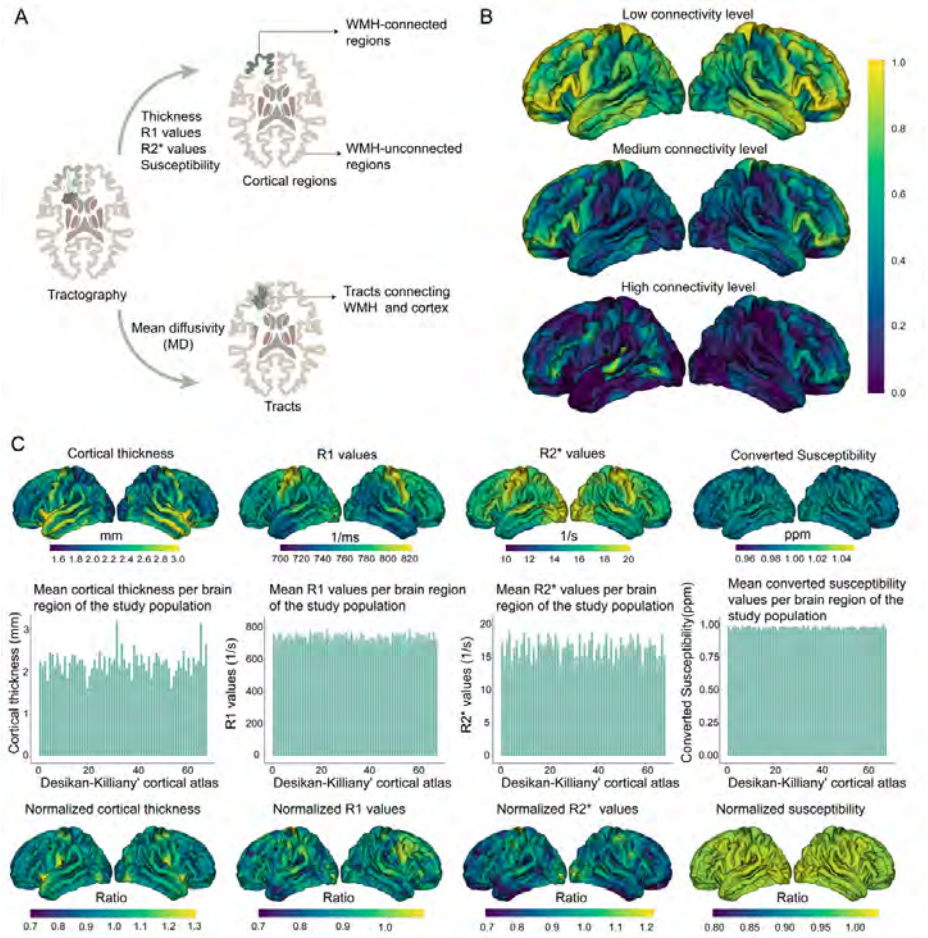

Figure 1. Study design and methods. (A) probabilistic tractography was performed from white matter hyperintensities (WMH) to the white/grey matter boundary to determine the WMH-connected regions (dark green color), the WMH-unconnected regions (beige color) and the connecting white matter tracts (light green color); **(B)** the cortical terminations of the connecting white matter tracts were projected to the 'fsaverage' surface template and then averaged across the study population, which represents the connectivity probability originating from WMH. Color bars indicate the vertex-wise probabilities of the regions connected to the WMH at different threshold levels; **(C)** correction for the inter-regional differences of cortical thickness, R1, R2*, susceptibility values at the vertex level. The top row of panels shows the averaged cortical thickness, R1, R2* and susceptibility map of the study population; the middle row of panels illustrates the different brain regions having a different cortical thickness, R1, R2* and susceptibility values; the bottom row of panels shows the inter-regional differences after correction by dividing the value of each vertex in cortical thickness/R1/R2*/susceptibility maps by the mean values of the thickness/R1/R2*/susceptibility on the corresponding brain regions of the study population.

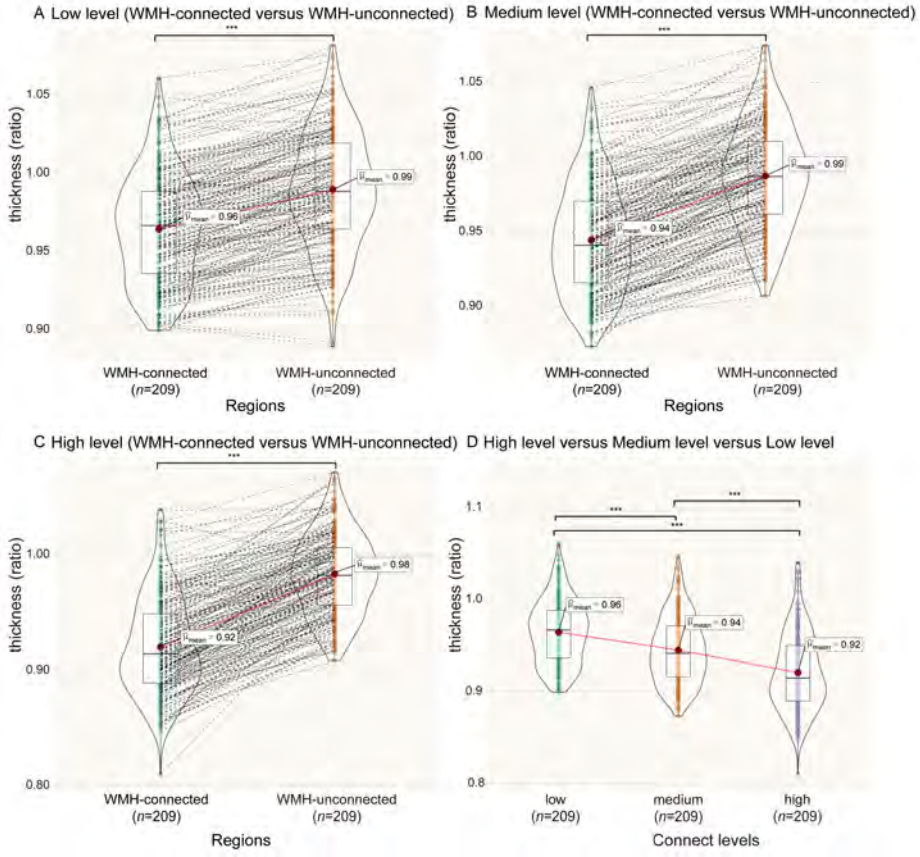

Figure 2. Comparison of cortical thickness between WMH-connected regions and WMH-unconnected regions, and between different connectivity levels. Four participants were identified as outliers, resulting 209 participants included. **(A-C)** compared with the WMH-unconnected regions, the cortical thickness in the WMH-connected regions showed significant decreases at all connectivity levels. **(D)** the WMH-connected regions with higher connectivity levels had more pronounced lower cortical thickness values. ***, *p-corrected* < 0.001.

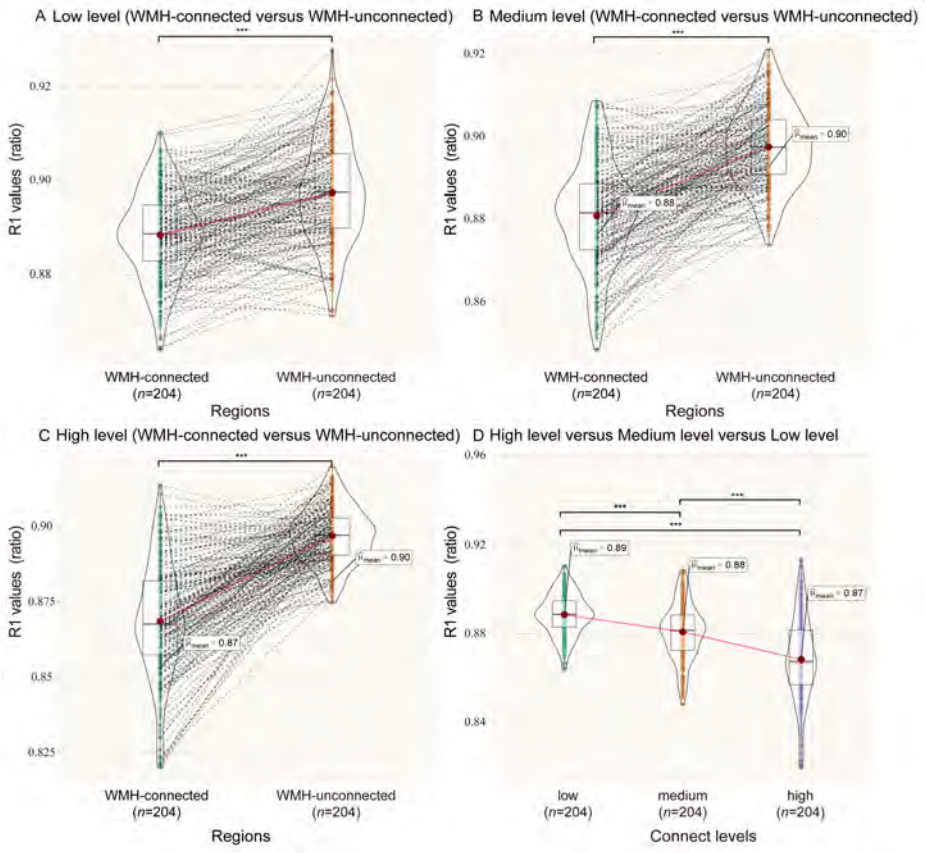

Figure 3. Comparison of R1 values between different WMH-connected regions and WMH-unconnected regions, and between different connectivity levels. Nine participants were identified as outliers, resulting 204 participants included. **(A-C)** compared with the WMH-unconnected regions, the R1 values in the WMH-connected regions showed significant decreases at all connectivity levels. **(D)** the WMH-connected regions with higher connectivity levels had more pronounced lower R1 values. ***, *p-corrected* < 0.001.

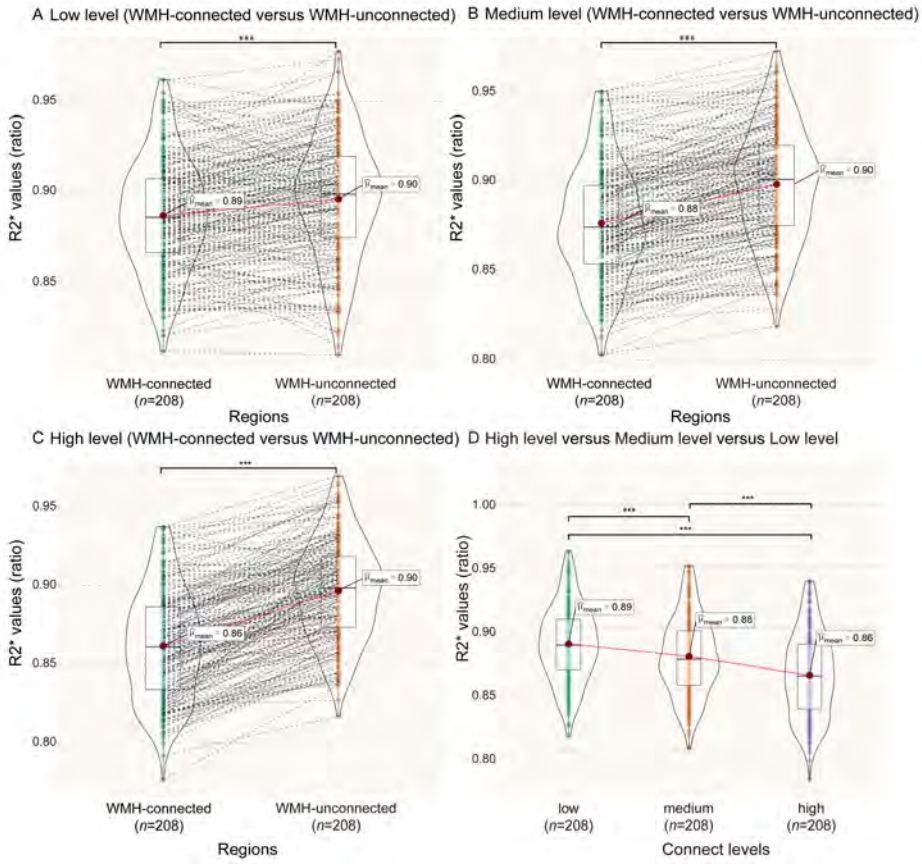

Figure 4. Comparison of R2* values between WMH-connected regions and WMH-unconnected regions, and between different connectivity levels. Five participants were identified as outliers, resulting 208 participants included. **(A-C)** compared with the WMH-unconnected regions, the R2* values in the WMH-connected regions showed significant decreases at three connectivity levels. **(D)** the WMH-connected regions with higher connectivity levels had more pronounced decreases in R2* values. ***, *p-corrected* < 0.001.

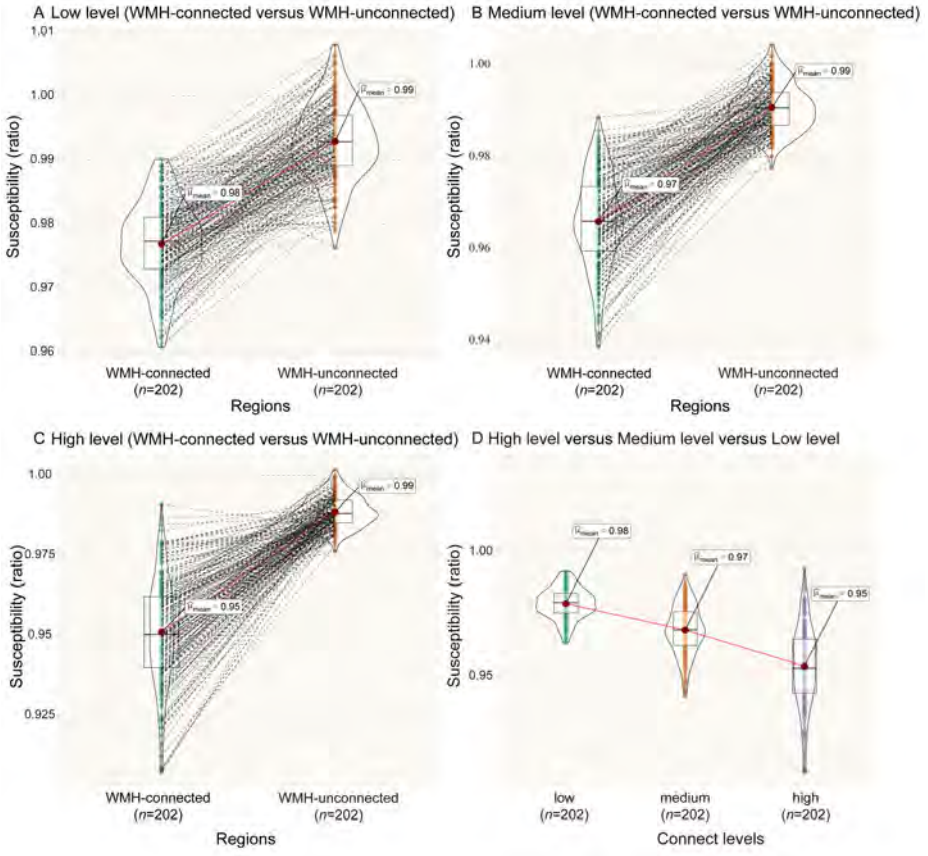

Figure 5. Comparison of susceptibility values between WMH-connected regions and WMH-unconnected regions, and different connectivity levels. Eleven participants were identified as outliers, resulting 202 participants included. **(A-C)** compared with the WMH-unconnected regions, the susceptibility values in the WMH-connected regions showed significant decreases at three connectivity levels. **(D)** the WMH-connected regions with higher connectivity levels had more pronounced decreases in susceptibility values. ***, *p-corrected* < 0.001.

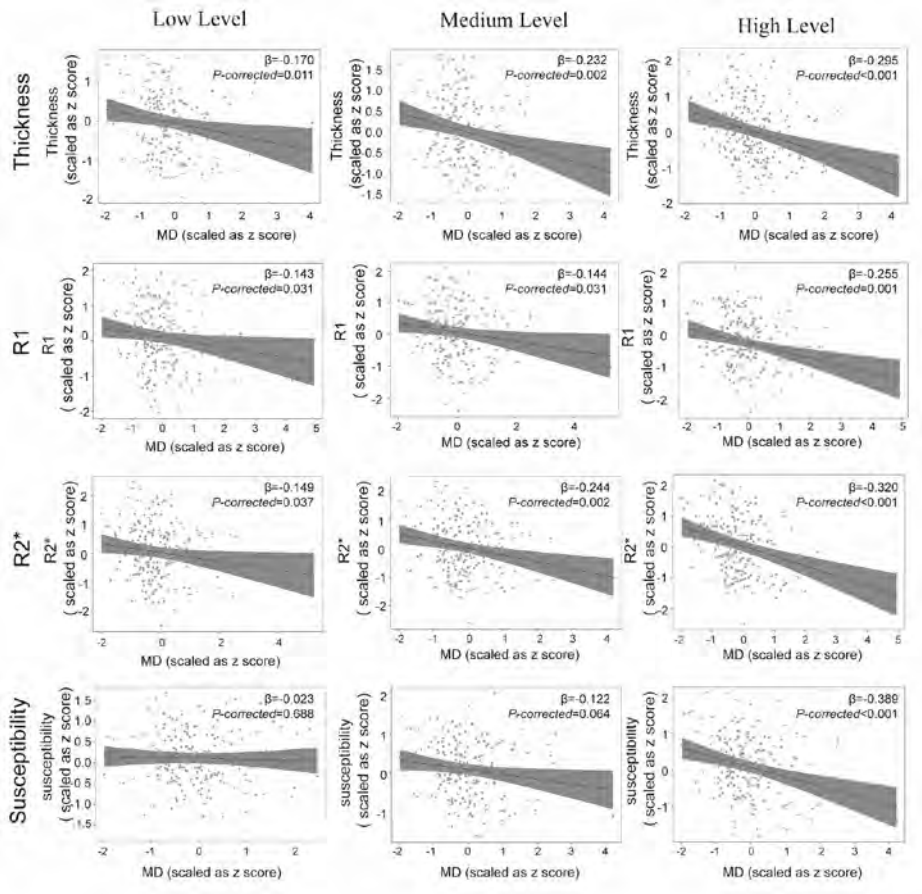

Figure 6. Relations between MD of connecting white matter tracts and the mean thickness, R1 and R2*, susceptibility values of the WMH-connected regions. In first panel, the higher MD of the connecting white matter tracts was related to the lower thickness of the WMH-connected regions at three connectivity levels; second panel, the higher MD of the connecting white matter tracts was related to lower R1 values of the WMH-connected regions at three connectivity levels; third panel, the higher MD of the connecting white matter tracts was related to lower R2* values of the WMH-connected regions at three connectivity levels; fourth panel, the higher MD of the connecting white matter tracts was related to lower susceptibility values of the WMH-connected regions at the high connectivity level; *p-corrected* values represent *p*-values corrected for multiple comparisons using the Hommel-Hochberg method.

Cortical thickness, R1, R2* and susceptibility in the connected regions and cognitive function

Lower scores on processing speed, but not any of the other cognitive domains, were significantly related to lower cortical thickness, lower R1 values, lower R2* values, and lower susceptibility values of the WMH-connected regions at three connectivity levels (Table 2). After additionally adjusting for the MD values of the connecting white matter tracts (model 2): the relations between processing speed and R1, R2* values of the WMH-connected regions at three connectivity levels, and the relations between processing speed and susceptibility values of the WMH-connected regions at the medium and low connectivity levels remained significant; the relations between processing speed and cortical thickness of the WMH-connected regions and the relation between the processing speed and susceptibility values of the WMH-connected regions at high connectivity level were not significant (Supplementary Table e-5).

Two latent variables were separately used to assess the global cortical abnormalities of the WMH-connected regions or the WMH-unconnected regions; both showed great model fit (Supplementary Table e-6). The mediation analysis showed that the global cortical abnormalities of WMH-connected regions significantly mediated the relations between the MD values of the connecting white matter tracts and the processing speed (indirect effect = -0.09, *p*-values = 0.011, direct effect = -0.04, *p*-values = 0.595, Supplementary Figure e-3).

Sensitivity analyses

In contrast to the WMH-connected regions, the mean MD values of the connecting white matter tracts were not related to the cortical thickness, R1, and R2* values of the WMH-unconnected regions across three connectivity levels. However, at medium and high connectivity levels, higher MD values of the connecting white matter tracts were significantly correlated with higher susceptibility values of the WMH-unconnected regions (Supplementary Table e-7). Furthermore, at the low connectivity level, higher WMH volumes were related to reduced cortical thickness of the WMH-unconnected regions (Supplementary Table e-8).

After adjusting for cortical thickness, the results for group differences in R1, R2*, and susceptibility values between the WMH-connected and WMH-unconnected regions and between the WMH-connected regions across three connectivity levels and for the relations between the WMH volumes/mean MD values of the connecting tracts and the R1, R2*, and susceptibility values of WMH-connected regions remained largely unchanged (Figure e-4, Table e-9).

Discussion

In this present study, we employed a multimodal neuroimaging study to systematically assess the cortical abnormalities connected to WMH in SVD. We found that 1) white matter tracts passing through WMH showed a specific connectivity pattern to the cortex, with higher connectivity probabilities to the frontal and occipital regions; 2) compared to WMH-unconnected cortical regions, WMH-connected cortical regions showed significantly lower thickness, R1, R2* and susceptibility values; 3) higher MD of the connecting white matter tracts were related to lower cortical thickness, R1, R2* and susceptibility values in the WMH-connected regions; 4) lower cortical thickness, R1, R2* and susceptibility values in the WMH-connected regions were significantly and specifically related to lower scores on processing speed; and 5) these cortical abnormalities of the WMH-connected regions mediated the relations between MD values of the connecting white matter tracts and processing speed. Taken together, our results suggest that WMH is related to changes in the connected cortex (e.g., cortical thinning, demyelination and iron loss), most likely through the disruption of connecting white matter tracts. These cortical tissue changes may lead to processing speed impairment, a key clinical feature of SVD.[51] These findings advance our understanding of the mechanisms of cognitive impairment in SVD.

In our study, WMH displayed a higher connectivity probability to the frontal and occipital regions. This finding corroborates with Mayer[8] C et al.'s study, showing a similar connectivity pattern of WMH to the cortex. Notably, that same employed a different tractography approach (whole-brain tractography) and focused on a community-based population, as opposed to the SVD population in the present study. Nevertheless, our findings confirmed the robustness of the connectivity pattern of WMH (of presumed vascular origin) to the cortex across different tractography methods and populations. However, it's worth noting that WMH resulting from other pathologies, such as in multiple sclerosis (MS) or Alzheimer's diseases, may have different connectivity patterns,[52,53] which requires further investigation.

We found that, compared to WMH-unconnected regions, WMH-connected regions showed a significantly lower cortical thickness. Cortical thinning was more pronounced in cortical regions with a higher probability connected to the WMH. This finding is in line with a previous study, which showed that a higher connectivity probability between WMH and the cortex was associated with a reduced cortical thickness.[8] Moreover, we found that higher MD values of the connecting white matter

tracts were specifically related to lower cortical thickness of WMH-connected regions, but not to that of the WMH-unconnected regions. This pattern of regional cortical thinning linked to the microstructural integrity of connecting tracts strengthens the suggestion that cortical thinning occurs, at least partially, as a result of secondary neurodegeneration of white matter tracts between WMH and the cortex. This mechanism is further substantiated by the finding that subcortical ischemic lesions could induce regional connected cortical alterations remote from the lesions through disruption of white matter tracts in studies involving CADASIL or stroke participants.[6,7] In addition, we found that higher WMH volumes were significantly related to lower cortical thickness of WMH-unconnected regions, which may be explained by other cortical pathological processes accompanying WMH, such as cortical microinfarction, increased blood-brain barrier (BBB) permeability, and inflammation.[54]

Furthermore, we found that, compared to the WMH-unconnected regions, the R1 and R2* values were significantly lower in WMH-connected regions that were associated with higher MD values of the connecting white matter tracts. These findings are suggestive of cortical demyelination of the connected cortex. No studies have previously examined cortical myelination changes in SVD. In multiple sclerosis, however, the demyelination of the cortex is well-established.[55,56] A longitudinal study in multiple sclerosis reported that microstructural damages of white matter tracts at baseline predicted myelin loss in the connected cortical regions at the 2-year follow-up.[57] This evidence strengthened our hypothesis that WMH can lead to cortical demyelination through secondary degeneration of the connecting white matter tracts. In addition, it can be speculated that the cortical thinning observed in the WMH-connected region may not solely arise from neuronal loss but also from reduction in myelinated fibers.

We also found decreased susceptibility values in the WMH-connected regions compared with the WMH-unconnected regions. Given that susceptibility values have demonstrated a predominant positive correlation with iron and a negative correlation with myelin,[12] the decreased susceptibility values observed in the WMH-connected regions strongly indicate iron loss. Similar iron loss in the cortex has been found in multiple sclerosis.[56,58] Furthermore, multiple sclerosis patients with long disease duration showed decreased iron concentration in the thalamus, whereas those with short disease duration or diagnosed as clinically isolated syndrome did not exhibit such changes.[59,60] Given that oligodendrocytes stores most of the iron and that iron is involved in various metabolic processes,[61] the iron loss during the progression of the disease may signify a reduction in oligodendrocyte density or depletion of iron due to repair of oligodendrocytes.[59] Studies with long-term

follow-up and histology data are required to verify whether iron level of the WMH-connected regions decreases with time in SVD patients.

Besides, we found a positive relationship between susceptibility values of the WMH-unconnected regions and MD values of the connecting white matter tracts, which was unexpected. This finding suggests that there are mechanisms other than secondary degeneration of the connecting white matter tracts that can lead to cortical iron abnormalities in SVD. For example, a previous study found increased R2* values at the site of the acute micro-cortical infarcts,[35] and studies in CADASIL reported that an increased BBB permeability was associated with increased susceptibility values in the cortex.[62] Further work is warranted to better understand these observations.

Lastly, we found that decreased thickness R1, R2*, and susceptibility values in WMH-connected regions were related to lower scores on processing speed, independent of global tissue composition abnormalities unrelated to WMH. Moreover, these global cortical abnormalities of the WMH-connected regions mediated the relations between microstructural damage of the connecting white matter tract and processing speed. This relation could be explained by a distinctive connectivity pattern of WMH to the cortex and specific tissue changes of WMH-connected regions. Previous studies in SVD have argued that the effects of lesions in the frontal subcortical network are mediated by frontal cortical changes (i.e., cortical thinning) and in combination underlie processing speed deficits.[63,64] In addition, cortical demyelination and obstructed remyelination (i.e., suggested by iron loss) in the connected cortical regions may also be contributing factors to processing speed deficits in SVD. Myelinating oligodendrocytes contribute to cortical information processing through their dual role of accelerating impulse propagation and supplying metabolic support to the spiking axons.[65] Our findings, combined with the fact that processing speed is the earliest and the most prominent cognitive domain affected,[51,66] highlight the significance of cortical pathologies caused by secondary degeneration in determining cognitive deficits in SVD. Interventions targeting the secondary degeneration of the cortex and the myelin repair might ameliorate the cognitive impairment in SVD.

The strengths of our study include a deeply phenotyped cohort sample of SVD with comprehensive and detailed cognitive data. In addition, we used a state-of-the-art multimodal neuroimaging approach for identification of WMH-connected cortical regions and the in-vivo cortical histopathological measurements. Futhermore, we corrected the nonuniform distribution of cortical thickness, myelin, and iron across brain regions by dividing the thickness, R1, R2* and susceptibility values of each

vertex in the cortical maps by the average values of the corresponding metrics of the corresponding cortical region of the study population. This method allowed us to compare changes between different cortical regions (i.e., the WMH-connected regions and unconnected regions) within one subject, thereby excluding cortical changes caused by other factors, such as normal ageing and global brain atrophy. Lastly, we excluded the lacunes located within or at the edge of WMH from the WMH mask, thereby minimizing the potential confounding effects of lacunes on the cortical abnormalities.[6]

Several limitations should be acknowledged. First, the availability of MP2RAGE, multi-echo GRE, and multi-shell DWI images enabled us to comprehensively assess the cortical abnormalities but limited us to only use the third follow-up data from the RUN DMC cohort and to only conduct cross-sectional analyses. Future longitudinal data are needed to test the directionality of the observed relations between the microstructural damage of connecting white matter tracts and cortical measures in the WMH-connected cortex, but also the speculated iron dynamic changes with the disease progression. Second, our cohort lacked age-matched healthy controls. We performed comparisons between changes in WMH-connected regions and WMH-unconnected regions within one subject. This limited the interpretation of our results, since the observed cortical differences between WMH-connected and WMH-unconnected regions may come from the nonuniform distribution of cortical features across brain regions, even though we have minimized this effect through the normalization. Third, in the context of cortical thinning in the WMH-connected regions, the measures of R1, R2*, and susceptibility could be more vulnerable to contamination from CSF or WM signals (i.e., the increased partial volume effects). To minimize this effect, we applied a threshold range [(5-30)1/s] in the R2* map to exclude signals from CSF or the white matter. We also repeated the analyses involving R1, R2* and susceptibility values while adjusting for cortical thickness, which did not alter our main findings. Fourth, the tissue composition probed by qMRI are based on the different contributions of various components to the magnetic time and/or susceptibility. Beyond the myelin and iron, R1, R2* and susceptibility values are also affected by other sources, such as the cell density or other trace elements.[67] Further histopathological and longitudinal studies are required to confirm our results. Lastly, our cohort lacked data regarding enlarged PVS, an emergent and promising MRI marker in SVD.[68] The assessment of PVS should be included in future SVD studies.

In conclusion, our study demonstrated that the microstructural integrity of white matter tracts passing from WMH is related to regional cortical abnormalities as

measured by thickness, R1, R2* and susceptibility values in the connected cortical regions. These findings indicate cortical thinning, demyelination and iron loss in the cortex, which is most likely through the disruption of the connecting white matter tracts, and these cortical abnormalities may contribute to processing speed dysfunction in SVD. These findings highlight the role of secondary degeneration in determining cortical thinning, histopathological changes, and deficits in processing speed and may have implications for finding intervention targets for the treatment of cognitive impairment in SVD by preventing secondary degeneration.

Supplementary material

Materials and methods

Neuropsychological assessment

Processing speed was assessed using the Trail Making Test A (TMT-A) and Symbol-Digit Modalities Test (SDMT); executive function was assessed using the TMT-A, TMT-B, the Verbal Fluency test (animal and job naming); memory was assessed using the forward and backward scores of the Digit Span test, the immediate and delayed recall scores of the Rey Auditory Verbal Learning Test (RAVLT) and the delayed recall score of Rey-Osterrieth Complex Figure Test (RCFT). The raw test scores were standardized as z-scores. Next, compound scores were computed per cognitive domain: processing speed was calculated by the sum of (1) the inverse Z score of the TMT-A, (2) the Z score of SDMT; executive function was calculated by the sum of (1) the inverse Z score of the TMT ratio (TMT-B/TMT-A), (2) the average Z score of Verbal Fluency Test of animal naming and job naming; memory was calculated as the sum of (1) the Z score of DST, (2) the average Z score of RAVLT of immediate recall and delayed recall; (3) the average Z score of ROCF of immediate recall and delayed recall. (Supplementary Table e-1).

Table e-1. Calculation of each cognitive domain

Cognitive domain	Cognitive test	Calculation of compound score
Processing speed	Trail Making Test A	$Z_{TMT\text{-}A} \times -1 + Z_{SDMT}/2$
	Symbol-Digit Modalities Test	
Executive function	Trail Making Test A	$Z_{(TMT\text{-}B/TMT\text{-}A)} \times -1 + (Z_{VFT\text{-}A} + Z_{VFT\text{-}J})/2$
	Trail Making Test B	
	Verbal Fluency Test (Animals and jobs)	
Memory	Digit span test (Forward and backward)	$Z_{(DST\text{-}f + DST\text{-}b)} + (Z_{RAVLT\text{-}I} + Z_{RAVLT\text{-}D})/2 + (Z_{ROCF\text{-}I} + Z_{ROCF\text{-}D})/2$
	Rey's Auditory Verbal learning test (Immediate recall and delayed recall)	
	Rey–Osterrieth Complex Figure Test (Immediate recall and delayed recall)	

Z, the Z transformed score; DST-f, Digit span forward test; DST-b, Digit span backward test; RAVLT-I, the Immediate recall of Rey's Auditory Verbal learning test; RAVLT-D, the delayed recall of Rey's Auditory Verbal learning test; ROCF-I, the Immediate recall of Rey–Osterrieth Complex Figure Test; ROCF -D, the delayed recall of Rey–Osterrieth

Complex Figure Test; TMT, Trail Making Test; SDMT, Symbol-Digit Modalities Test, VFT-A, Verbal Fluency Test (animals); VFT-A, Verbal Fluency Test (jobs).

MRI acquisition

Parameters for each sequence: 3D T1-weighted Magnetization Prepared 2 Rapid Acquisition Gradient Echoes (MP2RAGE): 0.85mm isotropic voxels, repetition time (TR) = 5500 ms, inversion time (TI1 and TI2) = 700 and 2500 ms, field of view (FOV) = 218×272mm^2, Flip Angle = 4; 3D multi-echo fast low-angle shot images (9 echoes): 0.85mm isotropic voxels, TR = 44ms, ΔTE = 4ms, FOV = 197×245mm^2, Flip angle = 20; 3D fluid-attenuated inversion recovery (FLAIR) image: 0.85mm isotropic voxels, TR = 5000ms, TE = 394 ms, TI = 1800ms, FOV = 163×272mm^2, Flip angle = 120; Multi-shell DWI using multi-band accelerated echo planar imaging (EPI): 99 diffusion-weighted directions (3 × b = 200, 6 × b = 500, 30 × b = 1,000, and 60 × b = 3,000s/mm2), 10 × b = 0 images, 1.7mm isotropic voxels, TR = 3220ms, TE = 74 ms, FOV = 221×221mm^2 , Flip angle = 90; one b=0 image with acquisition parameters equal to the previous b=0 images, but acquired in opposite phase-encoding direction.

Identification of connected cortex

The WMH masks derived from the FLAIR images were linearly registered to T1 images and then to diffusion images using Functional MRI of the brain linear image registration tool (FLIRT).[69,70] The white/grey matter boundaries were also linearly registered to the diffusion images. Probabilistic tractography was performed from the WMH masks to the white/grey matter boundaries in the diffusion spaces. This was done using the probtractx2 function from FSL with the following parameters: number of samples = 5000, number of steps per sample = 2000, step length in mm = 0.5, curvature threshold = 0.2.[71] The WM/GM matter boundary was additional used to constrain tractography. Resulting tracts were registered to T1 images using the inversed transformation matrix from T1 images to diffusion images generated in above registering steps. Regions where the tracts reached the white/grey matter boundaries were defined as the WMH-connected regions. To determine different levels of the connectivity probability between the cortex and the WMH lesion, the resulting WMH-connected regions were thresholded at different levels. Based a previously published study,[72-74] the threshold of the lowest level set at 3.08 x 10^{-5} percent of the total streamlines sent out from the seed masks (5000 times per voxel). WMH-connected regions with the medium and high levels of connectivity probability were determined by gradually increasing the values of the threshold until the volumes of thresholded the WMH-connected regions reached 50% (medium level) or 25% (high level) of the volumes of the low-level WMH-connected regions, as used in previous similar studies.[6,7]

Results

Table e-2. Results on each cognitive task

Cognitive task	Raw score
DST	
Forward, median (IQR)	9.0 (7.0-10.0)
backward, median (IQR)	5.0 (4.0-7.0)
RAVLT	
Immediate recall, median (IQR)	22.0 (19.0-25.0)
Delayed recall, median (IQR)	7.0 (4.0-8.8)
ROCF (Delayed recall)	
Immediate recall, median (IQR)	21.0 (16.0-25.0)
Delayed recall, median (IQR)	20.0 (16.0-24.0)
TMT-A, median (IQR)	45.2 (36.3-63.0)
TMT-B, median (IQR)	103.0 (81.3-153.1)
SDMT, median (IQR)	41.0 (32.0-47.8)
VFT, median (IQR)	
Animals	20.0 (16.0-23.0)
Jobs	15.0 (11.0-18.0)

DST, Digit span forward test; RAVLT, Rey's Auditory Verbal learning test; ROCF, Rey–Osterrieth Complex Figure Test; TMT, Trail Making Test; SDMT, Symbol-Digit Modalities Test; VFT, Verbal Fluency Test.

Table e-3.the connectivity probabilities of WMH to different cortical regions at three connectivity levels

Location	Desikan-Killiany atlas	High level	Medium level	Low level
Frontal	superiorfrontal	**0.24888**	**0.53337**	0.838535
	caudalmiddlefrontal	0.13648	0.291265	0.63656
	rostralmiddlefrontal	0.20227	0.361045	0.70671
	frontalpole	**0.53674**	**0.8502**	**0.978905**
	parsopercularis	**0.25371**	0.47833	0.785365
	parsorbitalis	0.21318	**0.551245**	**0.880005**
	parstriangularis	**0.37015**	**0.577375**	**0.872145**
	lateralorbitofrontal	0.07688	0.186365	0.523905
	medialorbitofrontal	0.21972	0.3239	0.666365
	precentral	0.20678	0.374775	0.72977
	paracentral	0.142375	0.47744	**0.851065**
parietal	postcentral	0.18307	0.250905	0.59474
	superiorparietal	0.170905	0.37492	0.714645
	inferiorparietal	0.1724	0.23677	0.585205
	supramarginal	0.148655	0.22152	0.58727
	precuneus	0.158025	0.48017	**0.838675**
Temporal	bankssts	0.144465	0.192505	0.587905
	transversetemporal	0.020885	0.138355	0.539115
	superiortemporal	0.16161	0.397985	0.82154
	temporalpole	0.06608	0.3185	0.723
	entorhinal	0.06187	0.113065	0.413925
	middletemporal	0.142515	0.32702	0.767805
	inferiortemporal	0.142755	0.353315	0.749355
	fusiform	0.07921	0.20098	0.602855
occipital	lateraloccipital	0.127265	0.24399	0.62291
	cuneus	0.17711	0.446875	0.79251
	lingual	0.169145	0.3489	0.711615
	pericalcarine	**0.231805**	**0.53718**	0.814345
insula	insula	0.158465	0.39924	0.716645
limbic	caudalanteriorcingulate	0.215755	0.513365	0.80609
	rostralanteriorcingulate	0.182145	0.28347	0.64236
	posteriorcingulate	0.164535	0.401485	0.734815
	isthmuscingulate	0.205405	0.5194	0.825865
	parahippocampal	0.099665	0.275955	0.69001

Values in bold are the top-five ranking of cortical regions with highest connectivity probabilities to the WMH at each connectivity level.

Table e-4. Relation between normalized WMH volumes and the cortical thickness, R1, R2*, susceptibility values of the WMH-connected regions at three connectivity levels

	WMH volumes	
	β	***p-corrected value***
Cortical thickness (WMH-connected regions)		
Low level	-0.25	**0.006**
Medium level	-0.23	**0.046**
High level	-0.09	0.395
R1 values (WMH-connected regions)		
Low level	-0.05	0.632
Medium level	0.09	0.632
High level	0.14	0.510
R2* values (WMH-connected regions)		
Low level	-0.08	0.908
Medium level	0.09	0.836
High level	-0.01	0.908
Susceptibility values (WMH-connected regions)		
Low level	-0.04	0.846
Medium level	-0.05	0.846
High level	0.02	0.846

WMH, white matter hyperintensities; normalized WMH volumes, WMH volumes were normalized by the intracranial volume (ICV); bold values: *p-corrected* < 0.05, p values were corrected for multiple comparisons using *Hommel-Hochberg* method.

Table e-5. Relation between the cortical thickness, R1, R2*, susceptibility values of the WMH-connected regions and cognitive function at three connectivity levels (Model 2)

	Processing speed		Executive function		Memory	
	β	*p*-corrected value	β	*p*-corrected value	β	*p*-corrected value
Cortical Thickness of the WMH-connected regions						
High level	0.15	0.131	-0.09	0.946	-0.02	0.993
Medium level	0.20	0.131	0.06	0.946	0.04	0.993
Low level	0.30	0.131	0.36	0.154	0.10	0.993
R1 of the WMH-connected regions						
High level	0.18	**0.035**	0.06	0.946	0.04	0.993
Medium level	0.20	**0.018**	0.09	0.915	0.08	0.993
Low level	0.21	**0.030**	0.10	0.898	0.10	0.993
R2* of the WMH-connected regions						
High level	0.28	**0.014**	-0.14	0.800	0.01	0.993
Medium level	0.42	**0.002**	-0.26	0.253	0.02	0.993
Low level	0.37	**0.011**	-0.21	0.458	0.09	0.993
Susceptibility of WMH-connected regions						
High level	0.14	0.131	-0.04	0.946	0.00	0.993
Medium level	0.22	**0.025**	-0.02	0.946	0.00	0.993
Low level	0.25	**0.030**	0.01	0.946	-0.02	0.993

Model 2 is adjusted for age, education years, the areas of WMH-connected regions, the normalized WMH volumes, the mean cortical thickness or R1 or R2* or susceptibility values of the WMH-unconnected regions, and the mean MD values of the connecting tracts; WMH, white matter hyperintensities, MD, mean diffusivity; bold values: *p*-corrected < 0.05, *p* values were corrected for multiple comparisons using *Hommel-Hochberg* method.

Table e-6. Factor load and model fit indicators of the latent variables using confirmatory factor analysis.

	Latent variable 1 (WMH-connected regions)	Latent variable 2 (WMH-unconnected regions)
Standardized factor load		
Cortical thickness	0.490	0.066
R1 values	0.955	0.590
R2* values	0.595	0.766
Susceptibility values	0.862	0.364
Model fit indicators		
CFI	0.999	>0.999
RMSEA	0.035	<0.001
SRMR	0.020	0.021

Latent variable 1, representing global cortical abnormalities of WMH-connected; Latent variable 2, representing global cortical abnormalities of WMH-unconnected; WMH-connected and WMH-unconnected regions were identified at the high connectivity level. WMH, white matter hyperintensities; CFI, Comparative Fit Index; RMSEA, Root Mean Square Error of Approximation; SRMR, Standardized Root Mean Residual.

Table e-7. Relation between MD of the connecting tracts and the cortical thickness, R1, R2*, susceptibility values of the WMH-unconnected regions at three connectivity levels

	MD of the connecting tracts	
	β	*p-corrected value*
Cortical thickness (WMH-unconnected regions)		
Low level	-0.00	0.997
Medium level	-0.03	0.997
High level	-0.05	0.959
R1 values (WMH-unconnected regions)		
Low level	-0.08	0.392
Medium level	-0.06	0.392
High level	-0.06	0.392
R2* values (WMH-unconnected regions)		
Low level	-0.15	0.060
Medium level	-0.16	0.062
High level	-0.13	0.064
Susceptibility values (WMH-unconnected regions)		
Low level	0.10	0.201
Medium level	0.04	**0.018**
High level	0.21	**0.006**

WMH, white matter hyperintensities; MD, mean diffusivity; bold values: *p*-corrected < 0.05, *p* values were corrected for multiple comparisons using *Hommel-Hochberg* method.

Table e-8. Relation between normalized WMH volumes and the cortical thickness, R1, R2*, susceptibility values of the WMH-unconnected at three connectivity levels

	Normalized WMH volumes	
	β	***p-corrected value***
Cortical thickness (WMH-unconnected regions)		
Low level	-0.23	**0.012**
Medium level	-0.15	0.057
High level	-0.15	0.057
R1 values (WMH-unconnected regions)		
Low level	-0.07	0.926
Medium level	-0.05	0.926
High level	-0.01	0.926
R2* values (WMH-unconnected regions)		
Low level	-0.14	0.480
Medium level	-0.05	0.652
High level	-0.06	0.652
Susceptibility values (WMH-unconnected regions)		
Low level	-0.19	0.189
Medium level	-0.05	0.622
High level	-0.05	0.622

WMH, white matter hyperintensities, normalized WMH volumes, WMH volumes were normalized by the intracranial volume (ICV); bold values: *p*-corrected < 0.05, p values were corrected for multiple comparisons using *Hommel-Hochberg* method.

Table e-9. Relation between MD of the connecting tracts, normalized WMH volumes and the R1, R2*, susceptibility values of the WMH-connected regions while adjusting for cortical thickness at three connectivity levels.

	Normalized WMH volumes		MD of the connecting tracts	
	β	***p-corrected***	**β**	***p-corrected***
R1 values (WMH-connected regions)				
Low	-0.06	0.559	-0.14	0.069
Medium	0.09	0.559	-0.12	0.069
High	0.13	0.438	-0.11	0.069
R2* values (WMH-connected regions)				
Low	-0.01	0.937	-0.15	**0.031**
Medium	0.11	0.937	-0.22	**0.008**
High	0.01	0.937	-0.29	**<0.001**
Susceptibility values (WMH-connected regions)				
Low	-0.03	0.763	-0.02	0.792
Medium	-0.02	0.763	-0.10	0.142
High	0.04	0.763	-0.15	**0.042**

WMH, white matter hyperintensities, normalized WMH volumes, WMH volumes were normalized by the intracranial volume (ICV); MD, mean diffusivity; bold values: *p*-corrected < 0.05, p values were corrected for multiple comparisons using *Hommel-Hochberg* method.

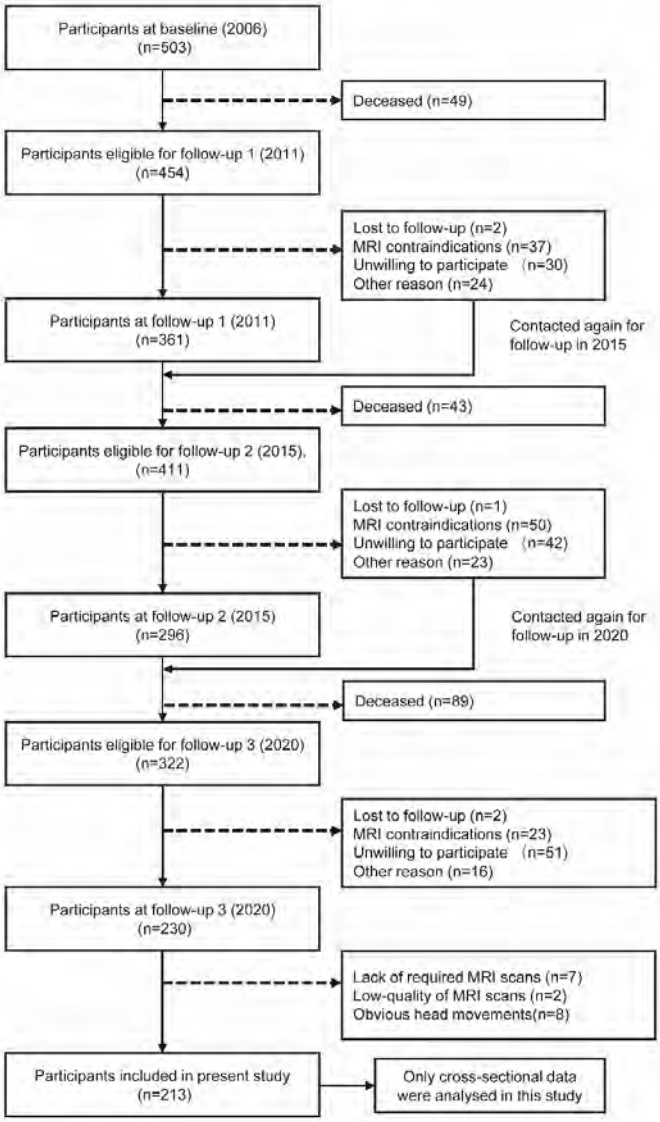

Figure e-1. Flow chart of the present study.

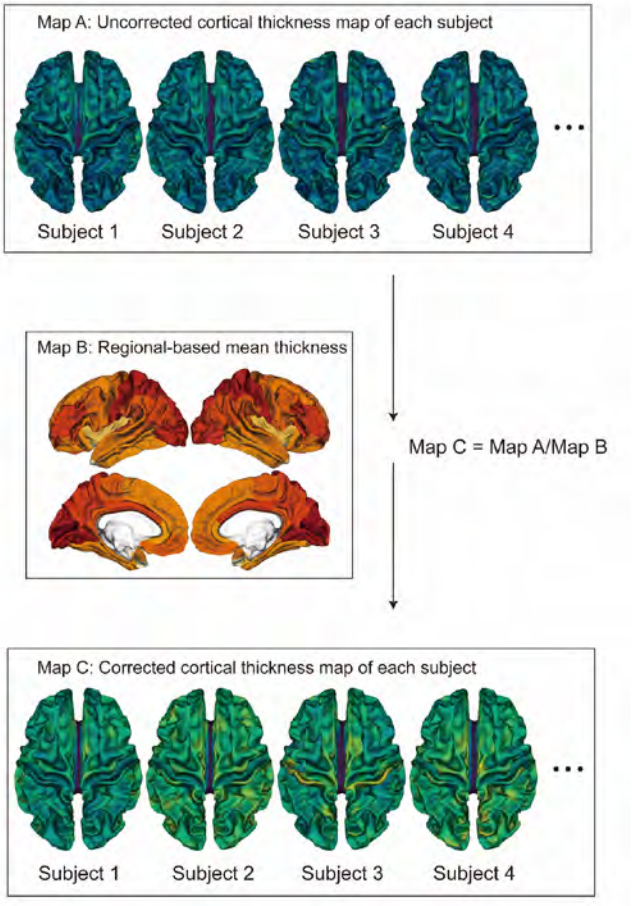

Figure e-2 Schematic diagram of correcting the inter-regional differences in cortical thickness. Similar steps were performed in the surface-based R1, R2* and susceptibility maps of each participant to correct the inter-regional differences in myelin and iron.

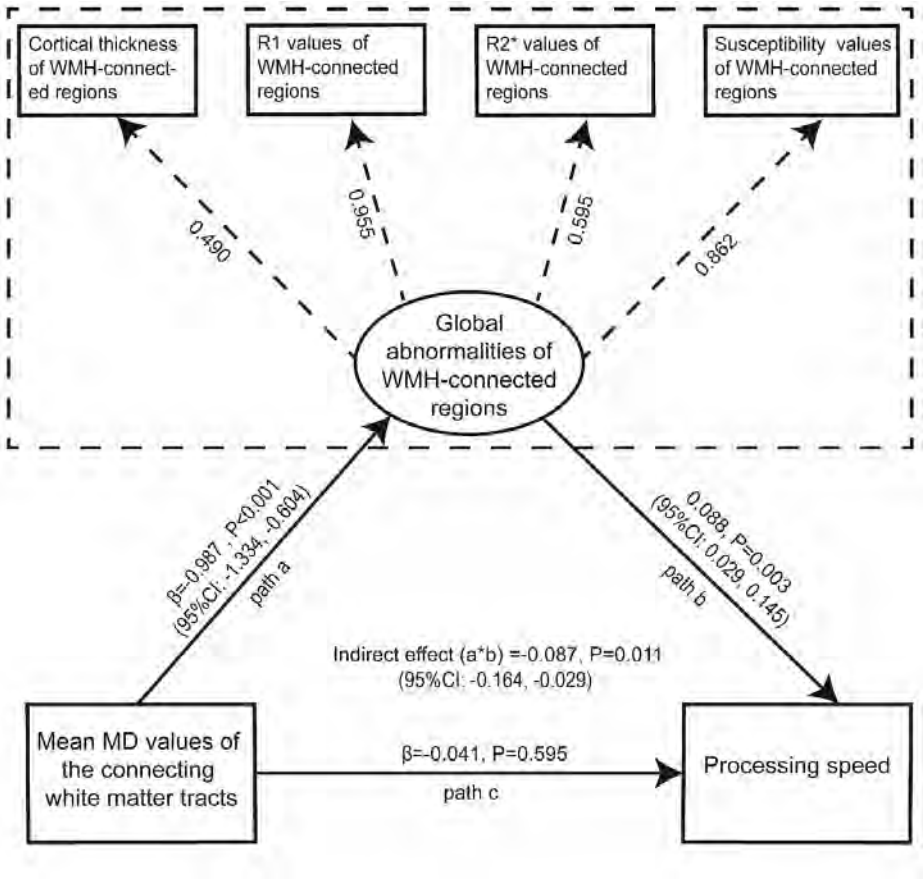

Figure e-3. Structural equation model for the relations between the microstructural damage of the connecting white matter tract, the abnormalities of WMH-connected regions and cognitive performances. WMH-connected regions were identified at the high-connectivity level. Covariances and control variables were omitted for readability. Upper panel: the confirmatory factor analysis (CFA) used to fit the latent variable representing global cortical abnormalities of the WMH-connected regions, the values attached to each dashed arrow are standardized factor load of each cortical measurements on the constructed latent variable; Lower panel: the mediation analysis, of mean MD values of the connecting white matter tract, the global cortical abnormalities of the WMH-connected regions and processing speed, path a: relationship between mean MD values of the connecting white matter tract and global cortical abnormalities of the WMH-connected regions, path b: relationship between global cortical abnormalities of the WMH-connected regions and processing speed. path c: direct relationship between mean MD values of the connecting white matter tract and processing speed. MD, mean diffusivity; WMH, white matter hyperintensities; 95%CI, 95% confidence interval.

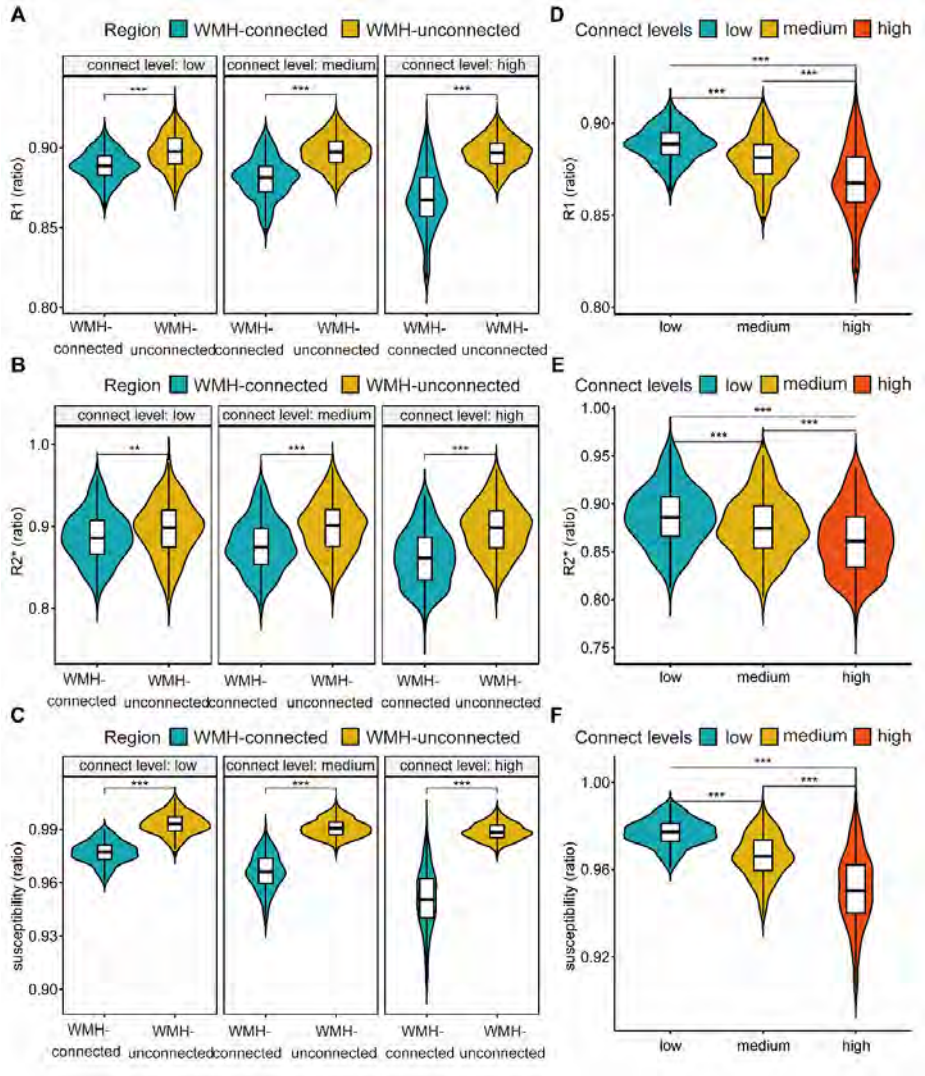

Figure e-4. Comparison of R1, R2*, susceptibility values between WMH-connected regions and WMH-unconnected regions (A-C), and between different connectivity levels (D-F) while adjusting cortical thickness. **, *p-corrected* < 0.01, ***, *p-corrected* < 0.001

Reference

1. Wardlaw JM, et al. Neuroimaging standards for research into small vessel disease and its contribution to ageing and neurodegeneration. Lancet Neurol. Aug 2013;12(8):822-38. doi:10.1016/s1474-4422(13)70124-8
2. Wardlaw JM, Smith C, Dichgans M. Small vessel disease: mechanisms and clinical implications. Lancet Neurol. Jul 2019;18(7):684-696. doi:10.1016/s1474-4422(19)30079-1
3. Tuladhar AM, Reid AT, Shumskaya E, de Laat KF, van Norden AG, van Dijk EJ, Norris DG, de Leeuw FE. Relationship between white matter hyperintensities, cortical thickness, and cognition. Stroke. Feb 2015;46(2):425-32. doi:10.1161/strokeaha.114.007146
4. Lambert C, Sam Narean J, Benjamin P, Zeestraten E, Barrick TR, Markus HS. Characterising the grey matter correlates of leukoaraiosis in cerebral small vessel disease. Neuroimage Clin. 2015;9:194-205. doi:10.1016/j.nicl.2015.07.002
5. Lambert C, Benjamin P, Zeestraten E, Lawrence AJ, Barrick TR, Markus HS. Longitudinal patterns of leukoaraiosis and brain atrophy in symptomatic small vessel disease. Brain. Apr 2016;139(Pt 4):1136-51. doi:10.1093/brain/aww009
6. Duering M, Righart R, Csanadi E, Jouvent E, Hervé D, Chabriat H, Dichgans M. Incident subcortical infarcts induce focal thinning in connected cortical regions. Neurology. Nov 13 2012;79(20):2025-8. doi:10.1212/WNL.0b013e3182749f39
7. Duering M, Righart R, Wollenweber FA, Zietemann V, Gesierich B, Dichgans M. Acute infarcts cause focal thinning in remote cortex via degeneration of connecting fiber tracts. Neurology. Apr 21 2015;84(16):1685-92. doi:10.1212/wnl.0000000000001502
8. Mayer C, Frey BM, Schlemm E, Petersen M, Engelke K, Hanning U, Jagodzinski A, Borof K, Fiehler J, Gerloff C, Thomalla G, Cheng B. Linking cortical atrophy to white matter hyperintensities of presumed vascular origin. J Cereb Blood Flow Metab. Jul 2021;41(7):1682-1691. doi:10.1177/0271678x20974170
9. van den Brink H, Doubal FN, Duering M. Advanced MRI in cerebral small vessel disease. Int J Stroke. Jan 2023;18(1):28-35. doi:10.1177/17474930221091879
10. Lutti A, Dick F, Sereno MI, Weiskopf NJN. Using high-resolution quantitative mapping of R1 as an index of cortical myelination. 2014;93:176-188.
11. Langkammer C, Krebs N, Goessler W, Scheurer E, Ebner F, Yen K, Fazekas F, Ropele S. Quantitative MR imaging of brain iron: a postmortem validation study. Radiology. Nov 2010;257(2):455-62. doi:10.1148/radiol.10100495
12. Langkammer C, Schweser F, Krebs N, Deistung A, Goessler W, Scheurer E, Sommer K, Reishofer G, Yen K, Fazekas F, Ropele S, Reichenbach JR. Quantitative susceptibility mapping (QSM) as a means to measure brain iron? A post mortem validation study. Neuroimage. Sep 2012;62(3):1593-9. doi:10.1016/j.neuroimage.2012.05.049
13. Cai M, Jacob MA, van Loenen MR, Bergkamp M, Marques J, Norris DG, Duering M, Tuladhar AM, de Leeuw FE. Determinants and Temporal Dynamics of Cerebral Small Vessel Disease: 14-Year Follow-Up. Stroke. Sep 2022;53(9):2789-2798. doi:10.1161/strokeaha.121.038099
14. Shelhamer E, Long J, Darrell T. Fully Convolutional Networks for Semantic Segmentation. IEEE transactions on pattern analysis and machine intelligence. Apr 2017;39(4):640-651. doi:10.1109/tpami.2016.2572683
15. Fazekas F, Chawluk JB, Alavi A, Hurtig HI, Zimmerman RA. MR signal abnormalities at 1.5 T in Alzheimer's dementia and normal aging. AJR Am J Roentgenol. Aug 1987;149(2):351-6. doi:10.2214/ajr.149.2.351

16. Amin Al Olama A, Wason JMS, Tuladhar AM, van Leijsen EMC, Koini M, Hofer E, Morris RG, Schmidt R, de Leeuw FE, Markus HS. Simple MRI score aids prediction of dementia in cerebral small vessel disease. Neurology. Mar 24 2020;94(12):e1294-e1302. doi:10.1212/wnl.0000000000009141

17. Li H, Cai M, Jacob MA, Norris DG, Marques JP, Chamberland M, Duering M, Kessels RPC, de Leeuw FE, Tuladhar AM. Dissociable Contributions of Thalamic-Subregions to Cognitive Impairment in Small Vessel Disease. Stroke. May 2023;54(5):1367-1376. doi:10.1161/strokeaha.122.041687

18. Kellner E, Dhital B, Kiselev VG, Reisert M. Gibbs-ringing artifact removal based on local subvoxel-shifts. Magn Reson Med. Nov 2016;76(5):1574-1581. doi:10.1002/mrm.26054

19. Veraart J, Novikov DS, Christiaens D, Ades-Aron B, Sijbers J, Fieremans E. Denoising of diffusion MRI using random matrix theory. Neuroimage. Nov 15 2016;142:394-406. doi:10.1016/j.neuroimage.2016.08.016

20. Andersson JLR, Sotiropoulos SN. An integrated approach to correction for off-resonance effects and subject movement in diffusion MR imaging. Neuroimage. Jan 15 2016;125:1063-1078. doi:10.1016/j.neuroimage.2015.10.019

21. Smith SM, Jenkinson M, Woolrich MW, Beckmann CF, Behrens TE, Johansen-Berg H, Bannister PR, De Luca M, Drobnjak I, Flitney DE, Niazy RK, Saunders J, Vickers J, Zhang Y, De Stefano N, Brady JM, Matthews PM. Advances in functional and structural MR image analysis and implementation as FSL. NeuroImage. 2004;23 Suppl 1:S208-19. doi:10.1016/j.neuroimage.2004.07.051

22. Tustison NJ, Avants BB, Cook PA, Zheng Y, Egan A, Yushkevich PA, Gee JC. N4ITK: improved N3 bias correction. IEEE Trans Med Imaging. Jun 2010;29(6):1310-20. doi:10.1109/tmi.2010.2046908

23. Jbabdi S, Sotiropoulos SN, Savio AM, Graña M, Behrens TE. Model-based analysis of multishell diffusion MR data for tractography: how to get over fitting problems. Magn Reson Med. Dec 2012;68(6):1846-55. doi:10.1002/mrm.24204

24. Marques JP, Kober T, Krueger G, van der Zwaag W, Van de Moortele PF, Gruetter R. MP2RAGE, a self bias-field corrected sequence for improved segmentation and T1-mapping at high field. NeuroImage. Jan 15 2010;49(2):1271-81. doi:10.1016/j.neuroimage.2009.10.002

25. O'Brien KR, Kober T, Hagmann P, Maeder P, Marques J, Lazeyras F, Krueger G, Roche A. Robust T1-weighted structural brain imaging and morphometry at 7T using MP2RAGE. PloS one. 2014;9(6):e99676. doi:10.1371/journal.pone.0099676

26. Fukutomi H, Glasser MF, Zhang H, Autio JA, Coalson TS, Okada T, Togashi K, Van Essen DC, Hayashi T. Neurite imaging reveals microstructural variations in human cerebral cortical gray matter. NeuroImage. Nov 15 2018;182:488-499. doi:10.1016/j.neuroimage.2018.02.017

27. Desikan RS, Ségonne F, Fischl B, Quinn BT, Dickerson BC, Blacker D, Buckner RL, Dale AM, Maguire RP, Hyman BT, Albert MS, Killiany RJ. An automated labeling system for subdividing the human cerebral cortex on MRI scans into gyral based regions of interest. NeuroImage. Jul 1 2006;31(3):968-80. doi:10.1016/j.neuroimage.2006.01.021

28. Muthuraman M, Fleischer V, Kroth J, Ciolac D, Radetz A, Koirala N, Gonzalez-Escamilla G, Wiendl H, Meuth SG, Zipp F, Groppa S. Covarying patterns of white matter lesions and cortical atrophy predict progression in early MS. Neurology(R) neuroimmunology & neuroinflammation. May 4 2020;7(3)doi:10.1212/nxi.0000000000000681

29. Coalson TS, Van Essen DC, Glasser MF. The impact of traditional neuroimaging methods on the spatial localization of cortical areas. Proceedings of the National Academy of Sciences of the United States of America. Jul 3 2018;115(27):E6356-e6365. doi:10.1073/pnas.1801582115

30. Shams Z, Norris DG, Marques JP. A comparison of in vivo MRI based cortical myelin mapping using T1w/T2w and R1 mapping at 3T. PloS one. 2019;14(7):e0218089. doi:10.1371/journal.pone.0218089

31. Ganzetti M, Wenderoth N, Mantini D. Whole brain myelin mapping using T1- and T2-weighted MR imaging data. Frontiers in human neuroscience. 2014;8:671. doi:10.3389/fnhum.2014.00671
32. Khabipova D, Wiaux Y, Gruetter R, Marques JP. A modulated closed form solution for quantitative susceptibility mapping--a thorough evaluation and comparison to iterative methods based on edge prior knowledge. NeuroImage. Feb 15 2015;107:163-174. doi:10.1016/j.neuroimage.2014.11.038
33. Greve DN, Fischl B. Accurate and robust brain image alignment using boundary-based registration. NeuroImage. Oct 15 2009;48(1):63-72. doi:10.1016/j.neuroimage.2009.06.060
34. Weiskopf N, Suckling J, Williams G, Correia MM, Inkster B, Tait R, Ooi C, Bullmore ET, Lutti A. Quantitative multi-parameter mapping of R1, PD(*), MT, and R2(*) at 3T: a multi-center validation. Front Neurosci. 2013;7:95. doi:10.3389/fnins.2013.00095
35. Wiegertjes K, Chan KS, Telgte AT, Gesierich B, Norris DG, Klijn CJ, Duering M, Tuladhar AM, Marques JP, Leeuw FE. Assessing cortical cerebral microinfarcts on iron-sensitive MRI in cerebral small vessel disease. Journal of cerebral blood flow and metabolism : official journal of the International Society of Cerebral Blood Flow and Metabolism. Dec 2021;41(12):3391-3399. doi:10.1177/0271678x211039609
36. Chan KS, Marques JP. SEPIA-Susceptibility mapping pipeline tool for phase images. NeuroImage. Feb 15 2021;227:117611. doi:10.1016/j.neuroimage.2020.117611
37. Smith SM. Fast robust automated brain extraction. Hum Brain Mapp. Nov 2002;17(3):143-55. doi:10.1002/hbm.10062
38. Karsa A, Shmueli K. SEGUE: A Speedy rEgion-Growing Algorithm for Unwrapping Estimated Phase. IEEE transactions on medical imaging. Jun 2019;38(6):1347-1357. doi:10.1109/tmi.2018.2884093
39. Liu T, Khalidov I, de Rochefort L, Spincemaille P, Liu J, Tsiouris AJ, Wang Y. A novel background field removal method for MRI using projection onto dipole fields (PDF). NMR in biomedicine. Nov 2011;24(9):1129-36. doi:10.1002/nbm.1670
40. Liu T, Liu J, de Rochefort L, Spincemaille P, Khalidov I, Ledoux JR, Wang Y. Morphology enabled dipole inversion (MEDI) from a single-angle acquisition: comparison with COSMOS in human brain imaging. Magnetic resonance in medicine. Sep 2011;66(3):777-83. doi:10.1002/mrm.22816
41. Brumer I, De Vita E, Ashmore J, Jarosz J, Borri M. Reproducibility of MRI-based white matter tract estimation using multi-fiber probabilistic tractography: effect of user-defined parameters and regions. Magma (New York, NY). Jun 2022;35(3):365-373. doi:10.1007/s10334-021-00965-6
42. Dauguet J, Peled S, Berezovskii V, Delzescaux T, Warfield SK, Born R, Westin CF. Comparison of fiber tracts derived from in-vivo DTI tractography with 3D histological neural tract tracer reconstruction on a macaque brain. Neuroimage. Aug 15 2007;37(2):530-8. doi:10.1016/j.neuroimage.2007.04.067
43. van Norden AG, van Uden IW, de Laat KF, van Dijk EJ, de Leeuw FE. Cognitive function in small vessel disease: the additional value of diffusion tensor imaging to conventional magnetic resonance imaging: the RUN DMC study. Journal of Alzheimer's disease : JAD. 2012;32(3):667-76. doi:10.3233/jad-2012-120784
44. Hu HY, Ou YN, Shen XN, Qu Y, Ma YH, Wang ZT, Dong Q, Tan L, Yu JT. White matter hyperintensities and risks of cognitive impairment and dementia: A systematic review and meta-analysis of 36 prospective studies. Neuroscience and biobehavioral reviews. Jan 2021;120:16-27. doi:10.1016/j.neubiorev.2020.11.007
45. Coenen M, et al. Strategic white matter hyperintensity locations for cognitive impairment: A multicenter lesion-symptom mapping study in 3525 memory clinic patients. Alzheimer's & dementia : the journal of the Alzheimer's Association. Dec 12 2022;doi:10.1002/alz.12827

46. Yeo IK, Johnson RA. A new family of power transformations to improve normality or symmetry. Biometrika. 2000;87(4):954-959. doi:10.1093/biomet/87.4.954 %J Biometrika
47. Cook RDJT. Detection of influential observation in linear regression. 1977;19(1):15-18.
48. Akinwande MO, Dikko HG, Samson AJOjos. Variance inflation factor: as a condition for the inclusion of suppressor variable (s) in regression analysis. 2015;5(07):754.
49. Goretzko D, Siemund K, Sterner PJE, Measurement P. Evaluating Model Fit of Measurement Models in Confirmatory Factor Analysis. 2023:00131644231163813.
50. Hommel GJB. A stagewise rejective multiple test procedure based on a modified Bonferroni test. 1988;75(2):383-386.
51. Salvadori E, Brambilla M, Maestri G, Nicotra A, Cova I, Pomati S, Pantoni L. The clinical profile of cerebral small vessel disease: Toward an evidence-based identification of cognitive markers. Alzheimer's & dementia : the journal of the Alzheimer's Association. Jan 2023;19(1):244-260. doi:10.1002/alz.12650
52. Garnier-Crussard A, Cotton F, Krolak-Salmon P, Chételat G. White matter hyperintensities in Alzheimer's disease: Beyond vascular contribution. Alzheimer's & dementia : the journal of the Alzheimer's Association. Apr 7 2023;doi:10.1002/alz.13057
53. Brown RB, Traylor M, Burgess S, Sawcer S, Markus HS. Do Cerebral Small Vessel Disease and Multiple Sclerosis Share Common Mechanisms of White Matter Injury? Stroke. Aug 2019;50(8):1968-1972. doi:10.1161/strokeaha.118.023649
54. Wardlaw JM, Smith C, Dichgans M. Mechanisms of sporadic cerebral small vessel disease: insights from neuroimaging. Lancet Neurol. May 2013;12(5):483-97. doi:10.1016/s1474-4422(13)70060-7
55. Lommers E, Simon J, Reuter G, Delrue G, Dive D, Degueldre C, Balteau E, Phillips C, Maquet P. Multiparameter MRI quantification of microstructural tissue alterations in multiple sclerosis. Neuroimage Clin. 2019;23:101879. doi:10.1016/j.nicl.2019.101879
56. Mainero C, Louapre C, Govindarajan ST, Giannì C, Nielsen AS, Cohen-Adad J, Sloane J, Kinkel RP. A gradient in cortical pathology in multiple sclerosis by in vivo quantitative 7 T imaging. Brain. Apr 2015;138(Pt 4):932-45. doi:10.1093/brain/awv011
57. Bodini B, Chard D, Altmann DR, Tozer D, Miller DH, Thompson AJ, Wheeler-Kingshott C, Ciccarelli O. White and gray matter damage in primary progressive MS: The chicken or the egg? Neurology. Jan 12 2016;86(2):170-6. doi:10.1212/wnl.0000000000002237
58. Bian W, Tranvinh E, Tourdias T, Han M, Liu T, Wang Y, Rutt B, Zeineh MM. In Vivo 7T MR Quantitative Susceptibility Mapping Reveals Opposite Susceptibility Contrast between Cortical and White Matter Lesions in Multiple Sclerosis. AJNR Am J Neuroradiol. Oct 2016;37(10):1808-1815. doi:10.3174/ajnr.A4830
59. Schweser F, Raffaini Duarte Martins AL, Hagemeier J, Lin F, Hanspach J, Weinstock-Guttman B, Hametner S, Bergsland N, Dwyer MG, Zivadinov R. Mapping of thalamic magnetic susceptibility in multiple sclerosis indicates decreasing iron with disease duration: A proposed mechanistic relationship between inflammation and oligodendrocyte vitality. NeuroImage. Feb 15 2018;167:438-452. doi:10.1016/j.neuroimage.2017.10.063
60. Burgetova A, Dusek P, Vaneckova M, Horakova D, Langkammer C, Krasensky J, Sobisek L, Matras P, Masek M, Seidl Z. Thalamic Iron Differentiates Primary-Progressive and Relapsing-Remitting Multiple Sclerosis. AJNR American journal of neuroradiology. Jun 2017;38(6):1079-1086. doi:10.3174/ajnr.A5166
61. Meguro R, Asano Y, Odagiri S, Li C, Shoumura K. Cellular and subcellular localizations of nonheme ferric and ferrous iron in the rat brain: a light and electron microscopic study by the perfusion-Perls and -Turnbull methods. Archives of histology and cytology. Dec 2008;71(4):205-22. doi:10.1679/aohc.71.205

62. Uchida Y, Kan H, Sakurai K, Arai N, Inui S, Kobayashi S, Kato D, Ueki Y, Matsukawa N. Iron leakage owing to blood-brain barrier disruption in small vessel disease CADASIL. Neurology. Sep 1 2020;95(9):e1188-e1198. doi:10.1212/wnl.0000000000010148

63. Righart R, Duering M, Gonik M, Jouvent E, Reyes S, Hervé D, Chabriat H, Dichgans M. Impact of regional cortical and subcortical changes on processing speed in cerebral small vessel disease. Neuroimage Clin. 2013;2:854-61. doi:10.1016/j.nicl.2013.06.006

64. Duering M, Gonik M, Malik R, Zieren N, Reyes S, Jouvent E, Hervé D, Gschwendtner A, Opherk C, Chabriat H, Dichgans M. Identification of a strategic brain network underlying processing speed deficits in vascular cognitive impairment. Neuroimage. Feb 1 2013;66:177-83. doi:10.1016/j.neuroimage.2012.10.084

65. Moore S, Meschkat M, Ruhwedel T, Trevisiol A, Tzvetanova ID, Battefeld A, Kusch K, Kole MHP, Strenzke N, Möbius W, de Hoz L, Nave KA. A role of oligodendrocytes in information processing. Nature communications. Oct 30 2020;11(1):5497. doi:10.1038/s41467-020-19152-7

66. Charlton RA, Morris RG, Nitkunan A, Markus HS. The cognitive profiles of CADASIL and sporadic small vessel disease. Neurology. May 23 2006;66(10):1523-6. doi:10.1212/01.wnl.0000216270.02610.7e

67. Weiskopf N, Edwards LJ, Helms G, Mohammadi S, Kirilina EJNRP. Quantitative magnetic resonance imaging of brain anatomy and in vivo histology. 2021;3(8):570-588.

68. Wardlaw JM, Benveniste H, Nedergaard M, Zlokovic BV, Mestre H, Lee H, Doubal FN, Brown R, Ramirez J, MacIntosh BJ, Tannenbaum A, Ballerini L, Rungta RL, Boido D, Sweeney M, Montagne A, Charpak S, Joutel A, Smith KJ, Black SE. Perivascular spaces in the brain: anatomy, physiology and pathology. Nat Rev Neurol. Mar 2020;16(3):137-153. doi:10.1038/s41582-020-0312-z

69. Jenkinson M, Smith S. A global optimisation method for robust affine registration of brain images. Medical image analysis. Jun 2001;5(2):143-56. doi:10.1016/s1361-8415(01)00036-6

70. Jenkinson M, Bannister P, Brady M, Smith S. Improved optimization for the robust and accurate linear registration and motion correction of brain images. NeuroImage. Oct 2002;17(2):825-41. doi:10.1016/s1053-8119(02)91132-8

71. Behrens TE, Berg HJ, Jbabdi S, Rushworth MF, Woolrich MW. Probabilistic diffusion tractography with multiple fibre orientations: What can we gain? Neuroimage. Jan 1 2007;34(1):144-55. doi:10.1016/j.neuroimage.2006.09.018

72. Rilling JK, Glasser MF, Preuss TM, Ma X, Zhao T, Hu X, Behrens TE. The evolution of the arcuate fasciculus revealed with comparative DTI. Nature neuroscience. Apr 2008;11(4):426-8. doi:10.1038/nn2072

73. Zhuo J, Fan L, Liu Y, Zhang Y, Yu C, Jiang T. Connectivity Profiles Reveal a Transition Subarea in the Parahippocampal Region That Integrates the Anterior Temporal-Posterior Medial Systems. The Journal of neuroscience : the official journal of the Society for Neuroscience. Mar 2 2016;36(9):2782-95. doi:10.1523/jneurosci.1975-15.2016

74. Seifert R, Telli T, Opitz M, Barbato F, Berliner C, Nader M, Umutlu L, Stuschke M, Hadaschik B, Herrmann K, Fendler WP. Unspecific (18)F-PSMA-1007 Bone Uptake Evaluated Through PSMA-11 PET, Bone Scanning, and MRI Triple Validation in Patients with Biochemical Recurrence of Prostate Cancer. Journal of nuclear medicine : official publication, Society of Nuclear Medicine. May 2023;64(5):738-743. doi:10.2967/jnumed.118.215434

Chapter 6.

Temporal and spatial effects of cortical micro-infarcts on the cortical and subcortical microstructure abnormalities in cerebral small vessel disease.

Submitted as:
Hao Li, Annemieke ter Telgte, Marco Duering, David G Norris, José P. Marques, Frank-Erik de Leeuw, Anil M. Tuladhar. Spatial and temporal effects of cortical cerebral microinfarcts on the cortical and subcortical regions in cerebral small vessel disease.

Abstract

Background: Cortical cerebral microinfarcts (CMIs) have emerged as imaging markers of cerebral small vessel disease (SVD) and are associated with cortical atrophy, impaired white matter (WM) connectivity.

Purpose: To investigate the mechanisms by which CMIs contribute to brain structural damage by assessing cortical thickness and micro-structural abnormalities in cortical and sub-cortical regions surrounding CMIs, and the temporal changes of these measures in SVD.

Materials and Methods: In a longitudinal cohort, 54 participants with SVD underwent monthly MRI scans over a ten-month period. We identified recent and chronic MIs along with their contralateral control regions. These regions were expanded within the cortex (cortical expansion) and along WM tracts toward the subcortex (subcortical expansion). Cortical thickness, R1 from quantitative T1-images, and neurite density index (NDI) from multi-diffusion images were extracted from these expansions to assess spatial effects. For recent CMIs, these measures were longitudinally extracted to assess temporal effects.

Results: Of 54 included participants (median age 68 years; 63% male), 22 (41%) had recent or chronic CMIs. Within cortical expansions, recent CMIs showed higher NDI in the immediate expansion (within 1.7mm), whereas chronic CMIs showed lower NDI and higher R1 values in the first two expansions (within 3.4 mm) compared to control regions. In sub-cortical expansions, recent CMIs showed no significant differences, but chronic CMIs consistently showed lower NDI values compared to contralateral regions, with these effects extending up to approximately 10 mm. Longitudinally, recent CMIs showed lower R1 and higher NDI values compared to control regions during acute phase, which normalized in follow-up scans.

Conclusion: Chronic CMIs are associated with significant microstructural changes in subcortical regions along the WM tracts, but show limited effects on adjacent cortical regions (likely related to partial volume effects). Alterations seen with recent CMIs are confined to lesion site and tend to be transient.

Introduction

Cortical cerebral microinfarcts (CMIs) are small ischemic lesions frequently observed through microscopic neuropathological examination.[1] Larger CMIs (up to 4 mm in diameter) can be in-vivo detected through MRI, appearing as hypointense on T1-weighted (T1W) images (i.e., chronic lesions), or hyperintense on diffusion-weighted imaging (DWI) (i.e., recent lesions).[1] The presence of CMIs has been associated with cognitive impairment, particularly in cerebrovascular diseases and dementia population.[2,3] This association could be partially attributed to cortical atrophy and disruption of white matter (WM) connectivity associated with CMIs.[4-6] However, the mechanisms by which CMIs lead to cortical atrophy and WM connectivity disruption remain unclear.

CMI-induced damage may spread horizontally within cortex and vertically to subcortical regions along descending fibers. Previous studies partially supported this hypothesis, showing perilesional cortical atrophy beyond CMI lesion core.[4,5] However, in vivo human studies of subcortical spread are lacking. Current evidence is limited to studies in mice models, which suggest a possible migration pathway from CMI lesions to subcortical regions along WM tracts.[7] Moreover, specific microstructural abnormalities associated with cortical and subcortical damage remain unexplored. Quantitative MRI techniques, including R1 (1/T1) mapping and neurite orientation dispersion and density imaging (NODDI) based on biophysical diffusion modelling, could more sensitively detect alterations of tissue microstructure.[8-10]

In addition to the spatial spread, understanding the temporal changes of the CMI-induced alterations is crucial for assessing their full impact. In our previous study with ten monthly MRI scans, we detected recent CMIs in 13% of participants with small vessel disease (SVD), which disappeared in follow-up scans.[11] Yet, these lesions may induce persistent underlying microstructural abnormalities, which could be detectable using advanced imaging. For example, we previously found increased R2* values (indicative of iron accumulation) at recent CMI lesion sites after lesion disappearance.[12] However, evidence of other abnormalities, such as cortical thinning and microstructural tissue changes, is still lacking.

We aimed to systematically assess the spatial and temporal effects of CMI-induced microstructural abnormalities in SVD patients using multi-modal quantitative MRI. Spatially, we assessed microstructural abnormalities in cortical and subcortical regions surrounding both recent and chronic CMIs. Temporally, we examined

longitudinal microstructural changes exclusively for recent CMIs. We hypothesized that CMI-induced microstructural abnormalities extend beyond the lesion core into adjacent cortex and subcortical regions through WM tracts. Furthermore, for recent CMIs, we proposed that these lesion-induced changes persist over time, even though these lesions visually disappeared on follow-up scans.

Methods

Participants and MRI acquisition

Data were obtained from the Radboud University Nijmegen Diffusion tensor and Magnetic resonance imaging Cohort – Investigating The origin and EvolutioN of cerebral small vessel disease (RUN DMC – InTENse) study.[13] RUN DMC-InTENse is a longitudinal observational study aiming to investigate the origin and short-term dynamical evolution of SVD. A total of 54 participants with SVD and without other identified causes of cerebral ischemia were recruited from the original RUN DMC study (Figure 1).[11] All participants underwent a pre-screening visit to determine eligibility, followed by 10 consecutive monthly MRI assessments at Radboud University Medical Centre between March 2016 and November 2017. A schematic diagram of this study is presented in Figure 2. All participants provided informed consent, and the study was approved by the Medical Review Ethics Committee of the Region Arnhem-Nijmegen.

MRI scans were performed on a 3T MAGNETOM Prisma scanner (Siemens) with the following sequences: Magnetization Prepared 2 Rapid Acquisition Gradient Echoes (MP2RAGE), multi-shell diffusion weighted image (DWI), 3D fluid-attenuated inversion recovery (FLAIR), multiple spin-echo T2 image and 3D multi-echo gradient echo sequence (GRE). Detailed MRI parameters were described elsewhere.[13]

Identification of cortical cerebral microinfarcts

Assessment of chronic and recent CMIs has been reported elsewhere.11 Briefly, CMIs were defined as MRI-visible lesions smaller than 4 mm in the cortex. Recent CMIs were hyperintense on DWI, chronic CMIs were hypointense on T1W, T2W, and FLAIR images, without hyperintensity on DWI.[1,2,11,14,15] For the detection of recent CMIs all monthly images were assessed. Recent CMIs were segmented in DWI space, while chronic CMIs were segmented in T1W space (example images in Figure e-1). For each segmented lesion, a corresponding contralateral control region was identified. These control regions underwent visual inspection and manual adjustment to ensure the accuracy.

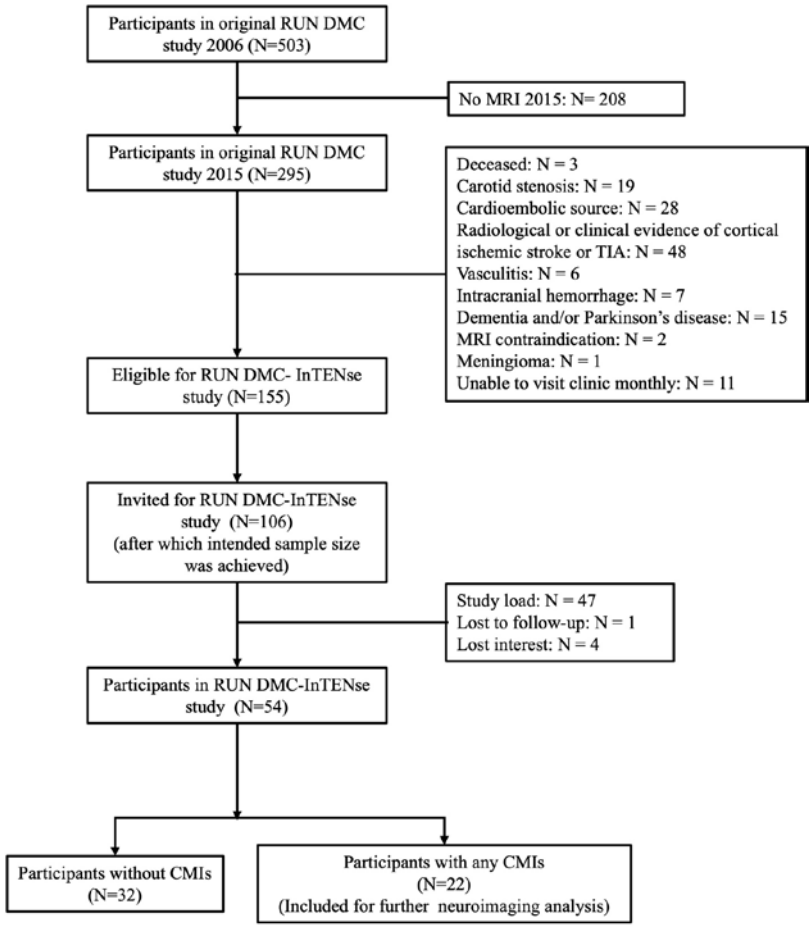

Figure 1. Flow diagram of the study sample. RUN DMC, the Radboud University Nijmegen Diffusion tensor and Magnetic resonance imaging Cohort; RUN DMC-InTENse, the Radboud University Nijmegen Diffusion tensor and Magnetic resonance imaging Cohort – Investigating The origin and EvolutioN of cerebral small vessel disease. CMIs, cortical cerebral microinfarcts.

Quantitative MRI measures: cortical thickness, R1 and Neurite Density Index

Three quantitative MRI measures: cortical thickness (CT), R1 and neurite density index (NDI), were employed in our study. R1 and NDI were chosen to probe microstructural changes underlying cortical thinning. Higher R1 values are generally associated with increased myelination, while higher NDI values reflect greater neurite density.[8-10] The combination of R1 and NDI indices is particularly effective for investigating the microstructural basis of cortical thinning by providing complementary information. Considering the potential registration errors between

volume space and surface space, these MRI measures were directly computed in the volume space. CT and R1 maps were derived from the MP2RAGE sequence (taking into account transmit field inhomogeneities),[16] while NDI maps were generated from fully pre-processed multi-shell DWI images using the NODDI toolbox in Matlab.[10] Note that NDI maps were calculated separately for gray matter (GM) and WM, resulting in two NDI maps (i.e., GM-NDI and WM-NDI) for each participant.[17] Details are provided in the supplementary materials.

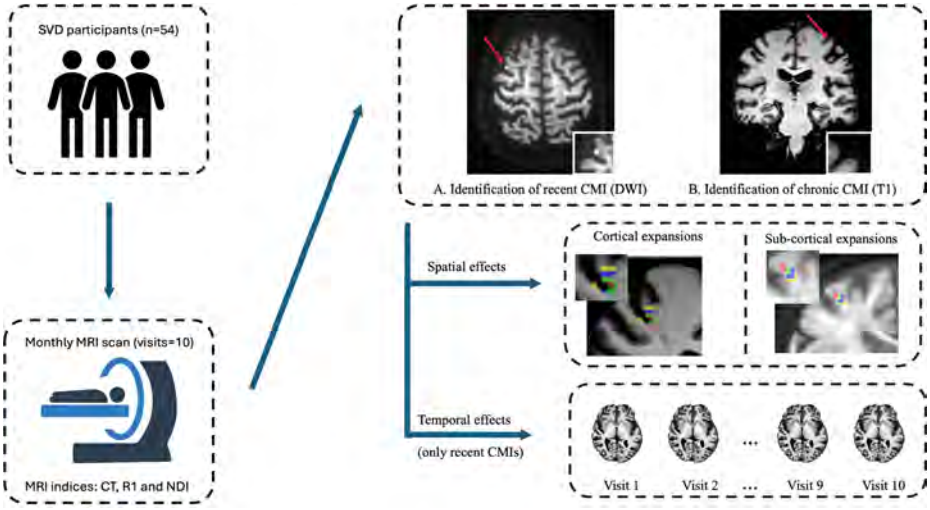

Figure 2. Study design and methods. Participants with SVD underwent ten consecutive monthly MRI assessments. Cortical thickness, R1, and NDI were quantified from the collected T1 and diffusion MRI. Both recent and chronic CMIs were identified and segmented from diffusion-weighted and T1-weighted images for each participant. The effects of these CMIs on CT, R1, and NDI was examined both temporally and spatially. SVD, small vessel disease, CMI, cerebral microinfarcts, NDI, neurite density index.

Cortical and subcortical expansion

For all lesion and control regions, expansion was performed in two ways: 1) cortical expansion within adjacent cortex areas in T1 space, and (2) subcortical expansion along WM tracts that connect with the lesions or control regions in DWI space. WM tracts connecting with cortical ROIs were reconstructed using MRtrix 3.0. These cortical and subcortical expansions resulted in three concentric rings at distances of 1.7 mm, 3.4 mm, and 5.1 mm from the lesion core (example images in Figure e-1). These distances correspond to the diffusion image voxel size (1.7 mm isotropic) and twice the voxel size of the T1W image (0.85 mm isotropic). In addition, based on the observation that chronic CMIs consistently showed lower NDI values across all three subcortical expansions compared to the control regions, we performed an extended

expansion, increasing sub-cortical expansion numbers from three (5.1 mm) to ten (17 mm). This extended expansion allowed a comprehensive assessment of NDI changes in subcortical regions along WM tracts. Details are provided in the supplementary material.

Extraction of quantitative MRI measures

To assess the cortical spatial effects, we extracted mean CT, R1, GM-NDI values from each cortical expansion of CMIs and control regions; for subcortical spatial effects, we similarly extracted the mean R1 and WM-NDI values from their subcortical expansions.

To examine the temporal effects of recent CMIs, we defined the image visit at which a lesion was first identified as the "lesion-visit", visits prior to this as "pre-lesion-visits", and those after it as "post-lesion-visits". CT, R1, and NDI maps from all visits were registered to the T1W image obtained at the lesion-visit. These MRI measures (CT, R1, GM-NDI) were then extracted from lesion sites and corresponding control ROIs across all visits (further details provided in the supplementary material). To control for global changes unrelated to lesions over time, we calculated the normalized values as ratios of these MRI measures at lesion sites to those in matched control regions.

Statistical analysis

Baseline characteristics of participants with any (old or recent) CMIs were compared to those without using the two-sample t-test or Mann-Whitney U test for continuous variables and the Chi-squared test for categorical variables.

First, we tested the spatial (both cortical and subcortical) effects of recent and chronic CMIs. For cortical expansions, we compared the mean CT, R1, GM-NDI values between lesion expansion and matched control regions using paired-sample t-tests. The same approach was applied to the initial three subcortical expansions, comparing mean R1 and WM-NDI values. For extended subcortical expansions, we calculated normalized WM-NDI values (i.e., lesion/control ratios) and tested whether these normalized values were significantly less than 1 using one-sample t-tests.

Next, to assess the temporal effects of recent CMIs, we first compared the mean CT, R1, and GM-NDI values at the recent CMI lesion sites to corresponding controls on lesion-visit using paired-sample t-tests. Then, for each recent CMI, we averaged these normalized values separately for pre-lesion and post-lesion visits. Subsequently, we employed analysis of variance (ANOVA), followed by post-hoc paired-sample t-test, to compare the normalized values at three time points: (pre-lesion-visits, lesion-visit, and post-lesion-visits). These analyses focused exclusively

on recent CMIs, as chronic CMIs appear as fluid-filled cavities on MRI, making assessments of these MRI measures no meaningful.

All statistical analyses were performed using R software (version 4.1.1), with alpha set at 0.05 (two-tailed). Multiple comparisons were corrected using Bonferroni method.

Sensitivity analysis

Given consistently lower NDI values across three initial subcortical expansions of chronic CMIs compared to controls, we tested the specificity of WM-NDI index by comparing MD values between lesion and control regions across the three subcortical expansion using paired-sample t-tests.

Results

A total of 54 participants were included, with a median age of 68 years (interquartile range [IQR] 65-73) and 63% male. Baseline characteristics comparing participants with any (recent or old) CMIs (n = 22) and without (n = 32) are presented in Table 1. 472 MRI scans were collected over a median follow-up of 39.5 weeks for these participants. On these scans, 21 recent CMIs were identified in 7 participants and 81 chronic CMIs were found in 19 participants at baseline. No new chronic CMIs appeared during follow-up. All recent CMIs were only visible on the MRI conducted at the time they first appeared and were not detectable on any subsequent follow-up scans.

Cortical spatial effects of CMIs

For recent CMIs, GM-NDI values were higher in the first lesion expansion compared to the corresponding control regions, with no significant differences at the second or third expansions. (Figure e-2). For chronic CMIs, GM-NDI values were lower at the first and second lesion expansions compared to corresponding control regions (Figure 3). Additionally, for chronic CMIs, R1 values at the first cortical expansion were higher than those at the corresponding control regions (Figure 3).

Subcortical spatial effects of CMIs

For recent CMIs, no MRI measure differences were found between lesion and control regions at any subcortical expansion (Figure e-3). For chronic CMIs, WM-NDI values were consistently lower at all three initial lesion expansions compared to corresponding control regions, while R1 values showed no significant differences between lesion and control regions at any of the three expansions (Figure 4).

Additionally, in the extended subcortical expansions, normalized WM-NDI values were significantly lower than 1 within the first six subcortical expansions (10.2 mm) (Figure 5).

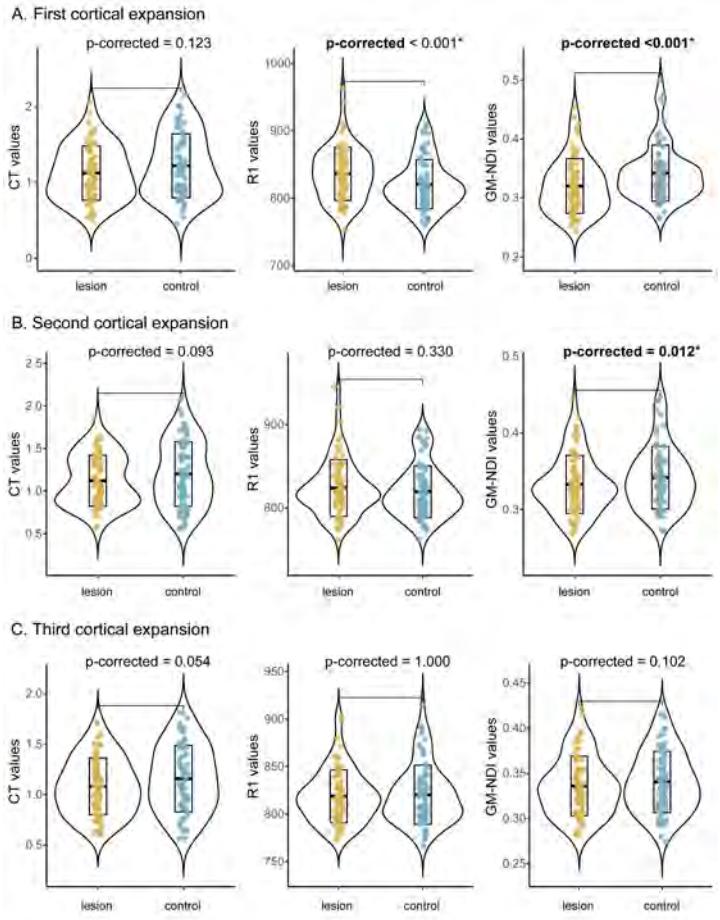

Figure 3. Comparisons of CT, R1 and GM-NDI values between chronic CMIs and control regions at each of their three cortical expansions. A. First cortical expansion, chronic CMIs showed higher R1 values and lower GM-NDI values compared to control regions; B. Second cortical expansion, chronic CMIs showed lower GM-NDI values compared to control regions. C. Third cortical expansion, chronic CMIs no differences at these MRI measures compared to control regions. CT, cortical thickness, GM-NDI, neurite density index for grey matter. Significant differences (p-corrected < 0.05) are indicated by an asterisk (*) and bold font. Among the 81 identified chronic CMIs, 7 lesions located too close to the pial surface and 2 lesions with poor cortical expansion characteristics were excluded, resulting in a total of 72 chronic CMIs included in the analysis.

Table 1 Demographic, clinical and imaging characteristics of the study sample.

	No CMIs (n = 32)	Acute or chronic CMIs (n = 22)	P values
Baseline demographics			
Age, years, mean (SD)	67.7 (4.0)	73.1 (8.0)	**0.007**
Male, n (%)	17 (53.1%)	17 (77.3%)	0.090
Education levels, median (IQR)	5.0 (5.0 – 6.0)	5.0 (5.0 – 6.0)	0.628
Baseline cardiovascular risk factors			
Systolic blood pressure, mmHg, mean (SD)	138.3 (18.6)	148.9 (19.2)	**0.0496**
Diastolic blood pressure, mmHg, median (IQR)	79.7 (74.2 – 85.8)	83.3 (77.8 – 90.6)	0.307
Hypertension, n (%)	24 (75.0%)	21 (95.5%)	0.067
Diabetes, n (%)	4 (12.5%)	2 (9.1%)	1.000
Hypercholesterolemia, n (%)	16 (50.0%)	11 (50.0%)	1.000
BMI, kg/m2, mean (SD)	25.7 (4.0)	25.9 (3.5)	0.881
Smoking history, n (%)	22 (68.8 %)	16 (72.7%)	0.991
Antithrombotic agents, n (%)	13 (40.6%)	13 (59.0%)	0.290
Baseline SVD MRI markers			
WMH volume, ml, median (IQR)	3.4 (2.1 – 9.4)	7.2 (3.9 – 10.4)	0.138
WMH volume, % of WM Volume, median (IQR)	0.8 (0.5 – 2.0)	1.5 (0.9 – 8.3)	0.138
Lacunes, n (%)	5 (15.6%)	7 (31.8%)	0.194
Microbleeds, n (%)	14 (43.8%	11 (50.0%)	0.861

Educational level was assessed using a 7-point Dutch rating scale with 1 indicating primary school not 17 completed and 7 academic degrees. CMIs, cerebral microinfarcts, BMI, body mass index. WM, white matter. WMH, white matter hyperintensity. *P*-values in bold represent *P* value < 0.05.

Temporal effects of CMIs at the lesion site

On the lesion visit, recent CMI lesion sites showed significantly lower R1 values and higher GM-NDI values compared to the control regions (Figure e-4). For recent CMIs, no MRI measure differences were found between lesion and control regions at any subcortical expansion (Figure e-3). For chronic CMIs, WM-NDI values were consistently lower at all three initial lesion expansions compared to corresponding control regions, while R1 values showed no significant differences between lesion and control regions at any of the three expansions (Figure 4). Additionally, in the extended subcortical expansions, normalized WM-NDI values were significantly lower than 1 within the first six subcortical expansions (10.2 mm) (Figure 5).

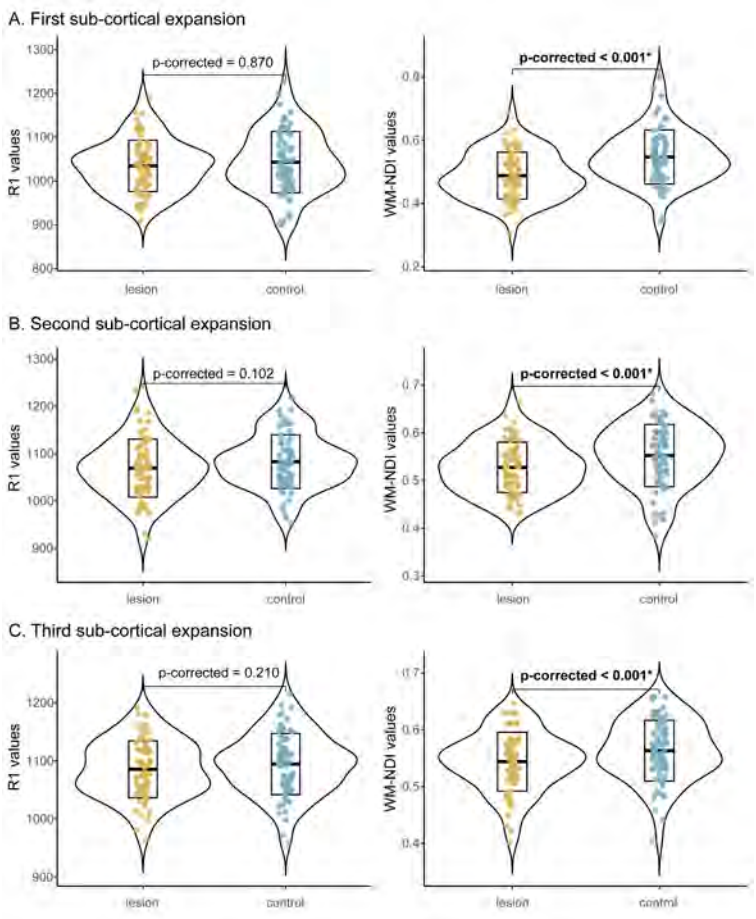

Figure 4. Comparisons of CT, R1 and WM-NDI values between chronic CMIs and control regions at each of their three sub-cortical expansions. A. First sub-cortical expansion, chronic CMIs showed lower WM-NDI values compared to control regions. B. Second sub-cortical expansion, chronic CMIs showed lower WM-NDI values compared to control regions. C. Third sub-cortical expansion, chronic CMIs showed lower WM-NDI values compared to control regions. Significant differences (p-corrected < 0.05) are indicated by an asterisk (*) and bold font. Among the 81 identified chronic CMIs, 7 lesions located too close to the pial surface and 3 lesions with poor cortical expansion characteristics were excluded, resulting in a total of 71 chronic CMIs were included in the analysis.

Sensitivity analysis

For chronic CMIs, MD values at the first sub-cortical expansion were lower than those at the corresponding control regions, while no differences were found at the second and third sub-cortical expansions (Figure e-6).

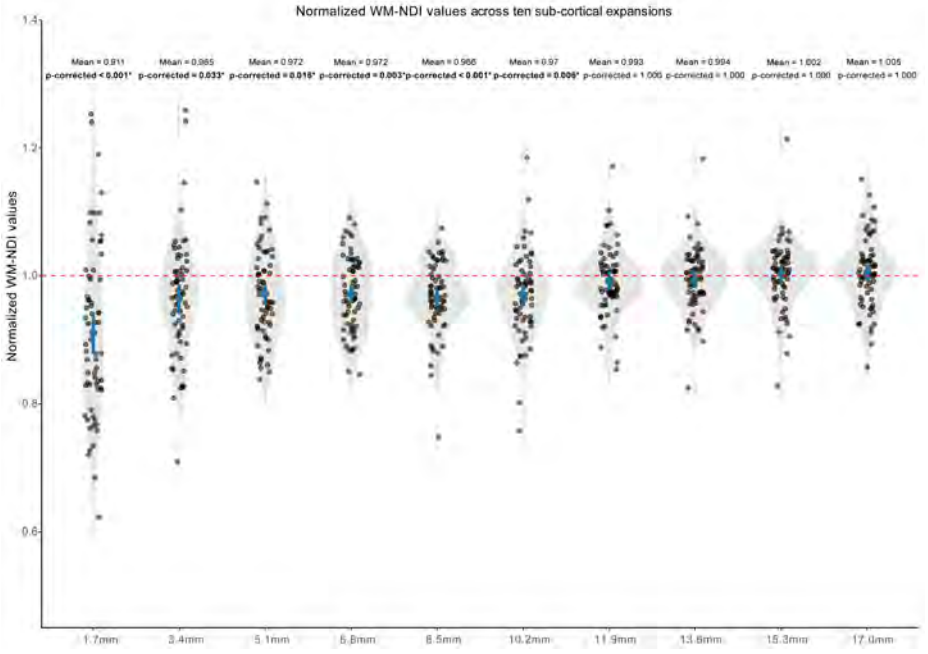

Figure 5. Normalized WM-NDI values of chronic CMIs across ten sub-cortical expansions. Normalized WM-NDI values within the first six subcortical expansions (10.2 mm) were lower than one. Significant differences (p-corrected < 0.05) are indicated by an asterisk (*) and bold font.

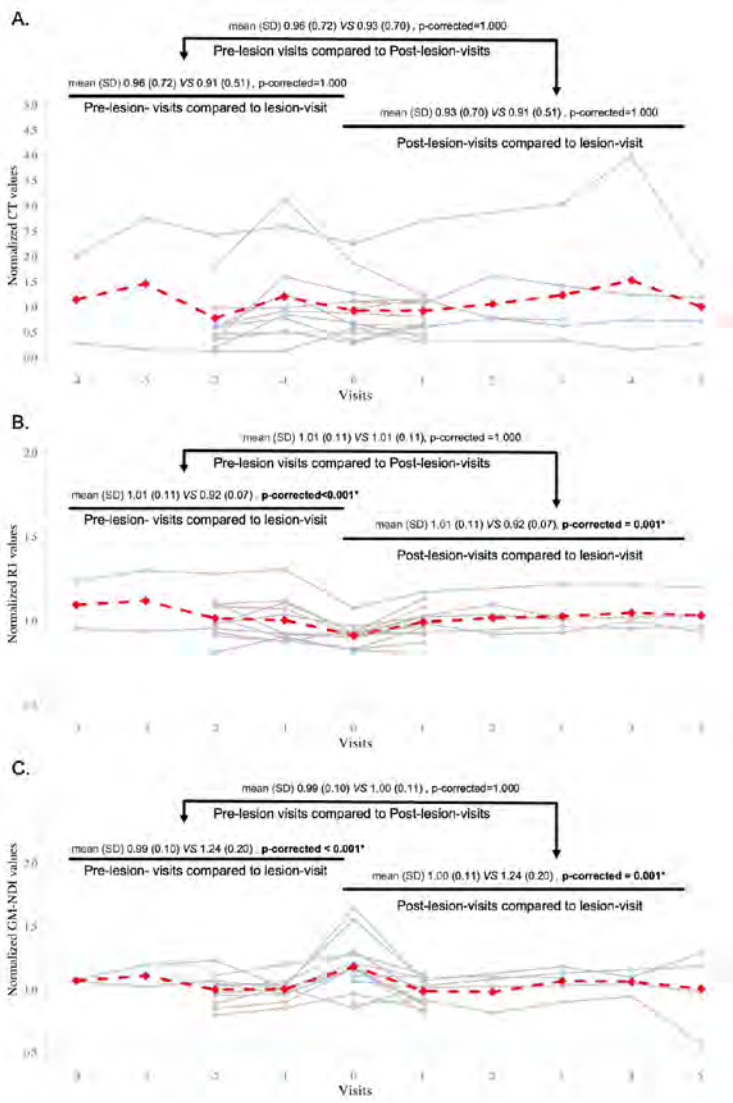

Figure 6. Comparison of normalized CT, R1 and GM-NDI values of recent CMIs at the lesion site between pre-lesion-visits, lesion-visit and post-lesion-visits. A, recent CMIs showed no differences of the normalized CT values at the lesion site between pre-lesion-visits, lesion-visit and post-lesion-visits; B, recent CMIs showed lower normalized R1 values at the lesion site on the lesion-visit compared to pre-lesion-visits and post-lesion-visits. C, recent CMIs showed higher normalized GM-NDI values at the lesion site on the lesion-visit compared to pre-lesion-visits and post-lesion-visits. Visit = 0 represents the lesion-visit, i.e., the visit when the lesion identified, visit < 0 represents pre-lesion-visits, i.e., visits prior to the lesion-visit, visit > 0 represents post-lesion-visits, i.e., visits after the lesion-visit. CT, cortical thickness, GM-NDI, neurite density index for grey matter. Significant differences (p-corrected < 0.05) are indicated by an asterisk (*) and bold font. Among the 21 identified recent CMIs, 2 lesions located too close to the pial surface were excluded, resulting in a total of 19 recent CMIs included in the analysis.

Discussion

In the present study, we found that (1) chronic CMIs were associated with lower WM-NDI values in surrounding subcortical regions along the WM tracts, extending up to 10.2 mm; (2) longitudinally, recent CMIs showed lower R1 values and higher NDI values compared to the control regions at the time of lesion detection, which normalized during follow-up. These findings suggest that chronic CMIs could cause sub-cortical microstructural changes along descending WM tracts, reflecting a vertical spread of damage, while sparing adjacent cortical regions. By contrast, microstructural changes induced by recent CMIs remained confined to the lesion site and do not persist over time.

We found that chronic CMIs showed lower NDI values at the surrounding cortical and sub-cortical regions. Notably, these effects were significantly more pronounced in the subcortical regions (up to 10.2 mm subcortically vs 3.4 mm cortically). A decrease in NDI values typically indicate axonal or dendritic damage.[10] Our findings provide the first in-vivo evidence suggesting that chronic CMIs can induce subcortical damage, most likely axonal damage, along white matter tracts connecting with the lesion. This finding supports secondary neurodegeneration as a factor in the non-local effects caused by chronic CMIs, potentially explaining previously observed associations between CMIs, disrupted overall WM connectivity and cognitive impairment.[6] By contrast, we did not find similar pronounced differences in MD or R1 values between lesions and controls in sub-cortical expansions. This may be because MD index from diffusion tensor imaging (DTI) model is less specific to microstructure compared to NDI index from the biophysical NODDI diffusion model.[10] Additionally, since white matter is rich in myelin and R1 is primarily associated with myelination, R1 values may be less susceptible to white matter damages when the myelin structure is relatively preserved.

Regarding cortical expansions of chronic CMIs, our findings contrast with previous studies.[4,5] Specifically, we observed a considerably smaller extent of perilesional damage compared to previous reports. Previous study showed that CMIs (defined as <5 mm) may induce cortical thinning extending up to 20 mm from the lesion core.[5] In contrast, our findings showed peri-lesional micro-structure changes, reflected by reduced NDI values, are limited to approximately 3 mm from the lesion core and occur without accompanying cortical thinning. Considering the voxel size (1.7 mm) of the diffusion data and the multiple co-registration of images involved, these observed perilesional changes are attributable to partial volume effects or, at most, represent mild and spatially limited tissue damage. This discrepancy between cortical and subcortical damages caused by chronic CMIs

could be attributed to the anatomical organization of cortical fibbers. Compared to horizontal fibbers within cortex, vertical nerve fibbers extending to subcortical areas are more numerous, forming the basic structural unit of the cortex, i.e., the cortex column.[18] Consequently, secondary neurodegeneration processes may preferentially propagate along these vertical fibbers, resulting in more pronounced subcortical than cortical damage following chronic CMIs. Additionally, we found higher R1 values at the first cortical expansion of chronic CMIs compared to control regions. This result cannot be attributed to partial volume effects, as R1 values at the lesion core itself were lower than in controls (Figure e-6). Instead, higher R1 values may result from gliosis in response to tissue injury,[19,20] where denser glial content restricts water mobility and alters the interaction between tissue-bound water and macromolecules, leading to shortened T1 (1/R1).[21] Nevertheless, further validation with high-resolution MRI and histopathological studies are warranted.

Regarding the spatial effects of recent CMIs, we found higher NDI values in the first cortical expansion compared to control regions, likely reflecting partial volume effects rather than perilesional damage. As suggested by previous histopathological studies, tissue injury of recent CMIs is relatively minor.[22] In the present study, at the lesion site, recent CMIs showed higher NDI values and lower R1 values compared to control regions. The increased NDI values can be explained by the neuronal swelling due to cytotoxic edema in the early phase following CMI onset.[23,24] Alternatively, the assumptions of fixed diffusivity and tortuosity constraints in NODDI model may not fully apply during the acute stage of infarction.[25] Decrease in R1 values may result from increased water content due to vasogenic edema or from demyelination, which increase water mobility. When damage is confined to myelin while axon remain preserved, it is less likely to induce secondary neurodegeneration.[26]

Furthermore, we found that the changes in R1 and NDI values at recent CMI lesion sites normalized on subsequent follow-up MRI scans. This is consistent with our previous findings that all recent CMIs became undetectable over time.[11] Additionally, this further supports our speculation that changes in R1 and NDI at the recent CMI lesion site reflect neuronal swelling transient edema rather than irreversible tissue damages. However, another study from our group suggested that increased R2* values at the recent CMIs sites persist in the follow-up scans.12 The may suggest that iron accumulation (as indicated by increased R2*) may arise not from ongoing myelin or neurite disruption, but from increased cell membrane permeability or vascular leakage of blood cells.[27]

The strengths of this study include a high-frequency serial imaging design using state-of-the-art multimodal neuroimaging. Monthly MRI scans allowed us to capture

acute events and characterize their dynamics in a short-term. Some limitations should be acknowledged. First, MRI measures, particularly R1 and NDI indices, are indirect measures of tissue properties, and the underlying microstructure can only be speculated. Caution is warranted when relating these measures to specific tissue compositions. Second, in the present study, all chronic CMIs were identified at baseline, with no new chronic lesions detected during follow-up. Therefore, associations between chronic CMIs and subcortical WM damage could only be examined cross-sectionally. Future studies with long-term follow-up are needed to clarify the temporal or causal relationships between the onset of chronic CMIs and subsequent subcortical WM damages. Third, due to the small size of these lesions, measurement accuracy at lesion sites could be confounded by registration errors and partial volume effects. To minimize these effects, we directly calculated CT in individuals' native volume space and minimized spatial transformations. We employed a state-of-the-art registration algorithm, with additional visual inspection and manual correction to ensure accuracy. We excluded lesions located too close to the pial surface to reduce partial volume effects from CSF. Nonetheless, future studies employing high-field MRI with optimal spatial resolution may further improve measurement precision. Finally, our cohort has a relatively small sample size (n=54) with a short follow-up (median: 39.5 weeks), which may limit statistical power and increase the risk of Type II errors. Larger cohorts with extended follow-up are warranted to validate these findings.

In conclusion, the present study provided a comprehensive assessment on the temporal and spatial effects of CMI-induced damages using high-frequency serial multi-modal images. Our findings showed that microstructural abnormalities from recent CMI are largely confined to lesion site and tend to be transient. By contrast, chronic CMIs may induce sub-cortical damages along WM tracts but are not likely to affect adjacent cortical regions. These findings clarified the distinct spatial and temporal effects of recent versus chronic CMIs on cortical and subcortical microstructural changes, thereby advancing our understanding of CMIs and their impact on brain structure, potentially explaining the mechanisms of cognitive impairment in SVD.

Supplementary material

Materials and methods

Quantitative MRI measures: cortical thickness, R1 and Neurite Density Index

For cortical thickness (CT), we first used a homemade MATLAB (R2016b; MathWorks, Natick, MA) script to create the robust T1W image based on MP2RAGE sequence.[28] Subsequently, we performed this volumetric CT calculation on the robust T1W image using DL + DiReCT, a tool based on diffeomorphic registration-based CT measurement.[29] This approach has demonstrated accuracy and reliability in CT measurements, comparable to those obtained from surface-based methods using FreeSurfer.[30]

For R1, MP2RAGE images were processed to obtain the quantitative T_1 map using an in-house MATLAB script.[9] The quantitative R1 map was created by taking the reciprocal of the T_1 map and scaling that in mHz (ms^{-1}). The R1 map and the robust T_1 image are intrinsically aligned since they are from the same data (i.e. MP2RAGE image).

For Neurite Density Index (NDI), we firstly preprocessed the multi-shell diffusion MRI data to denoise and remove Gibbs artifact, correct head motion and eddy current-induced distortions, mitigate susceptibility-induced distortions (topup) and intensity bias using the Functional Magnetic Resonance Imaging of the Brain Software Library (FSL; v6.0.1) and the Advanced Normalization Tools (ANTs, v 2.1.0).[31-35] The parameter of neurite compartment intrinsic parallel diffusivity [d∥] within the neurite orientation dispersion and density imaging (NODDI) model differs between white matter (WM) and grey matter (GM).[17] Consequently, when applying the NODDI model to WM, we set the d∥ value at 1.7 µm2/ms, which has been fixed using the corpus callosum as a reference, yielding the WM-NDI map for each participant; when employing NODDI model in the GM, we set its value to 1.2 µm2/ms, which is in the range of values proposed to minimise model residual for brain GM, yielding the GM-NDI map for each participant.[17]

Lesion expansion for cortical micro-infracts

For cortical expansion of recent CMIs and their control regions, these ROIs were registered from DWI space to T1W and then expanded six times in T1W space, each time increasing by one voxel (voxel size: 0.85 mm). To ensure these expanded regions were confined to the cortex, a cortical segmentation mask was applied during each expansion. Next, the ROIs and their three cortical expansions at 1.7 mm,

3.4 mm, and 5.1 mm in DWI space were registered back to T1W space. Regarding the subcortical expansion, probabilistic streamlines tractography using multi-shell DWI image were firstly performed to capture the WM tracts passing through the ROIs.[36,37] These ROIs in DWI space were expanded three times (1.7 mm, 3.4 mm, and 5.1 mm), each time increasing by one voxel (1.7 mm). Each expansion was restricted to the sub-cortical section of WM tracts connecting these ROIs by using a combination of WM and the corresponding tract-specific masks. The ROIs and their sub-cortical expansions were then registered to T1W space. The transformation between different modality within subject were performed using ANTs software.[38]

For cortical expansion of chronic CMIs and their control regions, ROIs in T1W space were incrementally expanded six times, each by one voxel (voxel size: 0.85 mm), with expansions confined to the cortical region using a cortical segmentation mask. The ROIs and their expansions at 1.7 mm, 3.4 mm, and 5.1 mm in T1 space were then registered to T1W space using ANTs software.[38] Regarding the sub-cortical expansions, these ROIs in T1W space were registered to DWI space using the ANTs software.[38] Subsequently, the sub-cortical sections of tracts passing through these ROIs in DWI space and their expansions were identified following the same methodology as with acute CMIs. These ROIs along with their expansions at 1.7 mm, 3.4 mm, 5.1 mm, 6.8 mm, and 8.5 mm, were registered to DWI space using ANTs software.[38]

For probabilistic streamlines tractography, fiber orientation distributions (FOD) images were estimated using the multi-tissue constrained spherical deconvolution (MT-CSD) algorithm in MRtrix 3.0 software.[36,39] These FOD images were then used to track fibers passing through the acute CMI lesions or control regions, employing these regions as seed masks and the second-order integration over fiber orientation distributions (iFOD2) algorithm.[37]

Extraction of quantitative MRI measures

All NDI maps from each visit were initially aligned with the corresponding T1W images of the same visit using using “antsRegistrationSyNQuick” function within ANTs software.[38] Subsequently, all T1W images from different visits were registered to the T1W image from the visit during which the lesion was identified using “antsRegistrationSyN” function.[38] Transformation matrices produced in this second registration step were then used to align the CT, R1, and GM-NDI maps from pre-lesion and post-lesion visits with the T1W image from the lesion-visit.

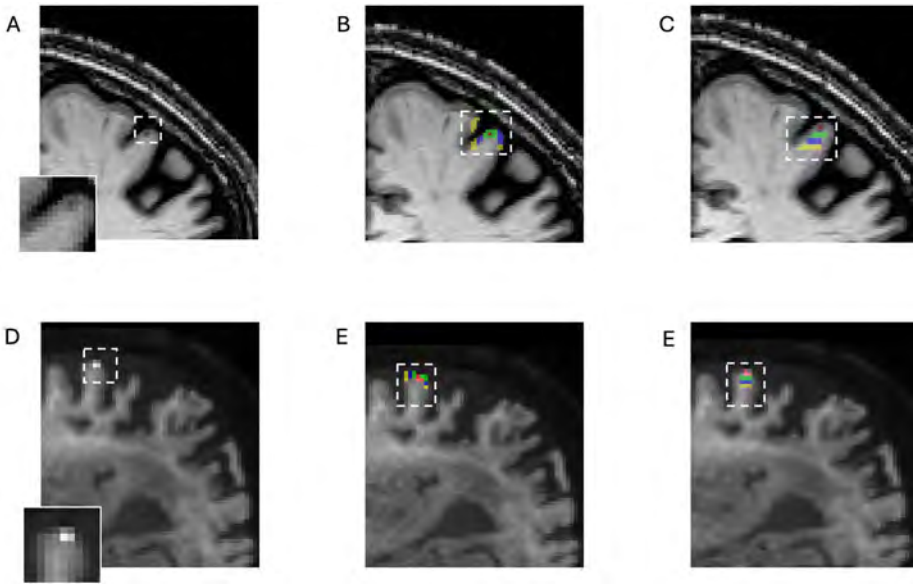

Figure e-1. Example images of recent and chronic CMIs and their cortical and sub-cortical expansions. A. chronic CMI; B, cortical expansions of chronic CMI; C, sub-cortical expansions of chronic CMI; D. recent CMI; E, cortical expansions of recent CMI; F, sub-cortical expansions of recent CMI. Red: original lesion site for recent or chronic CMIs; green: first expansion at 1.7mm; blue: second expansion at 3.4mm; yellow: third expansion at 5.1mm.

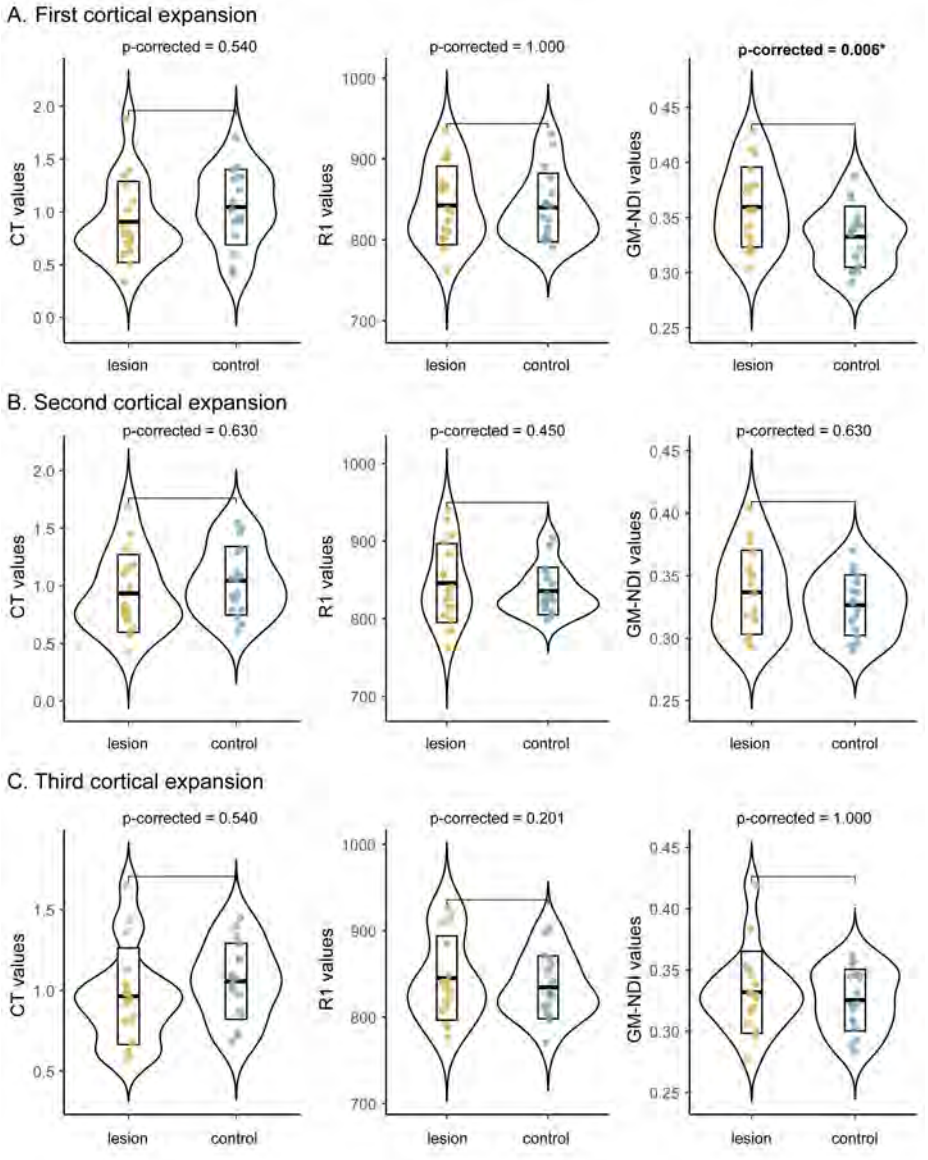

Figure e-2. Comparisons of CT, R1 and GM-NDI values between acute CMIs and control regions at each of their three cortical expansions. A. First cortical expansion, acute CMIs showed higher NDI values compared to control regions; B and C. Second and third cortical expansion, acute CMIs showed no differences at these MRI measures compared to control regions. CT, cortical thickness, GM-NDI, neurite density index for grey matter. Significant differences (p-corrected < 0.05) are indicated by an asterisk (*) and bold font. Among the 21 identified acute CMIs, 2 lesions located too close to the pial surface and 2 lesions with poor cortical expansion characteristics were excluded, resulting in a total of 17 acute CMIs included in the analysis.

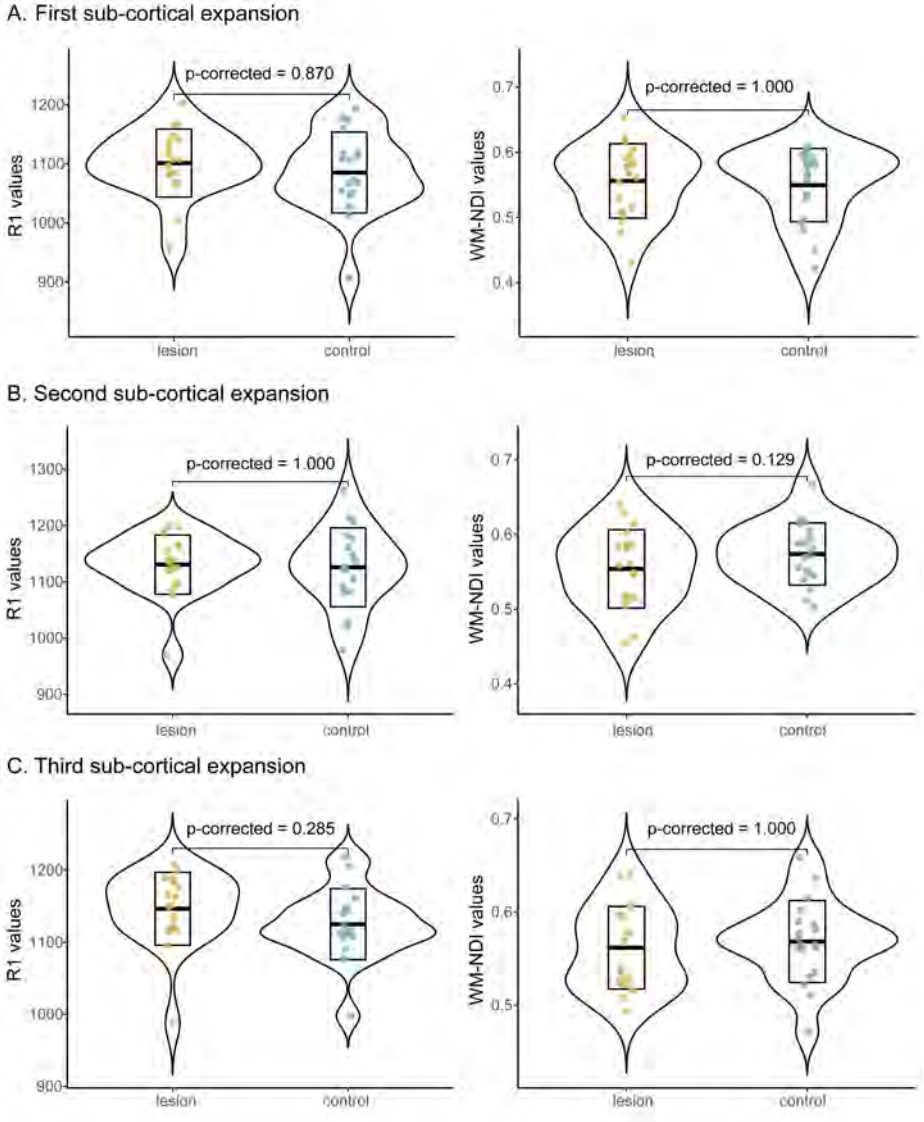

Figure e-3. Comparisons of CT, R1 and WM-NDI values between acute CMIs and control regions at each of their three sub-cortical expansions. All three sub-cortical expansion showed no differences at these MRI measures compared to control regions. CT, cortical thickness; WM-NDI, neurite density index for white matter. For acute CMIs, 21 lesions were identified, two lesions located too close to the pial surface were excluded, resulting in a total of 19 lesions included in the analysis.

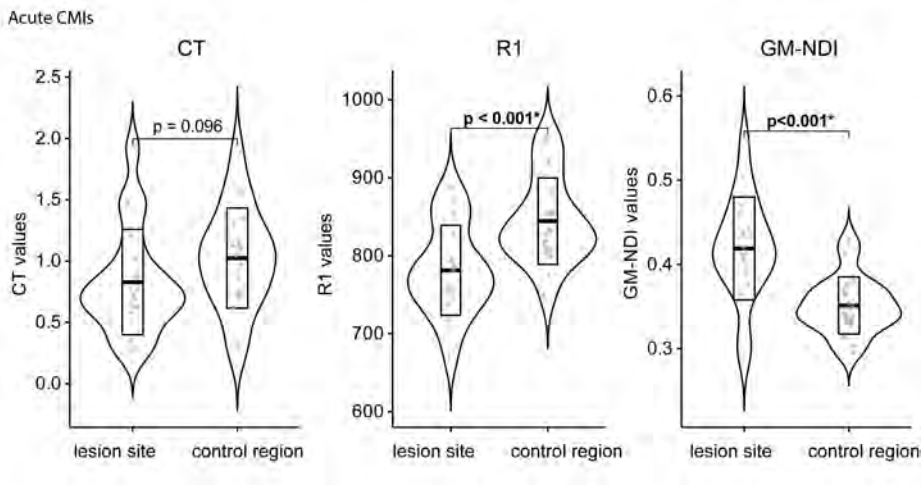

Figure e-4. Comparison of the cortical thickness, R1 and NDI values between the lesion site of acute CMIs and control regions. At the lesion site, acute CMIs showed lower R1, and higher NDI values compared to control regions. Significant differences ($p < 0.05$) are indicated by an asterisk (*) and bold font. Among the 21 acute identified, 2 acute located too close to the pial surface were excluded due to potential confounding from partial volume effects, resulting a total of 19 acute CMIs were included in the analysis.

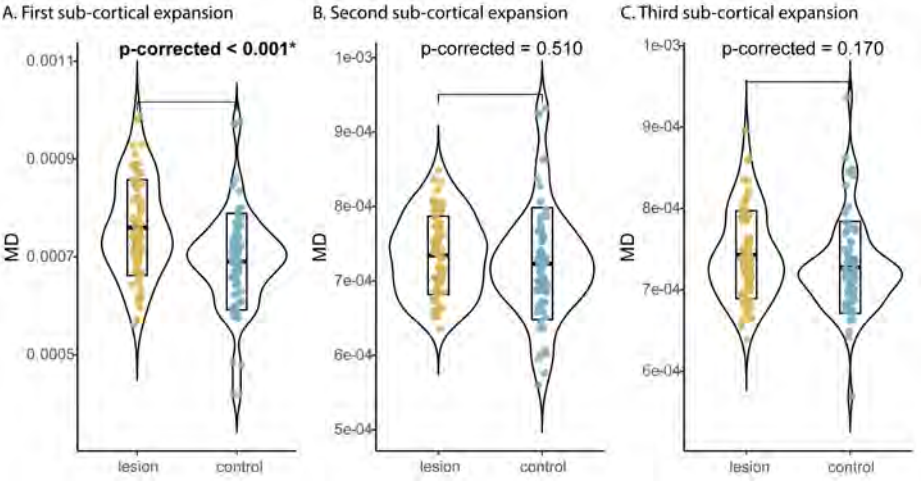

Figure e-5. Comparison of MD values between chronic CMIs and control regions at each of their three sub-cortical expansions. MD values at the first expansion were significantly lower than those at the corresponding control regions. MD, mean diffusivity, Significant differences (p-corrected < 0.05) are indicated by an asterisk (*) and bold font. Among the 81 identified chronic CMIs, 7 lesions located too close to the pial surface and 3 lesions with poor cortical expansion characteristics were excluded, resulting in a total of 71 chronic CMIs were included in the analysis.

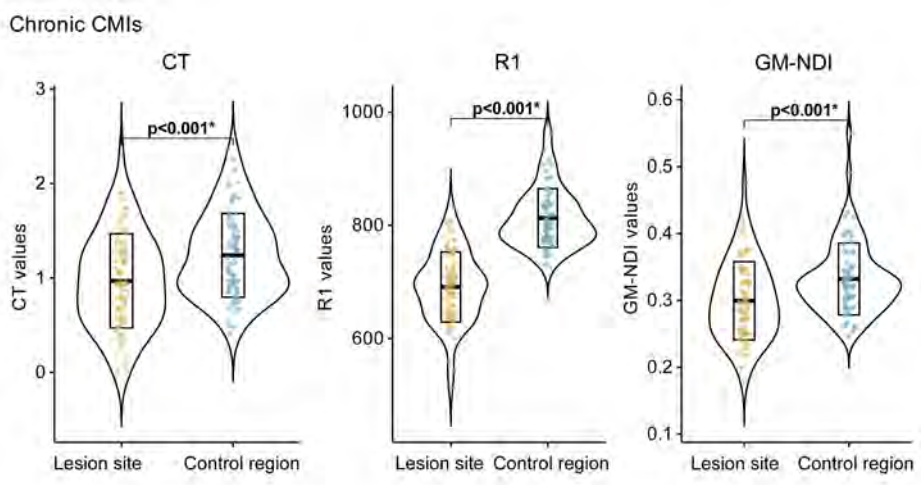

Figure e-6. Comparison of the cortical thickness, R1 and NDI values between the lesion site of chronic CMIs and control regions. At the lesion site, chronic CMIs showed lower CT, lower R1, and lower GM-NDI values compared to control regions. Significant differences ($p < 0.05$) are indicated by an asterisk (*) and bold font. Among the 81 chronic CMIs identified, 7 lesions located too close to the pial surface were excluded due to potential confounding from partial volume effects, resulting a total of 74 chronic CMIs were included in the analysis.

Reference

1. Duering M, et al. Neuroimaging standards for research into small vessel disease-advances since 2013. Lancet Neurol. Jul 2023;22(7):602-618. doi:10.1016/s1474-4422(23)00131-x
2. van Veluw SJ, Shih AY, Smith EE, Chen C, Schneider JA, Wardlaw JM, Greenberg SM, Biessels GJ. Detection, risk factors, and functional consequences of cerebral microinfarcts. Lancet Neurol. Sep 2017;16(9):730-740. doi:10.1016/s1474-4422(17)30196-5
3. Hilal S, Tan CS, van Veluw SJ, Xu X, Vrooman H, Tan BY, Venketasubramanian N, Biessels GJ, Chen C. Cortical cerebral microinfarcts predict cognitive decline in memory clinic patients. J Cereb Blood Flow Metab. Jan 2020;40(1):44-53. doi:10.1177/0271678x19835565
4. Summers PM, Hartmann DA, Hui ES, Nie X, Deardorff RL, McKinnon ET, Helpern JA, Jensen JH, Shih AY. Functional deficits induced by cortical microinfarcts. J Cereb Blood Flow Metab. Nov 2017;37(11):3599-3614. doi:10.1177/0271678x16685573
5. Ferro DA, Kuijf HJ, Hilal S, van Veluw SJ, van Veldhuizen D, Venketasubramanian N, Tan BY, Biessels GJ, Chen C. Association Between Cerebral Cortical Microinfarcts and Perilesional Cortical Atrophy on 3T MRI. Neurology. Feb 8 2022;98(6):e612-e622. doi:10.1212/wnl.0000000000013140
6. Huang J, Oh M, Robert C, Huang X, Egle M, Tozer DJ, Chen C, Hilal S. Loss of white matter integrity mediates the association between cortical cerebral microinfarcts and cognitive dysfunction: A longitudinal study. J Cereb Blood Flow Metab. May 26 2024:271678x241258563. doi:10.1177/0271678x241258563
7. Lubart A, Benbenishty A, Har-Gil H, Laufer H, Gdalyahu A, Assaf Y, Blinder P. Single Cortical Microinfarcts Lead to Widespread Microglia/Macrophage Migration Along the White Matter. Cereb Cortex. Jan 1 2021;31(1):248-266. doi:10.1093/cercor/bhaa223
8. Lutti A, Dick F, Sereno MI, Weiskopf N. Using high-resolution quantitative mapping of R1 as an index of cortical myelination. Neuroimage. Jun 2014;93 Pt 2:176-88. doi:10.1016/j.neuroimage.2013.06.005
9. Shams Z, Norris DG, Marques JP. A comparison of in vivo MRI based cortical myelin mapping using T1w/T2w and R1 mapping at 3T. PLoS One. 2019;14(7):e0218089. doi:10.1371/journal.pone.0218089
10. Zhang H, Schneider T, Wheeler-Kingshott CA, Alexander DC. NODDI: practical in vivo neurite orientation dispersion and density imaging of the human brain. Neuroimage. Jul 16 2012;61(4):1000-16. doi:10.1016/j.neuroimage.2012.03.072
11. Ter Telgte A, Wiegertjes K, Gesierich B, Baskaran BS, Marques JP, Kuijf HJ, Norris DG, Tuladhar AM, Duering M, de Leeuw FE. Temporal Dynamics of Cortical Microinfarcts in Cerebral Small Vessel Disease. JAMA Neurol. May 1 2020;77(5):643-647. doi:10.1001/jamaneurol.2019.5106
12. Wiegertjes K, Chan KS, Telgte AT, Gesierich B, Norris DG, Klijn CJ, Duering M, Tuladhar AM, Marques JP, Leeuw FE. Assessing cortical cerebral microinfarcts on iron-sensitive MRI in cerebral small vessel disease. J Cereb Blood Flow Metab. Dec 2021;41(12):3391-3399. doi:10.1177/0271678x211039609
13. Ter Telgte A, Wiegertjes K, Tuladhar AM, Noz MP, Marques JP, Gesierich B, Huebner M, Mutsaerts HM, Elias-Smale SE, Beelen MJ, Ropele S, Kessels RP, Riksen NP, Klijn CJ, Norris DG, Duering M, de Leeuw FE. Investigating the origin and evolution of cerebral small vessel disease: The RUN DMC - InTENse study. Eur Stroke J. Dec 2018;3(4):369-378. doi:10.1177/2396987318776088
14. Ter Telgte A, Wiegertjes K, Gesierich B, Marques JP, Huebner M, de Klerk JJ, Schreuder F, Araque Caballero MA, Kuijf HJ, Norris DG, Klijn CJM, Dichgans M, Tuladhar AM, Duering M, de Leeuw FE. Contribution of acute infarcts to cerebral small vessel disease progression. Ann Neurol. Oct 2019;86(4):582-592. doi:10.1002/ana.25556

15. Wardlaw JM, Smith C, Dichgans M. Small vessel disease: mechanisms and clinical implications. Lancet Neurol. Jul 2019;18(7):684-696. doi:10.1016/s1474-4422(19)30079-1

16. Marques JP, Gruetter R. New developments and applications of the MP2RAGE sequence--focusing the contrast and high spatial resolution R1 mapping. PLoS One. 2013;8(7):e69294. doi:10.1371/journal.pone.0069294

17. Guerrero JM, Adluru N, Bendlin BB, Goldsmith HH, Schaefer SM, Davidson RJ, Kecskemeti SR, Zhang H, Alexander AL. Optimizing the intrinsic parallel diffusivity in NODDI: An extensive empirical evaluation. PLoS One. 2019;14(9):e0217118. doi:10.1371/journal.pone.0217118

18. Mountcastle VB. The columnar organization of the neocortex. Brain. Apr 1997;120 (Pt 4):701-22. doi:10.1093/brain/120.4.701

19. Smith EE, Schneider JA, Wardlaw JM, Greenberg SM. Cerebral microinfarcts: the invisible lesions. Lancet Neurol. Mar 2012;11(3):272-82. doi:10.1016/s1474-4422(11)70307-6

20. Lee J, Kim JG, Hong S, Kim YS, Ahn S, Kim R, Chun H, Park KD, Jeong Y, Kim DE, Lee CJ, Ku T, Kim P. Longitudinal intravital imaging of cerebral microinfarction reveals a dynamic astrocyte reaction leading to glial scar formation. Glia. May 2022;70(5):975-988. doi:10.1002/glia.24151

21. Weiskopf N, Edwards LJ, Helms G, Mohammadi S, Kirilina E. Quantitative magnetic resonance imaging of brain anatomy and in vivo histology. Nature Reviews Physics. 2021/08/01 2021;3(8):570-588. doi:10.1038/s42254-021-00326-1

22. Yilmazer-Hanke D, Mayer T, Müller HP, Neugebauer H, Abaei A, Scheuerle A, Weis J, Forsberg KME, Althaus K, Meier J, Ludolph AC, Del Tredici K, Braak H, Kassubek J, Rasche V. Histological correlates of postmortem ultra-high-resolution single-section MRI in cortical cerebral microinfarcts. Acta Neuropathol Commun. Mar 13 2020;8(1):33. doi:10.1186/s40478-020-00900-1

23. Colgan N, Siow B, O'Callaghan JM, Harrison IF, Wells JA, Holmes HE, Ismail O, Richardson S, Alexander DC, Collins EC, Fisher EM, Johnson R, Schwarz AJ, Ahmed Z, O'Neill MJ, Murray TK, Zhang H, Lythgoe MF. Application of neurite orientation dispersion and density imaging (NODDI) to a tau pathology model of Alzheimer's disease. Neuroimage. Jan 15 2016;125:739-744. doi:10.1016/j.neuroimage.2015.10.043

24. Wang Z, Zhang S, Liu C, Yao Y, Shi J, Zhang J, Qin Y, Zhu W. A study of neurite orientation dispersion and density imaging in ischemic stroke. Magn Reson Imaging. Apr 2019;57:28-33. doi:10.1016/j.mri.2018.10.018

25. Kamiya K, Hori M, Aoki S. NODDI in clinical research. Journal of neuroscience methods. 2020;346:108908.

26. Smith CM, Cooksey E, Duncan ID. Myelin loss does not lead to axonal degeneration in a long-lived model of chronic demyelination. J Neurosci. Feb 6 2013;33(6):2718-27. doi:10.1523/jneurosci.4627-12.2013

27. Fazekas F, Kleinert R, Roob G, Kleinert G, Kapeller P, Schmidt R, Hartung HP. Histopathologic analysis of foci of signal loss on gradient-echo T2*-weighted MR images in patients with spontaneous intracerebral hemorrhage: evidence of microangiopathy-related microbleeds. AJNR Am J Neuroradiol. Apr 1999;20(4):637-42.

28. Marques JP, Kober T, Krueger G, van der Zwaag W, Van de Moortele PF, Gruetter R. MP2RAGE, a self bias-field corrected sequence for improved segmentation and T1-mapping at high field. Neuroimage. Jan 15 2010;49(2):1271-81. doi:10.1016/j.neuroimage.2009.10.002

29. Rebsamen M, Rummel C, Reyes M, Wiest R, McKinley R. Direct cortical thickness estimation using deep learning-based anatomy segmentation and cortex parcellation. Hum Brain Mapp. Dec 2020;41(17):4804-4814. doi:10.1002/hbm.25159

30. Das SR, Avants BB, Grossman M, Gee JC. Registration based cortical thickness measurement. Neuroimage. Apr 15 2009;45(3):867-79. doi:10.1016/j.neuroimage.2008.12.016
31. Kellner E, Dhital B, Kiselev VG, Reisert M. Gibbs-ringing artifact removal based on local subvoxel-shifts. Magnetic resonance in medicine. 2016;76(5):1574-1581.
32. Veraart J, Novikov DS, Christiaens D, Ades-Aron B, Sijbers J, Fieremans E. Denoising of diffusion MRI using random matrix theory. Neuroimage. 2016;142:394-406.
33. Smith SM, Jenkinson M, Woolrich MW, Beckmann CF, Behrens TE, Johansen-Berg H, Bannister PR, De Luca M, Drobnjak I, Flitney DE. Advances in functional and structural MR image analysis and implementation as FSL. Neuroimage. 2004;23:S208-S219.
34. Andersson JL, Sotiropoulos SN. An integrated approach to correction for off-resonance effects and subject movement in diffusion MR imaging. Neuroimage. 2016;125:1063-1078.
35. Tustison NJ, Avants BB, Cook PA, Zheng Y, Egan A, Yushkevich PA, Gee JC. N4ITK: improved N3 bias correction. IEEE transactions on medical imaging. 2010;29(6):1310-1320.
36. Tournier JD, Smith R, Raffelt D, Tabbara R, Dhollander T, Pietsch M, Christiaens D, Jeurissen B, Yeh CH, Connelly A. MRtrix3: A fast, flexible and open software framework for medical image processing and visualisation. Neuroimage. Nov 15 2019;202:116137. doi:10.1016/j.neuroimage.2019.116137
37. Tournier JD, Calamante F, Connelly A. Improved probabilistic streamlines tractography by 2nd order integration over fibre orientation distributions. John Wiley & Sons, Inc New Jersey, NJ; 2010:
38. Avants BB, Tustison NJ, Song G, Cook PA, Klein A, Gee JC. A reproducible evaluation of ANTs similarity metric performance in brain image registration. Neuroimage. Feb 1 2011;54(3):2033-44. doi:10.1016/j.neuroimage.2010.09.025
39. Jeurissen B, Tournier JD, Dhollander T, Connelly A, Sijbers J. Multi-tissue constrained spherical deconvolution for improved analysis of multi-shell diffusion MRI data. Neuroimage. Dec 2014;103:411-426. doi:10.1016/j.neuroimage.2014.07.061

Part IV.

The waste clean system in cerebral small vessel disease

Chapter 7.

Perivascular spaces, diffusivity along perivascular spaces, and free water in cerebral small vessel disease.

Published as:
Hao Li, Mina A Jacob, Mengfei Cai, Roy PC Kessels, David G Norris, Marco Duering, Frank-Erik De Leeuw, Anil Man Tuladhar. Perivascular spaces, diffusivity along perivascular spaces, and free water in cerebral small vessel disease. Neurology, 102(9): e209306, 2024.

Abstract

Background: Previous studies have linked the MRI measures of perivascular spaces (PVS), diffusivity along the perivascular spaces (DTI-ALPS) and free water (FW) to cerebral small vessel disease (SVD) and SVD-related cognitive impairments. However, studies tested the longitudinal associations between these MRI measures, SVD progression and cognitive decline are lacked. This study aimed to explore how PVS, DTI-ALPS, and FW contribute to SVD progression and cognitive decline.

Methods: This is a cohort study that included SVD participants who underwent neuroimaging and cognitive assessment, specifically measuring Mini-Mental State Examination (MMSE), cognitive index and processing speed, at two time points. Three MRI measures were quantified: PVS in basal-ganglia (BG-PVS) volumes, FW fraction and DTI-ALPS. We performed latent change score model to test inter-relations between the three MRI measures and linear regression mixed models to test their longitudinal associations with the changes of other SVD MRI markers and cognitive performances.

Results: In baseline assessment, we included 289 participants with SVD, characterized by a median age of 67.0 years and 42.9% women. Of which, 220 participants underwent the follow-up assessment, with a median follow-up time of 3.4 years. Baseline DTI-ALPS was associated with the changes of BG-PVS volumes (β=-0.09, p=0.030), but not vice versa (β=-0.08, p=0.110). Baseline BG-PVS volumes were associated with the changes of WMH volumes (β=0.33, p-corrected<0.001) and lacune numbers (β=0.28, p-corrected<0.001); FW fraction was associated with the changes of WMH volumes (β=0.30, p-corrected<0.001), lacune numbers (β=0.28, p-corrected<0.001) and brain volumes (β=-0.45, p-corrected<0.001); DTI-ALPS were associated with the changes of WMH volumes (β=-0.20, p-corrected=0.002) and brain volumes (β=0.23, p-corrected<0.001). Furthermore, baseline FW fraction was associated with decline in MMSE score (β=-0.17, *p-corrected*=0.006); baseline FW fraction and DTI-ALPS were associated with the changes of cognitive index (FW fraction: β=-0.25, p-corrected<0.001; DTI-ALPS: β=0.20, p-corrected=0.001) and processing speed over time (FW fraction: β=-0.29, p-corrected<0.001; DTI-ALPS: β=0.21, p-corrected<0.001).

Conclusion: Our results showed that increased BG-PVS volumes, increased FW fraction and decreased DTI-ALPS are related to progression of MRI markers of SVD, along with SVD-related cognitive decline over time. These findings may suggest that the glymphatic dysfunction is related to SVD progression, but further studies are needed.

Keywords: cerebral small vessel disease; perivascular spaces; diffusivity along perivascular spaces; free water.

Introduction

Cerebral small vessel disease (SVD) encompasses various pathologies affecting the brain's small vessels. SVD is the leading cause of vascular cognitive impairment and dementia.[1,2] A range of MRI features, including white matter hyperintensities (WMH), lacunes of presumed vascular origin, and cerebral microbleeds (CMBs) are thought to be pathological alterations caused by SVD.[1] However, the underlying mechanisms driving SVD development, progression, and the concomitant cognitive impairment remain largely unknown.

The glymphatic system has been considered as a highly dynamic waste clearance pathway in the central nervous system,[3] and may potentially be related in the pathophysiology of SVD.[4] MRI-visible perivascular spaces (PVS), free water (FW) and Diffusion Tensor Imaging along the Perivascular Space (DTI-ALPS) have been used to assess the glymphatic function (Figure 1).[5-8] MRI-visible perivascular spaces (PVS) showed a spatial correlation with small arteries rather than small veins,[9,10] suggesting that these spaces mostly represent periarterial spaces.[11] Free water (FW) estimates the extracellular water volume fraction, which could be regulated by interstitial fluid (ISF) in the brain parenchyma.[12] DTI-ALPS is based on the assumption that it measures the diffusivity capacity of the perivenous space surrounding the deep medullary vein at the lateral ventricle body level.[13] Although the three MRI measures are not formally validated as parameters for glymphatic function, DTI-ALPS has demonstrated a significant correlation with glymphatic clearance rates, as measured through invasive MRI with intrathecal gadolinium injection.[6] Note that this study was not performed in a SVD cohort. While the MRI measures of PVS volumes and FW values were suspected to be the consequence of blockage in glymphatic outflow based on previous studies, yet this lacks direct validations.

In SVD, several studies have demonstrated that higher PVS counts (mostly located in the basal ganglia),[14,15] higher FW and lower DTI-ALPS are related to the radiological severity and cognitive impairment in SVD.[6,8,16] However, most studies employed only one or two of the afore-mentioned measures with cross-sectional study design, resulting in inconsistent findings. Currently, there is a lack of longitudinal studies to disentangle the trajectories and the inter-relations of these measures, as well as their associations with radiological and clinical progression of SVD over time.

In this study, we aimed to examine the longitudinal changes and the inter-relations of PVS, FW and DTI-ALPS, as well as their longitudinal associations with MRI markers of SVD and cognitive function. We hypothesized that changes in these measures

over time are associated with progression of SVD MRI markers and cognitive decline in SVD patients.

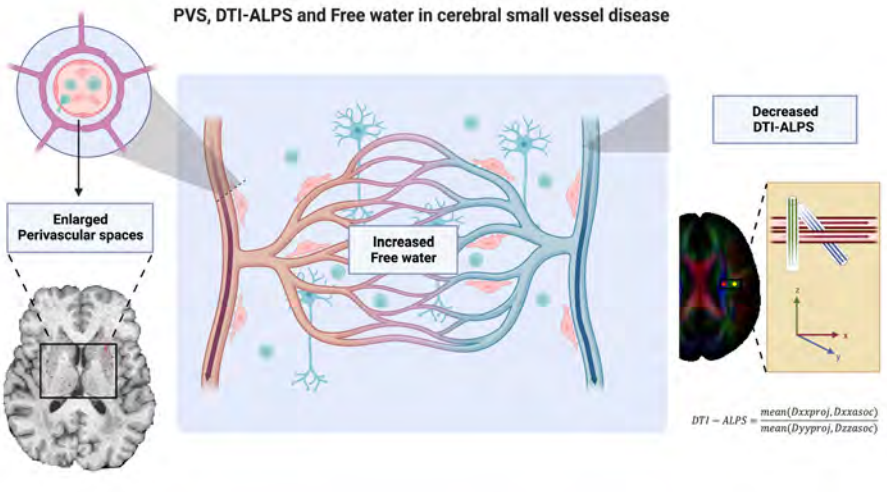

Figure 1. Perivascular spaces, diffusivity along the perivascular spaces and free water in cerebral small vessel disease. Note that formal validation studies are still lacking linking these measures to glymphatic function. It is hypothesized that PVS may serve as a proxy for the CSF inflow channel; FW estimates the extracellular water volume fraction, which could be regulated by ISF in the brain parenchyma; DTI-ALPS measures the diffusivity capacity of the perivenous space surrounding the deep medullary vein at the lateral ventricle body level, enabling the assessment of the CSF outflow channel within this system. It is suggested that glymphatic dysfunction in SVD may be characterized by the enlarged PVS, increased FW and decreased DTI-ALPS. SVD, small vessel disease; CSF, cerebrospinal fluid; PVS, perivascular spaces; FW, free water; DTI-ALPS, diffusion tensor imaging along the perivascular space. Created with *BioRender.com*.

Materials and methods

Study population

This study is a part of the Radboud University Nijmegen Diffusion tensor and Magnetic resonance imaging Cohort (RUN DMC) study, which is an ongoing prospective study that aims to investigate the causes and clinical consequences of sporadic SVD. Detailed information on this study has been described previously.[17] In brief, participants who met the following criteria were included: 1) age between 50 and 85 years; 2) cerebral SVD on MRI (i.e., lacunes or WMH); 3) clinical symptoms that could be attributed to SVD. Baseline inclusion was in 2006, with three follow-up assessments in 2011, 2015 and 2020. However, due to the scanner upgrade between baseline (2006) and first follow-up (2011), and between the second (2015) and the third follow-ups (2020), we only used the data from 2011 and 2015 (Figure

e-1). In the present study, we set the assessment in 2011 as baseline and assessment in 2015 as follow-up, since we only used data from these two time points.

Neuropsychological Assessment

All participants underwent a standardized cognitive assessment battery, including the immediate and delayed recall of the Rey Auditory Verbal Learning Test (RAVLT), the immediate and delayed recall of Rey Complex Figure Test (RCFT), Paper-Pencil Memory Scanning Task (PPMST), Stroop Colour-Word Test (SCWT), Symbol-Digit Substitution Task (SDST), Verbal fluency test (VFT) and Verbal Series Attention Test (VSAT). To minimize practice effects, the alternative versions of the tests were used whenever possible. For PPMST, SCWT and VSAT, we employed the Speed-Accuracy Trade-Off (SAT) score to quantify the balance between response time and correct responses. The SAT scores were computed as the percentage of correct responses divided by the response time, as described in previous study.[18] Raw scores of all time points were converted to z-scores by using the difference between the raw score and the mean of the baseline study population, divided by the SD of the baseline study population. Our analysis focused on global cognitive function as a compound measure of cognition and on processing speed, as this domain is the most prominent cognitive area and showed the strongest associations with neuroimaging markers in SVD.[19,20] For the global cognitive function, we calculated the cognitive index by first averaging the z-scores of the sub-scores for each cognitive test, followed by averaging the z scores of all tests in the cognitive test battery; for the processing speed, we calculated the mean of the z-scores of the PPMST, the reading and colour naming tasks of the Stroop Test, and the SDST. In addition, we employed the Mini-Mental State Examination (MMSE) as a measure of global cognitive function.

MRI acquisitions

All participants were scanned on a 1.5T MRI scanner (Magnetom Avanto, Simens) with an 8-channel head coil including the following sequences: T1-weighted 3D Magnetization Prepared Rapid Gradient Echo (MPRAGE), gradient echo (GRE) sequence for T2*-weighted image, Fluid Attenuated Inversion Recovery (FLAIR) image and diffusion weight image (DWI, voxel size=2.5*2.5*2.5 mm, 7 volumes with b=0 s/mm^2, 61 volumes with b=900 s/mm^2,). Detailed parameters of each sequence were provided in Table e-1.

SVD MRI markers

MRI markers of SVD (i.e., WMH, lacunes, CMBs) and brain atrophy were assessed according to version 2 of the Standards for Reporting Vascular Changes on Neuroimaging criteria (STRIVE-2).[1] WMH volumes at two time points were semi-

automatically calculated based on FLAIR and T1 images.[21] The lacunes on T1 and FLAIR images and the CMBs on T2* images were manually counted by two well-trained raters who were blind to the clinical data, followed by a consensus meeting. Intra- and interrater reliability were excellent, that is, weighted kappa of 0.87 and 0.95 for lacunes and 0.85 and 0.86 for microbleeds.[22] Grey matter (GM), white matter (WM) and cerebrospinal fluid (CSF) volumes were calculated on T1 images using FreeSurfer software. Brain volumes were determined by the ratio between the sum of GM and WM volumes and the sum of GM, WM, and CSF volumes (i.e., intracranial volumes [ICV]) and served as a proxy of brain atrophy. WMH volumes were normalized to the ICV.

Vascular Risk Factors

The prevalence of hypertension, smoking, diabetes, and hypercholesterolemia was assessed using a standardized questionnaire at baseline,[17] and a cumulative risk factor score (0-4) was derived based on the presence of these factors, representing the vascular risk factor burden.[23]

Diffusion MRI pre-processing

Diffusion MRI data were pre-processed to remove the noise and Gibbs artifacts, correct head motion, eddy currents-induced distortion, susceptibility-induced distortion (top-up) and intensity bias using MRtrix 3.0 software (http://www.mrtrix.org),[24] Functional Magnetic Resonance Imaging of the Brain Software Library (FSL; v6.0.3) software,[25] Synb0-DISCO,[26] and Advanced Normalization Tools (ANTs, v 2.1.0).[27] Due to the absence of a b0 image with reversed phase encoding in our DWI scans, 'topup' was performed based on a synthesized b0 image from the T1 image using Synb0-DISCO.[26] Next, with the pre-processed diffusion data, we calculated the mean diffusivity (MD) and fractional anisotropy (FA) maps of each participant using the 'dtifit' function within FSL.

PVS Segmentation

A PVS probability map was generated from 3D T1 images using a previously validated deep learning model (https://github.com/pboutinaud/SHIVA_PVS).[28] A threshold of 0.5 was applied to this PVS probability map to create a PVS mask for each participant. The threshold was selected based on the developer's recommendation and the visual assessment on segmented PVS masks. Subsequently, considering the partial volume effects arising from CSF, we removed the part of PVS mask located within 2 mm of the ventricle.[5] The resulting PVS masks were visually inspected. PVS segmentations in deep WM presented low quality. As such, PVS volumetry in present study focused only on the basal ganglia (BG). Note that previous studies have shown that PVS in deep white matter were mainly

associated with cerebral amyloid-β pathologies in Alzheimer's disease and cerebral amyloid angiopathy.[29] In contrast, PVS in the basal ganglia (BG-PVS) were related to arteriolosclerosis in SVD.[30] BG-PVS volumes were corrected for ICV. To validate the effectiveness/robustness of BG-PVS segmentation, we performed Pearson correlation analysis between the visual rating scores (4-point PVS visual rating scale: 0 score, no PVS; 1 score, 1-10 PVS; 2 score, 11,20 PVS; 3 score, 21,40 PVS; 4 score, >40 PVS) and the volumes for BG-PVS, using a 10% random participant subset from each time point. The correlation coefficients of 0.61 and 0.64 were found in the two timepoints of 2011 and 2015, respectively (Table e-2).

DTI-ALPS calculation

DTI-ALPS index was calculated using a semi-automated method in SVD.[6] We placed four 5-mm-diameter spherical ROIs in the areas of bilateral projection fibers and association fibers at the level of the lateral ventricular body using ICBM-DTI-81 white matter atlas.[31] Next, the four ROIs in the ICBM template were registered to the individual's diffusion image using the 'fnirt' function within FSL. The positions of registered ROIs were visual inspected. DTI-ALPS was computed as the ratio between the mean of the x-axis diffusivity on the projection fibres (Dxproj) and association fibres (Dxassoc) and the mean of the y-axis diffusivity on the projection fibres (Dyproj) and the z-axis diffusivity on association fibres (Dzassoc).

$$DTI - ALPS = \frac{mean(Dxproj + Dxassoc)}{mean(Dyproj + Dzassoc)} \quad (1)$$

Additionally, we calculated the mean MD values of the ROIs and performed Pearson correlation analyses between the MD values and DTI-ALPS from each time point (2011: r=-0.37, p<0.001; 2015: r=-0.33, p<0.001).

Free water mapping

A single-shell free water estimation model was performed using the DIPY (version 1.4.0, https://dipy.org/) package in Python.[12,32] Briefly, the signal of each voxel was fit based on a two-compartment model, resulting in a FW (isotropic tensor with fixed diffusion constant of water at 37°C) map and a FW-corrected tensor map. The FW map represents the relative fraction of FW in each voxel, ranging from 0 to 1. Subsequently, the mean FW fraction across the white matter, excluding the PVS regions, was calculated using the FW map.

Statistical analysis

The continuous variables were presented as mean (standard deviation, SD) or median (interquartile ranges, IQRs) according to the data distribution, categoric

variables were presented as counts and percentage (n, %). Demographic and neuroimaging characteristics of participants with follow-up assessments in 2015 were compared to those without follow-up assessments using two-sample *t*-tests or Mann-Whitney *U* tests for continuous variables and chi-squared ($\chi 2$) tests for categorical variables, as appropriate.

Temporal trajectories and inter-relations of BG-PVS volumes, FW fraction and DTI-ALPS

To estimate the temporal trajectories of BG-PVS volumes, FW fraction and DTI-ALPS, we employed linear mixed models analyses by using the 'lmer' package in R. The employment of linear mixed model allowed us to include all participants (n=289), including those with only baseline data. In these mixed models, follow-up time, age at baseline, sex, and vascular risk factors were treated as fixed effects, with random effects of intercept. For DTI-ALPS, we additionally incorporated fixed effects for the mean MD values of the ROIs which were used for the calculation of DTI-ALPS. This adjustment was essential for two reasons: 1) the reported effects of WM integrity on DTI-ALPS in previous studies,[5, 7,33] and 2) the results from our previous analyses, which showed a weak correlation between DTI-ALPS and the mean MD values of the DTI-ALPS related ROIs.

To explore dynamic inter-relations between the three measures, we employed the latent change score (LCS) model, as used in previous study.[34] The latent change score (LCS) model is a category of structural equation model that affords the unique advantage of modelling changes in multiple variables (i.e., three measures in present study) and their longitudinal inter-relations simultaneously.[35] To preclude the effects of confounding variables and maintain simplicity of the LCS model and subsequent statistical models, the three measures were adjusted for age, sex, and vascular risk factors through residualization with regression as in a previous study.[34] DTI-ALPS was additionally adjusted for the mean MD values of the ROIs employed in the DTI-ALPS calculation.[5,7,33] The Comparative Fit Index (CFI), Root Mean Square Error of Approximation (RMSEA), and Standardized Root Mean Residual (SRMR) were employed as the indicators of model fit.[36] This model showed a good model fit (CFI=0.991, RMSEA=0.078, SRMR=0.038).[36]

Relation between BG-PVS volumes, FW Fraction, DTI-ALPS, and SVD MRI markers

To determine the effects of BG-PVS, FW fraction and DTI-ALPS on SVD burden, we performed linear regression analyses between each measure, and each SVD MRI marker at each time point. To examine the association between these baseline measures and SVD burden progression, we fitted linear mixed models for each

baseline measure and respective SVD MRI marker. In these models, each baseline measure and follow-up time were treated as fixed effects, with random effects of intercept to account for variability across participants. Furthermore, to assess the associations between the changes of BG-PVS volumes, FW fraction and DTI-ALPS, and SVD progression over time, we also employed linear mixed models. These models incorporated each measure, follow-up time, and their interaction term as fixed effects, while considering random effects for the intercept.

Relation between BG-PVS volumes, FW Fraction, DTI-ALPS, and cognitive function

The cognitive function measures in present study included MMSE, cognitive index and processing speed. First, we adjusted three cognitive function measures for age, education, and vascular risk factors through residualization with regression. Subsequently, we tested cross-sectional associations between BG-PVS volumes, FW Fraction, DTI-ALPS and cognitive function at each time point, using linear regression analyses. Next, we tested the association between these baseline measures and cognitive decline, as well as the associations between the changes of these measures and the changes of cognitive function over follow-up time, using linear mixed models with random effects for the intercept. To correct for potential confounding effects of SVD on cognitive function, we repeated above analyses by including SVD MRI markers as the covariates into the models.

A correlation matrix of the independent variables in the regression model was employed to evaluate multicollinearity, with a correlation coefficient between any pair of independent variables greater than 0.7 indicating the presence of multicollinearity.

All statistical analyses were performed using R software (version 4.1.1), with a significance level set at a two-tailed p-value < 0.05. The *Bonferroni* method was employed to correct for multiple comparisons.

Standard Protocol Approvals, Registrations, and Patient Consents

The study was approved by the Medical Review Ethics Committee Region Arnhem-Nijmegen, and written informed consent was obtained from all participants.

Data Availability and Access

The data supporting the findings of this study can be obtained from the corresponding author upon reasonable request by qualified investigators after the approval of relevant regulatory bodies.

Table 1. Baseline demographic, neuroimaging characteristics and cognitive function of the whole cohort

	All Participants (n=289)
Demographic	
Age, years, median (IQR)	67.00 (61.00-75.00)
Female, n (%)	124 (42.9%)
Education, years, median (IQR)	10.00 (9.00-11.00)
Vascular risk factors	
Hypertension, n (%)	192 (66.4%)
Diabetes, n (%)	27 (9.3%)
hypercholesterolemia, n (%)	116 (40.1%)
Smoking, n (%)	204 (70.6%)
Vascular risk factors, median (IQR)	2.00 (1.00-3.00)
Medications	
Antihypertensive drugs, n (%)	186 (64.4%)
Antithrombotic drugs, n (%)	158 (54.7%)
Antidiabetic drugs, n (%)	39 (13.5%)
Statins, n (%)	131 (45.3%)
Cognitive function	
MMSE, median (IQR)	29.00 (28.00-30.00)
Cognitive index, Z score, median (IQR)	0.23 (-0.43-0.64)
Processing speed, Z score, mean (SD)	0.13 (0.85)
MRI markers	
WMH volumes, ml, median (IQR)	2.96 (1.29-8.67)
Lacunes, n (%)	70 (24.2%)
CMBs, n (%)	59 (20.4%)
brain volumes, ml, mean (SD)	1073.17 (109.65)
BG-PVS volumes, ml, median (IQR)	0.94 (0.85-1.03)
Free water fraction, median (IQR)	0.35 (0.34-0.37)
DTI-ALPS, mean (SD)	1.37 (0.17)

WMH, white matter hypersensitivity; CMBs, cerebral microbleeds; BG-PVS, perivascular spaces in basal ganglia; DTI-ALPS, Diffusion Tensor Imaging along the Perivascular Space; MMSE, Mini-Mental State Examination.

Results

Detailed demographic, neuroimaging, and cognitive data are presented in Table 1 and Table e-3. A total of 289 participants were included in the baseline assessments in 2011, with a median age of 67.0 (IQR [61.0-75.0]) years; 124 (42.9%) participants were women. Of the 289 participants, 220 participated in the follow-up assessment in 2015, with a median follow-up time of 3.4 (IQR [3.3-3.5]) years. Compared to participants with the follow-up assessments, participants without follow-up assessments were older, had lower scores of MMSE, cognitive index and processing speed, higher WMH volumes, lower brain volumes, a higher FW fraction, and a lower DTI-ALPS at baseline. (Table e-4).

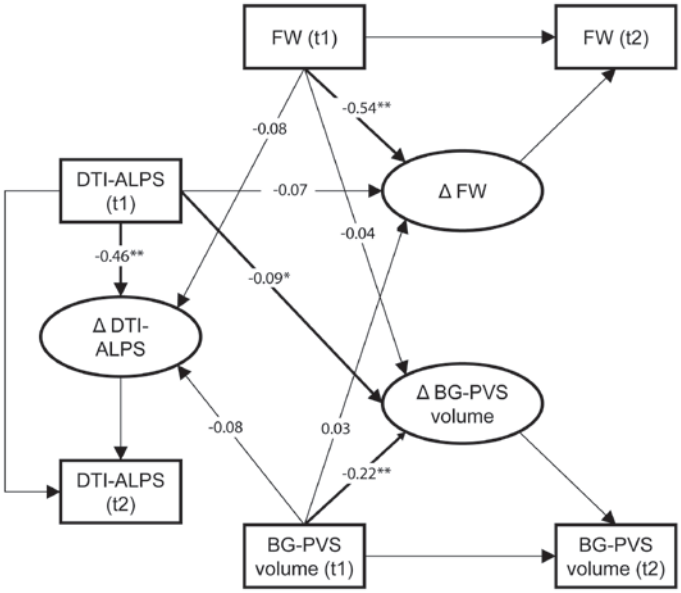

Figure 2. Inter-relations between BG-PVS volumes, FW fraction and DTI-ALPS over time based on latent change score (LCS) model. LCS model is a category of structural equation model and was employed to model the longitudinal inter-relations between BG-PVS volumes, FW fraction and DTI-ALPS simultaneously in present study. Baseline DTI-ALPS was associated with changes of BG-PVS volumes (β=-0.09, p=0.030), but not vice versa (β=-0.081, p=0.110). No significant associations between FW fraction and either BG-PVS volumes or DTI-ALPS were found. BG-PVS volumes, FW fraction and DTI-ALPS in this model were adjusted for age, sex, and vascular risk factors through revisualization with regression. DTI-ALPS was additionally adjusted for the mean MD values of the ROIs employed in the DTI-ALPS calculation. This model showed a good model fit (CFI=0.991, RMSEA=0.078, SRMR=0.038). The reported regression coefficients reflect standardized estimates. BG-PVS, perivascular spaces in basal ganglia; FW, free water; DTI-ALPS, diffusivity along perivascular spaces; CFI: comparative Fit Index; RMESA: Root Mean Square Error of Approximation; SRMR: Standardized Root Mean Residual. *, p-value<0.05, **, p-value<0.001. t1: 2011 (baseline assessment); t2: 2015 (follow-up assessment).

Temporal trajectories and relations of BG-PVS volumes, FW fraction and DTI-ALPS

There was no significant change in BG-PVS volumes, FW fraction or DTI-ALPS over time (Table e-5). The changes in DTI-ALPS were related to the MD values of the ROIs that were used for the DTI-ALPS calculation (β =-0.23, p<0.001).

The LCS model showed that baseline DTI-ALPS was associated with the increase of BG-PVS volumes over follow-up time (β=-0.093, p=0.030, Figure 2). However, baseline BG-PVS volumes were not associated with the changes in DTI-ALPS over time (β=-0.081, p=0.110, Figure 2). Furthermore, no association was found between FW fraction and either BG-PVS volumes or DTI-ALPS.

Relation between BG-PVS volumes, FW fraction and DTI-ALPS, and SVD MRI markers

Cross-sectional linear regression analyses showed that higher BG-PVS volumes were significantly related to higher WMH volumes and higher lacune numbers (Table 2). A higher FW fraction was also related to higher WMH volumes, higher lacune numbers, higher CMBs numbers at both two-time points and lower brain volumes at baseline. Higher DTI-ALPS were related to lower WMH volumes, and higher brain volumes at both time points (Table 2).

Table 2. Cross-sectional associations between BG-PVS volumes, FW fraction, DTI-ALPS and SVD markers at two time points.

	WMH volumes		Lacune numbers		CMBs numbers		Brain volumes	
	β	***P****	***β***	***P****	***β***	***P****	***β***	***P****
2011								
BG-PVS volume	0.32 (0.21, 0.43)	**<0.001**	0.29 (0.18, 0.40)	**<0.001**	0.03 (-0.08, 0.15)	1.000	-0.12 (-0.24, -0.01)	0.107
FW fraction	0.28 (0.17, 0.40)	**<0.001**	0.27 (0.16, 0.38)	**<0.001**	0.04 (-0.07, 0.16)	1.000	-0.46 (-0.56, -0.36)	**<0.001**
DTI-ALPS	-0.18 (-0.30, -0.07)	**<0.001**	-0.09 (-0.20, 0.03)	0.414	-0.03 (-0.15, 0.08)	1.000	0.23 (0.12, 0.35)	**<0.001**
2015								
BG-PVS volume	0.24 (0.11, 0.37)	**<0.001**	0.29 (0.17, 0.42)	**<0.001**	0.12 (-0.01, 0.25)	0.233	0.01 (-0.14, 0.13)	1.000
FW fraction	0.36 (0.24, 0.49)	**<0.001**	0.30 (0.17, 0.43)	**<0.001**	0.13 (0.00, 0.27)	0.804	-0.46 (-0.58, -0.34)	**<0.001**
DTI-ALPS	-0.18 (-0.31, -0.04)	**0.027**	-0.06 (-0.19, 0.08)	1.000	-0.08 (-0.21, 0.05)	0.726	0.17 (0.04, 0.30)	**0.034**

WMH, white matter hypersensitivity; CMBs, cerebral microbleeds; BG-PVS, perivascular spaces in basal ganglia; DTI-ALPS, Diffusion Tensor Imaging along the Perivascular Space. *P**, *p* values *corrected* for multiple comparisons; p values in bold indicates significance after *Bonferroni* correction.

Linear mixed model analyses showed that: 1) higher baseline BG-PVS volume was associated with increase in WMH volumes and increase in lacune numbers; 2) a higher baseline FW fraction was associated with increase in WMH volumes, increase in lacune numbers and decrease in brain volumes; 3) lower baseline DTI-ALPS was associated with increase in WMH volumes and decrease in brain volumes (Figure 3). Changes of BG-PVS volumes, FW fraction and DTI-ALPS over follow-up time did not show any associations with the changes of SVD markers (Table e-6).

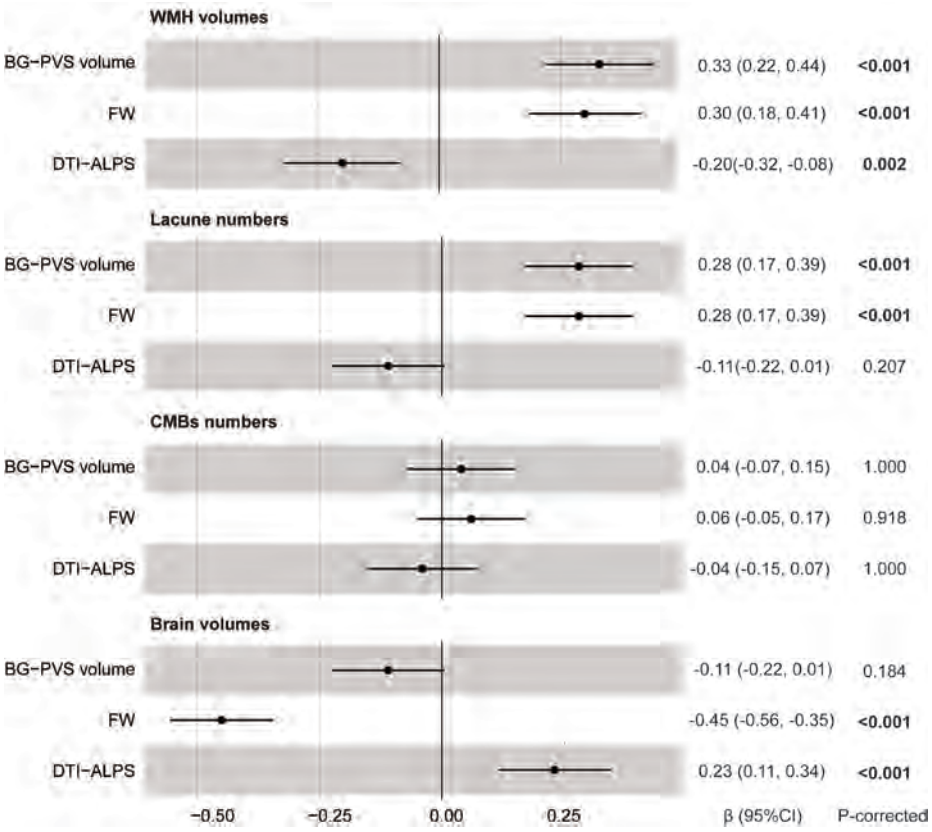

Figure 3. Linear mixed model results of the relations between baseline BG-PVS volumes, FW fraction, DTI-ALPS and changes of MRI markers of SVD over time. SVD MRI markers included WMH volumes, lacune numbers, CMBs numbers and brain volumes. BG-PVS, perivascular spaces in basal ganglia; FW, free water; DTI-ALPS, diffusivity along perivascular spaces; SVD, small vessel disease; WMH, white matter hyperintensity; CMBs, cerebral microbleeds. *P-corrected* values in bold indicates significance after *Bonferroni* correction.

Relation between BG-PVS volumes, FW fraction and DTI-ALPS, and cognitive function

In the cross-sectional analyses, we found that a higher FW fraction was associated with a lower MMSE, cognitive index score and slower processing speed; higher DTI-ALPS was associated a higher cognitive index score and faster processing speed (Table 3). BG-PVS volumes did not show any significant associations with cognitive function at any time point (Table 3). The association between FW fraction and processing speed, between DTI-ALPS and processing speed at baseline remained significant after additionally adjustment of SVD MRI markers (Table e-7).

Table 3. Cross-sectional associations between BG-PVS volumes, FW fraction, DTI-ALPS and cognitive function at two time points.

	MMSE		Cognitive index		Processing speed	
	β	***p-corrected***	***β***	***p-corrected***	***β***	***p-corrected***
2011						
BG-PVS volume	0.07 (-0.05, -0.18)	0.792	-0.09 (-0.21, 0.02)	0.324	-0.11 (-0.22, 0.01)	0.213
FW fraction	-0.16 (-0.27, -0.04)	**0.021**	-0.22 (-0.33, -0.11)	**<0.001**	-0.27 (-0.38, -0.16)	**<0.001**
DTI-ALPS	0.06 (-0.05, 0.18)	0.837	0.18 (0.06, 0.29)	**0.007**	0.19 (0.08, 0.31)	**0.003**
2015						
BG-PVS volume	0.06 (-0.07, 0,19)	1.000	-0.04 (-0.18, 0.09)	1.000	-0.06 (-0.19, 0.07)	1.000
FW fraction	-0.15 (-0.28, -0.02)	0.075	-0.15 (-0.29, -0.02)	0.069	-0.20 (-0.33, -0.07)	**0.009**
DTI-ALPS	0.08 (-0.05, 0.22)	0.651	0.17 (0.04, 0.30)	**0.032**	0.12 (-0.01, 0.26)	0.201

BG-PVS, perivascular spaces in basal ganglia; DTI-ALPS, Diffusion Tensor Imaging along the Perivascular Space; MMSE, Mini-Mental State Examination, *P-corrected* values in bold indicates significance after *Bonferroni* correction.

The longitudinal analyses showed that baseline FW fraction was associated with decline in MMSE score (β=-0.17, *p-corrected*=0.006), both baseline FW fraction and DTI-ALPS were associated with decline in cognitive index (FW: β=-0.25, *p-corrected*<0.001; DTI-ALPS: β=0.20, *p-corrected*=0.001) and processing speed (FW: β=-0.29, *p-corrected*<0.001; DTI-ALPS: β=0.21, *p-corrected*<0.001) (Figure 4). These associations remained largely significant after additionally adjusting for the changes in SVD MRI markers (Figure 4). BG-PVS volumes did not show any significant associations with changes in MMSE, cognitive index or processing speed over time. Changes of BG-PVS volumes, FW fraction and DTI-ALPS over follow-

up time did not show any associations with the changes of cognitive function in general or processing speed in specific (Table e-8).

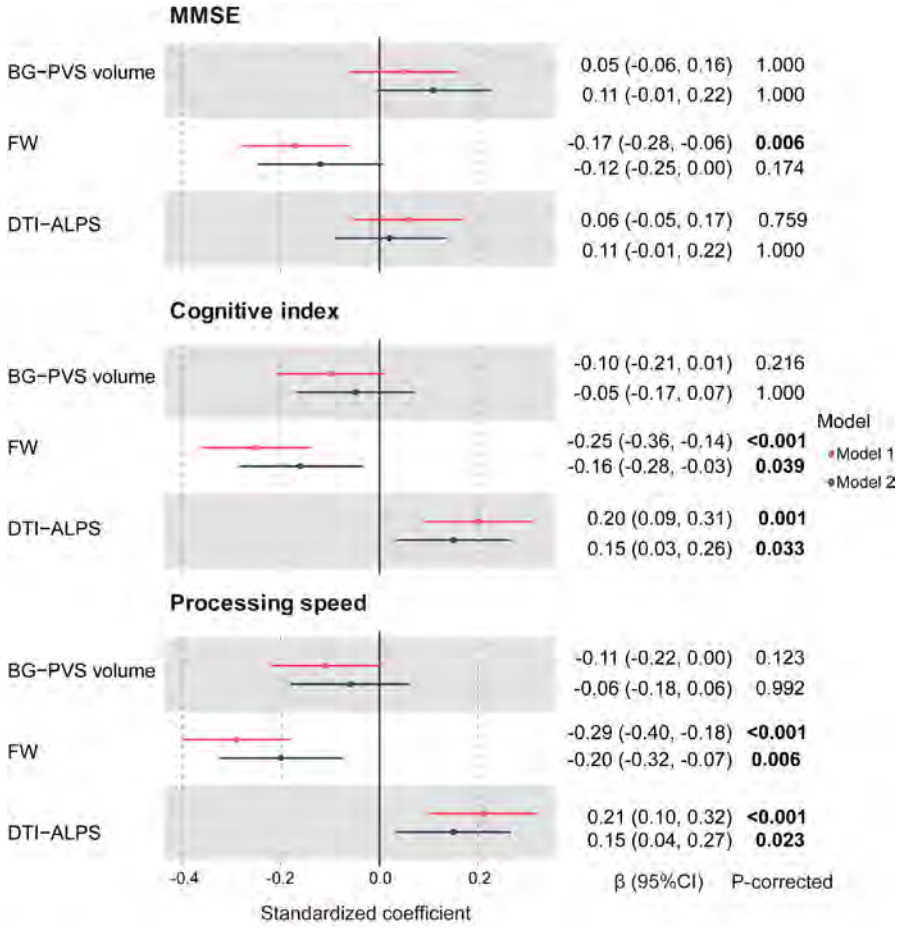

Figure 4. Linear mixed model results of the relations between baseline BG-PVS volumes, FW fraction and DTI-ALPS and cognitive decline over time. Model 1, adjusted for age, education, and vascular risk factors; Model 2, additionally adjusted for SVD MRI markers based on model 1. SVD MRI markers included WMH volumes, lacune numbers, CMBs numbers and brain volumes. BG-PVS, perivascular spaces in basal ganglia; FW, free water; DTI-ALPS, diffusivity along perivascular spaces; SVD, small vessel disease; WMH, white matter hyperintensity; CMBs, cerebral microbleeds. *P-corrected* values in bold indicates significance after *Bonferroni* correction.

Discussion

In this present study, we measured BG-PVS volumes, FW fraction and DTI-ALPS and examined their cross-sectional and longitudinal associations with MRI markers of SVD and cognitive function in a sporadic SVD cohort. We found that 1) baseline DTI-ALPS was associated with the increase of BG-PVS volumes over time, but not the reverse, suggesting a time-lagged association between DTI-ALPS and BG-PVS volumes; 2) increased BG-PVS volumes, increased FW fraction, and decreased DTI-ALPS were related to severity and progression of SVD; 3) increased FW fraction and decreased DTI-ALPS were associated with impairment and decline of cognitive function. Taken together, our results showed that BG-PVS volumes, FW fraction and DTI-ALPS independently contributed to the progression of SVD burden and cognitive decline in SVD population.

We showed that baseline DTI-ALPS was associated with the increase of BG-PVS volumes, but not vice versa. This finding builds upon previous studies that merely tested the cross-sectional association between DTI-ALPS and PVS,[6,8] by showing that decrease of DTI-ALPS precedes the increase of BG-PVS volumes. This time-lagged association supports the concept of decreased DTI-ALPS being an early contributing mechanism for enlarged BG-PVS, which is proposed to represent the blockage of brain drainage pathways.[11] In addition, we found that FW fraction was not related to either BG-PVS volumes or DTI-ALPS. This could be due to the exact mechanisms underlying the increased FW in SVD is highly complex and remains largely unclear yet. Although several studies suggested that increased FW-WM was related to the stagnation of ISF drainage,[5,7] an increase of FW may also be a consequence of other pathological processes, including the disruption of blood-brain barrier, neuroinflammation, vasogenic edema and intramyelinic vacuolization in SVD.[16] Therefore, caution is warranted in interpreting an increased FW fraction as a glymphatic dysfunction. Moreover, we did not find any significant changes in BG-PVS volumes, FW fraction and DTI-ALPS over time. This could mainly be due to the relatively short follow-up time (median: 3.4 years) in the study, leading to an insufficient observation window for the changes of these measures. In addition, another explanation could be the confounding effects of test-retest variations, especially in 1.5T MRI scanner, which could either reduce or enlarge the observed changes over time of the three measures.

We also found that increased BG-PVS volumes, increased FW fraction and decreased DTI-ALPS were related to the baseline severity and progression of SVD burden (mainly WMH volumes, lacune count and brain volumes). Similar associations have

previously been shown.[6,8,14,37] Our findings corroborate these associations and provide further evidence supporting the hypothesis that early-stage changes of BG-PVS, FW and DTI-ALPS may contribute to the progression of SVD. Nevertheless, we did not find any association between changes of BG-PVS volumes, FW fraction or DTI-ALPS and progression of MRI markers of SVD. This may suggest that the changes of BG-PVS volumes, FW fraction, DTI-ALPS and the progression of MRI markers appear at different times. Another explanation could be that the follow-up time-period was too short to detect significant changes in these measures that could truly lead to progression of SVD.

The association between DTI-ALPS and cognitive performance has been previously explored in cross-sectional studies that have shown that lower DTI-ALPS was related to worse performance in multiple cognitive domains.[38,39] Our findings extended this link by showing that DTI-ALPS at baseline was associated with decline in cognitive index and processing speed over time. Interestingly, we found that the significant association between decreased DTI-ALPS and cognitive impairment remained after adjusting for SVD MRI markers (including white matter integrity), suggesting an independent role of DTI-ALPS in cognitive decline.

We also found that increased FW fraction was related to cognitive decline over time, which is consistent with previous studies.[16] Increased FW could cause extensive cerebral structural abnormalities through various pathophysiological mechanisms, which in turn contribute to cognitive impairment in SVD.[5,16] We did not find any association between BG-PVS volumes and cognitive function based on the cross-sectional or longitudinal analyses. This result is consistent with previous study, which employed whole-brain PVS volumetry in SVD and Alzheimer Disease.[5,40] Nevertheless, several studies reported significant association between higher BG-PVS numbers and cognitive impairments.[41,42] An independent contribution of PVS on cognitive impairment remains to be established in SVD.

The strength of this study is the comprehensive longitudinal imaging assessment in a relatively large sample size of SVD participants with detailed cognitive data. However, there are some limitations that should be acknowledged. First, although DTI-ALPS have shown to have a substantial correlation with glymphatic clearance rates measured via invasive MRI with intrathecal injection of gadolinium, it fundamentally captures the diffusivity along the peri-vascular spaces, which may originate from different compartments, such as tissue and blood, rather than along the peri-vascular spaces.[6,13] In addition, this index was measured only at the level of lateral ventricle body,[13] while the glymphatic changes occurs throughout the brain.

Therefore, DTI-ALPS could only serve as an approximate measure of a regional brain area. Further validations are therefore needed for DTI-ALPS in the assessments of glymphatic function. Until then, no conclusion can be made whether DTI-ALPS can be used as a proxy for glymphatic function. Second, the PVS volumetry was limited in the basal ganglia in this present study due to the low-quality of PVS segmentations in deep WM. Although SVD-related PVS are typically concentrated within the basal ganglia,[30] the lack of PVS volumetry in other regions (e.g., the centrum semiovale and hippocampus) could potentially underestimate the association between PVS volumes and other markers of SVD, as well as cognitive function. Future studies employing higher resolution structural MRI, particularly using a high-field strength, could enable an accurate PVS volumetry of whole-brain, thereby providing a better understanding of the role of PVS in SVD and SVD-related cognitive impairments. Third, the statistical models used in our study, specifically the linear mixed model and latent change score model for longitudinal analyses are not able to draw a casual association. These models, at most, could infer temporal associations, which should not be equal with causal associations. As the temporal associations could be caused by other concurrent factors, including aging and the accumulation of vascular risk factors. Further work employing more precise methods for assessing glymphatic function, such as MRI with intrathecal injection of gadolinium and with extended follow-up periods, is needed to validate our findings.

In conclusion, our study demonstrated that decreases in DTI-ALPS precede increases in BG-PVS volumes, suggesting a time-lagged association between the two measures Increased BG-PVS volumes, increased FW fraction and decreased DTI-ALPS are independently related to SVD progression, along with SVD-related cognitive decline over time. However, it is essential to formally validate whether these measures accurately represent glymphatic dysfunction in SVD in further studies.

Supplementary material

Table e-1. The MRI acquisition details of RUN DMC cohort in 2011 and 2015

Sequences	TR/ TE/ (TI) ms	Voxel size	Number of Weighted/ unweighted scans	b-value
3D T1 MPRAGE	2250/2.95/850 ms	1.0x1.0x1.0 mm	NA	NA
T2*-weighted GRE	800/26 ms	1.3x1.0x5.0 mm	NA	NA
FLAIR sequence	14240/89/2200 ms	0.5x0.5x2.5 mm	NA	NA
DWI sequence	10200/95 ms	2.5x2.5x2.5 mm	30/4	900 s/mm^2

MPRAGE: magnetization-prepared rapid gradient echo, FLAIR: fluid-attenuated inversion recovery, DWI= diffusion weighted imaging, GRE: gradient echo sequence, TR: repetition time, TE: echo time, TI: inversion time, ms: milliseconds, mm: millimeter.

Table e-2. Correlation analysis between visual rating scores and volumetry for basal ganglia perivascular spaces.

	BG-PVS scores, median (IQR)	BG-PVS volumes, cm^3, median (IQR)	Correlation coefficient	*P*
2011 (*n*=29)	2 (1-2)	0.93 (0.88, 1.00)	0.61	**<0.001**
2015 (*n*=22)	2 (2-2)	0.92 (0.87-1.09)	0.64	**0.001**

BG-PVS, perivascular spaces in basal ganglia; P values in bold indicates significance.

Table e-3. Baseline cognitive performances of the whole cohort on each cognitive test.

Cognitive tests	Raw score
RAVLT	
Immediate recall, median (IQR)	5.33 (4.00-6.67)
Delayed recall, median (IQR)	4.00 (2.00-6.00)
RCFT	
Immediate recall, mean (SD)	19.15 (6.58)
Delayed recall, mean (SD)	18.91 (6.59)
PPMST, SAT score	
Number Scanning, mean (SD)	2.18 (0.64)
Letter Scanning, mean (SD)	1.40 (0.42)
Shape Scanning, mean (SD)	1.18 (0.38)
SCWT, SAT score	
Colour Naming, mean (SD)	4.02 (0.83)
Word Reading, mean (SD)	3.18 (0.63)
Interference, mean (SD)	1.85 (0.56)
SDST, median (IQR)	26.00 (16.00-23.00)
VFT	
Animals, median (IQR)	20.00 (16.00-23.00)
Jobs, median (IQR)	15.00 (12.00-18.00)
VSAT, SAT score, mean (SD)	1.22 (0.38)

Note: RAVLT, Rey's Auditory Verbal learning test; RCFT, Rey Complex Figure Test; PPMST, Paper-Pencil Memory Scanning Task; SCWT, Stroop Colour-Word Test; SDMT, Symbol-Digit Modalities Test; VFT, Verbal Fluency Test; VSAT, Verbal Series Attention Test. SAT score.

Table e-4 Baseline demographic, neuroimaging characteristics and cognitive function of participants with and with-out follow-up assessments.

	Participants with follow-up (n=220)	Participants without complete follow-up (n=69)	*P*
Demographic			
Age, years, median (IQR)	65 (60-73)	74 (66-80)	**<0.001**
Female, n (%)	95 (43.2%)	29 (42.0%)	0.976
Education, years, median (IQR)	10 (10-11)	10 (9-11)	**0.038**
Vascular risk factors			
Hypertension, n (%)	144 (65.5%)	48 (69.6%)	0.628
Diabetes, n (%)	14 (6.4%)	13 (18.8%)	**0.004**
hypercholesterolemia, n (%)	85 (38.6%)	31 (44.9%)	0.430
Smoking, n (%)	153 (69.5%)	51 (73.9%)	0.587
Vascular risk factors, median (IQR)	2 (1-3)	2 (1-3)	0.132
Medications			
Antihypertensive drugs, n (%)	136 (61.8%)	50 (72.5%)	0.107
Antithrombotic drugs, n (%)	121 (55.0%)	37 (53.6%)	0.841
Antidiabetic drugs, n (%)	25 (11.4%)	14 (20.3%)	0.058
Statins, n (%)	94 (21.4%)	37 (53.6%)	0.113
Cognitive function			
MMSE, median (IQR)	29.00 (28.00-30.00)	28.00 (27.00-29.00)	**0.001**
Cognitive index, Z score, median (IQR)	0.29 (-0.23-0.72)	-0.37 (-0.78-0.35)	**<0.001**
Processing speed, Z score, mean (SD)	0.27 (0.80)	-0.29 (0.88)	**<0.001**
MRI markers			
WMH volumes, ml, median (IQR)	2.52 (1.14-6.54)	6.74 (2.57-18.07)	**<0.001**
Lacunes, n (%)	47 (21.4%)	23 (33.3%)	0.062
CMBs, n (%)	39 (17.7%)	20 (29.0%)	0.064
Brain volumes, ml, mean (SD)	1090.28 (109.87)	1018.64 (89.82)	**<0.001**
BG-PVS volume, ml, median (IQR)	0.94 (0.84-1.02)	0.96 (0.87-1.04)	0.150
Free water fraction, median (IQR)	0.35 (0.34-0.37)	0.34 (0.33-0.35)	**0.001**
DTI-ALPS, mean (SD)	1.39 (0.17)	1.32 (0.15)	**0.001**

MMSE, Mini-Mental State Examination; WMH, white matter hypersensitivity; CMBs, cerebral microbleeds; BG-PVS, perivascular spaces in basal ganglia; DTI-ALPS, Diffusion Tensor Imaging along the Perivascular Space.

Table e-5. Linear mixed model for temporal changes of BG-PVS volumes, DTI-ALPS and FW fraction.

Fixed effects	BG-PVS volumes		FW fraction		DTI-ALPS	
	Standardized β (95%CI)	***p-corrected***	**Standardized β (95%CI)**	***p-corrected***	**Standardized β (95%CI)**	***p-corrected***
Age	0.14 (0.02, 0.25)	0.054	0.43 (0.33, 0.53)	**<0.001**	-0.19 (-0.30, -0.08)	**0.002**
Sex	0.10 (-0.01, 0.21)	0.201	0.13 (0.04, 0.23)	**0.021**	0.04 (-0.06, 0.13)	1.000
Follow-up time	0.30 (-0.09, 0.68)	0.396	-0.50 (-1.00, 0.01)	0.168	-0.03 (-0.48, 0.41)	1.000
Vascular risk factor	0.058 (-0.05, 0.17)	0.903	0.16 (0.06, 0.25)	**0.003**	-0.13 (-0.23, -0.04)	**0.022**
Age*follow-up time	-0.00 (-0.01, 0.00)	1.000	0.01 (-0.00, 0.01)	0.216	0.00 (-0.00, 0.01)	1.000
MD					-0.23 (-0.33, -0.13)	**<0.001**

MD, the mean MD values of the regions employed in the DTI-ALPS calculation. P values in bold indicates significance. BG-PVS, peri-vascular spaces in the basal ganglia; FW, free water; DTI-ALPS, Diffusion Tensor Imaging along the Perivascular Space; CI, Confidence intervals.

Table e-6. The relation between changes of BG-PVS volumes, DTI-ALPS and FW and the changes of SVD MRI markers over time.

Fixed effects	WMH volumes		Lacune numbers		CMBs numbers		Brain percent	
	β	***p-corrected***	***β***	***p-corrected***	***β***	***p-corrected***	***β***	***p-corrected***
BG-PVS Volume*time	0.02 (0.00, 0.04)	0.108	0.00 (-0.02, 0.02)	1.000	0.01 (-0.01, 0.03)	1.000	0.01 (-0.01, 0.04)	0.615
FW*time	0.02 (0.00, 0.04)	0.135	0.00 (-0.02, 0.02)	1.000	0.00 (-0.02, 0.02)	1.000	0.02 (-0.01, 0.04)	0.459
DTI-ALPS*time	-0.02 (-0.04, -0.02)	0.081	-0.01 (-0.03, 0.01)	0.837	-0.01 (-0.04, 0.01)	0.756	-0.01 (-0.03, 0.01)	1.000

WMH, white matter hypersensitivity; CMBs, cerebral microbleeds; BG-PVS, perivascular spaces in basal ganglia; DTI-ALPS, Diffusion Tensor Imaging along the Perivascular Space. BG-PVS*time: interaction term between BG-PVS and follow-up time; FW*time: interaction term between FW and follow-up time; DTI-ALPS*time: interaction term between DTI-ALPS and follow-up time. P-corrected values in bold indicates significance after Bonferroni correction.

Table e-7. Linear regression analyses between BG-PVS volumes, DTI-ALPS and FW and cognitive function at two time points while adjusting for SVD MRI markers.

	MMSE		Cognitive index		Processing speed	
	β	***p-corrected***	***β***	***p-corrected***	***β***	***p-corrected***
2011						
BG-PVS volume	0.11 (-0.01, 0.24)	0.228	-0.05 (-0.18, 0.07)	1.000	-0.05 (-0.17, 0.07)	1.000
FW	-0.12 (-0.26, 0.01)	0.225	-0.17 (-0.30, -0.04)	**0.039**	-0.21 (-0.34, -0.08)	**0.006**
DTI-ALPS	0.03 (-0.09, 0.15)	1.000	0.14 (0.02, 0.26)	0.060	0.15 (0.03, 0.26)	**0.039**
2015						
BG-PVS volume	0.15 (0.02, 0.29)	0.084	0.03 (-0.11, 0.16)	1.000	0.00 (-0.13, 0.14)	1.000
FW	-0.06 (-0.21, 0.10)	1.000	-0.03 (-0.18, 0.13)	1.000	-0.11 (-0.26, 0.05)	0.537
DTI-ALPS	0.05 (-0.09, 0.18)	1.000	0.14 (0.01, 0.27)	0.117	0.09 (-0.04, 0.22)	0.537

SVD, small vessel disease; BG-PVS, perivascular spaces in basal ganglia; DTI-ALPS, Diffusion Tensor Imaging along the Perivascular Space. P-corrected values in bold indicates significance after Bonferroni correction.

Table e-8. Linear mixed models for the association between the changes of BG-PVS volumes, DTI-ALPS and FW measures and the changes of cognitive function.

	MMSE		Cognitive index		Processing speed	
	β	***p-corrected***	***β***	***p-corrected***	***β***	***p-corrected***
Model 1						
BG-PVS volume*time	-0.01 (-0.07, 0.06)	1.000	-0.00 (-0.04, 0.04)	1.000	-0.01 (-0.05, 0.03)	1.000
FW*time	-0.00 (-0.07, 0.06)	1.000	-0.04 (-0.08, 0.00)	0.174	-0.03 (-0.07, 0.01)	0.336
DTI-ALPS*time	0.04 (-0.02, 0.10)	0.525	0.02 (-0.02, 0.06)	1.000	0.01 (-0.03, 0.05)	1.000
Model 2						
BG-PVS volume*time	0.01 (-0.03, 0.05)	1.000	0.00 (-0.02, 0.03)	1.000	-0.00 (-0.03, 0.02)	1.000
FW*time	0.01 (-0.03, 0.06)	1.000	-0.01 (-0.04, 0.02)	1.000	-0.02 (-0.05, 0.01)	0.522
DTI-ALPS*time	0.02 (-0.02, 0.06)	0.864	0.00 (-0.02, 0.03)	1.000	0.00 (-0.02, 0.03)	1.000

Model 2. Additionally adjusted for SVD MRI markers and their interaction term with follow-up time based on Model 1. BG-PVS, perivascular spaces in basal ganglia; DTI-ALPS, Diffusion Tensor Imaging along the Perivascular Space. BG-PVS*time: interaction term between BG-PVS and follow-up time; FW*time: interaction term between FW and follow-up time; DTI-ALPS*time: interaction term between DTI-ALPS and follow-up time. P-corrected values in bold indicates significance after Bonferroni correction.

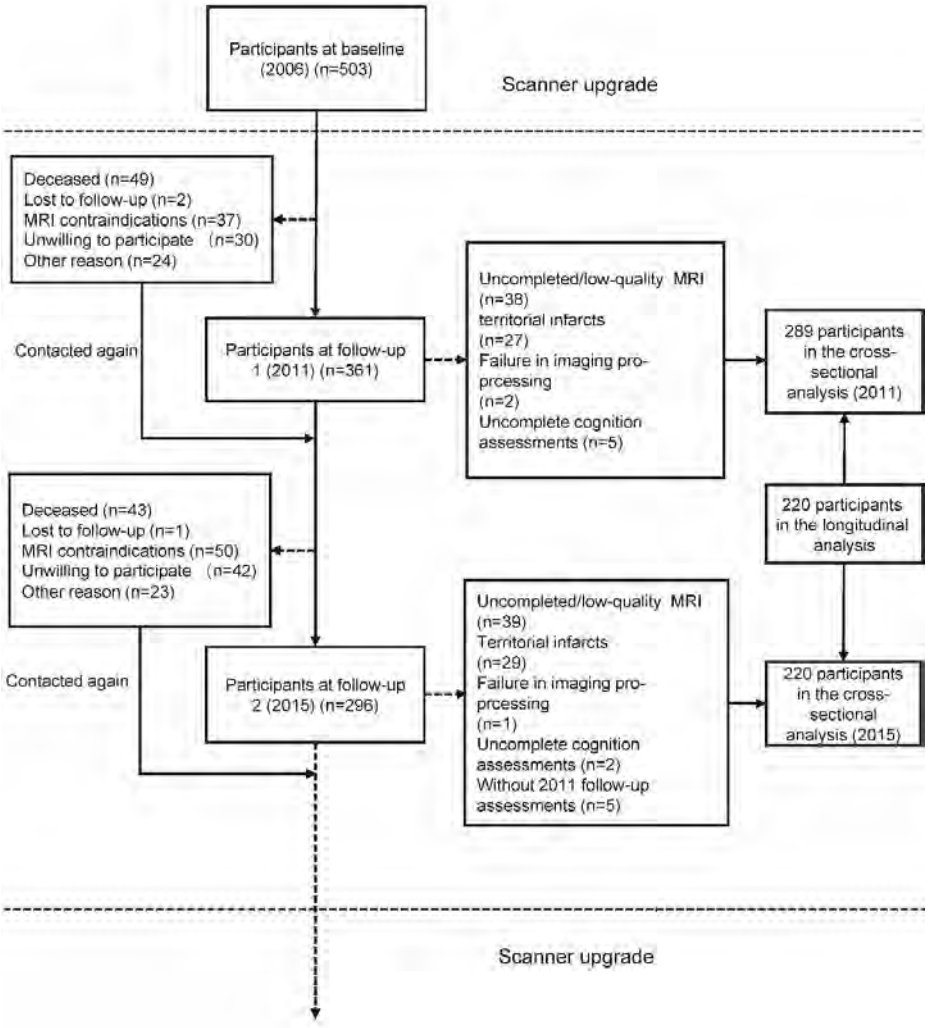

Figure e-1. Flow chart of included participants. Only data from 2011 and 2015 were used in the present study. Of the 361 participants in 2011, participants were excluded due to incomplete or low-quality MRI scans (n=38), presence of territory infarcts (n=27), image processing failure (n=2) and incomplete cognitive assessments (n=5). Of the 291 participants who participated in both 2011 and 2015, 39 participants were excluded due to incomplete or low-quality MRI scans (n=39), presence of territory infarcts (n=29), image processing failure (n=1) and incomplete cognitive assessments (n=2). This brought our total sample size used in the study to 289 participants in 2011 (cross-sectional analysis) and 220 participants in 2015 (longitudinal analysis).

Reference

1. Duering M, et al. Neuroimaging standards for research into small vessel disease-advances since 2013. The Lancet Neurology. May 23 2023;doi:10.1016/s1474-4422(23)00131-x
2. Wardlaw JM, Smith C, Dichgans M. Small vessel disease: mechanisms and clinical implications. Lancet Neurol. Jul 2019;18(7):684-696. doi:10.1016/s1474-4422(19)30079-1
3. Mestre H, Mori Y, Nedergaard M. The Brain's Glymphatic System: Current Controversies. Trends Neurosci. Jul 2020;43(7):458-466. doi:10.1016/j.tins.2020.04.003
4. Xu J, Su Y, Fu J, Shen Y, Dong Q, Cheng X. Glymphatic pathway in sporadic cerebral small vessel diseases: From bench to bedside. Ageing Res Rev. Apr 2023;86:101885. doi:10.1016/j.arr.2023.101885
5. Kamagata K, Andica C, Takabayashi K, Saito Y, Taoka T, Nozaki H, Kikuta J, Fujita S, Hagiwara A, Kamiya K, Wada A, Akashi T, Sano K, Nishizawa M, Hori M, Naganawa S, Aoki S. Association of MRI Indices of Glymphatic System With Amyloid Deposition and Cognition in Mild Cognitive Impairment and Alzheimer Disease. Neurology. Sep 19 2022;99(24):e2648-60. doi:10.1212/wnl.0000000000201300
6. Zhang W, Zhou Y, Wang J, Gong X, Chen Z, Zhang X, Cai J, Chen S, Fang L, Sun J, Lou M. Glymphatic clearance function in patients with cerebral small vessel disease. Neuroimage. Sep 2021;238:118257. doi:10.1016/j.neuroimage.2021.118257
7. Andica C, Kamagata K, Takabayashi K, Kikuta J, Kaga H, Someya Y, Tamura Y, Kawamori R, Watada H, Taoka T, Naganawa S, Aoki S. Neuroimaging findings related to glymphatic system alterations in older adults with metabolic syndrome. Neurobiology of disease. Feb 2023;177:105990. doi:10.1016/j.nbd.2023.105990
8. Tian Y, Cai X, Zhou Y, Jin A, Wang S, Yang Y, Mei L, Jing J, Li S, Meng X, Wei T, Liu T, Wang Y, Pan Y, Wang Y. Impaired glymphatic system as evidenced by low diffusivity along perivascular spaces is associated with cerebral small vessel disease: a population-based study. Stroke and vascular neurology. Apr 12 2023;doi:10.1136/svn-2022-002191
9. Bouvy WH, Biessels GJ, Kuijf HJ, Kappelle LJ, Luijten PR, Zwanenburg JJ. Visualization of perivascular spaces and perforating arteries with 7 T magnetic resonance imaging. Investigative radiology. May 2014;49(5):307-13. doi:10.1097/rli.0000000000000027
10. SCHLESINGER B. THE VENOUS DRAINAGE OF THE BRAIN, WITH SPECIAL REFERENCE TO THE GALENIC SYSTEM. Brain : a journal of neurology. 1939;62(3):274-291. doi:10.1093/brain/62.3.274 %J Brain
11. Wardlaw JM, Benveniste H, Nedergaard M, Zlokovic BV, Mestre H, Lee H, Doubal FN, Brown R, Ramirez J, MacIntosh BJ, Tannenbaum A, Ballerini L, Rungta RL, Boido D, Sweeney M, Montagne A, Charpak S, Joutel A, Smith KJ, Black SE. Perivascular spaces in the brain: anatomy, physiology and pathology. Nat Rev Neurol. Mar 2020;16(3):137-153. doi:10.1038/s41582-020-0312-z
12. Pasternak O, Sochen N, Gur Y, Intrator N, Assaf Y. Free water elimination and mapping from diffusion MRI. Magn Reson Med. Sep 2009;62(3):717-30. doi:10.1002/mrm.22055
13. Taoka T, Masutani Y, Kawai H, Nakane T, Matsuoka K, Yasuno F, Kishimoto T, Naganawa SJJjor. Evaluation of glymphatic system activity with the diffusion MR technique: diffusion tensor image analysis along the perivascular space (DTI-ALPS) in Alzheimer's disease cases. 2017;35:172-178.
14. Ding J, Sigurðsson S, Jónsson PV, Eiriksdottir G, Charidimou A, Lopez OL, van Buchem MA, Guðnason V, Launer LJ. Large Perivascular Spaces Visible on Magnetic Resonance Imaging, Cerebral Small Vessel Disease Progression, and Risk of Dementia: The Age, Gene/Environment Susceptibility-Reykjavik Study. JAMA Neurol. Sep 1 2017;74(9):1105-1112. doi:10.1001/jamaneurol.2017.1397

15. Evans TE, Knol MJ, Schwingenschuh P, Wittfeld K, Hilal S, Ikram MA, Dubost F, van Wijnen KMH, Katschnig P, Yilmaz P, de Bruijne M, Habes M, Chen C, Langer S, Völzke H, Ikram MK, Grabe HJ, Schmidt R, Adams HHH, Vernooij MW. Determinants of Perivascular Spaces in the General Population: A Pooled Cohort Analysis of Individual Participant Data. Neurology. Jan 10 2023;100(2):e107-e122. doi:10.1212/wnl.0000000000201349

16. Duering M, Finsterwalder S, Baykara E, Tuladhar AM, Gesierich B, Konieczny MJ, Malik R, Franzmeier N, Ewers M, Jouvent E, Biessels GJ, Schmidt R, de Leeuw FE, Pasternak O, Dichgans M. Free water determines diffusion alterations and clinical status in cerebral small vessel disease. Alzheimers Dement. Jun 2018;14(6):764-774. doi:10.1016/j.jalz.2017.12.007

17. van Norden AG, de Laat KF, Gons RA, van Uden IW, van Dijk EJ, van Oudheusden LJ, Esselink RA, Bloem BR, van Engelen BG, Zwarts MJ, Tendolkar I, Olde-Rikkert MG, van der Vlugt MJ, Zwiers MP, Norris DG, de Leeuw FE. Causes and consequences of cerebral small vessel disease. The RUN DMC study: a prospective cohort study. Study rationale and protocol. BMC Neurol. Feb 28 2011;11:29. doi:10.1186/1471-2377-11-29

18. Cai M, Jacob MA, Norris DG, de Leeuw FE, Tuladhar AM. Longitudinal Relation Between Structural Network Efficiency, Cognition, and Gait in Cerebral Small Vessel Disease. J Gerontol A Biol Sci Med Sci. Mar 3 2022;77(3):554-560. doi:10.1093/gerona/glab247

19. Charlton RA, Morris RG, Nitkunan A, Markus HS. The cognitive profiles of CADASIL and sporadic small vessel disease. Neurology. May 23 2006;66(10):1523-6. doi:10.1212/01.wnl.0000216270.02610.7e

20. Salvadori E, Brambilla M, Maestri G, Nicotra A, Cova I, Pomati S, Pantoni L. The clinical profile of cerebral small vessel disease: Toward an evidence-based identification of cognitive markers. Alzheimer's & dementia : the journal of the Alzheimer's Association. Jan 2023;19(1):244-260. doi:10.1002/alz.12650

21. Ghafoorian M, Karssemeijer N, van Uden IW, de Leeuw FE, Heskes T, Marchiori E, Platel B. Automated detection of white matter hyperintensities of all sizes in cerebral small vessel disease. Medical physics. Dec 2016;43(12):6246. doi:10.1118/1.4966029

22. Cai M, Jacob MA, Marques J, Norris DG, Duering M, Esselink RAJ, Zhang Y, de Leeuw FE, Tuladhar AM. Structural network efficiency predicts conversion to incident parkinsonism in patients with cerebral small vessel disease. J Gerontol A Biol Sci Med Sci. Aug 1 2023;doi:10.1093/gerona/glad182

23. Putaala J, Haapaniemi E, Kaste M, Tatlisumak T. How does number of risk factors affect prognosis in young patients with ischemic stroke? Stroke. Feb 2012;43(2):356-61. doi:10.1161/strokeaha.111.635276

24. Tournier JD, Smith R, Raffelt D, Tabbara R, Dhollander T, Pietsch M, Christiaens D, Jeurissen B, Yeh CH, Connelly A. MRtrix3: A fast, flexible and open software framework for medical image processing and visualisation. Neuroimage. Nov 15 2019;202:116137. doi:10.1016/j.neuroimage.2019.116137

25. Smith SM, Jenkinson M, Woolrich MW, Beckmann CF, Behrens TE, Johansen-Berg H, Bannister PR, De Luca M, Drobnjak I, Flitney DE, Niazy RK, Saunders J, Vickers J, Zhang Y, De Stefano N, Brady JM, Matthews PM. Advances in functional and structural MR image analysis and implementation as FSL. NeuroImage. 2004;23 Suppl 1:S208-19. doi:10.1016/j.neuroimage.2004.07.051

26. Schilling KG, Blaber J, Huo Y, Newton A, Hansen C, Nath V, Shafer AT, Williams O, Resnick SM, Rogers B, Anderson AW, Landman BA. Synthesized b0 for diffusion distortion correction (Synb0-DisCo). Magn Reson Imaging. Dec 2019;64:62-70. doi:10.1016/j.mri.2019.05.008

27. Tustison NJ, Avants BB, Cook PA, Zheng Y, Egan A, Yushkevich PA, Gee JC. N4ITK: improved N3 bias correction. IEEE Trans Med Imaging. Jun 2010;29(6):1310-20. doi:10.1109/tmi.2010.2046908

28. Boutinaud P, Tsuchida A, Laurent A, Adonias F, Hanifehlou Z, Nozais V, Verrecchia V, Lampe L, Zhang J, Zhu YC, Tzourio C, Mazoyer B, Joliot M. 3D Segmentation of Perivascular Spaces on T1-Weighted 3 Tesla MR Images With a Convolutional Autoencoder and a U-Shaped Neural Network. Front Neuroinform. 2021;15:641600. doi:10.3389/fninf.2021.641600

29. Banerjee G, Kim HJ, Fox Z, Jäger HR, Wilson D, Charidimou A, Na HK, Na DL, Seo SW, Werring DJ. MRI-visible perivascular space location is associated with Alzheimer's disease independently of amyloid burden. Brain : a journal of neurology. Apr 1 2017;140(4):1107-1116. doi:10.1093/brain/awx003

30. Charidimou A, Meegahage R, Fox Z, Peeters A, Vandermeeren Y, Laloux P, Baron JC, Jäger HR, Werring DJ. Enlarged perivascular spaces as a marker of underlying arteriopathy in intracerebral haemorrhage: a multicentre MRI cohort study. Journal of neurology, neurosurgery, and psychiatry. Jun 2013;84(6):624-9. doi:10.1136/jnnp-2012-304434

31. Mori S, Oishi K, Jiang H, Jiang L, Li X, Akhter K, Hua K, Faria AV, Mahmood A, Woods R, Toga AW, Pike GB, Neto PR, Evans A, Zhang J, Huang H, Miller MI, van Zijl P, Mazziotta J. Stereotaxic white matter atlas based on diffusion tensor imaging in an ICBM template. Neuroimage. Apr 1 2008;40(2):570-582. doi:10.1016/j.neuroimage.2007.12.035

32. Golub M. Implementation of an algorithm for estimating free-water fraction in Diffusion-Weighted Magnetic Resonance Imaging. 2018:

33. He P, Shi L, Li Y, Duan Q, Qiu Y, Feng S, Gao Y, Luo Y, Ma G, Zhang Y, Wang L, Nie K. The Association of the Glymphatic Function with Parkinson's Disease Symptoms: Neuroimaging Evidence from Longitudinal and Cross-sectional Studies. Annals of neurology. Jun 28 2023;doi:10.1002/ana.26729

34. Vikner T, Karalija N, Eklund A, Malm J, Lundquist A, Gallewicz N, Dahlin M, Lindenberger U, Riklund K, Bäckman L, Nyberg L, Wåhlin A. 5-Year Associations among Cerebral Arterial Pulsatility, Perivascular Space Dilation, and White Matter Lesions. Annals of neurology. Nov 2022;92(5):871-881. doi:10.1002/ana.26475

35. Kievit RA, Brandmaier AM, Ziegler G, van Harmelen AL, de Mooij SMM, Moutoussis M, Goodyer IM, Bullmore E, Jones PB, Fonagy P, Lindenberger U, Dolan RJ. Developmental cognitive neuroscience using latent change score models: A tutorial and applications. Developmental cognitive neuroscience. Oct 2018;33:99-117. doi:10.1016/j.dcn.2017.11.007

36. Hu Lt, Bentler PMJSemamj. Cutoff criteria for fit indexes in covariance structure analysis: Conventional criteria versus new alternatives. 1999;6(1):1-55.

37. Evans TE, Knol MJ, Schwingenschuh P, Wittfeld K, Hilal S, Ikram MA, Dubost F, van Wijnen KM, Katschnig P, Yilmaz PJN. Determinants of perivascular spaces in the general population: a pooled cohort analysis of individual participant data. 2023;100(2):e107-e122.

38. Tang J, Zhang M, Liu N, Xue Y, Ren X, Huang Q, Shi L, Fu J. The Association Between Glymphatic System Dysfunction and Cognitive Impairment in Cerebral Small Vessel Disease. Frontiers in aging neuroscience. 2022;14:916633. doi:10.3389/fnagi.2022.916633

39. Ke Z, Mo Y, Li J, Yang D, Huang L, Yang Z, Qin R, Mao C, Lv W, Huang Y, Hu Z, Zhang B, Xu Y. Glymphatic Dysfunction Mediates the Influence of White Matter Hyperintensities on Episodic Memory in Cerebral Small Vessel Disease. Brain sciences. Nov 24 2022;12(12)doi:10.3390/brainsci12121611

40. Benjamin P, Trippier S, Lawrence AJ, Lambert C, Zeestraten E, Williams OA, Patel B, Morris RG, Barrick TR, MacKinnon AD, Markus HS. Lacunar Infarcts, but Not Perivascular Spaces, Are Predictors of Cognitive Decline in Cerebral Small-Vessel Disease. Stroke. Mar 2018;49(3):586-593. doi:10.1161/strokeaha.117.017526

41. Huijts M, Duits A, Staals J, Kroon AA, de Leeuw PW, van Oostenbrugge RJ. Basal ganglia enlarged perivascular spaces are linked to cognitive function in patients with cerebral small vessel disease. Current neurovascular research. May 2014;11(2):136-41. doi:10.2174/1567202611666140310102248

42. Passiak BS, Liu D, Kresge HA, Cambronero FE, Pechman KR, Osborn KE, Gifford KA, Hohman TJ, Schrag MS, Davis LT, Jefferson AL. Perivascular spaces contribute to cognition beyond other small vessel disease markers. Neurology. Mar 19 2019;92(12):e1309-e1321. doi:10.1212/wnl.0000000000007124

Chapter 8.

Disruptions of deep medullary veins and MRI indices of glymphatic function in cerebral small vessel disease.

Published as:
Mengshi Liao, Meng Wang, Wenli Zhou, Yixin Chen, Jiayu Guo, Gemma Solé-Guardia, Anil M Tuladhar, Yuhua Fan+, Hao Li+. Disruption of deep medullary veins and MRI indices of glymphatic function in cerebral small vessel disease.

Abstract

Background: Disruptions of deep medullary veins (DMV) have been associated with the radiological severity and cognitive impairment observed in cerebral small vessel disease (SVD). Glymphatic dysfunction may serve as a potential mechanism underlying these associations. We aimed to clarify the associations between DMV disruptions, MRI indices previously hypothesized as related to glymphatic function, white matter hyperintensity (WMH), and cognitive impairment in SVD.

Methods: This cross-sectional study included 133 participants with SVD. DMV disruptions were visually rated on susceptibility-weighted imaging (SWI). Five MRI indices related to glymphatic function were measured: the diffusion tensor imaging along the perivascular space (DTI-ALPS), free water (FW) fraction, choroid plexus (Cp) volumes, perivascular spaces in basal ganglia (BG-PVS) and white matter (WM-PVS). Partial Pearson correlation analyses were performed to assess the correlations between DMV scores and these five MRI indices. Linear regression models tested the associations between DMV scores, WMH volumes, and MoCA scores. Parallel mediation analyses were conducted to determine whether these MRI five indices mediated the associations between DMV scores, WMH volumes, and MoCA scores.

Results: Higher DMV scores were associated with higher WMH volumes ($\beta = 0.55$, $p < 0.001$) and lower MoCA scores ($\beta = -0.24$, $p = 0.003$). Higher DMV scores were correlated with lower DTI-ALPS values, higher FW fraction, higher volumes in Cp, BG-PVS, and WM-PVS (all $p < 0.001$). DTI-ALPS values and BG-PVS volumes mediated the associations between DMV scores and WMH volumes, with only BG-PVS volumes mediating the associations between DMV scores and MoCA scores.

Conclusion: Our results suggested that DMV disruptions contribute to WMH burden and cognitive impairment in SVD. This effect could be mediated by MRI markers indicative of glymphatic dysfunction, particularly the enlargement of BG-PVS.

Keywords: Deep medullary veins, glymphatic function, White matter hyperintensities, Cognitive impairment, Cerebral small vessel disease

Introduction

Cerebral small vessel disease (SVD) is a leading causes of vascular cognitive impairment and dementia, characterized by neuroimaging features such as white matter hyperintensities (WMH), lacunes of presumed vascular origin, and cerebral microbleeds (CMBs).[1] Although these imaging markers are primarily considered to originate from pathological abnormalities in the arteriolar components of small vessels, the venous components also plays a significant role in the development and progression of SVD and its associated clinical manifestations.[2,3] [2, 3]

Deep medullary veins (DMV), which drain deep white matter in the brain, have been implicated in SVD pathophysiology.[3] Previous studies have identified associations between DMV disruptions, WMH, and cognitive impairment in SVD.[4, 5] However, the precise mechanisms linking these factors remain unclear. Emerging evidence suggests that glymphatic dysfunction may serve as a potential mechanism connecting DMV disruptions to both radiological manifestations and cognitive impairment in SVD.[6, 7] The glymphatic system refers to a waste clearance system in the brain that facilitates the removal of interstitial solutes through the production, circulation, and reabsorption of cerebrospinal fluid (CSF).[8, 9] Several MRI indices, although not validated, are hypothesized to reflect glymphatic function and have been widely used to assess it in previous studies.[7,9-12] These indices include diffusion tensor imaging along the perivascular space (DTI-ALPS), free water (FW) fraction, choroid plexus (Cp) volumes, and perivascular space (PVS) volumes.[7,9-12] Some of these MRI indices have been linked to disruptions of DMV in SVD. Specifically, DMV disruptions have been associated with an increased number of enlarged PVS in basal ganglia (BG-PVS) and higher FW fraction in SVD.[6,13] Moreover, a recent study found that DMV disruptions correlated with lower DTI-ALPS values, which further relate to higher WMH volumes.[14] However, these studies were limited by small sample size (n=32), reliance on single measures of glymphatic function, and insufficient exploration of clinical outcomes.

Therefore, the purpose of this study is to comprehensively assess the associations between DMV disruptions, glymphatic dysfunction, radiological severity, and cognitive impairment in SVD. We hypothesized that DMV disruptions are associated with glymphatic dysfunction, which subsequently contributes to radiological severity (as evidenced by WMH), and cognitive impairment in SVD (Figure 1). To test our hypothesis, we performed a visual rating of DMV disruptions using high-quality susceptibility-weighted imaging (SWI) and measured multiple MRI indices hypothesized as related to glymphatic function based on multi-modal imaging.

These MRI indices included the DTI-ALPS index, FW fraction, Cp volumes, and PVS volumes in the basal ganglia and deep white matter (BG-PVS and WM-PVS, respectively). We then tested the relations between DMV rating score, these MRI indices hypothesized as related to glymphatic function, WMH volumes, and cognitive function.

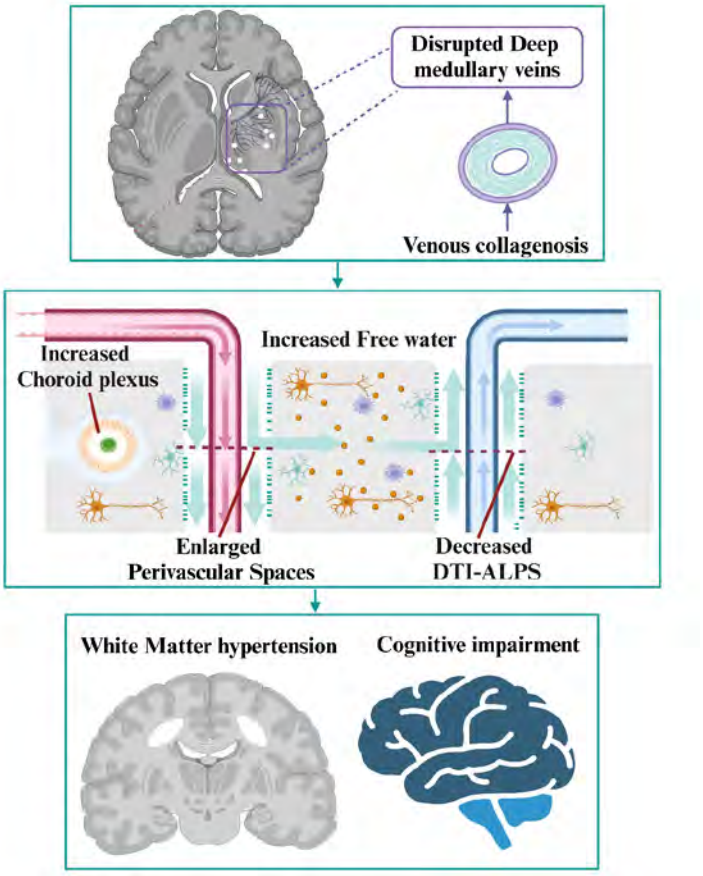

Figure 1. The association between DMV scores, five MRI indices hypothesized as related to glymphatic function (i.e., DTI-ALPS, FW fraction, Cp volumes, BG-PVS volumes, and WM-PVS volumes), WMH burden, and cognition impairment in cerebral small vessel disease. Abbreviations: DTI-ALPS, Diffusion tensor imaging along the perivascular space; FW, free water; Cp, Choroid plexus; BG-PVS, Basal Ganglia Perivascular Space; WM-PVS, White matter Perivascular Space. Created in BioRender. Liao, M. (2024) BioRender.com/u96b162.

Materials and methods

Study population

We consecutively recruited participants with SVD at the Department of Neurology, First Affiliated Hospital of Sun Yat-sen University, between December 2018 and July 2023. Detailed information about the study methodology has been described elsewhere.[5,15] Briefly, participants meeting the following criteria were included: (1) age between 50 and 80 years; and (2) at least two MRI markers of SVD, e.g., the presence of Lacunes, WMH (Fazekas score ≥ 2), the presence of CMBs, or enlarged PVS ≥10.[16] All participants provided written informed consent, and the study was approved by the Human Ethics Committee of the First Affiliated Hospital of Sun Yat-sen University (Approval No: 2018109).

Clinical assessment

Vascular risk factors, including hypertension, diabetes mellitus, hypercholesterolemia, and smoking status were assessed using a standardized questionnaire. Each participant received a cumulative vascular risk scores ranging from 0 to 4, based on the presence of these risk factors, serving as an indicator of their overall vascular risk burden.[17] Cognitive function was assessed using the Beijing version of the Montreal Cognitive Assessment (MoCA).[18] Cognitive assessments were conducted by a trained examiner (W.L.Z.) who was blinded to the imaging results to minimize detection bias.

MRI acquisition

All participants underwent MRI scans on a 3.0T scanner (GE Medical Solutions) equipped with a standard head coil. The imaging sequences included T1-weighted (T1W) imaging with 0.5 mm isotropic voxels, T2-weighted (T2W) imaging with $0.5 \times 0.5 \times 5.5\,mm^3$ voxels, fluid attenuated inversion recovery (FLAIR) imaging with $0.5 \times 0.5 \times 5.5\,mm^3$ voxels, susceptibility-weighted imaging (SWI) with $0.5 \times 0.5 \times 1.0\,mm^3$ voxels, and single-shell diffusion weight image (DWI, 2 volumes with $b = 0\ s/mm^2$, 30 volumes with $b = 900\ s/mm^2$) with $1.0 \times 1.0 \times 2.0\,mm^3$ voxels. Additional details of the MRI acquisition are provided elsewhere.[5,15]

WMH volumetry and other SVD MRI markers

WMH, as the most common and prominent MRI marker of SVD,[1,19] was used as a primary proxy for SVD burden. Specifically, WMH was segmented from FLAIR and T1W images using LST-AI (https://github.com/CompImg/LST-AI), an advanced deep learning-based toolbox.[20] The entire WMH lesion mask was further divided into periventricular (pWMH) and deep (dWMH) regions based on a 12 mm threshold from the ventricles.[21] Gray matter (GM), white matter (WM), and cerebrospinal fluid

(CSF) were segmented using FreeSurfer software. Due to the similar intensities between WMH and GM, the WMH mask was used to correct the GM and WM segmentation. Intracranial volumes (ICV) were determined as the sum of GM, WM, and CSF volumes. The total WMH volumes, as well as the pWMH and dWMH volumes, were normalized to ICV to account for individual head size variations.

Additionally, we performed visual assessment of traditional SVD MRI markers based on the version 2 of the Standards for Reporting Vascular Changes on Neuroimaging (STRIVE-2).[1] WMH was visually rated using Fazekas scale (mild: 0–1 score, moderate: 2 score, severe: 3 score) on FLAIR images.[22] Lacunes were identified on T1W and FLAIR images, while CMBs were identified on SWI images.

Assessment of DMV disruptions

Following established methods, DMV from the level of the ventricles above the basal ganglia to the centrum semi-ovale were evaluated on SWI.[5] A region of interest (ROI) measuring 1 × 4 cm was placed over five consecutive 2 mm-thick axial slices to capture the majority of DMV. DMV disruptions were visually graded by signal appearance: Grade 0 (continuous, homogeneous), Grade 1 (continuous, nonhomogeneous), Grade 2 (discontinuous with spot-like hyperintensity), and Grade 3 (absence of continuous veins) (Figure S1 in the supplementary materials). Scores were averaged per slice and summed across slices (range: 0–15), with higher scores indicating greater disruptions.

Diffusion MRI Preprocessing

Pre-processing steps of diffusion MRI data included removing noise and Gibbs artifacts, correcting head motion, eddy-current–induced and susceptibility-induced distortions (top-up), and adjusting intensity bias. These steps were performed using MRtrix 3.0, FSL (version 6.0.3), and Advanced Normalization Tools (ANTs; version 2.1.0).[23-25] Due to the lack of a b0 image with reversed phase encoding in our DWI scans, the "top-up" was conducted using a synthesized b0 image generated from the T1 image using Synb0-DISCO.[26]

MRI indices related to glymphatic function

According to previous studies,[7,9-12] five MRI indices derived from T1W and diffusion images were calculated to reflect glymphatic function: DTI-ALPS, FW fraction, Cp volumes, BG-PVS volumes and WM-PVS volumes.

The DTI-ALPS was determined by placing four 5-mm spherical ROIs in the projection and association fibers at the level of the lateral ventricles. The index was calculated

as the ratio of x-axis diffusivity to the combined y- axis and z-axis diffusivities in these fibers. More details were provided in the supplementary material.[7, 27]

To calculate the FW fraction, a FW map was generated by applying the FW imaging model to pre-processed diffusion images using a custom MATLAB script.[7,28] The FW represents the unrestricted extracellular water component, which is hypothesized to increase due to multiple pathological processes, including glymphatic dysfunction-induced fluid stagnation, blood–brain barrier (BBB) disruption and neuroinflammation in SVD.[10,29] The mean FW fraction across the white matter, excluding PVS regions, was subsequently calculated using the FW map.

For Cp volumetry, the left and right Cp were segmented from the T1W images using the "Samseg" function in Freesurfer software, followed by visual inspection and manual correction when necessary.[30] The total Cp volumes were then calculated by summing the left and right Cp volumes.

For PVS volumetry, a probability map of PVS was generated from preprocessed T1W images using a deep learning-based model (details in the supplementary material).[31] A threshold of 0.5 was applied to the probability map to produce a binarized PVS mask. This threshold was selected based on previous studies and visual inspection.[7,31] To minimize partial volumes effects arising from CSF and potential confounding effects from WMH, regions of the PVS mask located within 2 mm of the ventricles and within WMH were excluded PVS volumes were subsequently calculated for the white matter and basal ganglia, which were segmented from T1W images using "samseg" function within Freesurfer.[32]

Statistical analysis

Continuous variables were assessed for normality and described using the mean and standard deviation (SD) or the median and interquartile range (IQR), depending on their distribution. Categorical variables were described as count and percentage (n and %).

First, partial Pearson correlation analyses were performed to examine the correlations of DMV scores with the five MRI indices hypothesized as related to glymphatic function (i.e., DTI-ALPS, FW fraction, Cp volumes, BG-PVS volumes, and WM-PVS volumes), adjusting for age, sex, and vascular risk factors.

Second, to assess the effects of DMV disruptions on radiological severity in SVD, linear regression analyses were conducted with total WMH volumes as the dependent

variable and DMV scores as the independent variable. Two different adjustment models were employed: Model 1 included age, sex, and vascular risk factors, while Model 2 included adjustments from Model 1 and the five MRI indices hypothesized as related to glymphatic function. The same analyses were repeated for pWMH and dWMH volumes to explore potential location dependent effects of WMH.

Similarly, to assess the effects of DMV disruptions on clinical severity in SVD, linear regression analyses were conducted performed with MoCA scores as the dependent variable and DMV scores as the independent variable. Model 1 adjusted for age, sex, vascular risk factors, and education level, while Model 2 additionally included the five MRI indices hypothesized as related to glymphatic function.

Lastly, parallel mediation analyses were performed to determine whether glymphatic dysfunction mediated the associations between DMV disruptions and both radiological and clinical severity in SVD. Parallel mediation models were performed using the "bruceR" package (PROCESS function) in R, with 1000 bootstrapping samples to determine the 95% confidence interval (CI) and statistical significance. The five MRI indices were included as mediators in the model, with DMV scores as the independent variable and WMH volumes (total, periventricular, and deep) or MoCA scores as the outcome variables. Adjustments included age, sex, vascular risk factors, and education level (only for MoCA scores). The parallel mediation model was selected due to its ability to account for inter-correlations among the mediators.[33]

For all linear regression models, multicollinearity was assessed with variance inflation factors (VIFs), where values over 5 indicate significant multicollinearity.[34] Outliers were excluded if their Cook's distance exceeded four times the group mean to minimize outlier bias.[35]

All statistical analyses were conducted using R software (version 4.1.0), with a two-tailed significance level of $\alpha = 0.05$. To account for multiple comparisons, Bonferroni correction was applied.

Results

A total of 133 participants were included in the study, with a median age of 64 years (IQR, 54.5–69.0) and 68.4% were male. The median WMH volumes were 12.64 mL (IQR, 2.86–31.25), and the median MoCA scores were 23.0 (IQR, 20.0-25.0). More details are presented in Table 1.

Table 1. Baseline demographic, vascular risk factors, and imaging characteristics of the SVD patient.

	All Participants (n=133)
Demographic	
Male, n (%)	91(68.4%)
Age, years, median (IQR)	64(54.5, 69.0)
Education, high school or higher, n (%)	55(41.4%)
Vascular risk factors	
Hypertension, n (%)	90(67.7%)
Hyperlipidaemia, n (%)	10(7.5%)
Diabetes mellitus, n (%)	42(31.6%)
Smoking history, n (%)	76(57.1%)
Vascular risk factor scores, median (IQR)	2(1, 2)
SVD MRI markers	
Total WMH volumes, ml, median (IQR)	12.64(2.86, 31.25)
Deep WMH volumes, median (IQR)	2.91(1.23, 7.34)
Periventricular WMH volumes, median (IQR)	8.84(1.42, 22.67)
Lacunes≥1, n (%)	122(91.7%)
Cerebral microbleed≥1, n (%)	74(55.6%)
ICV, ml, mean (SD)	1427.2(138.5)
MRI indices of glymphatic function	
DMV scores, median (IQR)	7.0(5.0, 9.50)
DTI-ALPS, mean (SD)	1.38(0.19)
FW fraction, median (IQR)	0.20(0.18, 0.24)
Cp volumes, median (IQR)	1.38(0.99, 1.98)
BG-PVS volumes, ml, median (IQR)	0.60(0.44, 0.84)
WM-PVS volumes, ml, median (IQR)	0.77(0.50, 1.14)
MoCA, median (IQR)	23(20, 25)

WMH, White Matter Hyperintensity; ICV, Intracranial volumes; DMV, deep medullary veins; DTI-ALPS, Diffusion tensor imaging along the perivascular space; FW, free water; Cp, Choroid plexus; BG-PVS, Basal Ganglia Perivascular Space; WM-PVS, White matter Perivascular Space; MoCA, Montreal cognitive assessment scores.

Correlation between DMV disruptions and MRI indices related to glymphatic function

Partial correlation analyses showed that higher DMV scores correlated with lower DTI-ALPS ($r = -0.52$, p-corrected < 0.001), higher FW fraction ($r = 0.29$, p-corrected < 0.001), higher Cp volumes ($r = 0.43$, p-corrected < 0.001), higher BG-PVS volumes ($r = 0.40$, p-corrected < 0.001), and higher WM-PVS volumes ($r = 0.44$, p-corrected < 0.001), while adjusting for age, sex and vascular risk factors (Figure 2).

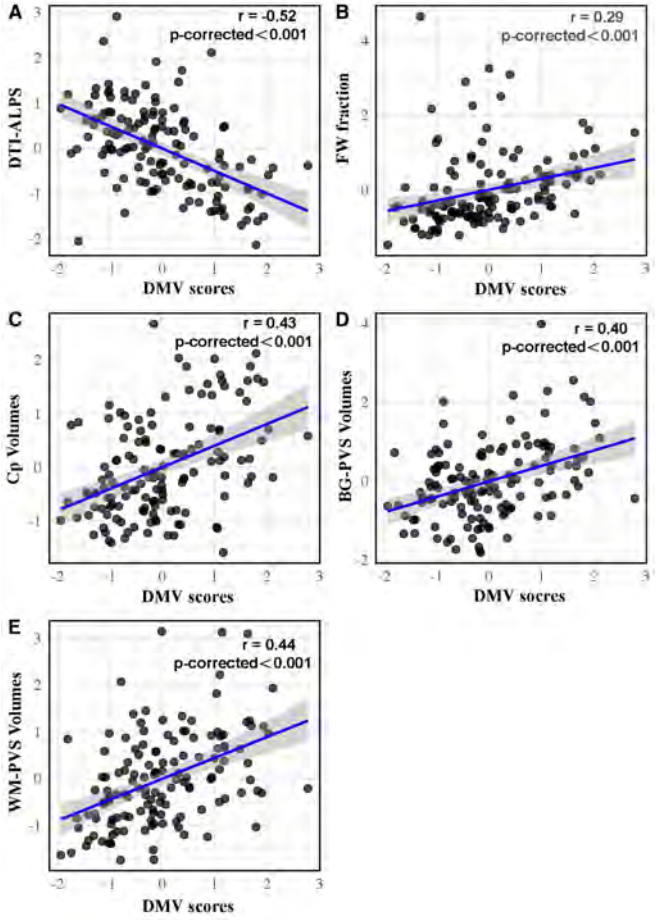

Figure 2. Correlations between DMV scores and five MRI indices in cerebral small vessel disease (SVD) based on partial Pearson correlation tests. Blue lines depict partial correlation with 95% confidence intervals (shaded areas). Abbreviations: DMV, Deep medullary veins; DTI-ALPS, Diffusion tensor imaging along the perivascular space; FW, Free Water; Cp, Choroid plexus; BG-PVS, Basal Ganglia Perivascular Space; WM-PVS, White Matter Perivascular Space. P-values presented in bold with asterisks (*) indicate statistical significance. P-corrected, p values corrected for multiple comparisons using Bonferroni method.

Associations between DMV disruptions and SVD burden

Linear regression analyses showed that higher DMV scores were associated with higher total WMH volumes (β = 0.55, p < 0.001), while adjusting for age, sex and vascular risk factors. For the sub-group analyses in pWMH and dWMH, higher DMV scores were associated with both higher volumes in pWMH (β = 0.54, p-corrected < 0.001) and dWMH (β = 0.38, p-corrected < 0.001) in Model 1. These associations remained unchanged after additionally adjusting for these MRI indices hypothesized as related to glymphatic function in Model 2 (Table 2).

Table 2. Associations between the DMV scores and WMH volumes

	Total WMH volumes		pWMH volumes		dWMH volumes	
	β	p	β	p-corrected	β	p-corrected
Model 1	0.55	**<0.001***	0.54	**<0.001***	0.38	**<0.001***
Model 2	0.45	**<0.001***	0.43	**< 0.001***	0.34	**0.002***

Model 1 was adjusted for age, sex, and vascular risk factors. The adjusted R^2 values were 48.0% for total white matter hyperintensity (WMH) volumes, 47.8% for periventricular WMH volumes (pWMH), and 31.3% for deep WMH volumes (dWMH). Model 2, which was additionally adjusted for the five MRI indices hypothesized as related to glymphatic function (i.e., DTI-ALPS, FW fraction, Cp volumes, BG-PVS volumes, and WM-PVS volumes), showed adjusted R^2 values of 60.0% for total WMH volumes, 63.4% for pWMH volumes, and 22.2% for dWMH volumes. P-values presented in bold with asterisks (*) indicate statistical significance. P-corrected, p values corrected for multiple comparisons using Bonferroni method. Abbreviations: DTI-ALPS, Diffusion tensor imaging along the perivascular space; FW, free water; Cp, Choroid plexus; BG-PVS, Basal Ganglia Perivascular Space; WM-PVS, White matter Perivascular Space.

Associations between DMV disruptions and cognition

Linear regression analyses showed that higher DMV scores were associated with lower MoCA scores (β = -0.24, p = 0.003), while adjusting for age, sex, vascular risk factors and education levels in Model 1. After additionally adjusting for the five MRI indices hypothesized as related to glymphatic function in Model 2, the association between DMV scores and MoCA scores became non-significant (β = -0.18, p = 0.100) (Table 3).

Table 3. Cross-sectional association between the DMV scores and MoCA scores

	Model 1		Model 2	
	β	P	β	p
DMV scores	-0.24	**0.003***	-0.18	0.100
Age	-0.19	**0.022***	-0.27	**0.005***
Sex	0.30	0.108	0.24	0.202
Vascular risk factor	-0.13	0.134	-0.14	0.103
Education	0.21	**0.012***	0.22	0.011
DTI-ALPS	-	-	0.07	0.515
FW fraction	-	-	0.06	0.491
Cp volumes	-	-	0.04	0.706
BG-PVS volumes	-	-	-0.25	**0.012***
WM-PVS volumes	-	-	0.09	0.368

Model 1 (R^2 adjusted = 15.9%) was adjusted for age, sex, vascular risk factors, and education level, while Model 2 (R^2 adjusted = 17.6%) additionally adjusted for the five MRI indices hypothesized as related to glymphatic function (i.e., DTI-ALPS, FW fraction, Cp volumes, BG-PVS volumes, and WM-PVS volumes). DMV, deep medullary veins; DTI-ALPS, Diffusion tensor imaging along the perivascular space; FW, free water; Cp, Choroid plexus; BG-PVS, Basal Ganglia Perivascular Space; WM-PVS, White matter Perivascular Space. P-values presented in bold with asterisks (*) indicate statistical significance.

Mediation effects of MRI indices linked to glymphatic function on the associations between DMV disruptions, SVD burden, and cognition

Parallel mediation analysis showed significant mediation effects of DTI-ALPS (indirect effects = 0.06, p = 0.015) and BG-PVS volumes (indirect effects = 0.05, p = 0.017) in the associations between DMV scores and total WMH volumes (Figure 3). While other three MRI indices (i.e., FW fraction, Cp volumes and WM-PVS volumes) showed no significant mediation effects (Figure 3). In the sub-group analyses for pWMH and dWMH, the mediation effects of the DTI-ALPS (indirect effects = 0.06, p-corrected = 0.019) and BG-PVS volumes (indirect effects = 0.06, p-corrected = 0.028) remained significant for pWMH volumes, but not for dWMH (Figure S2 in the supplementary material).

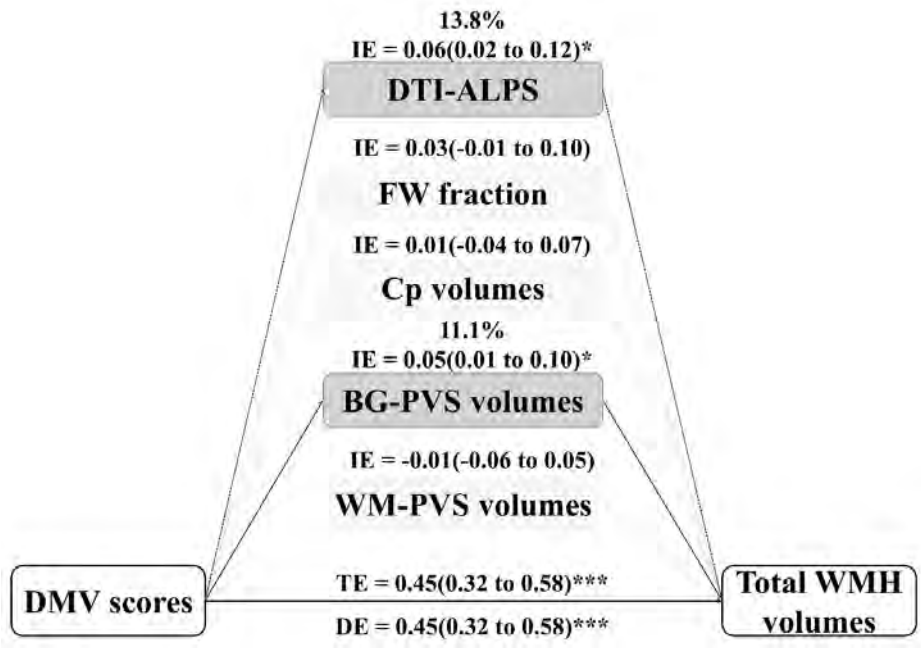

Figure 3. Multiple parallel mediation models illustrating the effects of five MRI indices on the associations between DMV scores and WMH volumes. Models are adjusted for age, sex, and vascular risk factors. Direct effects (DE), indirect effects (IE), and total effects (TE) are shown for whole WMH volumes. Key mediators include diffusion tensor imaging along the perivascular space (DTI-ALPS), free water (FW) fraction, choroid plexus (Cp) volumes, perivascular spaces in basal ganglia (BG-PVS) and white matter (WM-PVS) volumes. Statistical significance is denoted as *p < 0.05, **p < 0.01, ***p < 0.001.

For cognitive impairment, parallel mediation analyses identified BG-PVS volumes (indirect effects = 0.06, p = 0.011) as the only mediator in the associations between DMV scores and MoCA scores (Figure 4).

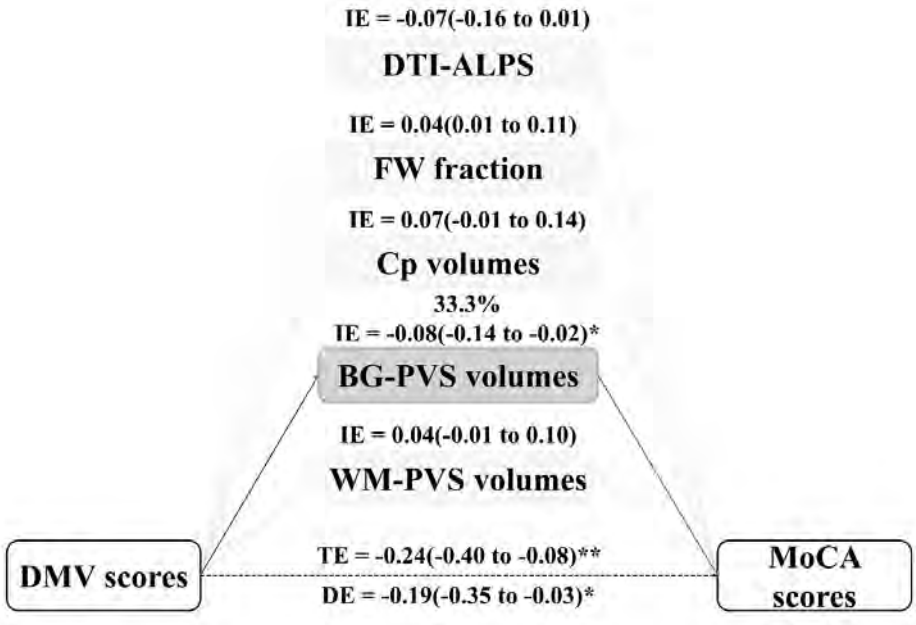

Figure 4. Multiple parallel mediation models illustrating the effects of five MRI indices on the associations between DMV scores and MoCA scores. Models are adjusted for age, sex, vascular risk factors, and education. Direct effects (DE), indirect effects (IE), and total effects (TE) are shown for MoCA scores. Key mediators include diffusion tensor imaging along the perivascular space (DTI-ALPS), free water (FW) fraction, choroid plexus (Cp) volumes, perivascular spaces in basal ganglia (BG-PVS) and white matter (WM-PVS) volumes. Statistical significance is denoted as *p < 0.05, **p < 0.01, ***p < 0.001.

Discussion

In this study, we employed multi-modal neuroimaging approaches and comprehensively assessed the associations between DMV disruptions, multiple MRI indices hypothesized as related to glymphatic function, WMH, and cognitive impairment in SVD. We found that 1) higher DMV scores were significantly correlated with lower DTI-ALPS values, higher FW fraction, higher volumes of Cp, BG-PVS, and WM-PVS; 2) higher DMV scores were associated with higher WMH volumes and lower MoCA scores; 3) DTI-ALPS values and BG-PVS volumes mediated the associations between DMV scores and WMH (particularly periventricular WMH) volumes, with only BG-PVS volumes mediating the associations between DMV scores and MoCA scores. Taken together, our findings suggested that DMV disruptions may contribute to SVD burden and cognitive impairment through these MRI markers indicative of glymphatic dysfunction, particularly the enlargement of BG-PVS.

Our analyses showed that higher DMV scores were correlated with lower DTI-ALPS values, higher FW fraction, higher volumes of Cp, BG-PVS, and WM-PVS. The relations between DMV scores, DTI-ALPS values and BG-PVS volumes align with previous studies.[13,14] Higher DMV scores suggest higher heterogeneity or discontinuity observed on SWI, potentially caused by venous wall thickening, stenosis, or occlusion.[3] These venous abnormalities may reduce venous flow velocity and increase static pulse pressure due to venous insufficiency.[36,37] Additionally, according to the glymphatic system hypothesis, DTI-ALPS measures the diffusivity of CSF outflow in perivenous space surrounding the DMV, thereby reflecting glymphatic system clearance function.[7,11,14] The enlargement of PVS is considered a secondary manifestation of blocked brain drainage pathways.[38] Consequently, it can be speculated that DMV disruption could compromise glymphatic function, appearing as decreased activity of CSF outflow and secondary accumulation of interstitial fluid and metabolic waste products in brain. However, DTI-ALPS validation was initially conducted in non-SVD populations,[9] where diffusion data with high b-values (1000 s/mm^2) are less affected by blood flow signals.[39] In SVD patients with DMV disruptions, reduced venous flow velocity may have a more substantial confounding effect on DTI-ALPS measurements. Additional validation studies are necessary to assess the reliability of DTI-ALPS in assessing glymphatic outflow function in SVD, thereby confirming our findings.

Furthermore, our results expanded these previous findings by showing the correlations between DMV scores, Cp volumes and FW fraction. DMV disruption may induce structural changes in Cp, the primary site of CSF production, likely through changes in CSF dynamics.[40,41] The increase in the FW fraction may result from DMV-disruption-induced obstruction of CSF circulation, compounded by other pathological processes in SVD, such as BBB dysfunction and neuroinflammation.[29] These coexisting pathologies may further impair glymphatic function through exacerbating the accumulation of metabolic waste and inflammatory factors.[6,7,42]

We also found higher DMV scores were associated with higher WMH volumes. Moreover, the association between DMV scores and periventricular WMH volumes were partially mediated by DTI-ALPS and BG-PVS volumes. This aligns with a previous study that showed DTI-ALPS mediates the association between DMV scores and WMH volumes.[14] These venous disruptions may lead to a decline in the drainage capacity of the glymphatic system and the blockage of the perivascular space, thereby contributing to the accumulation of interstitial fluid and metabolic waste and subsequent white matter damages.[11,43,44] Notably, the mediation effects observed in this study were evident only for pWMH volumes,

but not for dWMH, suggesting a potential location-dependent difference in the underlying mechanisms. Pathological studies indicated that the primary changes in dWMH involve demyelination, axonal degeneration, and gliosis, which are generally attributed to vascular ischemia or hypoperfusion.[45,46] In contrast, pWMH changes are characterized by extracellular fluid accumulation and endothelial damages, involving multiple pathological process beyond vascular ischemia, such as venous insufficiency, CSF leakage induced by BBB dysfunction and neuroinflammation.[36,47,48] Furthermore, previous studies have suggested that systemic inflammation is more strongly associated with pWMH than with dWMH.[49, 50] In this context, DMV disruptions-induced glymphatic dysfunction may play a central role in the formation of pWMH but not dWMH. Additionally, the observed differential associations between DMV scores and pWMH versus dWMH might partially result from statistical bias, as pWMH constitutes a larger proportion of total WMH volume, providing greater statistical power compared to dWMH. Further studies with larger sample sizes are needed to validate these findings.

Other MRI indices, including FW fraction, Cp volumes and WM-PVS volumes, did not mediate the associations between DMV scores and WMH volumes, either in the periventricular or deep white matter. This finding contrasts with previous study showing that an increased FW fraction mediated the association between DMV scores and white matter integrity.[6] This inconsistency could be explained by the inclusion of multiple mediators in our study, which accounts for inter-correlations between these MRI indices. Thus, this may suggest that FW changes and other measures (i.e., Cp volumes and WM-PVS volumes) are not directly or predominantly affected by DMV disruptions.

Finally, we found that higher DMV scores were associated with lower MoCA scores, with a partially mediating effect of BG-PVS volumes in this association. Several studies have reported the associations between DMV disruptions and cognitive impairment in SVD.[5,49,50] Our finding further underscored the role of the enlargement of BG-PVS volumes in linking DMV disruptions and cognitive impairment. Previous study also suggested a time-lagged association between changes in DTI-ALPS values and BG-PVS volumes.[7] Specifically, increases in BG-PVS volumes occur after the decreases in DTI-ALPS values. Thus, the presence of enlarged BG-PVS may indicate advanced stages of glymphatic dysfunction, where accumulated effects could lead to clinical deficits. However, the contribution of BG-PVS to cognitive impairment remains debated. While some studies have reported associations between higher BG-PVS volumes/counts and cognitive impairment,[13,51] others have not.[7] It is noteworthy that the inclusion of patients with medium-to-

severe SVD (with at least two SVD MRI markers) and the high resolution (0.5 mm isotropic voxels) of images used for PVS segmentation in the present study may explain these inconsistencies. Future studies with longitudinal designs and high-resolution imaging are needed to validate our findings.

The strength of this study relied on the inclusion of comprehensive MRI indices previously hypothesized as related to glymphatic function and the application of parallel mediation models. However, serval limitations that should be acknowledged. First, the cross-sectional design limits causal inferences, and longitudinal studies are required to clarify the temporal relationships between DMV disruptions, these MRI indices, WMH burden, and cognitive impairment. Second, although these MRI indices, especially the DTI-ALPS index, have been widely used in prior studies.[7,9-12] and correlated with glymphatic clearance rates measured via invasive MRI with intrathecal gadolinium, they lack robust validation, they lack fully convinced validations. Consequently, these MRI indices could consider indirect and approximate measure of glymphatic function.[7,9,52] Future study should prioritize using more accurate glymphatic assessment tools, such as MRI with intrathecal gadolinium, to validate these findings. Third, the semi-quantitative DMV scores may not fully capture DMV disruptions, and the automatic segmentation of the whole Cp volumes may oversimplify its structure and miss crucial details.[53] Quantitative volumetric or morphological analyses of DMV and detailed assessments of Cp subregions in future studies could help further clarify their effects in SVD.

In conclusion, this study showed that DMV disruptions significantly related with these MRI markers hypothesized as related to glymphatic function and are also independently associated with WMH volumes and cognitive impairment in patients with SVD. These findings highlight the crucial role of glymphatic dysfunction, particularly reflected by increased BG-PVS volumes, in linking DMV disruptions, radiological severity and cognitive impairment in SVD. However, future studies employing fully validated measures of glymphatic function and longitudinal follow-up are essential to confirm our findings and elucidate the temporal and causal relationships among these variables.

Supplementary

Methods

DTI-ALPS calculation

The DTI-ALPS was calculated using a semi-automated method in participants with SVD.[9] Four spherical regions of interest (ROIs), each with a 5 mm diameter, were placed in bilateral projection and association fibers at the lateral ventricular body level, using the ICBM-DTI-81 white matter atlas as a reference.[27] These ROIs were registered to each participant's diffusion images via the 'fnirt' function in FSL, with the alignment of the ROIs visually verified for accuracy. The DTI-ALPS was then computed as the ratio of the average x-axis diffusivity values in the projection fibers (Dxproj) and association fibers (Dxassoc), to the combined mean of the y-axis diffusivity in the projection fibers (Dyproj) and the z-axis diffusivity in the association fibers (Dzassoc). The formula used for the calculation was as follows: DTI-ALPS = mean (Dxproj + Dxassoc) / mean (Dyproj + Dzassoc).[7]

PVS Segmentation

Before calculating the PVS probability map, T1W images were preprocessed using FreeSurfer and ANTs software.[31] Specifically, skull stripping was performed using the "SynthStrip" function in FreeSurfer,[54] followed by N4 bias field correction to address intensity inhomogeneities caused by uneven magnetic field distribution.[25] Voxel intensities within each T1W image were then rescaled between 0 and 1, with the 99th percentile of each image's data serving as the upper limit, and values exceeding this threshold set to 1. A fixed bounding box (160 × 214 × 176 voxels) was applied to each subject's T1W image to remove the neck and background signals and to reduce computational load. Finally, the "samseg" function within FreeSurfer was used for tissue segmentation, generating the masks of the ventricles, basal ganglia, and white matter.[32]

Results

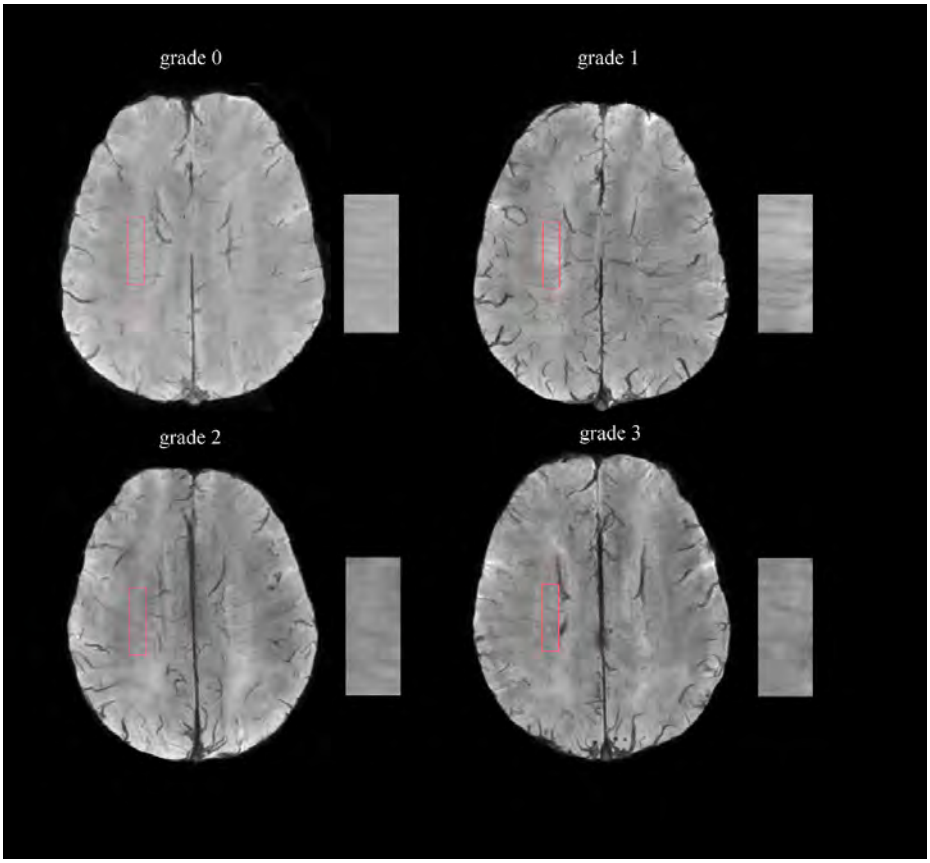

Figure S1. A visual grading scores for deep medullary veins (DMV). Grade 0, each vein was continuous and had a homogeneous signal; Grade 1, each vein was continuous; however, one or more veins had an inhomogeneous signal; Grade 2, one or more than one vein was not continuous, presenting with spot-like hyperintensity; Grade 3, no observed vein was found to be continuous.

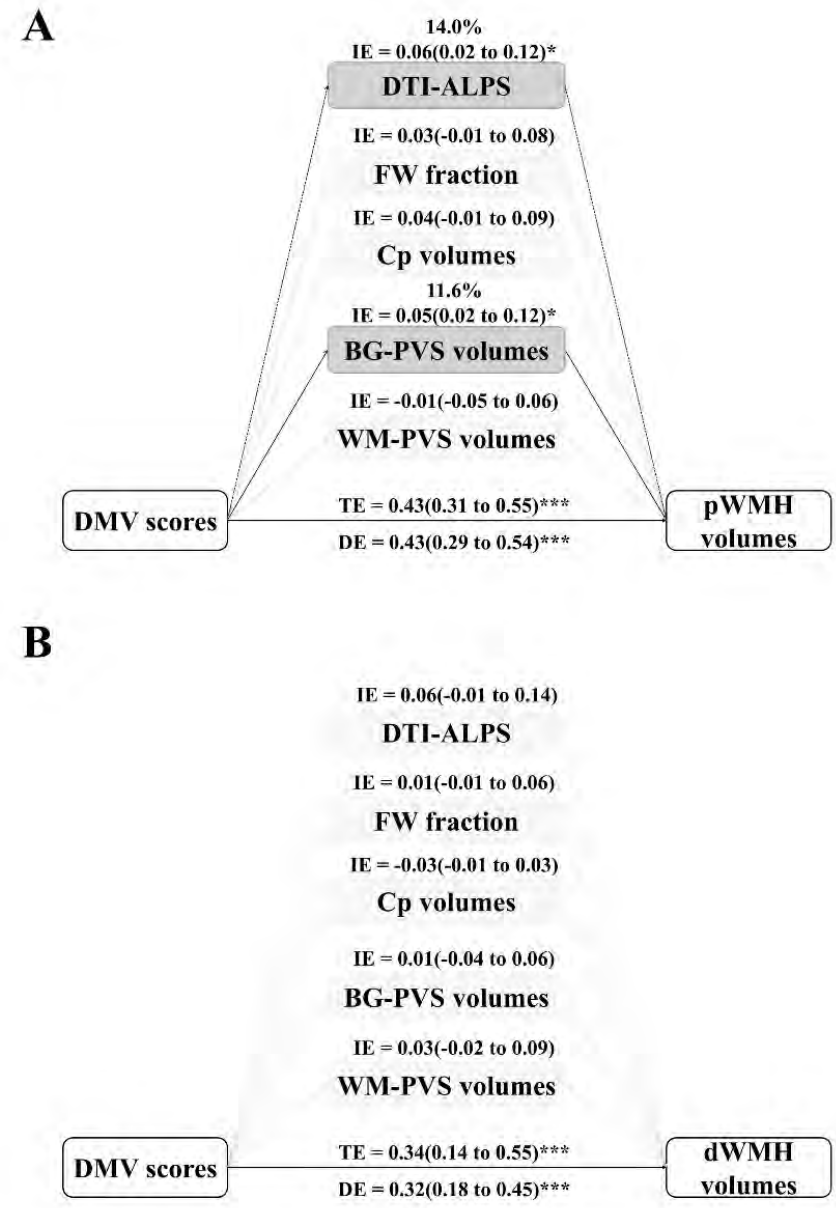

Figure S2. Multiple parallel mediation models illustrating the effects of five MRI indices on the associations between DMV scores and subgroup analyses for periventricular WMH (pWMH) and deep WMH (dWMH) volumes. Models are adjusted for age, sex, and vascular risk factors. Direct effects (DE), indirect effects (IE), and total effects (TE) are displayed for pWMH volumes (A) and dWMH volumes (B). Key mediators include diffusion tensor imaging along the perivascular space (DTI-ALPS), free water (FW) fraction, choroid plexus (Cp) volumes, perivascular spaces in basal ganglia (BG-PVS) and white matter (WM-PVS) volumes. Statistical significance is indicated as *p < 0.05, **p < 0.01, ***p < 0.001.

Reference

1. Duering M, et al. Neuroimaging standards for research into small vessel disease-advances since 2013. Lancet Neurol. Jul 2023;22(7):602-618. doi:10.1016/s1474-4422(23)00131-x
2. Fulop GA, Tarantini S, Yabluchanskiy A, Molnar A, Prodan CI, Kiss T, Csipo T, Lipecz A, Balasubramanian P, Farkas E, Toth P, Sorond F, Csiszar A, Ungvari Z. Role of age-related alterations of the cerebral venous circulation in the pathogenesis of vascular cognitive impairment. Am J Physiol Heart Circ Physiol. May 1 2019;316(5):H1124-h1140. doi:10.1152/ajpheart.00776.2018
3. Nan D, Cheng Y, Feng L, Zhao M, Ma D, Feng J. Potential Mechanism of Venous System for Leukoaraiosis: From post-mortem to in vivo Research. Neurodegener Dis. 2019;19(3-4):101-108. doi:10.1159/000505157
4. Ao DH, Zhang DD, Zhai FF, Zhang JT, Han F, Li ML, Ni J, Yao M, Zhang SY, Cui LY, Jin ZY, Zhou LX, Zhu YC. Brain deep medullary veins on 3-T MRI in a population-based cohort. J Cereb Blood Flow Metab. Mar 2021;41(3):561-568. doi:10.1177/0271678x20918467
5. Liao M, Wang M, Li H, Li J, Yi M, Lan L, Ouyang F, Shi L, Fan Y. Discontinuity of deep medullary veins in SWI is associated with deep white matter hyperintensity volume and cognitive impairment in cerebral small vessel disease. J Affect Disord. Apr 1 2024;350:600-607. doi:10.1016/j.jad.2024.01.124
6. Zhang R, Huang P, Jiaerken Y, Wang S, Hong H, Luo X, Xu X, Yu X, Li K, Zeng Q, Wu X, Lou M, Zhang M. Venous disruption affects white matter integrity through increased interstitial fluid in cerebral small vessel disease. J Cereb Blood Flow Metab. Jan 2021;41(1):157-165. doi:10.1177/0271678x20904840
7. Li H, Jacob MA, Cai M, Kessels RPC, Norris DG, Duering M, De Leeuw FE, Tuladhar AM. Perivascular Spaces, Diffusivity Along Perivascular Spaces, and Free Water in Cerebral Small Vessel Disease. Neurology. May 2024;102(9):e209306. doi:10.1212/wnl.0000000000209306
8. Xu J, Su Y, Fu J, Shen Y, Dong Q, Cheng X. Glymphatic pathway in sporadic cerebral small vessel diseases: From bench to bedside. Ageing Res Rev. Apr 2023;86:101885. doi:10.1016/j.arr.2023.101885
9. Zhang W, Zhou Y, Wang J, Gong X, Chen Z, Zhang X, Cai J, Chen S, Fang L, Sun J, Lou M. Glymphatic clearance function in patients with cerebral small vessel disease. Neuroimage. Sep 2021;238:118257. doi:10.1016/j.neuroimage.2021.118257
10. Kamagata K, Andica C, Takabayashi K, Saito Y, Taoka T, Nozaki H, Kikuta J, Fujita S, Hagiwara A, Kamiya K, Wada A, Akashi T, Sano K, Nishizawa M, Hori M, Naganawa S, Aoki S. Association of MRI Indices of Glymphatic System With Amyloid Deposition and Cognition in Mild Cognitive Impairment and Alzheimer Disease. Neurology. Dec 12 2022;99(24):e2648-e2660. doi:10.1212/wnl.0000000000201300
11. Tian Y, Cai X, Zhou Y, Jin A, Wang S, Yang Y, Mei L, Jing J, Li S, Meng X, Wei T, Liu T, Wang Y, Pan Y, Wang Y. Impaired glymphatic system as evidenced by low diffusivity along perivascular spaces is associated with cerebral small vessel disease: a population-based study. Stroke Vasc Neurol. Oct 2023;8(5):413-423. doi:10.1136/svn-2022-002191
12. Li Y, Zhou Y, Zhong W, Zhu X, Chen Y, Zhang K, He Y, Luo Z, Ran W, Sun J, Lou M. Choroid Plexus Enlargement Exacerbates White Matter Hyperintensity Growth through Glymphatic Impairment. Ann Neurol. Jul 2023;94(1):182-195. doi:10.1002/ana.26648
13. Zhang K, Zhou Y, Zhang W, Li Q, Sun J, Lou M. MRI-visible perivascular spaces in basal ganglia but not centrum semiovale or hippocampus were related to deep medullary veins changes. J Cereb Blood Flow Metab. Jan 2022;42(1):136-144. doi:10.1177/0271678x211038138

14. Zhang X, Pei X, Shi Y, Yang Y, Bai X, Chen T, Zhao Y, Yang Q, Ye J, Leng X, Yang Q, Bai R, Wang Y, Sui B. Unveiling connections between venous disruption and cerebral small vessel disease using diffusion tensor image analysis along perivascular space (DTI-ALPS): A 7-T MRI study. Int J Stroke. Apr 2025;20(4):497-506. doi:10.1177/17474930241293966

15. Li H, Cui L, Wang M, Liao M, Li JB, Ouyang F, Mei T, Zen H, Fan Y. Apathy is associated with striatal atrophy and cognitive impairment in cerebral small vessel disease. J Affect Disord. May 1 2023;328:39-46. doi:10.1016/j.jad.2023.02.004

16. Wardlaw JM, et al. Neuroimaging standards for research into small vessel disease and its contribution to ageing and neurodegeneration. Lancet Neurol. Aug 2013;12(8):822-38. doi:10.1016/s1474-4422(13)70124-8

17. Putaala J, Haapaniemi E, Kaste M, Tatlisumak T. How does number of risk factors affect prognosis in young patients with ischemic stroke? Stroke. Feb 2012;43(2):356-61. doi:10.1161/strokeaha.111.635276

18. Lu J, Li D, Li F, Zhou A, Wang F, Zuo X, Jia XF, Song H, Jia J. Montreal cognitive assessment in detecting cognitive impairment in Chinese elderly individuals: a population-based study. J Geriatr Psychiatry Neurol. Dec 2011;24(4):184-90. doi:10.1177/0891988711422528

19. Sargurupremraj M, et al. Cerebral small vessel disease genomics and its implications across the lifespan. Nat Commun. Dec 8 2020;11(1):6285. doi:10.1038/s41467-020-19111-2

20. Wiltgen T, McGinnis J, Schlaeger S, Kofler F, Voon C, Berthele A, Bischl D, Grundl L, Will N, Metz M, Schinz D, Sepp D, Prucker P, Schmitz-Koep B, Zimmer C, Menze B, Rueckert D, Hemmer B, Kirschke J, Mühlau M, Wiestler B. LST-AI: A deep learning ensemble for accurate MS lesion segmentation. Neuroimage Clin. 2024;42:103611. doi:10.1016/j.nicl.2024.103611

21. Jiang J, Liu T, Zhu W, Koncz R, Liu H, Lee T, Sachdev PS, Wen W. UBO Detector - A cluster-based, fully automated pipeline for extracting white matter hyperintensities. Neuroimage. Jul 1 2018;174:539-549. doi:10.1016/j.neuroimage.2018.03.050

22. Fazekas F, Chawluk JB, Alavi A, Hurtig HI, Zimmerman RA. MR signal abnormalities at 1.5 T in Alzheimer's dementia and normal aging. AJR Am J Roentgenol. Aug 1987;149(2):351-6. doi:10.2214/ajr.149.2.351

23. Tournier JD, Smith R, Raffelt D, Tabbara R, Dhollander T, Pietsch M, Christiaens D, Jeurissen B, Yeh CH, Connelly A. MRtrix3: A fast, flexible and open software framework for medical image processing and visualisation. Neuroimage. Nov 15 2019;202:116137. doi:10.1016/j.neuroimage.2019.116137

24. Jenkinson M, Beckmann CF, Behrens TE, Woolrich MW, Smith SM. FSL. Neuroimage. Aug 15 2012;62(2):782-90. doi:10.1016/j.neuroimage.2011.09.015

25. Tustison NJ, Avants BB, Cook PA, Zheng Y, Egan A, Yushkevich PA, Gee JC. N4ITK: improved N3 bias correction. IEEE Trans Med Imaging. Jun 2010;29(6):1310-20. doi:10.1109/tmi.2010.2046908

26. Schilling KG, Blaber J, Huo Y, Newton A, Hansen C, Nath V, Shafer AT, Williams O, Resnick SM, Rogers B, Anderson AW, Landman BA. Synthesized b0 for diffusion distortion correction (Synb0-DisCo). Magn Reson Imaging. Dec 2019;64:62-70. doi:10.1016/j.mri.2019.05.008

27. Mori S, Oishi K, Jiang H, Jiang L, Li X, Akhter K, Hua K, Faria AV, Mahmood A, Woods R, Toga AW, Pike GB, Neto PR, Evans A, Zhang J, Huang H, Miller MI, van Zijl P, Mazziotta J. Stereotaxic white matter atlas based on diffusion tensor imaging in an ICBM template. Neuroimage. Apr 1 2008;40(2):570-582. doi:10.1016/j.neuroimage.2007.12.035

28. Pasternak O, Sochen N, Gur Y, Intrator N, Assaf Y. Free water elimination and mapping from diffusion MRI. Magn Reson Med. Sep 2009;62(3):717-30. doi:10.1002/mrm.22055

29. Duering M, Finsterwalder S, Baykara E, Tuladhar AM, Gesierich B, Konieczny MJ, Malik R, Franzmeier N, Ewers M, Jouvent E, Biessels GJ, Schmidt R, de Leeuw FE, Pasternak O, Dichgans M. Free water determines diffusion alterations and clinical status in cerebral small vessel disease. Alzheimers Dement. Jun 2018;14(6):764-774. doi:10.1016/j.jalz.2017.12.007

30. Sederevičius D, Vidal-Piñeiro D, Sørensen Ø, van Leemput K, Iglesias JE, Dalca AV, Greve DN, Fischl B, Bjørnerud A, Walhovd KB, Fjell AM. Reliability and sensitivity of two whole-brain segmentation approaches included in FreeSurfer - ASEG and SAMSEG. Neuroimage. Aug 15 2021;237:118113. doi:10.1016/j.neuroimage.2021.118113

31. Boutinaud P, Tsuchida A, Laurent A, Adonias F, Hanifehlou Z, Nozais V, Verrecchia V, Lampe L, Zhang J, Zhu YC, Tzourio C, Mazoyer B, Joliot M. 3D Segmentation of Perivascular Spaces on T1-Weighted 3 Tesla MR Images With a Convolutional Autoencoder and a U-Shaped Neural Network. Front Neuroinform. 2021;15:641600. doi:10.3389/fninf.2021.641600

32. Puonti O, Iglesias JE, Van Leemput K. Fast and sequence-adaptive whole-brain segmentation using parametric Bayesian modeling. Neuroimage. Dec 2016;143:235-249. doi:10.1016/j.neuroimage.2016.09.011

33. Preacher KJ, Hayes AF. Asymptotic and resampling strategies for assessing and comparing indirect effects in multiple mediator models. Behav Res Methods. Aug 2008;40(3):879-91. doi:10.3758/brm.40.3.879

34. Kim JH. Multicollinearity and misleading statistical results. Korean J Anesthesiol. Dec 2019;72(6):558-569. doi:10.4097/kja.19087

35. Cook RD. Detection of influential observation in linear regression. Technometrics. 1977;19(1):15-18.

36. Lahna D, Schwartz DL, Woltjer R, Black SE, Roese N, Dodge H, Boespflug EL, Keith J, Gao F, Ramirez J, Silbert LC. Venous Collagenosis as Pathogenesis of White Matter Hyperintensity. Ann Neurol. Dec 2022;92(6):992-1000. doi:10.1002/ana.26487

37. Keith J, Gao FQ, Noor R, Kiss A, Balasubramaniam G, Au K, Rogaeva E, Masellis M, Black SE. Collagenosis of the Deep Medullary Veins: An Underrecognized Pathologic Correlate of White Matter Hyperintensities and Periventricular Infarction? J Neuropathol Exp Neurol. Apr 1 2017;76(4):299-312. doi:10.1093/jnen/nlx009

38. Wardlaw JM, Benveniste H, Nedergaard M, Zlokovic BV, Mestre H, Lee H, Doubal FN, Brown R, Ramirez J, MacIntosh BJ, Tannenbaum A, Ballerini L, Rungta RL, Boido D, Sweeney M, Montagne A, Charpak S, Joutel A, Smith KJ, Black SE. Perivascular spaces in the brain: anatomy, physiology and pathology. Nat Rev Neurol. Mar 2020;16(3):137-153. doi:10.1038/s41582-020-0312-z

39. Szubert-Franczak AE, Naduk-Ostrowska M, Pasicz K, Podgórska J, Skrzyński W, Cieszanowski A. Intravoxel incoherent motion magnetic resonance imaging: basic principles and clinical applications. Pol J Radiol. 2020;85:e624-e635. doi:10.5114/pjr.2020.101476

40. Jiang D, Liu L, Kong Y, Chen Z, Rosa-Neto P, Chen K, Ren L, Chu M, Wu L. Regional Glymphatic Abnormality in Behavioral Variant Frontotemporal Dementia. Ann Neurol. Sep 2023;94(3):442-456. doi:10.1002/ana.26710

41. Tu Y, Li Z, Xiong F, Gao F. Decreased DTI-ALPS and choroid plexus enlargement in fibromyalgia: a preliminary multimodal MRI study. Neuroradiology. Dec 2023;65(12):1749-1755. doi:10.1007/s00234-023-03240-8

42. Zhou Y, Xue R, Li Y, Ran W, Chen Y, Luo Z, Zhang K, Zhang R, Wang J, Fang M, Chen C, Lou M. Impaired Meningeal Lymphatics and Glymphatic Pathway in Patients with White Matter Hyperintensity. Adv Sci (Weinh). Jul 2024;11(26):e2402059. doi:10.1002/advs.202402059

43. Wang X, Lyu J, Duan Q, Li C, Huang J, Meng Z, Wu X, Chen W, Wang G, Niu Q, Li X, Bian Y, Han D, Guo W, Yang S, Bian X, Lan Y, Wang L, Zhang T, Duan C, Lou X. Deep medullary vein damage

correlates with small vessel disease in small vessel occlusion acute ischemic stroke. Eur Radiol. Sep 2024;34(9):6026-6035. doi:10.1007/s00330-024-10628-4

44. Sabayan B, Westendorp RGJ. Neurovascular-glymphatic dysfunction and white matter lesions. Geroscience. Aug 2021;43(4):1635-1642. doi:10.1007/s11357-021-00361-x
45. Humphreys CA, Smith C, Wardlaw JM. Correlations in post-mortem imaging-histopathology studies of sporadic human cerebral small vessel disease: A systematic review. Neuropathol Appl Neurobiol. Dec 2021;47(7):910-930. doi:10.1111/nan.12737
46. Gouw AA, Seewann A, van der Flier WM, Barkhof F, Rozemuller AM, Scheltens P, Geurts JJ. Heterogeneity of small vessel disease: a systematic review of MRI and histopathology correlations. J Neurol Neurosurg Psychiatry. Feb 2011;82(2):126-35. doi:10.1136/jnnp.2009.204685
47. Cai J, Sun J, Chen H, Chen Y, Zhou Y, Lou M, Yu R. Different mechanisms in periventricular and deep white matter hyperintensities in old subjects. Front Aging Neurosci. 2022;14:940538. doi:10.3389/fnagi.2022.940538
48. Black S, Gao F, Bilbao J. Understanding white matter disease: imaging-pathological correlations in vascular cognitive impairment. Stroke. Mar 2009;40(3 Suppl):S48-52. doi:10.1161/strokeaha.108.537704
49. Chen X, Luo Y, Zhang S, Yang X, Dong Z, Wang Y, Wu D. Deep medullary veins: a promising neuroimaging marker for mild cognitive impairment in outpatients. BMC Neurol. Jan 5 2023;23(1):3. doi:10.1186/s12883-022-03037-x
50. Xu Z, Li F, Xing D, Song H, Chen J, Duan Y, Yang B. A Novel Imaging Biomarker for Cerebral Small Vessel Disease Associated With Cognitive Impairment: The Deep-Medullary-Veins Score. Front Aging Neurosci. 2021;13:720481. doi:10.3389/fnagi.2021.720481
51. Ding J, Sigurðsson S, Jónsson PV, Eiriksdottir G, Charidimou A, Lopez OL, van Buchem MA, Guðnason V, Launer LJ. Large Perivascular Spaces Visible on Magnetic Resonance Imaging, Cerebral Small Vessel Disease Progression, and Risk of Dementia: The Age, Gene/Environment Susceptibility-Reykjavik Study. JAMA Neurol. Sep 1 2017;74(9):1105-1112. doi:10.1001/jamaneurol.2017.1397
52. Taoka T, Masutani Y, Kawai H, Nakane T, Matsuoka K, Yasuno F, Kishimoto T, Naganawa S. Evaluation of glymphatic system activity with the diffusion MR technique: diffusion tensor image analysis along the perivascular space (DTI-ALPS) in Alzheimer's disease cases. Jpn J Radiol. Apr 2017;35(4):172-178. doi:10.1007/s11604-017-0617-z
53. Lizano P, Lutz O, Ling G, Lee AM, Eum S, Bishop JR, Kelly S, Pasternak O, Clementz B, Pearlson G, Sweeney JA, Gershon E, Tamminga C, Keshavan M. Association of Choroid Plexus Enlargement With Cognitive, Inflammatory, and Structural Phenotypes Across the Psychosis Spectrum. Am J Psychiatry. Jul 1 2019;176(7):564-572. doi:10.1176/appi.ajp.2019.18070825
54. Hoopes A, Mora JS, Dalca AV, Fischl B, Hoffmann M. SynthStrip: skull-stripping for any brain image. Neuroimage. Oct 15 2022;260:119474. doi:10.1016/j.neuroimage.2022.119474.

Part VI.

General discussion

Chapter 9.

Summary

Part I | Introduction

Cerebral small vessel disease (SVD) affects the small vessels in the brain and is the leading cause of vascular cognitive impairment and dementia. Currently, SVD is mainly assessed using a spectrum of neuroimaging markers, including white matter hyperintensities (WMH), lacunes, and cortical microbleeds. Patients with similar radiological degrees of SVD exhibit significant heterogeneity in clinical manifestations. This discrepancy may result from the fact that traditional MRI markers of SVD reveal the *tip of the iceberg* of the total SVD-caused brain damage, thus failing to fully capture the extent of its association with clinical deficits. Recent advances in quantitative neuroimaging approaches, practically diffusion imaging, offer insights beyond conventional SVD markers, which may enhance our understanding of the mechanisms behind diverse symptoms in SVD. Therefore, in this thesis, I aimed to explore the mechanisms contributing to clinical symptoms, particularly cognitive impairment, in SVD using advanced multimodal neuroimaging techniques. Specifically, I focused on the following three aspects:

1. The strategic effects arising from damage to specific regions.
2. The remote effects resulting from local lesions through secondary neurodegeneration.
3. The dysfunction of brain's waste clean system involving peri-vascular spaces.

Part II | Strategic regions in cerebral small vessel disease

In **Chapter 2**, I assessed the associations between the structural alterations of thalamic subregions and the performances in three cognitive domains (i.e., processing speed, executive function and memory) in SVD. Data were retrieved from the third follow-up (2020) of the Radboud University Nijmegen Diffusion Tensor and Magnetic resonance Cohort (RUN DMC) study, comprising 205 participants with SVD but without thalamic lacunes. Using probabilistic tractography and connectivity-based thalamic segmentation, we delineated six thalamic subregions and quantified their volumes as well as their connectivity (measured by mean diffusivity [MD]) with cortex. We found that higher MD of the thalamic-motor tract was associated with worse processing speed; higher MD of the thalamic-frontal tract was associated with worse executive function and memory, respectively. Mediation analysis showed that MD of thalamocortical tracts mediated the association between corresponding thalamic subregion volumes and

the cognitive performances. These findings suggest that the structural alterations of thalamus are linked to cognitive impairment in SVD, largely depending on the damage pattern of the white matter tracts connecting specific thalamic subregions and cortical regions.

In **Chapter 3**, I investigated the potential inter-relations between cognitive impairment, apathy, and gait dysfunction, with a specific focus on determining whether these clinical features are associated with damage to the meso-cortical and meso-limbic pathways in SVD. I systematically investigated cognitive impairment, apathy and gait dysfunction using comprehensive cognitive test battery including processing speed, executive function, and memory, the Apathy Evaluation Scale (AES), and motor tests, including mean time and step numbers in the Timed Up and Go (TUG) test in 213 participants with sporadic SVD from the third follow-up (2020) of RUN DMC study. I related cognition, apathy and gait dysfunction together by showing close correlations among these measurements for cognition, apathy, and gait in this study sample. Furthermore, using principal component analysis (PCA), I identified a common component for these three symptoms, with higher values indicating worse composite performance in cognition, apathy, and gait. Based on the findings of a common component underlying cognitive impairment, apathy and gait dysfunction in SVD, I speculated that the three symptoms may share a neural basis, potentially involving the brain's dopaminergic system, especially the meso-cortical and meso-limbic pathways. To investigate this, I employed probabilistic tractography and reconstructed five white matter tracts within the meso-cortical pathway and meso-limbic pathway. I found that white matter damage, quantified by the diffusion metric (i.e., free water [FW]), across the four tracts within the meso-cortical pathway were related to cognitive impairment, apathy, gait dysfunction, as well as to the common principal component in our SVD sample. These findings suggested that the three clinical features (cognitive impairment, apathy, and gait dysfunction) of SVD are strongly inter-related and that the damage in meso-cortical pathway could be the common neural basis underlying the three features in SVD.

In **Chapter 4**, I investigated the cholinergic pathway, which may serve, next to the meso-cortical pathway and meso-limbic pathway, as another neural basis for cognitive and motor dysfunction, commonly referred to as motoric cognitive dysfunction, in SVD. Two white matter tracts within the cholinergic cortical pathways and one tract within the cholinergic thalamic pathways were reconstructed using probabilistic tractography. The disruptions in these tracts were quantified with diffusion metrics derived from the neurite orientation dispersion and density imaging (NODDI) model. I found that diffusion metrics (mainly neurite density index

[NDI] and isotropic volume fraction [ISOVF]) in the cholinergic cortical pathways mediated the relationship between these MRI markers of SVD and both cognitive and gait dysfunction. In contrast, the cholinergic thalamic pathways mediated only the relationship between these markers and cognition. These findings suggest that disruption in the cholinergic cortical pathways is central to the pathophysiology underlying the combined performance of cognition and gait, i.e., motoric cognitive dysfunction, in SVD.

Part III | Beyond focal lesion: the remote effects in cerebral small vessel disease

In **Chapter 5**, I hypothesized that WMH may induce structural changes in cortical regions that are remote but connected to subcortical WMH through fibers passing through the lesions, potentially contributing to cognitive deficits in SVD. To test this hypothesis, I conducted probabilistic tractography using WMH as the seed mask to identify cortical regions connected to WMH (termed "WMH-connected cortex") and the tracts linking WMH to the cortex (termed "connecting tracts"). Cortical thickness, quantitative R1, R2*, and susceptibility mapping were employed to determine the macroscopic atrophy and the underlying tissue composition changes, particularly in myelin and iron content, within both WMH-connected and WMH-unconnected cortical regions. MD index was employed to evaluate white matter damage in the connecting tracts. These analyses showed significantly lower values for cortical thickness, R1, R2*, and susceptibility in WMH-connected cortex compared to WMH-unconnected regions, indicating cortical thinning, demyelination, and iron loss. Higher MD values in connecting tracts associated with lower thickness, R1, R2*, and susceptibility values in WMH-connected cortical regions, which in turn were associated with slower processing speed. These findings, together, are indicative of cortical thinning, demyelination and iron loss in the WMH-connected cortical regions, which is most likely through disruption of white matter tracts connecting WMH and cortex and may contribute to processing speed impairment in SVD.

In **Chapter 6**, I focused on cerebral cortical microinfarcts (CMIs), an emerging imaging marker of SVD. We explored the potential remote effects caused by the localized CMI lesions on surrounding cortical and sub-cortical regions, along with the dynamic temporal changes associated with acute CMIs in SVD. Using data from the RUN DMC-Investigating The origin and EvolutioN of cerebral small vessel disease (RUN DMC – InTENse) cohort study, which includes 54 SVD participants undergoing ten monthly MRI scans, I identified acute and chronic CMIs along

with corresponding control regions in these participants. Surrounding cortical regions within the cortex and subcortical regions along white matter tracts were subsequently delineated. Cortical thickness (CT; cortex only), R1, and neurite density index (NDI) were employed to assess structural changes in the expanded regions surrounding the CMI lesion core. Spatially, we found that sub-cortical expansions of chronic CMIs exhibited lower NDI values compared to control regions, with effects extending up to approximately 10mm. Temporally, these analyses showed that acute CMIs displayed lower R1, and higher NDI values compared to control regions, which normalized in follow-up scans. These findings suggested that chronic CMIs are associated with damages of subcortical regions along the WM tracts, but show limited effects on adjacent cortical regions (likely related to partial volume effects). Additionally, the damages at the lesion site caused by acute CMIs are confined to lesion site and tend to be transient.

Part IV | The waste clean system in cerebral small vessel disease

In **Chapter 7**, my investigation was directed toward a highly dynamic waste clearance system in the brain that facilitates efficient elimination of metabolic products from the central nervous system through perivascular channels. I analyzed data from the RUN DMC cohort study, which included 289 SVD participants in 2011, with 220 completing follow-up assessments in 2015. For these participants, I measured three MRI indices hypothesized to be related to waste clean function: basal ganglia perivascular space (BG-PVS) volumes, free water (FW) fraction, and diffusion tensor imaging along the perivascular space (DTI-ALPS). I subsequently tested the dynamic inter-relations between the three MRI indices using a latent change score model and examined their longitudinal associations with changes in other SVD MRI markers and cognitive performance through linear mixed-effects regression models. These analyses suggested that baseline DTI-ALPS was associated with the changes of BG-PVS volumes, but not vice versa, indicating a time-lagged association between decreases in DTI-ALPS values and the enlargement of BG-PVS. Furthermore, baseline measures of the three MRI indices were associated with the changes of traditional SVD MRI markers, including increased WMH volumes, increased lacune numbers and decreased brain volumes. Additionally, DTI-ALPS and FW fraction at baseline were associated with the decline in MMSE score, cognitive index and processing speed over time. These findings suggested that these MRI indices, hypothesized to reflect brain's waste clean function, contributed to SVD progression and associated cognitive decline over time.

In **Chapter 8**, I explored the potential associations between deep medullary veins (DMV) disruptions, waste clearance dysfunction, WMH burden and cognitive impairment in SVD. I used the data from another independent SVD cohort from First Affiliated Hospital of Sun Yat-sen University, Guangzhou, China, with available rating scores of DMV disruption on high quality susceptibility-weighted imaging (SWI) (n=133). Five MRI indices related to waste clearance were measured: DTI-ALPS, FW fraction, choroid plexus (Cp) volumes, BG-PVS volumes and white matter PVS volumes (WM-PVS). Analyses suggested that higher DMV scores, indicative of greater DMV disruption, were correlated with lower DTI-ALPS values, higher FW fraction, higher volumes in Cp, BG-PVS, and WM-PVS. Furthermore, higher DMV scores were linked to increased WMH volumes and reduced MoCA scores. Parallel mediation analyses suggested that DTI-ALPS values and BG-PVS volumes mediated the associations between DMV scores and WMH volumes, with only BG-PVS volumes mediating the associations between DMV scores and MoCA scores. These findings suggested that DMV disruptions contribute to WMH burden and cognitive impairment in SVD. This effect could be mediated by MRI markers indicative of impaired waste clearance, particularly the enlargement of BG-PVS.

Chapter 10.

General discussion

Overview

The general aim of this thesis is to provide insights into the mechanisms contributing to the clinical symptoms, particularly cognitive impairment, in patients with cerebral small vessel disease (SVD). To achieve this, I conducted a series of studies primarily embedded within the Radboud University Nijmegen Diffusion Tensor and Magnetic Resonance Cohort (RUN DMC). I specifically focused on three potential mechanisms that may contribute to SVD-associated symptoms:

- the strategic effects arising from damage to specific regions
- the remote effects caused by localized lesions
- dysfunction of the waste clearance involving perivascular spaces

In this chapter, I provide a general discussion, starting with methodological considerations regarding the study population, internal validity, reproducibility and external validity of our findings. I then discuss our main findings in the context of existing literature and conclude with their clinical relevance and perspectives for future research directions.

Methodological considerations

Study population

This thesis is primarily based on the RUN DMC cohort, an ongoing hospital-based single-centre prospective cohort study initiated in 2006.[1] This cohort study aims to investigate the causes and clinical consequences of sporadic SVD. Patients visiting our outpatient clinic and undergoing routine diagnostic brain imaging for potentially SVD-related symptoms, such as transient ischemic attack and stroke, mood, cognitive or gait complaints, were assessed for eligibility. Those with MRI evidence of cerebral SVD, defined as white matter hyperintensities (WMH) or lacunes, were invited to participate. The main exclusion criteria included dementia, parkinsonism, WMH unrelated to SVD (e.g., multiple sclerosis), or a life expectancy of less than six months. At baseline, 503 participants were included. Follow-up assessments were conducted in 2011, 2015, and 2020. At each time point, participants underwent clinical evaluations of cognition, mood, and motor function, along with MRI scanning.

Internal validity

Internal validity refers to the extent to which the observed effects in a study can be confidently attributed to the variable of interest, rather than to other possible

causes.[2] The internal validity of a study may be compromised by various biases, including selection bias, information bias, as well as by confounding factors.[2]

Selection bias

Selection bias refers to the systematic differences between individuals who are included in a study and those in the target population, potentially leading to inaccurate estimates of exposure-outcome relationships.[3] In cohort studies, such bias can occur at both the initial recruitment stage and during follow-up (attrition bias). For instance, during recruitment, individuals who are willing and able to participate often differ in demographics, disease severity, and socioeconomic status compared to those who do not participate. These differences can influence both the likelihood of participation and the outcomes being measured. Similarly, over the follow-up of a longitudinal study, participant drop-out may be selective, thereby compromising the representativeness of included particpants.[4]

In the RUN DMC cohort, these forms of selection bias were apparent. During initial recruitment, the study achieved a relatively high response rate of 71% among eligible participants. However, non-responders were generally older and showed more severe WMH on pre-inclusion brain scans. These individuals likely experienced greater physical and cognitive impairments, which may have prevented their participation. Consequently, this selective non-response might have led to an underestimation of cognitive impairments and other deficits in the study population, potentially weakening the observed associations between the variables of interest and the clinical symptoms in the study population. Attrition bias emerged as a significant source of selection bias during the long-term follow-up of the RUN DMC cohort study. Over the 14-year period, three follow-up assessments were conducted, with participant numbers declining due to factors such as inability to attend or death. Loss to follow-up increased progressively across the study period, with rates of 20.9% at first follow-up, 31.2% at second follow-up, and 49.5% at third follow-up. Those participants lost to follow-up were generally older and exhibited a more severe SVD burden. Conversely, individuals who remained in the study for the full 14-year period may have experienced relatively slower disease progression. This selective attrition raised concerns about the representativeness of the remaining cohort and potentially resulted in underestimations of observed associations.

To address these concerns, we employed a linear mixed model in **Chapter 7**. This approach is particularly effective for reducing bias associated with missing data in longitudinal studies with multilevel or hierarchical structures.[5] It allows for the inclusion of subjects with missing values at certain time points by accounting for missing data

and considering correlations within and between participants. However, selection bias cannot be fully eliminated in this thesis. The increased accessibility of advanced MRI techniques and the establishment of an imaging research consortium may enable multi-center studies with larger sample sizes, such as Meta VCI Map consortium and VICA (Vascular, Imaging and Cognition Association of China) consortium,[6,7] which could help mitigate this bias to some extent and validate our findings.

Information bias

Information bias refers to a systematic error resulting from inaccurate measurement or misclassification of key study variables, including exposures, outcomes and confounders.[3] This bias arises when data are collected, recorded or interpreted incorrectly, potentially distorting the associations between variables under investigation.

The accuracy of clinical assessments in research heavily depends on the standardized assessment procedures and the reliability of measurement instruments. In our study, the clinical assessments were performed prior the MRI scans, or by trained raters who were blind to their neuroimaging features. This helped minimize interviewer bias. However, participant fatigue during lengthy testing sessions may have influenced performance, particularly in those with more severe SVD. Furthermore, mood status assessments (e.g., apathy and depression) relied solely on self-reported questionnaires. While this approach facilitated implementation in a large cohort, the results could be affected by recall bias, questionnaire misinterpretation or socially desirable answers, especially among individuals with cognitive impairment in SVD. Additionally, practice effects could affect longitudinal cognitive assessments, potentially masking subtle cognitive decline. To mitigate these effects, we employed alternate versions of cognitive tests when available.

Precise measurement of MRI parameters fundamentally depends on accurate image segmentation and registration. In the context of SVD, the presence of WMH poses specific challenges for tissue classification, as these lesions can be misclassified as grey matter due to their similar T1 intensities. To address this issue, I employed WMH masking to improve the accuracy of grey matter/white matter segmentation. Furthermore, the presence of lesions, combined with brain atrophy, can significantly complicate image registration processes. To minimize these potential sources of bias, visual quality control following segmentation and registration was performed.

Another technique in which information bias may play a role is tractography, which was extensively used throughout this thesis. We employed two common

probabilistic tractography approaches: FSL's bedpostX/probtrackx pipeline (**Chapters 2-5**), which uses a Bayesian framework to estimate multiple fibber orientations and tract fibers by repeated sampling,[8,9] and MRtrix3's constrained spherical deconvolution (**CSD**) algorithm (Chapter 6), which generates fiber orientation distributions for probabilistic streamline propagation.[10,11] While these probabilistic approaches, particularly when combined with multi-shell diffusion data, can account for multiple fiber orientations, there are still several limitations.[12] The most fundamental limitation is voxel size: an average axon is approximately 1 µm in diameter,[13] whereas a typical isotropic diffusion MRI voxel measures about 1.5 mm. This substantial difference in scale makes it difficult to resolve complex fiber patterns in smaller, deeper bundles and at grey matter/white matter junctions, where crossing, kissing, or bending fibers often coexist within a single voxel. Additionally, this approach is originally developed in healthy brains; therefore, their application in SVD requires additional consideration. Specifically, the extensive white matter damage can impact fiber orientation reconstruction, potentially affecting the accuracy of tractography.[14] Nevertheless, current tractography methods are generally effective at determining the primary diffusion direction of major white matter tracts. In this thesis, we have employed a combination of advanced tractography techniques and rigorous visual inspection to ensure the accurate reconstruction of key pathways like thalamic projections, dopaminergic mesocortical and mesolimbic pathways, and cholinergic pathways.

A further consideration involves partial volume effects (PVE), which arise when voxels contain multiple tissue types, such as grey matter, white matter, cerebrospinal fluid, lesions, or normal tissues.[15] These effects can result in inaccurate estimations of MRI parameters, particularly diffusion metrics. PVE could be more pronounced in the presences of tissue atrophy or in some small size lesions (such as cerebral cortical micro-infarcts) in SVD. To mitigate PVEs, I employed several strategies throughout this thesis. For example, in **Chapter 5**, I employed the surface-based analysis pipeline to reconstruct the grey matter–white matter boundary and the pial surface, thereby enhancing the robustness of parameter estimates at tissue borders. In addition, certain MRI parameters (e.g., Fractional Anisotropy [FA], R2*) typically fall within certain tissue-specific ranges, allowing us to minimize PVEs by applying appropriate thresholds. For instance, within the Tract-Based Spatial Statistics (TBSS) pipeline, an FA threshold of >0.2 is generally used to exclude non-white matter voxels. Similarly, I used an R2* threshold of 5–30 s^{-1} to include voxels more representative of grey matter while excluding white matter and CSF.[16,17] Furthermore, suboptimal image processing (e.g., imprecise image registration or the use of over-large smooth kernels that reduce image resolution) can further

exacerbate PVEs. Consequently, I employed robust registration algorithms, avoided repeated image registrations, and carefully selected appropriate smoothing kernels. Yet, it is important to acknowledge that these methods reduce but cannot eliminate PVEs. When interpreting findings, especially for some small effects observed in localized regions, the confounding effects arising from PVEs should be considered. Future studies using higher-field MRI (e.g., 7T) with superior spatial resolution may further minimizing PVEs.

In addition, the interpretation of diffusion MRI metrics requires careful consideration of model assumptions. The diffusion tensor imaging (DTI) model is widely used to assess the microstructural integrity of white matter. This model assumes Gaussian diffusion of water molecules at a microscopic scale.[18] While this assumption may be valid in regions with homogeneous, parallel white matter tracts, most brain regions exhibit complex white matter architecture where water diffusion is non-Gaussian. Consequently, interpretation of DTI-derived metrics, such as fractional anisotropy (FA) and mean diffusivity (MD), in these regions and their pathological relevance could be affected. For instance, although high FA typically indicates better white matter integrity, regions with crossing fibers in normal white matter can present inherently low FA values. Furthermore, FA values may increase if part of the crossing fibers is damaged. By contrast, MD is less influenced by crossing fibres.[19] Thus, throughout this thesis, MD is preferentially used over FA to reduce this source of bias. In addition, as an extension of the DTI model, the free water imaging model employs a two-compartment approach to differentiate signals from free water (FW) and tissue compartments, providing a more detailed characterization of subtle changes in brain microstructure in SVD.[20,21] Neurite Orientation Dispersion and Density Imaging (NODDI), another advanced model based on multi-shell diffusion data, estimates three key aspects of neural tissue at each voxel: neurite density index (NDI), orientation dispersion index (ODI), and the free water fraction (FWF).[22] NODDI further enhances sensitivity to subtle neuronal damage and allows for the quantification of distinct microstructural components.[22] However, it relies on fixed diffusivity and tortuosity assumptions that may not hold under certain pathological conditions, particularly during the acute phase of tissue ischemia.[23] For example, in acute CMI, neuronal swelling due to cytotoxic edema may instead lead to the increase of NDI (**Chapter 6**).

Confounding

Confounding factors pose significant challenges in SVD research due to the complex interplay between vascular risk factors, aging, and disease progression. In particular, age and vascular risk factors are major confounders because they are strongly associated with the determinant (SVD progression) and the outcome

(cognitive decline). When examining specific outcomes, we carefully considered corresponding confounders, for example, education years were controlled for in analyses with cognitive performance as the outcome, and depression levels were adjusted for in the assessment of apathy. Additional potential confounders include concurrent pathologies such as Alzheimer's disease and Parkinson's disease. We addressed these confounding effects by excluding participants with concurrent pathologies when appropriate. Nevertheless, residual confounding cannot be entirely ruled out, especially when related to unmeasured variables or imperfectly measured confounders.

Reproducibility and External Validation

Reproducibility refers to the ability to obtain consistent results under similar conditions as those were set on the original study.[24] Several critical factors may complicate reproducibility in neuroimaging research. The famous "dead salmon" study highlighted the issue of multiple comparisons correction, demonstrating how apparent brain activity could be detected in a deceased fish when proper statistical corrections were not applied.[25] Throughout this thesis, I carefully selected statistical approaches and applied corrections for multiple comparisons whenever necessary to minimize the risk of false-positive findings. Sample size present another significant factor. One study suggested that brain-wide association studies (BWAS) linking neuroimaging features with behavioral phenotypes require large sample sizes, potentially over 3000 participants, to achieve reproducible results.[26] Although the study was conducted on healthy population, its conclusions about the need for large sample sizes in BWAS hold significance for studies involving patients. I primarily used data from the RUN DMC cohort, which included 503 participants at baseline and underwent three follow-up assessments over 14 years. The longitudinal design of this cohort, combined with the inclusion of well-characterized SVD participants, could significantly improve replicability.[27] Furthermore, the establishment of imaging research consortia, such as the Meta VCI Map consortium and VICA (Vascular, Imaging and Cognition Association of China),[6,7] could facilitate multicenter studies with larger sample sizes, potentially improving the reproducibility of SVD imaging findings.

External validity refers to the extent to which study results can be generalized to populations beyond the original study sample.[2] The key determinant of generalizability is the representativeness of the study sample relative to the target population.[28] This thesis primarily analyzed data from the RUN DMC cohort, a single-center, hospital-based study. Given its hospital-based design, the sample likely includes individuals with higher SVD burden compared to the general

elderly population. As a result, these findings may have limited generalizability to community-dwelling populations with lower SVD burden. Additionally, baseline recruitment of RUN DMC cohort was conducted in the outpatient clinic and included non-demented participants with a largely preserved cognitive function (mean Mini-Mental State Examination [MMSE] score: 28.1). These participants had lower baseline WMH volumes compared to individuals with severe symptomatic SVD in other cohorts.[29] Furthermore, the 14-year follow-up data suggest that participants who participated during the whole follow-up period likely experienced relatively slow disease progression. Thus, caution is required when extrapolating these findings to individuals with more severe SVD or faster disease progression. Finally, as the cohort is based in the Netherlands and predominantly comprises Caucasian participants, the findings may not be generalizable to other ethnic groups. Replication of these results in diverse SVD populations is essential. An initial effort to address this limitation was presented in **Chapter 8**, which used data from an independent Chinese SVD cohort with higher SVD burden.

Causal Inference

Drawing causal inferences is challenging due to the observational nature of our studies. Most studies in this thesis employ a cross-sectional design, which captures data at a single point in time, making it impossible to determine the temporal sequence or causality. Advanced statistical methods such as mediation analysis may help elucidate causal relationships, but the possibility of reverse causation and limitations in our ability to measure all relevant variables must be acknowledged. For example, in **Chapter 5**, we found that white matter damage in tracts connecting WMH to the cortex is associated with the abnormalities in those connected cortical regions. Additionally, we identified a mediation effect of these cortical abnormalities in the relationship between white matter tract damage and processing speed. However, these associations could work in the opposite direction or be bidirectional. Specifically, white matter damage might not directly cause cortical thinning but instead reflect a downstream effect, as showed in **Chapter 6**. Furthermore, poor processing speed might relate to the system vascular risk factors or neuroinflammation process contributing to both white matter tract damage and cortical thinning.

Compared to cross-sectional analyses, longitudinal studies provide stronger evidence for causal mechanisms. For example, in **Chapter 7**, we found that baseline diffusion tensor imaging along the perivascular space (DTI-ALPS) values were associated with the changes of basal ganglia perivascular space (BG-PVS) volumes over time, but not vice versa. This strongly suggests a directional relationship. However, it still does not fully prove causality due to potential confounding and the possibility of bidirectional

relationships. Therefore, although these findings are highly valuable for generating hypotheses about potential mechanisms and informing further research, future studies employing targeted interventions or advanced causal inference techniques, such as mendelian randomization analysis,[30] are necessary to establish causality.

General discussion

The traditional markers of SVD observed on conventional MRI, such as WMH and lacunes, do not fully explain the complex clinical manifestations of the disease. This disparity may result from the fact that traditional MRI markers of SVD reveal the tip of the iceberg of the total SVD-caused brain damage. In this thesis, I investigated alternative mechanisms that may contribute to clinical deficits in SVD, including strategic effects arising from damage to specific regions, remote effects caused by secondary neurodegeneration from local lesions, and dysfunction of brain's waste clearance.

Strategic lesions in SVD

The thalamus functions as a crucial communication hub in the brain through its extensive connectivity with both cortical and subcortical regions.[31] This widespread connectivity, however, makes the thalamus particularly susceptible to subcortical damage associated with SVD. In **Chapter 2**, I investigated how volume and connectivity of thalamus relate to cognitive performance SVD. The analyses showed that thalamocortical disconnection, rather than thalamic volume loss, was the primary contributor to cognitive impairment in SVD. This finding aligns with other studies showing that WMH accumulation in thalamic-cortical tracts related with reduced processing speed, and that lesions in anterior thalamic radiations contributed to executive dysfunction in SVD.[32,33] Furthermore, by establishing links between disrupted connectivity in specific thalamic subregions and domain-specific cognitive deficits, these findings enhance our understanding of how SVD compromises the complex neuronal networks underlying cognition.[34] Collectively, this evidence supports a brain network perspective of SVD pathophysiology.[35] Localized SVD lesions disconnect specific white matter tracts such as the thalamocortical projections, leading to disruption of the white matter network, ultimately leading to cognitive impairment.

Building on this network perspective, the integrity of neurotransmitter systems represents another crucial aspect of interregional communication in brain. Within the context of SVD, damage to specific neurotransmitter pathways that subserve neurotransmitter release and transmission can disrupt these processes, thereby

contributing to a range of clinical manifestations. This thesis highlighted two neurotransmitter pathways: the dopaminergic mesocortical and mesolimbic pathways **(Chapters 3)**, and the cholinergic cortical and thalamic projections **(Chapters 4)**. The dopaminergic pathways are known to modulate cognitive, emotional, and motor functions.[36] **Chapter 3** showed that damages within the meso-cortical pathway were related to cognitive impairment, apathy, gait dysfunction in SVD. These findings complement and extend previous SVD studies, which reported that striatal atrophy or large-scale white matter microstructural damage involving the dopamine reward circuit contributed to apathy.[37] In parallel, white matter microstructural damage within cholinergic pathways, particularly the cortical projections of the nucleus basalis of Meynert (NBM), was associated with both cognitive and gait dysfunction in SVD **(Chapter 4)**. These pathways are implicated in cognitive and motor functions, with their disruption previously reported in other conditions, such as aging, AD, PD and dementia with Lewy bodies.[38-41] WMH volumes could be identified as the primary contributor to white matter integrity damage within the investigated dopaminergic pathways and cholinergic cortical projections..[38,42] These pathways are particularly vulnerable because of the following factors: first, these pathways' extensive distribution and reliance on long-axonal connections make them particularly vulnerable to WMH-related damage, which predominantly affects long-range white matter fibers;[43] second, the anatomical distribution of WMH lesions, occurring primarily in supratentorial regions, spatially corresponds with the trajectory of these projections **(Chapter 4)**. Thirdly, indirect damage through secondary neurodegeneration may occur even when lesions do not directly affect these pathways (as detailed in subsequent sections).

An interesting question concerns the interaction between dopaminergic and cholinergic systems in SVD. In SVD, the sub-cortical lesions might simultaneously affect dopaminergic and cholinergic projections. Additionally, there is a balance and crosstalk between these neuromodulators in the brain. For instance, the thalamus is one region where this interplay is evident: it receives cholinergic innervation from brainstem nuclei and is modulated by dopamine via basal ganglia circuits.[44,45] Consequently, the connectivity between thalamus and cortex could be modulated by the dynamic balance of dopaminergic and cholinergic system. However, it should be acknowledged that these MRI measures (i.e., diffusion abnormalities along the dopaminergic or cholinergic pathway) in this thesis **(Chapters 3 and 4)** do not directly assess dopamine or acetylcholine levels or function. Instead, they only reflect white matter integrity along these pathways that were reconstructed using diffusion-weighted imaging, constrained by anatomical information from relevant circuits. This indirect measurement poses several limitations: the identified

tract may include fibers innervated by other neurotransmitter systems, and the extent of white matter damage may not correlate directly with neurotransmitter function or concentration. Hence, caution is required when relating these tract damages with specific dopaminergic or cholinergic system dysfunction.

Beyond focal lesion: the remote effects in SVD

Another potential mechanism by which SVD causes clinical deficits involves the remote effects of local lesions, often manifested as secondary neurodegeneration along white matter tracts passing through lesions. This hypothesis is supported by multiple lines of evidence. First, many studies have showed a close association between WMH burden and cortical thinning.[46-48] Second, in cases of incident lacunes and subcortical infarcts, regional cortical thinning has been observed specifically in regions connected (via white matter tracts) to the initial lesion, suggesting that these remote cortical changes could be a result of degeneration of the associated white matter tracts.[49,50] **Chapter 5** extends these evidence by showing that cortical regions structurally connected to subcortical WMH lesions exhibit both cortical thinning and lower quantitative MRI parameters (i.e., R1, R2*, and susceptibility values). These changes are consistent with previous studies on cortical thickness.[51] Notably, the parametric MRI findings provide new insights into possible tissue composition changes underlying cortical thinning, including demyelination and iron loss (as interpreted in Box 1), similar to patterns observed in multiple sclerosis.[52-54] Critically, these region-specific cortical changes were associated with both the disruption of white matter tracts connecting WMH lesions to cortex and impaired processing speed in SVD. The specificity of these associations was validated by controlling for changes in WMH-unconnected regions, which represent cortical changes caused by other potential co-existing pathologies. Hence, these findings have highlighted the role of secondary neurodegeneration in WMH-associated cortical changes and its significance in determining cognitive deficits in SVD. A similar process may also extend to cortical lesions, such as cerebral cortical microinfarcts (CMIs) in SVD. **Chapter 6** showed that chronic CMIs were associated with lower neurite density index (NDI, Box 1) values in subcortical white matter tracts up to ~10 mm from the lesion. This finding provides, for the first time to the best our knowledge, *in-vivo* evidence suggesting that chronic CMIs can induce subcortical damage, most likely axonal damage, along white matter tracts passing through the lesion. It, therefore, supports the hypothesis of secondary neurodegeneration as a mechanism underlying the remote effects of cortical lesions, potentially explaining previously reported associations between CMIs, disrupted overall WM connectivity and cognitive impairment.[55] Taken together, these findings reinforce the concept of SVD as a global network-level disorder, where focal lesions initiate widespread

structural disruptions across interconnected brain regions.[56] This process involves both "upstream and downstream" effects along white matter tracts, linking cortical and subcortical damage and amplifying the initial lesions' effects. When integrated with the findings in previous section, it can be hypothesized that even when SVD lesions do not directly affect strategic regions or pathways, these areas may still be impacted through remote effects.

The waste clearance system in SVD

Lastly, dysfunction of the brain's waste clearance system may represent another crucial mechanism in SVD. This waste clearance system is hypothesized to be a brain-wide network of perivascular channels that allows cerebrospinal fluid (CSF) to flush out interstitial waste products from the brain tissue.[57] Given SVD's inherent pathologies in small arterioles, capillaries, and venules, it is plausible that these vascular abnormalities compromise perivascular fluid drainage.[58] Leveraging emerging MRI measures of this waste clearance system (as detailed in Box 1), **Chapter 7** provides longitudinal evidence (mean follow-up time: 3.4 years) that such dysfunction may drive SVD progression. Specifically, higher volumes of perivascular space in the basal ganglia (BG-PVS), higher free water (FW) fraction and lower diffusion tensor image analysis along the perivascular space (DTI-ALPS) values at baseline were related to progression of SVD burden (mainly WMH volumes, lacune count and brain atrophy). Moreover, reduced DTI-ALPS at baseline were linked to subsequent declines in cognitive performance over time. These findings in line with previous cross-sectional studies,[21,59-61] supporting impaired perivascular fluid drainage as an early contributing mechanism for SVD progression and cognitive decline. In addition, deep medullary veins (DMV) play a crucial role in white matter drainage, and accumulated evidence suggests that venous pathologies are significantly implicated in SVD.[62,63] DMV dysfunction may therefore be related to impaired perivascular waste clearance, potentially driving tissue damage and cognitive decline in SVD. The findings presented in **Chapter 8**, which showed significant correlations between DMV disruptions and several MRI measures related to waste clearance function (Box 1), offer preliminary support for this hypothesis. Moreover, DMV disruptions was related with higher WMH volumes and lower Montreal Cognitive Assessment (MoCA) scores, partly mediated by BG-PVS enlargement and reduced DTI-ALPS. These findings suggested that impaired waste clearance function, as indicated by decreased DTI-ALPS and enlarged BG-PVS, may represent one mechanistic pathway through which DMV disruptions contribute to WMH formation and cognitive impairments in SVD. However, the contributions of PVS in SVD-related cognitive impairments remains controversial, with inconsistent findings across studies.[64-67]

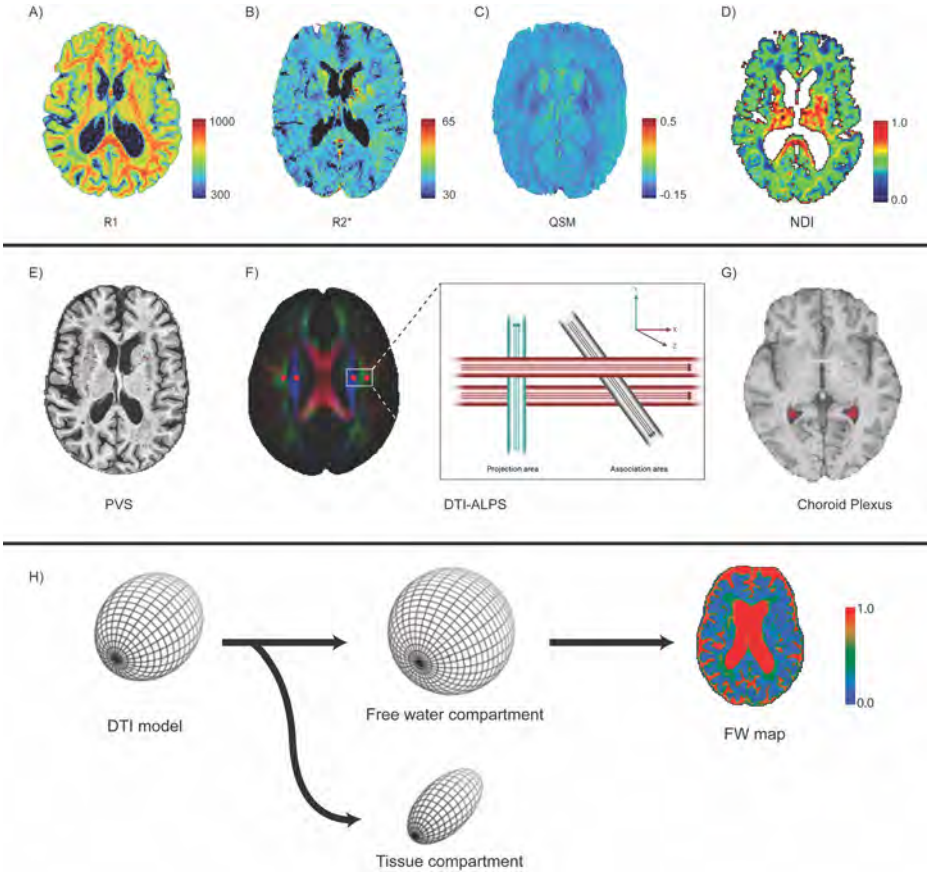

Box 1. Imaging tissue composition and the waste clean system function in brain.

First Row: MRI Measures of Microstructural Composition. (A) The longitudinal relaxation rate (R1, 1/T1), measures how quickly protons realign with the magnetic field after excitation. R1 provides insight into myelin-related changes in the brain; (B) The effective transverse relaxation rate (R2*, 1/T2*), reflects how quickly the MRI signal decays due to spin–spin dephasing and magnetic field inhomogeneities. R2* is highly sensitive to magnetic susceptibility effects, such as iron deposition, and is also influenced by myelin content; (C) Quantitative Susceptibility Mapping (QSM) computes maps of tissue magnetic susceptibility. By detecting local variations in magnetic properties, QSM is particularly useful for quantifying iron deposition and other susceptibility-related changes in the brain. (D) Neurite Density Index (NDI) is derived from Neurite Orientation Dispersion and Density Imaging (NODDI) models, this index specifically quantifies the fraction of tissue composed of neurites (axons and dendrites).

Second Row: MRI Measures of Brain Waste Clearance Function. (E) Perivascular Space (PVS) are fluid-filled spaces that surround small vessels in brain. On MRI, "visible" PVS typically represent dilated perivascular spaces, most probably around periarteriolar spaces, thus it is considered to act as the cerebrospinal fluid (CSF) inflow channel in brain's waste clean system. Larger PVS volumes may suggest impaired clearance along these perivascular channels; (F) DTI-ALPS (Diffusion Tensor Imaging Analysis along the Perivascular Space). DTI-ALPS is hypothesised to measure the diffusivity capacity of the perivenous space surrounding the deep medullary vein at the lateral ventricle body level. A

higher ALPS index may indicate more efficient CSF outflow and better waste clearance along these perivascular channels; (G) Choroid Plexus is a major site of CSF production, which helps drive the convective flow essential for waste removal. The volume of the choroid plexus could influence how much CSF is produced and, in turn, the brain's overall clearance capacity.

Third Row: (H) Free Water (FW) Imaging model is a two-compartment model that enhances traditional diffusion tensor imaging (DTI) models by modelling both a FW component and a FW-corrected tissue compartment. The FW compartment represents extracellular water fraction. A higher FW fraction is related to pathologic processes, such as the disruption of the blood-brain barrier and neuroinflammation.

Notably, it is crucial to acknowledge that while these proposed MRI metrics (Box 1, second row) are commonly used as proxies for waste clearance function, their validity remains unconfirmed due to a lack of formal validation. Among these metrics, only the DTI-ALPS index has demonstrated a correlation with waste clearance rates, as measured by invasive intrathecal gadolinium-enhanced MRI in one previous study; however, this validation was not performed in the SVD population.[68] It is possible that these measures do not directly reflect impaired waste clearance function but are instead influenced by coexisting pathologies such as disrupted white matter integrity, neuroinflammation, and blood-brain barrier impairment. Therefore, caution is warranted when interpreting MRI-based measures as direct indicators of waste clearance function. Future studies employing more precise assessments, such as intrathecal gadolinium-enhanced MRI, are needed to validate these findings **(Chapters 7 and 8)** and establish their clinical relevance.

Bringing It All Together: SVD as a Vascular-Driven Multifactorial Network Disease

From a broad view, the evidence across this thesis showed that the three proposed mechanism independently contributes to the clinical deficits observed in SVD while also interacting synergistically (Figure 1). This interplay highlights the complexity of SVD pathophysiology: small vessel pathology in SVD gradually leads to tissue damage and concurrently impairs the brain's waste clearance system. This impaired waste clearance system results in the accumulation of metabolic products, which further exacerbate both vascular and tissue injury in a vicious cycle. Additionally, secondary neurodegenerative processes trigged by localized tissue damage disproportionately amplify the initial injury by facilitating its propagation through inter-connected neural networks. Over time, these interacting mechanisms ultimately results in a diffuse brain damage characterized by extensive white matter disconnection and a range of clinical symptoms. Thus, this underscores the conceptualization of SVD as a vascular-derived multifactorial network disorder, where clinical deficits correspond more with the cumulative burden of brain connection disruption rather than with the MRI-visible lesions at a single time point.

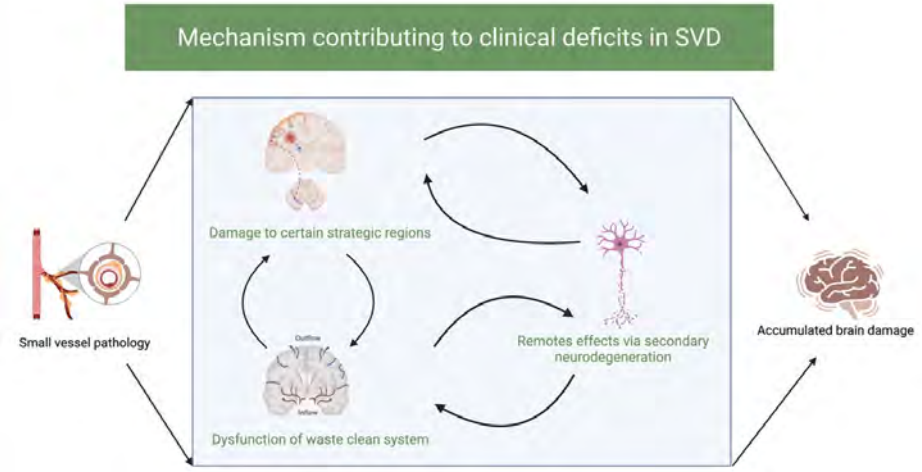

Figure 1. Schematic overview of the proposed mechanism in small vessel disease.

Clinical relevance

Clinical manifestations in SVD

Given the diversity of clinical manifestations of SVD, the comprehensive characterization of clinical manifestations in SVD represents a critical foundation for advancing disease management. This thesis showed that cognitive impairment, apathy, and gait dysfunction in SVD are inter- connected and likely share common underlying mechanisms, potentially involving dopaminergic meso-cortical pathway damage. This finding specifically underscores the need for an integrative approach in both clinical assessment and treatment. First, clinicians should adopt a more systematic approach to patient assessment. For instance, patients presenting with cognitive complaints should also be screened for apathy and gait disturbances, and vice versa. Second, the identification of common neural substrates underlying these manifestations, particularly within the dopaminergic pathway, suggests potential therapeutic opportunities. Interventions targeting dopaminergic function may yield broader clinical benefits, potentially addressing multiple symptom domains simultaneously.[69,70] Finally, the integration of composite outcome measures, rather than isolated assessments of cognition, apathy, or gait, may serve as a more robust and comprehensive endpoint in clinical trials. This approach would better detect meaningful treatment effects and quantify disease progression in relevant trials.

Surrogate markers of disease progression

Accurately tracking the progression of SVD is crucial for advancing both clinical management and mechanistic understanding of this condition. Traditional MRI

markers, such as WMH and lacunes, provide insights into established tissue damage. However, these conventional markers showed relatively modest correlations with clinical symptoms and inadequately capture the progressive, dynamic nature of SVD pathology. This limitation results in substantial unexplained variance in clinical presentations.

Advanced quantitative MRI techniques, particularly diffusion imaging, have emerged to help address these limitations by enabling detection of subtle microstructural alterations. The findings presented in this thesis suggest that damage to strategically important brain regions, such as the thalamocortical projections and specific neurotransmitter pathways (e.g., dopaminergic and cholinergic circuits), is closely associated with cognitive deficits and other key clinical manifestations of SVD, independently of conventional MRI markers. Identifying damage in these regions (such as lesions involving thalamus) may therefore provide a robust method for patient risk stratification.

Directions for future research

From the invisible to the visible: Ultra-High-Field MRI in Small Vessel Disease

An important direction for future research lies in leveraging ultra-high-field MRI (UHF-MRI) technologies (i.e., 7T and above) to visualize the currently "invisible" changes in SVD. These UHF-MRI scanners offer high spatial resolution and improved signal-to-noise ratios, which can facilitate the detection of structural and functional changes at an early stage of SVD. For instance, high-resolution 7T imaging modalities such as time-of-flight angiography (TOF) and susceptibility-weighted imaging (SWI) have demonstrated superior capability in visualizing small cerebral vessels, including lenticulostriate arteries branches and both deep and superficial medullary veins.[71,72] When combined with advanced computational methods, these imaging modalities enable to study the pathological origin of SVD, i.e., the vascular structural (e.g. the length, continuity and curvature) and functional (e.g., the blood flow velocity and pulsatility) changes, instead of their presumed pathological tissue alterations.[73,74] Furthermore, evidence in the thesis and other collaborative studies have suggested the significance of cerebral micro-infarcts (CMI) in SVD-related damage.[75] However, conventional 3T MRI detects only a fraction of the lesions identified in post-mortem studies.[76] The implementation of UHF-MRI could substantially improve *in-vivo* CMI detection, potentially bridging this diagnostic gap and enhancing our understanding of CMI's role in the progression

of SVD's pathology and clinical manifestations. Another part of particular interest is the potential application of detecting subtle changes in perivascular spaces (PVS), which serve as critical pathways in the brain's waste clearance system. The sub-millimeters voxel resolution achievable with UHF-MRI enables accurate measurements of PVS volume, morphology, and potentially fluid dynamics, thereby potentially advancing our understanding of PVS burden and its relationship with the glymphatic system in SVD pathophysiology.

Detection of Pathophysiology Alterations: Quantitative Imaging and Molecular Imaging

Research focusing on the pathophysiology changes is another important future step in advancing our understanding of the early stages of SVD. In this context, quantitative MRI techniques offer promising opportunities to detect and quantify subtle damages in SVD and potentially link these damages to specific changes in tissue composition. Advanced quantitative MRI parameters, including relaxometry, myelin water fraction, and susceptibility, provide specific markers of tissue composition, notably for myelin and iron content.[77] These measures may better characterize the SVD-related tissue damage, potentially serving as more sensitive outcome measures for clinical trials targeting early intervention. Yet, the main question lies in the non-specificity of these measurements, as they can be influenced by multiple tissue factors, including water content, macromolecular composition, and the presence of paramagnetic or diamagnetic substances.[77] Additionally, the validation of these parameters is not specifically performed in the pathological environment of SVD, potentially limiting their applicability and interoperation. A multiparametric approach that integrates various quantitative measures could provide comprehensive tissue characterization, but careful consideration is required when interpreting these measurements in the context of SVD pathology.

Molecular imaging, particularly using PET, represents another frontier in understanding SVD pathophysiology by enabling visualization of specific biological processes. PET imaging with targeted radioligands could help elucidate key pathogenic mechanisms like inflammation (using translocator protein [TSPO] ligands) in SVD.[78] Of particular interest is the combination of TSPO-PET with other advanced MRI techniques, such as Dynamic Contrast-Enhanced (DCE) MRI for blood-brain barrier (BBB) integrity and novel imaging approaches for waste clearance function evaluation.[79] This multimodal imaging paradigm holds the potential to provide comprehensive insights into the complex interplay between neuroinflammation, BBB dysfunction, and impaired waste clearance mechanisms in early-stage SVD. Additionally, PET imaging with neurotransmitter tracer enables the

specifically measure for various neurotransmitter level in brain, thus reflecting the function of each neurotransmitter system. The findings regarding the dopamine and cholinergic pathway damage in this thesis have underscored the importance of investigating the function of certain neurotransmitter system in SVD. Future studies employing neurotransmitter-specific PET imaging could elucidate the contributions of dopamine and cholinergic systems dysfunction in SVD, potentially identifying novel therapeutic targets.

Early-onset SVD: A Window into Disease Mechanisms and Progression

Given that SVD predominantly manifests in older populations (over 60 years), most existing research has focused on this demographic. Consequently, our understanding of SVD has left a critical knowledge gap for young population. Investigating young and middle-aged individual with SVD or at risk offer unique opportunity to elucidate disease mechanisms, since SVD-related pathological changes may precede visible lesions by years or even decades.[80] This extended temporal window provides two critical advantages. First, it enables observation of the complete natural history of SVD, from its earliest manifestations through disease progression. Second, it offers a unique window to study initial pathogenic mechanisms in the absence of confounding factors such as neurodegenerative processes and age-related changes, thereby potentially advancing our understanding of SVD etiology and progression. Moreover, examining SVD burden in younger populations could reveal age-specific variations in risk factors and disease manifestations. Such insights are crucial for developing age-dependent management approaches and interventions strategies, potentially improving outcomes across the disease spectrum.

From Bench to Bedside: Translating Novel Therapies for Small Vessel Disease

The work in this thesis informed several potential strategies that may slow disease progression and mitigate clinical symptoms in SVD. Apart from preventive strategies targeting disease progression are essential, developing therapeutic interventions for existing pathologies and clinical manifestations in SVD remains crucial. This thesis has identified several strategic brain regions and pathways contributing to clinical symptoms in SVD. For example, this thesis suggests that damage to the dopaminergic mesocortical pathway and cholinergic system contributes to SVD-related clinical symptoms, indicating therapeutic potential in targeting these neurotransmitter systems. Previous trials have demonstrated potential benefits of dopaminergic agents and cholinesterase inhibitors for improving apathy and cognition in various conditions, including Alzheimer's disease, vascular

dementia, and Parkinson's disease.[81,82] Additionally, rivastigmine has been shown to improve gait stability in Parkinson's disease.[83] These evidence, combined with the findings in present thesis, support further exploration of dopaminergic and cholinergic therapies as symptomatic treatments for cognitive impairment, apathy, and gait dysfunction in SVD. However, before initiating clinical trials with such pharmacological interventions, robust mechanistic studies must be performed to determine whether SVD patients (or which group of patients) exhibit specific neurotransmitter deficits and evaluate their contributions to clinical symptoms.

Concluding remarks

By leveraging advanced multimodal neuroimaging approaches, this thesis investigated several mechanisms underlying clinical symptoms in SVD. The results highlight how strategic regional damage, remote effects of localized lesions, and impaired brain waste clearance contribute to the progression and clinical manifestations of SVD. Collectively, these findings suggest that SVD should be conceptualized as a vascular-derived multifactorial network disorder, wherein various vascular and non-vascular mechanisms interact synergistically. The clinical deficits in SVD correspond more with the cumulative burden of brain connection disruption rather than with the MRI-visible lesions. Furthermore, these insights may inform the development of novel imaging biomarkers for disease severity assessment and therapeutic targets to slow progression and ameliorate symptoms. Future studies, preferably with large-scale sample size and multimodal MRI, are required to further explore both these established and additional mechanisms driving the progression and diverse clinical presentations of SVD, ultimately translating these findings into clinical practice.

Reference

1. van Norden AG, de Laat KF, Gons RA, van Uden IW, van Dijk EJ, van Oudheusden LJ, Esselink RA, Bloem BR, van Engelen BG, Zwarts MJ, Tendolkar I, Olde-Rikkert MG, van der Vlugt MJ, Zwiers MP, Norris DG, de Leeuw FE. Causes and consequences of cerebral small vessel disease. The RUN DMC study: a prospective cohort study. Study rationale and protocol. BMC Neurol. Feb 28 2011;11:29. doi:10.1186/1471-2377-11-29
2. Carlson MD, Morrison RS. Study design, precision, and validity in observational studies. J Palliat Med. Jan 2009;12(1):77-82. doi:10.1089/jpm.2008.9690
3. Alexander LK, Lopes B, Ricchetti-Masterson K, Yeatts KB. Sources of systematic error or bias: Information bias. Eric Notebook. 2015;2(14):1-5.
4. Nunan D, Aronson J, Bankhead C. Catalogue of bias: attrition bias. BMJ Evid Based Med. Feb 2018;23(1):21-22. doi:10.1136/ebmed-2017-110883
5. Welch CA, Sabia S, Brunner E, Kivimäki M, Shipley MJ. Does pattern mixture modelling reduce bias due to informative attrition compared to fitting a mixed effects model to the available cases or data imputed using multiple imputation?: a simulation study. BMC Med Res Methodol. Aug 29 2018;18(1):89. doi:10.1186/s12874-018-0548-0
6. Weaver NA, et al. The Meta VCI Map consortium for meta-analyses on strategic lesion locations for vascular cognitive impairment using lesion-symptom mapping: Design and multicenter pilot study. Alzheimers Dement (Amst). Dec 2019;11:310-326. doi:10.1016/j.dadm.2019.02.007
7. Cui M, Jin Z, Wang Y, Jiang J, Peng S, Wei Q, Zhang S, Tuo Q, Xie J, Leng H, Wang H, Zhao Y, Lei P, Xu J, Wang K, Zhang J, Jiang Y, Ding D, Xie F, Yu J, Dong Q. Imaging, biomarkers, and vascular cognitive impairment in China: Rationale and design for the VICA study. Alzheimers Dement. Nov 13 2024;doi:10.1002/alz.14352
8. Behrens TE, Berg HJ, Jbabdi S, Rushworth MF, Woolrich MW. Probabilistic diffusion tractography with multiple fibre orientations: What can we gain? Neuroimage. Jan 1 2007;34(1):144-55. doi:10.1016/j.neuroimage.2006.09.018
9. Jenkinson M, Beckmann CF, Behrens TE, Woolrich MW, Smith SM. FSL. Neuroimage. Aug 15 2012;62(2):782-90. doi:10.1016/j.neuroimage.2011.09.015
10. Tournier JD, Calamante F, Connelly A. Robust determination of the fibre orientation distribution in diffusion MRI: non-negativity constrained super-resolved spherical deconvolution. Neuroimage. May 1 2007;35(4):1459-72. doi:10.1016/j.neuroimage.2007.02.016
11. Tournier JD, Smith R, Raffelt D, Tabbara R, Dhollander T, Pietsch M, Christiaens D, Jeurissen B, Yeh CH, Connelly A. MRtrix3: A fast, flexible and open software framework for medical image processing and visualisation. Neuroimage. Nov 15 2019;202:116137. doi:10.1016/j.neuroimage.2019.116137
12. Grier MD, Zimmermann J, Heilbronner SR. Estimating Brain Connectivity With Diffusion-Weighted Magnetic Resonance Imaging: Promise and Peril. Biol Psychiatry Cogn Neurosci Neuroimaging. Sep 2020;5(9):846-854. doi:10.1016/j.bpsc.2020.04.009
13. Liewald D, Miller R, Logothetis N, Wagner HJ, Schüz A. Distribution of axon diameters in cortical white matter: an electron-microscopic study on three human brains and a macaque. Biol Cybern. Oct 2014;108(5):541-57. doi:10.1007/s00422-014-0626-2
14. Lipp I, Parker GD, Tallantyre EC, Goodall A, Grama S, Patitucci E, Heveron P, Tomassini V, Jones DK. Tractography in the presence of multiple sclerosis lesions. Neuroimage. Apr 1 2020;209:116471. doi:10.1016/j.neuroimage.2019.116471

15. Alexander AL, Hasan KM, Lazar M, Tsuruda JS, Parker DL. Analysis of partial volume effects in diffusion-tensor MRI. Magn Reson Med. May 2001;45(5):770-80. doi:10.1002/mrm.1105
16. Weiskopf N, Suckling J, Williams G, Correia MM, Inkster B, Tait R, Ooi C, Bullmore ET, Lutti A. Quantitative multi-parameter mapping of R1, PD(*), MT, and R2(*) at 3T: a multi-center validation. Front Neurosci. 2013;7:95. doi:10.3389/fnins.2013.00095
17. Langkammer C, Krebs N, Goessler W, Scheurer E, Ebner F, Yen K, Fazekas F, Ropele S. Quantitative MR imaging of brain iron: a postmortem validation study. Radiology. Nov 2010;257(2):455-62. doi:10.1148/radiol.10100495
18. Emsell L, Van Hecke W, Tournier J-D. Introduction to Diffusion Tensor Imaging. In: Van Hecke W, Emsell L, Sunaert S, eds. Diffusion Tensor Imaging: A Practical Handbook. Springer New York; 2016:7-19.
19. Dauguet J, Peled S, Berezovskii V, Delzescaux T, Warfield SK, Born R, Westin CF. Comparison of fiber tracts derived from in-vivo DTI tractography with 3D histological neural tract tracer reconstruction on a macaque brain. Neuroimage. Aug 15 2007;37(2):530-8. doi:10.1016/j.neuroimage.2007.04.067
20. Pasternak O, Sochen N, Gur Y, Intrator N, Assaf Y. Free water elimination and mapping from diffusion MRI. Magn Reson Med. Sep 2009;62(3):717-30. doi:10.1002/mrm.22055
21. Duering M, Finsterwalder S, Baykara E, Tuladhar AM, Gesierich B, Konieczny MJ, Malik R, Franzmeier N, Ewers M, Jouvent E, Biessels GJ, Schmidt R, de Leeuw FE, Pasternak O, Dichgans M. Free water determines diffusion alterations and clinical status in cerebral small vessel disease. Alzheimers Dement. Jun 2018;14(6):764-774. doi:10.1016/j.jalz.2017.12.007
22. Zhang H, Schneider T, Wheeler-Kingshott CA, Alexander DC. NODDI: practical in vivo neurite orientation dispersion and density imaging of the human brain. Neuroimage. Jul 16 2012;61(4):1000-16. doi:10.1016/j.neuroimage.2012.03.072
23. Kamiya K, Hori M, Aoki S. NODDI in clinical research. J Neurosci Methods. Dec 1 2020;346:108908. doi:10.1016/j.jneumeth.2020.108908
24. Sciences NAo, Policy, Affairs G, Data BoR, Information, Engineering Do, Sciences P, Applied Co, Statistics T, Sciences BoM. Reproducibility and replicability in science. National Academies Press; 2019.
25. Bennett B. Miller, & Wolford.(2011). Neural Correlates of Interspecies Perspective Taking in the Post-Mortem Atlantic Salmon: An Argument For Proper Multiple Comparisons Correction. Journal of Serendipitous and Unexpected Results. 1(1):1-5.
26. Marek S, et al. Reproducible brain-wide association studies require thousands of individuals. Nature. Mar 2022;603(7902):654-660. doi:10.1038/s41586-022-04492-9
27. Kang K, Seidlitz J, Bethlehem RAI, Xiong J, Jones MT, Mehta K, Keller AS, Tao R, Randolph A, Larsen B, Tervo-Clemmens B, Feczko E, Dominguez OM, Nelson SM, Alexander-Bloch AF, Fair DA, Schildcrout J, Fair DA, Satterthwaite TD, Alexander-Bloch A, Vandekar S, Lifespan Brain Chart C. Study design features increase replicability in brain-wide association studies. Nature. 2024/12/01 2024;636(8043):719-727. doi:10.1038/s41586-024-08260-9
28. Pannucci CJ, Wilkins EG. Identifying and avoiding bias in research. Plast Reconstr Surg. Aug 2010;126(2):619-625. doi:10.1097/PRS.0b013e3181de24bc
29. Chen Y, Tozer D, Li R, Li H, Tuladhar A, De Leeuw FE, Markus HS. Improved Dementia Prediction in Cerebral Small Vessel Disease Using Deep Learning-Derived Diffusion Scalar Maps From T1. Stroke. Sep 2024;55(9):2254-2263. doi:10.1161/strokeaha.124.047449

30. Emdin CA, Khera AV, Kathiresan S. Mendelian Randomization. Jama. Nov 21 2017;318(19):1925-1926. doi:10.1001/jama.2017.17219

31. Biesbroek JM, Verhagen MG, van der Stigchel S, Biessels GJ. When the central integrator disintegrates: A review of the role of the thalamus in cognition and dementia. Alzheimers Dement. Mar 2024;20(3):2209-2222. doi:10.1002/alz.13563

32. Duering M, Gesierich B, Seiler S, Pirpamer L, Gonik M, Hofer E, Jouvent E, Duchesnay E, Chabriat H, Ropele S, Schmidt R, Dichgans M. Strategic white matter tracts for processing speed deficits in age-related small vessel disease. Neurology. Jun 3 2014;82(22):1946-50. doi:10.1212/wnl.0000000000000475

33. Biesbroek JM, Weaver NA, Hilal S, Kuijf HJ, Ikram MK, Xu X, Tan BY, Venketasubramanian N, Postma A, Biessels GJ, Chen CP. Impact of Strategically Located White Matter Hyperintensities on Cognition in Memory Clinic Patients with Small Vessel Disease. PLoS One. 2016;11(11):e0166261. doi:10.1371/journal.pone.0166261

34. Menegaux A, Meng C, Bäuml JG, Berndt MT, Hedderich DM, Schmitz-Koep B, Schneider S, Nuttall R, Zimmermann J, Daamen M. Aberrant cortico-thalamic structural connectivity in premature-born adults. Cortex. 2021;141:347-362.

35. Ter Telgte A, Duering M. Cerebral Small Vessel Disease: Advancing Knowledge With Neuroimaging. Stroke. Jun 2024;55(6):1686-1688. doi:10.1161/strokeaha.123.044294

36. Weinstein AM. Reward, motivation and brain imaging in human healthy participants - A narrative review. Front Behav Neurosci. 2023;17:1123733. doi:10.3389/fnbeh.2023.1123733

37. Li H, Cui L, Wang M, Liao M, Li JB, Ouyang F, Mei T, Zen H, Fan Y. Apathy is associated with striatal atrophy and cognitive impairment in cerebral small vessel disease. J Affect Disord. May 1 2023;328:39-46. doi:10.1016/j.jad.2023.02.004

38. Nemy M, et al. Cholinergic white matter pathways along the Alzheimer's disease continuum. Brain. May 2 2023;146(5):2075-2088. doi:10.1093/brain/awac385

39. Schumacher J, Ray NJ, Hamilton CA, Bergamino M, Donaghy PC, Firbank M, Watson R, Roberts G, Allan L, Barnett N, O'Brien JT, Thomas AJ, Taylor JP. Free water imaging of the cholinergic system in dementia with Lewy bodies and Alzheimer's disease. Alzheimers Dement. Oct 2023;19(10):4549-4563. doi:10.1002/alz.13034

40. Ray NJ, Lawson RA, Martin SL, Sigurdsson HP, Wilson J, Galna B, Lord S, Alcock L, Duncan GW, Khoo TK, O'Brien JT, Burn DJ, Taylor JP, Rea RC, Bergamino M, Rochester L, Yarnall AJ. Free-water imaging of the cholinergic basal forebrain and pedunculopontine nucleus in Parkinson's disease. Brain. Mar 1 2023;146(3):1053-1064. doi:10.1093/brain/awac127

41. Nemy M, Cedres N, Grothe MJ, Muehlboeck JS, Lindberg O, Nedelska Z, Stepankova O, Vyslouzilova L, Eriksdotter M, Barroso J, Teipel S, Westman E, Ferreira D. Cholinergic white matter pathways make a stronger contribution to attention and memory in normal aging than cerebrovascular health and nucleus basalis of Meynert. Neuroimage. May 1 2020;211:116607. doi:10.1016/j.neuroimage.2020.116607

42. Cedres N, Ferreira D, Nemy M, Machado A, Pereira JB, Shams S, Wahlund LO, Zettergren A, Stepankova O, Vyslouzilova L, Eriksdotter M, Teipel S, Grothe MJ, Blennow K, Zetterberg H, Schöll M, Kern S, Skoog I, Westman E. Association of Cerebrovascular and Alzheimer Disease Biomarkers With Cholinergic White Matter Degeneration in Cognitively Unimpaired Individuals. Neurology. Oct 11 2022;99(15):e1619-e1629. doi:10.1212/wnl.0000000000200930

43. Wilmskoetter J, Marebwa B, Basilakos A, Fridriksson J, Rorden C, Stark BC, Johnson L, Hickok G, Hillis AE, Bonilha L. Long-range fibre damage in small vessel brain disease affects aphasia severity. Brain. Oct 1 2019;142(10):3190-3201. doi:10.1093/brain/awz251

44. Huerta-Ocampo I, Hacioglu-Bay H, Dautan D, Mena-Segovia J. Distribution of Midbrain Cholinergic Axons in the Thalamus. eNeuro. Jan/Feb 2020;7(1)doi:10.1523/eneuro.0454-19.2019

45. Ikemoto S, Yang C, Tan A. Basal ganglia circuit loops, dopamine and motivation: A review and enquiry. Behav Brain Res. Sep 1 2015;290:17-31. doi:10.1016/j.bbr.2015.04.018

46. Tuladhar AM, Reid AT, Shumskaya E, de Laat KF, van Norden AG, van Dijk EJ, Norris DG, de Leeuw FE. Relationship between white matter hyperintensities, cortical thickness, and cognition. Stroke. Feb 2015;46(2):425-32. doi:10.1161/strokeaha.114.007146

47. Lambert C, Sam Narean J, Benjamin P, Zeestraten E, Barrick TR, Markus HS. Characterising the grey matter correlates of leukoaraiosis in cerebral small vessel disease. Neuroimage Clin. 2015;9:194-205. doi:10.1016/j.nicl.2015.07.002

48. Lambert C, Benjamin P, Zeestraten E, Lawrence AJ, Barrick TR, Markus HS. Longitudinal patterns of leukoaraiosis and brain atrophy in symptomatic small vessel disease. Brain. Apr 2016;139(Pt 4):1136-51. doi:10.1093/brain/aww009

49. Duering M, Righart R, Csanadi E, Jouvent E, Hervé D, Chabriat H, Dichgans M. Incident subcortical infarcts induce focal thinning in connected cortical regions. Neurology. Nov 13 2012;79(20):2025-8. doi:10.1212/WNL.0b013e3182749f39

50. Duering M, Righart R, Wollenweber FA, Zietemann V, Gesierich B, Dichgans M. Acute infarcts cause focal thinning in remote cortex via degeneration of connecting fiber tracts. Neurology. Apr 21 2015;84(16):1685-92. doi:10.1212/wnl.0000000000001502

51. Mayer C, Frey BM, Schlemm E, Petersen M, Engelke K, Hanning U, Jagodzinski A, Borof K, Fiehler J, Gerloff C, Thomalla G, Cheng B. Linking cortical atrophy to white matter hyperintensities of presumed vascular origin. J Cereb Blood Flow Metab. Jul 2021;41(7):1682-1691. doi:10.1177/0271678x20974170

52. Lommers E, Simon J, Reuter G, Delrue G, Dive D, Degueldre C, Balteau E, Phillips C, Maquet P. Multiparameter MRI quantification of microstructural tissue alterations in multiple sclerosis. Neuroimage Clin. 2019;23:101879. doi:10.1016/j.nicl.2019.101879

53. Mainero C, Louapre C, Govindarajan ST, Giannì C, Nielsen AS, Cohen-Adad J, Sloane J, Kinkel RP. A gradient in cortical pathology in multiple sclerosis by in vivo quantitative 7 T imaging. Brain. Apr 2015;138(Pt 4):932-45. doi:10.1093/brain/awv011

54. Bian W, Tranvinh E, Tourdias T, Han M, Liu T, Wang Y, Rutt B, Zeineh MM. In Vivo 7T MR Quantitative Susceptibility Mapping Reveals Opposite Susceptibility Contrast between Cortical and White Matter Lesions in Multiple Sclerosis. AJNR Am J Neuroradiol. Oct 2016;37(10):1808-1815. doi:10.3174/ajnr.A4830

55. Huang J, Oh M, Robert C, Huang X, Egle M, Tozer DJ, Chen C, Hilal S. Loss of white matter integrity mediates the association between cortical cerebral microinfarcts and cognitive dysfunction: A longitudinal study. J Cereb Blood Flow Metab. Oct 2024;44(10):1723-1732. doi:10.1177/0271678x241258563

56. Ter Telgte A, van Leijsen EMC, Wiegertjes K, Klijn CJM, Tuladhar AM, de Leeuw FE. Cerebral small vessel disease: from a focal to a global perspective. Nat Rev Neurol. Jul 2018;14(7):387-398. doi:10.1038/s41582-018-0014-y

57. Mestre H, Mori Y, Nedergaard M. The Brain's Glymphatic System: Current Controversies. Trends Neurosci. Jul 2020;43(7):458-466. doi:10.1016/j.tins.2020.04.003

58. Xu J, Su Y, Fu J, Shen Y, Dong Q, Cheng X. Glymphatic pathway in sporadic cerebral small vessel diseases: From bench to bedside. Ageing Res Rev. Apr 2023;86:101885. doi:10.1016/j.arr.2023.101885

59. Ding J, Sigurðsson S, Jónsson PV, Eiriksdottir G, Charidimou A, Lopez OL, van Buchem MA, Guðnason V, Launer LJ. Large Perivascular Spaces Visible on Magnetic Resonance Imaging,

Cerebral Small Vessel Disease Progression, and Risk of Dementia: The Age, Gene/Environment Susceptibility-Reykjavik Study. JAMA Neurol. Sep 1 2017;74(9):1105-1112. doi:10.1001/jamaneurol.2017.1397

60. Evans TE, Knol MJ, Schwingenschuh P, Wittfeld K, Hilal S, Ikram MA, Dubost F, van Wijnen KMH, Katschnig P, Yilmaz P, de Bruijne M, Habes M, Chen C, Langer S, Völzke H, Ikram MK, Grabe HJ, Schmidt R, Adams HHH, Vernooij MW. Determinants of Perivascular Spaces in the General Population: A Pooled Cohort Analysis of Individual Participant Data. Neurology. Jan 10 2023;100(2):e107-e122. doi:10.1212/wnl.0000000000201349
61. Tian Y, Cai X, Zhou Y, Jin A, Wang S, Yang Y, Mei L, Jing J, Li S, Meng X, Wei T, Liu T, Wang Y, Pan Y, Wang Y. Impaired glymphatic system as evidenced by low diffusivity along perivascular spaces is associated with cerebral small vessel disease: a population-based study. Stroke Vasc Neurol. Oct 2023;8(5):413-423. doi:10.1136/svn-2022-002191
62. Fulop GA, Tarantini S, Yabluchanskiy A, Molnar A, Prodan CI, Kiss T, Csipo T, Lipecz A, Balasubramanian P, Farkas E, Toth P, Sorond F, Csiszar A, Ungvari Z. Role of age-related alterations of the cerebral venous circulation in the pathogenesis of vascular cognitive impairment. Am J Physiol Heart Circ Physiol. May 1 2019;316(5):H1124-h1140. doi:10.1152/ajpheart.00776.2018
63. Nan D, Cheng Y, Feng L, Zhao M, Ma D, Feng J. Potential Mechanism of Venous System for Leukoaraiosis: From post-mortem to in vivo Research. Neurodegener Dis. 2019;19(3-4):101-108. doi:10.1159/000505157
64. Benjamin P, Trippier S, Lawrence AJ, Lambert C, Zeestraten E, Williams OA, Patel B, Morris RG, Barrick TR, MacKinnon AD, Markus HS. Lacunar Infarcts, but Not Perivascular Spaces, Are Predictors of Cognitive Decline in Cerebral Small-Vessel Disease. Stroke. Mar 2018;49(3):586-593. doi:10.1161/strokeaha.117.017526
65. Hilal S, Tan CS, Adams HHH, Habes M, Mok V, Venketasubramanian N, Hofer E, Ikram MK, Abrigo J, Vernooij MW, Chen C, Hosten N, Volzke H, Grabe HJ, Schmidt R, Ikram MA. Enlarged perivascular spaces and cognition: A meta-analysis of 5 population-based studies. Neurology. Aug 28 2018;91(9):e832-e842. doi:10.1212/wnl.0000000000006079
66. Paradise M, Crawford JD, Lam BCP, Wen W, Kochan NA, Makkar S, Dawes L, Trollor J, Draper B, Brodaty H, Sachdev PS. Association of Dilated Perivascular Spaces With Cognitive Decline and Incident Dementia. Neurology. Mar 16 2021;96(11):e1501-e1511. doi:10.1212/wnl.0000000000011537
67. Passiak BS, Liu D, Kresge HA, Cambronero FE, Pechman KR, Osborn KE, Gifford KA, Hohman TJ, Schrag MS, Davis LT, Jefferson AL. Perivascular spaces contribute to cognition beyond other small vessel disease markers. Neurology. Mar 19 2019;92(12):e1309-e1321. doi:10.1212/wnl.0000000000007124
68. Zhang W, Zhou Y, Wang J, Gong X, Chen Z, Zhang X, Cai J, Chen S, Fang L, Sun J, Lou M. Glymphatic clearance function in patients with cerebral small vessel disease. Neuroimage. Sep 2021;238:118257. doi:10.1016/j.neuroimage.2021.118257
69. Schneider JS, Kortagere S. Current concepts in treating mild cognitive impairment in Parkinson's disease. Neuropharmacology. Feb 1 2022;203:108880. doi:10.1016/j.neuropharm.2021.108880
70. Cummings J, Lanctot K, Grossberg G, Ballard C. Progress in Pharmacologic Management of Neuropsychiatric Syndromes in Neurodegenerative Disorders: A Review. JAMA Neurol. Jun 1 2024;81(6):645-653. doi:10.1001/jamaneurol.2024.0586
71. Kang CK, Park CA, Park CW, Lee YB, Cho ZH, Kim YB. Lenticulostriate arteries in chronic stroke patients visualised by 7T magnetic resonance angiography. Int J Stroke. Oct 2010;5(5):374-80. doi:10.1111/j.1747-4949.2010.00464.x

72. van Harten TW, Heijmans A, van Rooden S, Wermer MJH, van Osch MJP, Kuijf HJ, van Veluw SJ, Greenberg SM, van Buchem MA, van der Grond J, van Walderveen MAA. Brain Deep Medullary Veins on 7T MRI in Dutch-Type Hereditary Cerebral Amyloid Angiopathy. J Alzheimers Dis. 2022;90(1):381-388. doi:10.3233/jad-220354

73. Ling C, Fang X, Kong Q, Sun Y, Wang B, Zhuo Y, An J, Zhang W, Wang Z, Zhang Z, Yuan Y. Lenticulostriate Arteries and Basal Ganglia Changes in Cerebral Autosomal Dominant Arteriopathy With Subcortical Infarcts and Leukoencephalopathy, a High-Field MRI Study. Front Neurol. 2019;10:870. doi:10.3389/fneur.2019.00870

74. Arts T, Meijs TA, Grotenhuis H, Voskuil M, Siero J, Biessels GJ, Zwanenburg J. Velocity and Pulsatility Measures in the Perforating Arteries of the Basal Ganglia at 3T MRI in Reference to 7T MRI. Front Neurosci. 2021;15:665480. doi:10.3389/fnins.2021.665480

75. Ferro DA, Kuijf HJ, Hilal S, van Veluw SJ, van Veldhuizen D, Venketasubramanian N, Tan BY, Biessels GJ, Chen C. Association Between Cerebral Cortical Microinfarcts and Perilesional Cortical Atrophy on 3T MRI. Neurology. Feb 8 2022;98(6):e612-e622. doi:10.1212/wnl.0000000000013140

76. van Veluw SJ, Shih AY, Smith EE, Chen C, Schneider JA, Wardlaw JM, Greenberg SM, Biessels GJ. Detection, risk factors, and functional consequences of cerebral microinfarcts. Lancet Neurol. Sep 2017;16(9):730-740. doi:10.1016/s1474-4422(17)30196-5

77. Weiskopf N, Edwards LJ, Helms G, Mohammadi S, Kirilina E. Quantitative magnetic resonance imaging of brain anatomy and in vivo histology. Nature Reviews Physics. 2021;3(8):570-588.

78. Gouilly D, Saint-Aubert L, Ribeiro MJ, Salabert AS, Tauber C, Péran P, Arlicot N, Pariente J, Payoux P. Neuroinflammation PET imaging of the translocator protein (TSPO) in Alzheimer's disease: An update. Eur J Neurosci. Mar 2022;55(5):1322-1343. doi:10.1111/ejn.15613

79. Heye AK, Culling RD, Valdés Hernández Mdel C, Thrippleton MJ, Wardlaw JM. Assessment of blood-brain barrier disruption using dynamic contrast-enhanced MRI. A systematic review. Neuroimage Clin. 2014;6:262-74. doi:10.1016/j.nicl.2014.09.002

80. Williamson W, Lewandowski AJ, Forkert ND, Griffanti L, Okell TW, Betts J, Boardman H, Siepmann T, McKean D, Huckstep O, Francis JM, Neubauer S, Phellan R, Jenkinson M, Doherty A, Dawes H, Frangou E, Malamateniou C, Foster C, Leeson P. Association of Cardiovascular Risk Factors With MRI Indices of Cerebrovascular Structure and Function and White Matter Hyperintensities in Young Adults. Jama. Aug 21 2018;320(7):665-673. doi:10.1001/jama.2018.11498

81. Birks J, Craig D. Galantamine for vascular cognitive impairment. Cochrane Database Syst Rev. Jan 25 2006;(4):Cd004746. doi:10.1002/14651858.CD004746.pub2

82. Harrison F, Aerts L, Brodaty H. Apathy in Dementia: Systematic Review of Recent Evidence on Pharmacological Treatments. Curr Psychiatry Rep. Nov 2016;18(11):103. doi:10.1007/s11920-016-0737-7

83. Henderson EJ, Lord SR, Brodie MA, Gaunt DM, Lawrence AD, Close JC, Whone AL, Ben-Shlomo Y. Rivastigmine for gait stability in patients with Parkinson's disease (ReSPonD): a randomised, double-blind, placebo-controlled, phase 2 trial. Lancet Neurol. Mar 2016;15(3):249-58. doi:10.1016/s1474-4422(15)00389-0

Chapter 11.

Nederlandse samenvatting

Deel I | Introductie

Aandoening van de kleine bloedvaten in de hersenen, in het Engels Cerebral Small Vessel Disease afgekort als SVD, vormt de belangrijkste vasculaire oorzaak van cognitieve stoornissen en dementie. Momenteel wordt SVD vastgesteld aan de hand van afwijkingen op de MRI-, waaronder wittestofafwijkingen (WSA), lacunaire infarcten en microbloedingen. Bij patiënten met vergelijkbare radiologische mate van SVD bestaat er echter een aanzienlijke heterogeniteit in de klinische verschijnselen. Deze discrepantie kan verklaard worden door het feit dat de bovengenoemde traditionele MRI-markers voor SVD slechts het topje van de ijsberg laten zien van de totale hersenschade die door SVD wordt veroorzaakt. Deze MRI-afwijkingen verklaren daarom niet volledig klinische symptomen. Recente ontwikkelingen in de kwantitatieve beeldvorming van de hersenen, met name diffusie-gewogen beeldvorming (een speciale MRI-techniek die de witte en grijze stof nauwkeuriger kan onderzoeken), bieden mogelijkheden om verder te kijken dan de traditionele SVD-markers. Dit kan leiden tot een beter begrip van de mechanismen achter de uiteenlopende symptomen bij SVD. In dit proefschrift heb ik daarom onderzocht welke mechanismen ten grondslag liggen aan de klinische symptomen van SVD, in het bijzonder de cognitieve stoornissen, door middel van geavanceerde multimodale beeldvormingstechnieken. Hierbij richtte ik me specifiek op de volgende drie aspecten:

1. De strategische effecten van schade in specifieke hersengebieden.
2. De effecten op afstand als gevolg van lokale afwijkingen door secundaire neurodegeneratie.
3. De disfunctie van het afvalverwerkende systeem van de hersenen, waarbij perivasculaire ruimten zijn betrokken.

Deel II | Strategische gebieden bij SVD

In **Hoofdstuk 2** onderzocht ik de associaties tussen structurele veranderingen in de thalamus en de prestaties in drie cognitieve domeinen (verwerkingssnelheid, executief functioneren en geheugen) bij SVD. De data zijn afkomstig uit de derde follow-up (2020) van de Radboud University Nijmegen Diffusion Tensor and Magnetic resonance Cohort (RUN DMC)-studie, bestaande uit 205 deelnemers met SVD, maar zonder lacunaire infarcten in de thamalus. Met behulp van probabilistische tractografie en connectiviteitsgebaseerde thalamus-segmentatie werden zes thalamische subregio's afgebakend en hebben we zowel hun volume

als hun connectiviteit met de grijze stof (gemeten met mean diffusivity [MD]) gekwantificeerd. We vonden dat een hogere MD-waarde in het thalamisch-motorische traject samenhing met slechtere verwerkingssnelheid; een hogere MD in het thalamisch-frontale traject hing samen met slechter executief functioneren en geheugen. Mediatie-analyses lieten zien dat de MD in de thalamocorticale trajecten de associatie medieerde tussen het volume van de corresponderende thalamische subregio's en de cognitieve prestaties. Deze bevindingen suggereren dat de structurele veranderingen in de thalamus bij SVD gerelateerd zijn aan cognitieve stoornissen, grotendeels afhankelijk van het patroon van schade in de witte-stofbanen die specifieke thalamische subregio's met corticale gebieden verbinden.

In **Hoofdstuk 3** onderzocht ik mogelijke onderlinge relaties tussen cognitieve stoornissen, apathie en loopstoornissen, met speciale aandacht voor de vraag of deze klinische symptomen samenhangen met schade aan de mesocorticale en mesolimbische banen bij SVD. Bij 213 deelnemers met SVD uit de derde follow-up (2020) van de RUN DMC-studie zijn cognitieve stoornissen, apathie en loopproblemen systematisch beoordeeld via een uitgebreide cognitieve testbatterij (waaronder testen voor verwerkingssnelheid, executief functioneren en geheugen), de Apathy Evaluation Scale (AES) en motortesten, waaronder de gemiddelde tijd en het aantal stappen tijdens de Timed Up and Go (TUG)-test. Ik bracht cognitie, apathie en loopstoornissen met elkaar in verband door de nauwe correlaties aan te tonen tussen de uitkomsten van deze drie domeinen in deze studiepopulatie. Vervolgens voerde ik een principal component analysis (PCA) uit waaruit één gemeenschappelijke component naar voren kwam voor deze drie symptomen. Hogere waarden van deze component duiden op slechtere prestaties op de gecombineerde metingen van cognitie, apathie en lopen. Op basis van de bevinding van zo'n gemeenschappelijke component, veronderstelde ik dat de drie symptomen mogelijk een gemeenschappelijke neurale basis delen, waarin het dopaminerge systeem van de hersenen - met name de mesocorticale en mesolimbische circuits - een hoofdrol zou kunnen spelen. Om dit te onderzoeken maakte ik gebruik van probabilistische tractografie en reconstrueerde ik vijf witte-stofbanen binnen de mesocorticale en mesolimbische banen. Daaruit bleek dat schade in vier witte-stofbanen binnen het mesocorticale circuit, gekwantificeerd door free water (FW) als diffusieparameter, gerelateerd was aan cognitieve stoornissen, apathie, loopstoornissen én de gemeenschappelijke PCA-component in onze SVD-studiepopulatie. Deze bevindingen wijzen erop dat de drie klinische kenmerken (cognitieve stoornissen, apathie en loopstoornissen) bij SVD onderling sterk verbonden zijn, en dat schade in de mesocorticale banen de gemeenschappelijke neurale basis zou kunnen vormen voor deze kenmerken.

In **Hoofdstuk 4** richtte ik me op het cholinerge circuit, die net als de mesocorticale en mesolimbische circuits kunnen bijdragen aan de cognitieve en motorische stoornissen, gezamenlijk ook wel 'motoric cognitive dysfunction' genoemd, bij SVD. Via probabilistische tractografie reconstrueerde ik twee witte-stoftrajecten binnen het cholinerg corticaal circuit en één traject in het cholinerg thalamisch circuit. De verstoringen in deze banen werden in kaart gebracht door gebruik te maken van diffusieparameters, gebaseerd op het neurite orientation dispersion and density imaging (NODDI)-model. Ik vond dat de diffusieparameters (vooral de neurite density index [NDI] en de isotrope volumefractie [ISOVF]) in het cholinerg corticaal circuit de relatie medieerden tussen traditionele MRI-markers van SVD en zowel cognitieve als loopstoornissen. De cholinerge thalamische trajecten medieerden daarentegen uitsluitend de relatie tussen deze MRI-markers en cognitieve stoornissen. Deze bevindingen suggereren dat verstoring van de cholinerge corticale banen een centrale rol speelt in de pathofysiologie die ten grondslag ligt aan de gecombineerde cognitieve en motorische stoornissen, oftewel 'motoric cognitive dysfunction', bij SVD.

Deel III | Voorbij de focale afwijking: effecten op afstand in SVD

In **Hoofdstuk 5** stelde ik de hypothese dat WMH mogelijk structurele veranderingen kunnen veroorzaken in corticale gebieden die op afstand liggen, maar via vezelverbindingen verbonden zijn met de subcorticale WMH, en dat dit kan bijdragen aan cognitieve stoornissen bij SVD. Om dit te toetsen, gebruikte ik probabilistische tractografie met het WMH masker als 'seed', oftewel als startpunt, om corticale gebieden in kaart te brengen die verbonden zijn met de WMH (de zogeheten "WMH-connected cortex"), evenals de witte-stofbanen die deze WMH met de cortex verbinden (de "connecting tracts"). De dikte van de cortex, en kwantitatieve R1, R2* en susceptibiliteitsmapping zijn gebruikt om het verlies van hersenvolume en onderliggende weefselveranderingen — met name in myeline en ijzer — in zowel de WMH-connected als de niet-verbonden (WMH-unconnected) corticale gebieden te bepalen. De MD-index werd toegepast om schade aan de connecting tracts te evalueren. Uit deze analyses bleek dat de WMH-connected corticale gebieden significant lagere waarden hadden voor corticale dikte, R1, R2* en susceptibiliteit in vergelijking met de WMH-unconnected gebieden, wat wijst op het dunner worden van de cortex, demyelinisatie en ijzerverlies. Daarnaast hing een hogere MD in de connecting tracts samen met lagere waarden voor corticale dikte, R1, R2* en susceptibiliteit in de WMH-connected cortex, wat vervolgens

geassocieerd was met een lagere verwerkingssnelheid. Deze bevindingen wijzen gezamenlijk op corticale atrofie, demyelinisatie en ijzerverlies in WMH-connected corticale gebieden, waarschijnlijk als gevolg van een verstoring van de witte-stofbanen die WMH met de cortex verbinden, en dit kan een bijdrage leveren aan vertraging in verwerkingssnelheid bij SVD.

In **Hoofdstuk 6** richtte ik me op cerebrale corticale micro-infarcten (CMI), een relatief nieuwe MRI-marker van SVD. We onderzochten de mogelijke effecten op afstand van lokale CMI-laesies in omliggende corticale en subcorticale gebieden, en de dynamische temporele veranderingen bij acute CMI's in SVD. Met behulp van data van de RUN DMC-Investigating The origin and EvolutioN of cerebral small vessel disease (RUN DMC-InTENse) cohortstudie, bestaande uit 54 SVD-deelnemers die tien maandelijkse MRI-scans ondergingen, identificeerde ik nieuwe en oude CMI's en bijbehorende controlegebieden. De omliggende gebieden binnen de cortex en de subcorticale gebieden langs de witte-stofbanen werden vervolgens afgebakend. Corticale dikte, R1 en de neurite density index (NDI) werden gebruikt om structurele veranderingen te evalueren in de gebieden rond de kern van de CMI-laesie. In de analyses zagen we dat de subcorticale gebieden van oude CMI's lagere NDI-waarden liet zien in vergelijking met controlegebieden, tot op ongeveer 10 mm afstand van CMI. Nieuwe CMI's hadden lagere R1- en hogere NDI-waarden dan de controlegebieden, maar dat deze waarden normaliseerden tijdens vervolgmetingen. Deze bevindingen suggereren dat oude CMI's gepaard gaan met schade aan subcorticale gebieden langs de witte-stofbanen, maar dat de effecten op naburige corticale gebieden beperkt zijn (vermoedelijk mede door partial volume-effecten). Daarnaast lijkt de door nieuwe CMI's veroorzaakte schade op de plaats van de afwijking vooral lokaal te zijn en van voorbijgaande aard.

Deel IV | Het afvalverwerkende systeem in SVD

In Hoofdstuk 7 richtte mijn onderzoek zich op een zeer dynamisch afvalverwerkend systeem in de hersenen, dat een efficiënte afvoer van metabolische restproducten uit het centrale zenuwstelsel via perivasculaire kanalen mogelijk maakt. Ik analyseerde data uit de RUN DMC-cohortstudie uit 2011, bestaande uit 289 SVD-deelnemers, waarvan er 220 in 2015 de follow-up voltooiden. Bij deze deelnemers berekende ik drie MRI-indices die mogelijk gerelateerd zijn aan de functie van het afvalverwerkingssysteem: de volumes van perivasculaire ruimten in de basale kernen (BG-PVS), de free water (FW)-fractie en de Diffusion Tensor Imaging Along the Perivascular Space (DTI-ALPS) index. Ik bracht vervolgens de dynamische

onderlinge relaties tussen deze drie MRI-indices in kaart met behulp van een latent change score-model. Daarnaast onderzocht ik in lineaire mixed-effecten regressiemodellen hun longitudinale associaties met veranderingen in andere SVD-MRI-markers en cognitieve prestaties. Deze analyses toonden aan dat de baseline DTI-ALPS-waarde samenhing met de verandering van BG-PVS-volumes, maar niet omgekeerd. Dit wijst op een tijdsvertraging waarbij afname in DTI-ALPS-waarden voorafgaat aan de toename van BG-PVS. Verder waren de baselinewaarden van deze drie MRI-indices geassocieerd met veranderingen in traditionele SVD-MRI-markers, zoals een toename in WMH-volumes, een toename in het aantal lacunaire infarcten en een afname van het hersenvolume. Bovendien hingen DTI-ALPS en de FW-fractie op baseline samen met de achteruitgang in MMSE-score, cognitieve index en verwerkingssnelheid over tijd. Deze bevindingen suggereren dat de hier onderzochte MRI-indices, die verondersteld worden de functie van het afvalverwerkingssysteem in de hersenen te weerspiegelen, bijdragen aan de progressie van SVD en de daarmee gepaard gaande cognitieve achteruitgang.

In Hoofdstuk 8 onderzocht ik de mogelijke associaties tussen verstoringen van de diepe medullaire venen (DMV), dysfunctie van het afvalverwerkingssysteem, de WMH-omvang en cognitieve stoornissen bij SVD. Ik maakte gebruik van data uit een onafhankelijk SVD-cohort van het First Affiliated Hospital of Sun Yat-sen University in Guangzhou (China), waar bij 133 deelnemers de mate van DMV-verstoring op kwalitatief hoogwaardige susceptibility-weighted imaging (SWI) werd beoordeeld. Vijf MRI-indices die gerelateerd zijn aan afvalverwerking zijn gemeten: DTI-ALPS-index, FW-fractie, plexus choroideus (Cp)-volume, BG-PVS-volume en witte-stof-PVS (WM-PVS)-volume. Analyses lieten zien dat hogere DMV-scores (wat duidt op grotere DMV-verstoringen) samenhingen met lagere DTI-ALPS-waarden, hogere FW-fractie en grotere volumes van Cp, BG-PVS en WM-PVS. Verder waren hogere DMV-scores gerelateerd aan toegenomen WMH-volumes en een lagere MoCA-score. Parallelle mediatie-analyses toonden vervolgens dat DTI-ALPS-index en BG-PVS-volume de relatie tussen DMV-scores en WMH-volumes medieerden, waarbij alleen BG-PVS-volume de relatie tussen DMV-scores en de MoCA-score medieerde. Deze bevindingen suggereren dat verstoring van de DMV bijdraagt aan zowel WMH-belasting als cognitieve stoornissen bij SVD, en dat deze invloed mogelijk wordt gemedieerd door MRI-markers die indicatief zijn voor een verminderde afvalverwerking in de hersenen, in het bijzonder de vergroting van BG-PVS.

Part VI.

Appendices

List of main abbreviations

AAL:	Anatomical Automatic Labelling
ACC:	Anterior cingulate cortex
AD:	Alzheimer's disease
AES-C:	clinician-rated version of Apathy Evaluation Scale
ANOVA:	analysis of variance
ANTs:	Advanced Normalization Tools
ATR:	anterior thalamic radiation
BBB:	blood-brain barrier
BG-PVS:	basal ganglia perivascular space
BF:	basal forebrain
BPF:	brain parenchymal fraction
CADASIL:	cerebral autosomal dominant arteriopathy with subcortical infarcts and leukoencephalopathy
CFI:	Comparative Fit Index
CMBs:	cerebral microbleeds
CMIs:	cerebral cortical microinfarcts
Cp:	choroid plexus
CSF:	cerebrospinal fluid
CSD:	constrained spherical deconvolution
DCE:	Dynamic Contrast-Enhanced
dlPFC:	dorsolateral prefrontal cortex
dWMH:	deep white matter hyperintensity
DTI:	diffusion tensor imaging
DTI-ALPS:	diffusion tensor imaging along the perivascular spaces
DWI:	diffusion-weighted imaging
FA:	fractional anisotropy
FLAIR:	fluid-attenuated inversion recovery
FSL:	Functional Magnetic Resonance Imaging of the Brain Software Library
FWF:	free water fraction
GM:	grey matter
GRE:	gradient echo sequence
ICV:	intracranial volume
IQR:	interquartile range
ISF:	interstitial fluid

ISOVF:	isotropic volume fraction
MCA:	middle cerebral artery
MD:	mean diffusivity
MD-t:	free water-corrected mean diffusivity
MoCA:	Montreal Cognitive Assessment
MP2RAGE:	Magnetization Prepared 2 Rapid Acquisition Gradient Echoes
MPRAGE:	Magnetization Prepared Rapid Gradient Echo
mOFC:	medial orbitofrontal cortex
NAWM:	normal-appearing white matter
NBM:	nucleus basalis of Meynert
NODDI:	Neurite Orientation Dispersion and Density Imaging
NDI:	neurite density index
ODI:	orientation dispersion index
PCA:	principal component analysis
PPN:	pedunculopontine nucleus
pWMH:	periventricular white matter hyperintensity
PFC:	prefrontal cortex
PVE:	partial volume effects
qMRI:	quantitative MRI
QSM:	quantitative susceptibility mapping
RAVLT:	Rey Auditory Verbal Learning Test
RUN DMC:	Radboud University Nijmegen Diffusion tensor and Magnetic resonance imaging Cohort
RUN DMC-InTENse:	Radboud University Nijmegen Diffusion tensor and Magnetic resonance imaging Cohort – Investigating The origin and EvolutioN of cerebral small vessel disease
RMSEA:	Root Mean Square Error of Approximation
SAMSEG:	Sequence Adaptive Multimodal SEGmentation
SD:	standard deviation
SDST:	Symbol Digit Substitution Test
SN:	substantia nigra
SRMR:	Standardized Root Mean Residual
STIRVE-2:	version 2 of the Standards for Reporting Vascular Changes on Neuroimaging criteria
SVD:	small vessel disease
SWI:	susceptibility-weighted imaging
T1W:	T1-weighted imaging
TMT:	Trail Making Test
TBV:	Total brain volumes

TUG:	Timed Up and Go
VICA:	Vascular, Imaging and Cognition Association of China
VIF:	variance inflation factor
vlPFC:	ventral lateral prefrontal cortex
VSAT:	Verbal Series Attention Test
VTA:	ventral tegmental area
WM:	white matter
WMH:	white matter hyperintensities

Research data management statement

Ethics and privacy

This thesis is based on the results of research involving human participants, which were conducted in accordance with relevant national and international legislation and regulations, guidelines, codes of conduct and Radboudumc policy. The studies presented in Chapters 2-7 were approved by the Medical Ethics Review Committee (METC) Oost-Nederland (file numbers NL69678.091.19 and NL53939.091.15). The study in Chapter 8 was approved by the Human Ethics Committee of the First Affiliated Hospital of Sun Yat-sen University (approval no. 2018109).

The privacy of the participants in these studies was warranted by the use of pseudonymization. The pseudonymization key was stored on a secured departmental network drive that was only accessible to members of the project who needed access to it because of their role within the project. The pseudonymization key was stored separately from the research data.

Informed consent was obtained from participants to collect and process their data for this research project. Consent was not obtained for sharing the (pseudonymized) data after research.

Data collection and Storage

Raw Data for Chapters 2-7 in this thesis were collected through electronic Case Report Forms (eCRF) of a prospective data collection in Castor EDC. Data were converged from (electronic) health records or Castor EDC to SPSS (SPSS Inc., Chicago, Illinois, USA) and are only accessible by project members working at the Radboudumc. Raw Data for Chapters 8 in this thesis were collected through the standardized Case Report Forms (CRF). Data are only accessible by project members working at the First Affiliated Hospital of Sun Yat-sen University. Processed data and documentation of all Chapters are archived in a Research Documentation Collection (RDC) in the Radboud Data Repository. These secure storage options safeguard the availability, integrity and confidentiality of the data.

Data sharing according to the FAIR principles

All studies are published with open access. The datasets from chapters 2-8 are archived with closed access in a Data Acquisition Collection (DAC) in the Radboud Data Repository: '*Mechanism behind clinical symptoms in cerebral small vessel disease*'

Data were made reusable by adding sufficient documentation and by using preferred and sustainable data formats.

The table details where the data and research documentation for each chapter can be found on the Radboud Data Repository (RDR). All data archived as a Data Acquisition Collection remain available for at least 15 years after termination of the studies.

Chapter	RDC	DAC
2-8	Mechanism behind clinical symptoms in cerebral small vessel disease	DOI: https://doi.org/10.34973/ve2t-qz05

RDC = Research Documentation Collection, DAC = Data Acquisition Collection

About the author

Hao Li was born on 17 November 1995 in Anhua, Hunan Province, China. He completed his medical education at Xiangya School of Medicine, Central South University, in 2018, majoring in psychiatry. Following this, he completed his residency training and obtained a Master's degree in Neurology at Sun Yat-sen University, where he developed a strong interest in neuroimaging and cerebral small vessel disease.

In 2021, Hao Li received the opportunity to pursue a PhD abroad with financial support from the China Scholarship Council. He subsequently moved to Nijmegen, the Netherlands, to begin his doctoral research at the Department of Neurology, Radboud University Medical Center, under the supervision of Dr. Anil M. Tuladhar and Prof. Frank-Erik de Leeuw. His PhD project, titled "Mechanisms behind clinical symptoms in cerebral small vessel disease: a neuroimaging perspective," aimed to disentangle the neural mechanisms linking cerebral small vessel disease to major clinical manifestations such as cognitive impairment.

During his PhD, he worked extensively with MRI data from the RUN DMC study, applying advanced multimodal neuroimaging techniques to investigate how localized vascular lesions contributes to widespread structural changes in the brain. Hao Li presented his research at several international conferences, including the European Stroke Organisation Conference (ESOC). His studies have resulted in multiple peer-reviewed publications in high-impact journals and and culminated in this thesis.

Currently, Hao Li continues his research as a postdoctoral fellow at Radboud University Medical Center, focusing on integrating imaging markers to better understand the mechanisms underlying cognitive impairment in cerebral small vessel disease. In the near future, he will return to China to work as a clinician while continuing his research, with the hope of translating scientific insights into improved clinical practice.

List of the publications

This thesis

1. **Hao Li**, Mengfei Cai, Mina A Jacob, David G Norris, José P Marques, Maxime Chamberland, Marco Duering, Roy PC Kessels, Frank-Erik de Leeuw, Anil M Tuladhar. Dissociable contributions of thalamic-subregions to cognitive impairment in small vessel disease. *Stroke*, 54(5): 1367-1376, 2023.
2. **Hao Li**, Mina A Jacob, Mengfei Cai, Roy PC Kessels, David G Norris, Marco Duering, Frank-Erik de Leeuw, Anil M Tuladhar. Meso-cortical pathway damage in cognition, apathy and gait in cerebral small vessel disease. *Brain*, awa145, 2024.
3. **Hao Li***, Mengfei Cai *, Milan Nemy, Mina A. Jacob, David G. Norris, Marco Duering, Yuhu Zhang, Roy P. C. Kessels, Stefan J Teipel, Daniel Ferreira, Frank-Erik de Leeuw,Anil M. Tuladhar. Cholinergic system disruption contributes to motoric cognitive dysfunction in cerebral small vessel disease. (Accepted in *Stroke*).
4. **Hao Li**, Mina A Jacob, Mengfei Cai, Marco Duering, Maxime Chamberland, David G Norris, Roy PC Kessels, Frank-Erik de Leeuw, José P Marques, Anil M Tuladhar. Regional cortical thinning, demyelination and iron loss in cerebral small vessel disease. *Brain*, 146(11): 4659-4673, 2023.
5. **Hao Li**, Annemieke ter Telgte, Marco Duering, David G Norris, José P. Marques, Frank-Erik de Leeuw, Anil M. Tuladhar. Spatial and temporal effects of cortical cerebral microinfarcts on the cortical and subcortical regions in cerebral small vessel disease (Submitted).
6. **Hao Li**, Mina A Jacob, Mengfei Cai, Roy PC Kessels, David G Norris, Marco Duering, Frank-Erik De Leeuw, Anil Man Tuladhar. Perivascular spaces, diffusivity along perivascular spaces, and free water in cerebral small vessel disease. *Neurology*, 102(9): e209306, 2024.
7. Mengshi Liao, Meng Wang, Wenli Zhou, Yixin Chen, Jiayu Guo, Gemma Solé-Guardia, Anil M Tuladhar, Yuhua Fan[+], **Hao Li**[+]. Disruption of deep medullary veins and MRI indices of glymphatic function in cerebral small vessel disease. *J Alzheimers Dis*. Published online September 3, 2025.

*, shared first authorship, [+], shared corresponding authorship.

Other Publications

8. **Hao Li**, Liqian Cui, Ziyi Chen, Yue Chen. Risk factors for early-onset seizures in patients with cerebral venous sinus thrombosis: A meta-analysis of observational studies. *Seizure*. 2019.
9. **Hao Li**, Liqian Cui, Liping Cao, Yizhi Zhang, Yueheng Liu, Wenhao Deng, Wenjin Zhou. Identification of bipolar disorder using a combination of multimodality magnetic resonance imaging and machine learning techniques. *BMC Psychiatry*, 20: 12-Jan, 2020.
10. **Hao Li**, Liqian Cui, Jinbiao Li, Yueheng Liu, Yue Chen. Comparative efficacy and acceptability of neuromodulation procedures in the treatment of treatment-resistant depression: a network meta-analysis of randomized controlled trials. *Journal of Affective Disorders*, 287: 115-124, 2021.
11. Liqian Cui, **Hao Li**, Jinbiao Li, Huixing Zeng, Yizhi Zhang, Wenhao Deng, Wenjin Zhou, Liping Cao. Altered cerebellar gray matter and cerebellar-cortex resting-state functional connectivity in patients with bipolar disorder I. *Journal of Affective Disorders*, 302: 50-57, 2022.
12. Fubing Ouyang, Meng Wang, Mengshi Liao, Linfan Lan, Xiaolu Liu, **Hao Li**, Rong Mo, Lin Shi, Yuhua Fan. Association between periodic limb movements during sleep and neuroimaging features of cerebral small vessel disease: A preliminary cross-sectional study. *Journal of Sleep Research*, 31(5): e13573, 2022.
13. Jinbiao Li, Liqian Cui, **Hao Li**. Optimal parameter determination of repetitive transcranial magnetic stimulation for treating treatment-resistant depression: A network meta-analysis of randomized controlled trials. *Frontiers in Psychiatry*, 13: 1038312, 2022.
14. **Hao Li**, Liqian Cui, Meng Wang, Mengshi Liao, Jinbiao Li, Fubing Ouyang, Ting Mei, Huixing Zen, Yuhua Fan. Apathy is associated with striatal atrophy and cognitive impairment in cerebral small vessel disease. *Journal of Affective Disorders*, 328: 39-46, 2023.
15. Anna M De Kort, Kanishk Kaushik, H Bea Kuiperij, Lieke Jäkel, **Hao Li**, Anil M Tuladhar, Gisela M Terwindt, Marieke JH Wermer, Jurgen AHR Claassen, Catharina JM Klijn. The relation of a cerebrospinal fluid profile associated with Alzheimer's disease with cognitive function and neuropsychiatric symptoms in sporadic cerebral amyloid angiopathy. *Alzheimer's Research & Therapy*, 16(1): 99, 2024.
16. Mengshi Liao, Meng Wang, **Hao Li**, Jinbiao Li, Ming Yi, Linfang Lan, Fubing Ouyang, Lin Shi, Yuhua Fan. Discontinuity of deep medullary veins in SWI is associated with deep white matter hyperintensity volume and cognitive impairment in cerebral small vessel disease. *Journal of Affective Disorders*, 350: 600-607, 2024.

17. Yutong Chen, Daniel Tozer, Rui Li, **Hao Li**, Anil Tuladhar, Frank Erik De Leeuw, Hugh S Markus. Improved dementia prediction in cerebral small vessel disease using deep learning–derived diffusion scalar maps from T1. *Stroke*, 55(9): 2254-2263, 2024.
18. Theresa J Van Lith, **Hao Li**, Marte W van der Wijk, Naomi T Wijers, Wouter M Sluis, Marieke JH Wermer, Frank-Erik De Leeuw, Frederick JA Meijer, Anil M Tuladhar. White matter integrity in hospitalized COVID-19 patients is not associated with short- and long-term clinical outcomes. *Frontiers in Neurology*, 15: 1440294, 2024.
19. Chentao He, Rui Yang, Siming Rong, Piao Zhang, Xi Chen, Qi Qi, Ziqi Gao, Yan Li, **Hao Li**, Frank-Erik de Leeuw, Anil M Tuladhar, Marco Duering, Rick C Helmich, Rick van der Vliet, Sirwan KL Darweesh, Zaiyi Liu, Lijuan Wang, Mengfei Cai, Yuhu Zhang. Temporal evolution of microstructural integrity in cerebellar peduncles in Parkinson's disease: Stage-specific patterns and dopaminergic correlates. *NeuroImage: Clinical*, 44: 103679, 2024.
20. **Hao Li**, Mengfei Cai, Anil M Tuladhar. Cognition, apathy, and gait dysfunction in cerebral small vessel disease: a shared neural basis? *Neural Regen Res*. Published online December 7, 2024.
21. Mijntje MI Schellekens, **Hao Li**, Esther M Boot, Jamie I Verhoeven, Merel S Ekker, Frederick JA Meijer, Roy PC Kessels, Frank-Erik de Leeuw, Anil M Tuladhar. White matter integrity and cognitive performance in the subacute phase after ischemic stroke in young adults. *NeuroImage: Clinical*, 45: 103711, 2025.
22. Theresa J van Lith, Esther Janssen, Jan-Willem van Dalen, **Hao Li**, Mats Koeneman, Wouter M Sluis, Naomi T Wijers, Marieke JH Wermer, Menno V Huisman, H Bart van der Worp, Frederick JA Meijer, Anil M Tuladhar, Sebastian JH Bredie, Frank-Erik de Leeuw. Higher blood pressure variability during hospitalization is associated with lower cerebral white matter integrity in COVID-19 patients. Blood Press. Published online April 17, 2025.
23. Kirsten CJ Kapteijns, Teije H van Prooije, **Hao Li**, Tom WJ Scheenen, Anil Tuladhar, Bart P van de Warrenburg. The pattern and dynamics of white matter alterations in Spinocerebellar ataxia type 1: A diffusion-weighted magnetic resonance imaging study. *NeuroImage: Clinical*. Published online April 21, 2025.
24. Gemma Solé-Guardia, **Hao Li,** Luc Willemse, Jessica Lebenberg, Eric Jouvent, Anil Tuladhar. Imaging brain fluid dynamics and waste clearance involving perivascular spaces in cerebral small vessel disease. *Alzheimer's & Dementia*. Published online April 25, 2025.
25. Xin Cai, Wei Sun, Mengfei Cai, Dawei Li, Zhenzhen Chen, **Hao Li**, Bo Yuan, Yan Li, Zaiyi Liu, Yuhu Zhang, Impaired glymphatic function contributes to high-frequency attacks in patients with episodic migraine, *J Headache Pain*. 2025;26(1):132. Published 2025 Jun 3.

26. Chentao He, Zhenzhen Chen, Mengfei Cai, Piao Zhang, **Hao Li,** Xi Chen, Qi Qi, Rui Yang, Yan Li, Zaiyi Liu, Lijuan Wang, Yuhu Zhang. Cerebellar large-scale network connectivity in Parkinson's disease: associations with emotion, cognition, and aging effects. *Brain Imaging Behav.* Published online June 6, 2025.
27. Mengfei Cai, Chentao He, **Hao Li,** Rui Yang, Siming Rong, Ziqi Gao, Qibing Luo, Zihao Li, Yan Li, Zaiyi Liu, Piao Zhang, Yuhu Zhang. Advanced brain aging, selective vulnerability in gray matter, and cognition in Parkinson's disease. *J Gerontol A Biol Sci Med Sci.* 2025;80(9):glaf124.
28. Theresa J van Lith, Esther Janssen, Jan-Willem van Dalen, **Hao Li,** Mats Koeneman, Wouter M Sluis, Naomi T Wijers, Marieke JH Wermer, Menno V Huisman, H Bart van der Worp, Frederick JA Meijer, Anil M Tuladhar, Sebastian JH Bredie, Frank-Erik de Leeuw. Higher blood pressure variability during hospitalisation is associated with lower cerebral white matter integrity in COVID-19 patients. *Blood Press.* 2025;34(1):2493828.

Portfolio

Courses

- Academic English Conversation and Pronunciation (2022)
- Statistics for clinical researchers (2023)
- Scientific Integrity course (2025)

Conferences

- European Stroke Organization Conference (ESOC), 2022, Lyon, France
- Thalamic Volume and Processing Speed in Cerebral Small Vessel Disease. *Oral presentation*
- European Stroke Organization Conference (ESOC), 2023, Munich, Germany
- Regional Cortical Thinning, Demyelination, and Iron Loss Related to White Matter Hyperintensities in Cerebral Small Vessel Disease. *Oral presentation*
- European Stroke Organization Conference (ESOC), 2024, Basel, Switzerland
- Meso-Cortical Pathway Damage in Cognition, Apathy, Gait Dysfunction in Cerebral Small Vessel Disease. *Oral presentation*
- European Stroke Organization Conference (ESOC), 2025, Helsinki, Finland
- Cortical Atrophy Patterns Associated with Cognitive, Apathy and Gait Impairments Map to Dopaminergic Distribution in Cerebral Small Vessel Disease. *Oral presentation*
- Lesion Network Mapping to Identify Personalized Strategic Regions for Cognitive Outcomes in Young Stroke Survivors. *Oral presentation*
- Spatial and Temporal Effects of Cortical Cerebral Microinfarcts on the Cortical and Subcortical Regions in Cerebral Small Vessel Disease. *Poster presentation*

Acknowledgements

As I reach the completion of this doctoral dissertation, countless thoughts come to mind. It feels as though a heavy burden has finally been lifted, allowing me to pause and look back on the long journey that has brought me here. Standing at this point, I realize how far this journey has carried me. When I was a child, I could never have imagined that life at thirty would find me here: walking along a road that once seemed far beyond my reach. This journey has carried me across countries and cultures, through moments of doubt and discovery. Every step, every challenge, and every small victory has held meaning that reaches far beyond research itself. It has quietly transformed how I see both science and life, an experience that will continue to shape the rest of my life. Along this journey, I owe my deepest gratitude to many people. Without their guidance, support, and kindness, I could never have come this far. Each person I met, mentors who guided me, colleagues who inspired me, friends who encouraged me, and family who loved me unconditionally, has left an indelible mark on this journey. To them, this work belongs as much as it does to me.

Dear Anil, as my supervisor, I would like to sincerely thank you for your unwavering support and personal guidance in every aspect of my PhD. From the very first project on the thalamus, you provided hands-on mentoring in both coding and writing. During the project on DTI-ALPS, although the process was full of struggles, it became an invaluable period of growth in which you trained and inspired my critical thinking. Before every presentation, the part I often feared the most, you were always willing to spend your time with me, patiently practicing again and again. All these experiences of guidance and training have shaped me into the researcher I am today. Before coming to the Netherlands, I could not have imagined how challenging it would be to pursue a PhD in a foreign country, surrounded by a new environment and language. Yet, with your guidance and support, I always found a sense of clarity and purpose. Your quick and thoughtful feedback, even late at night or during weekends, became the foundation of every project we completed together. Looking back at the first email I sent you, I did not realize then how profoundly that moment would change my life, but I feel truly grateful that I sent it.

Dear Frank-Erik, thank you for your continuous support throughout my PhD. Whenever I needed help, whether it was facing difficulties in my projects or preparing for a conference presentation, you were always there to offer your guidance and encouragement. For every piece of work, your thoughtful feedback and constant reminder of the clinical relevance behind each research question

have deeply influenced me. Your insights and experience have shaped the way I think about connecting scientific discoveries with meaningful impact for patients.

Dear Jose, Dear Marco, as imaging experts, you have been my safety net in every project. Whenever I had questions or concerns about methodology, you always found time to patiently explain and guide me. Through your generous guidance, I learned not only the technical methods, but also a way of approaching science with depth, precision, and care. Your insights allowed me to glimpse the vast landscape of neuroimaging, not merely at the surface, but with true understanding and respect for its complexity.

Dear Roy, I am deeply grateful for your constant help and generous sharing of neuropsychological knowledge. You were closely involved in nearly all of my projects, always responding promptly, offering help with great patience and care. Your expertise and thoughtful advice have guided me through many challenges and greatly enriched my understanding of neuropsychology.

Dear Mengfei (梦飞), I would like to express my heartfelt and special thanks to you. You have been like an academic brother to me,one of the most important people I have met in Nijmegen. My journey here began with your help, and I am truly grateful that, as this chapter comes to an end, we have remained closely connected. Every piece of work I have accomplished rests on the foundation built by your hard work (together with Mina), especially your high-quality data collection during the fourth wave of the RUN DMC study. You have been the giant whose shoulders I have stood on, guiding and inspiring me to see further and aim higher. Even now, your presence continues to shine like a light, reminding me of the direction I should keep striving toward. I truly hope that our paths will continue to cross in the future, and that we can keep working side by side toward new discoveries and shared goals.

Dear Mina, just like with Mengfei, all my projects are built upon the foundation of your contributions to the RUN DMC study. Whenever I needed help, you were always there to lend a hand. From you, I have truly felt the passion you hold for studying the brain. Your jokes always brought lightness and warmth to us, and I am genuinely happy to see that after your PhD, you have continued to devote this passion to the STOP study. That pursuit, to bring real change to clinical practice, is one of the highest callings of a clinician, and it is also the ultimate goal I hope my own research will one day reach. I look forward to seeing your results soon, and when that time comes, I will follow your findings in treating my future patients in China.

Many thanks to all my co-authors in the RUN DMC(-intense) study, especially to David for his generous administrative and technical assistance at the Donders Institute, and to Annemieke for her dedicated help in the cerebral cortical micro-infarct project. Dear Annemieke, although our time chatting has been limited, mostly during the ESOC conference, I strongly felt your kindness, enthusiasm, and willingness to help. Your positivity and encouragement left a lasting warmth that I will always remember.

Many thanks to all the participants of the RUN DMC study. Your trust, commitment, and willingness to take part in this long-term research have made possible all the discoveries in small vessel disease. Many of you have returned for follow-up visits over the years, often spending hours undergoing MRI scans and cognitive testing, your dedication is truly admirable.

Many thanks to the members of my Doctoral Examination Board: Prof. Dr. METC van den Muijsenbergh, Prof. dr. Geert Jan Biessels, Prof. Dr. GJS Litjens, Dr. M. Wiesmann, Prof. dr. J.F.A. Jansen, Dr. R.C.G. Helmich, and Dr. V. Piai, for taking the time to participate in my defense and for their thoughtful questions and comments on my thesis.

Thanks to all my other friends and colleagues in the Department of Neurology: Resa, Esther Janssen, Sanner, Gemma, Floor, Mina, Mijntje, Fang Yi (易芳),, Alex, Maikel, Anna, Esmée, Jamie, Anne Roos, Erin, Anne, Esther Boot. Thanks for a wonderful time. Thank you for bringing me beers and chesse (though thankfully not the blue one), for teaching me Ducth words and for every second we spent together during ESOC. Your friendship, encouragement, and laughter have made my PhD journey so much brighter and more memorable.

Dear Sanner and Gemma, I'm super glad to see you both continuing to work on small vessel disease research. I truly hope all your efforts will be rewarded and that your studies will go smoothly. Beyond research, you have both been incredibly kind, warm, and supportive, always offering help even before I asked. Your generosity and positivity have truly meant a lot to me, and I feel very lucky to have shared this journey with you.

Dear Resa, at the very beginning of my time in Nijmegen, it was you who helped me settle in and find my place. Before my first presentation, you even took time out of your own schedule to help me practice. You did all of this with such kindness and patience, and it's something I will always carry in my heart. I'm also very happy that we had the chance to work together on the COVID project, it was a wonderful experience to collaborate together.

Dear Floor, you've always been like a big sister in our group, caring for everyone with warmth and thoughtfulness. Without your help, my time here would certainly have been much more difficult. I'm truly grateful for all the kindness and support you've given me. I sincerely wish everything go smoothly for you in the future.

Dear Mijntje and Anna, I feel deeply honored to have contributed as a co-author to your research. I've learned so much from our discussions and teamwork, and I sincerely appreciate the enthusiasm and scientific rigor you have shown throughout our collaboration.

Thanks to all my Chinese friends all round me in Nijmegen: Mingqian Guo (郭鸣谦), Ting Mei (梅婷), Dan Wu (吴丹), Dongyue Zhou (周冬跃), Yuxuan Dai (戴雨萱), Menghan Sun (孙梦涵), Danting Meng (孟丹婷), JinBiao Yang (杨金鬻), Changrun Huang (黄长润), Zhen Zhang (张祯), Chao Tang (唐超), Weitao Zhang (张伟韬), for these moments we have or ever shared with each other.

Thanks to Dr. Liqian Cui (崔立谦) and Prof. Yuhua Fan (范玉华). I spent a wonderful period of time during my master's studies under your guidance. It was during that time that you both led me into the field of cerebral small vessel disease research. Even now, four years later and thousands of miles away, you continue to care for and support me in so many ways. I am deeply grateful for your lasting encouragement and mentorship.

Thanks to all my friends and classmates in Guangzhou and Changsha: Mengshi Liao (廖梦诗), Xingyang Niu (牛星阳), Minping Li (李敏屏), Chong Wu (伍翀), Shijie Lu (陆世杰), ZhenJiang Liao (廖振江), Yueheng Liu (刘岳衡), ZiWei Yin (尹子维). Every time I return to China and reunite with you, those joyful moments recharge me with energy and happiness. Meeting all of you along the way has truly been one of the greatest fortunes in my life.

Special thanks to Milan Nemy, Ziwei Teng (藤紫薇) & Zhuohui Chen (陈焯辉), Heyang Lu (卢鹤扬), and Siyu Wentian (温田思雨) for our collaboration. I have learned so much from working with you and truly value the experience and insights I gained from your side.

Special thanks to Alex (胡杨) for organizing the neuroimaging discussion group. Although we've never met in person, I've been deeply impressed by your willingness to help and truly grateful for the generous help you've given me.

衷心感谢我的父母与家人，感谢你们无尽的爱、理解与支持。即使相隔万里，你们的关怀始终是我最坚实的力量源泉。我走过的每一步，都凝结着你们的付出与鼓励。我所取得的一切，都凝结着你们的爱与支持。My deepest gratitude goes to my parents and family for their endless love, understanding, and support. Even from afar, your care has always been my greatest source of strength. Every step I've taken on this journey has been built upon your sacrifices and encouragement. No words can truly express how thankful I am. This achievement belongs to you as much as it does to me.

衷心感谢陈永雄叔叔与唐艳阿姨多年来的关心、鼓励与支持。七年来，你们待我如亲生子般照顾与关怀，让我在异乡也感受到了家的温暖。因为有你们的陪伴与呵护，广州早已成为我心中的第二个家。My heartfelt thanks to Uncle Yongxiong Chen and Aunt Yan Tang for your care, encouragement, and unwavering support over the years. For the past seven years, you have treated me like your own son, surrounding me with warmth and kindness. Because of you, Guangzhou has become more than just a city to me. It has become my second home.

Lastly, and most importantly, to my love, Yue Chen (陈悦). Thank you for walking with me through all the ups and downs of these years. Your companionship, understanding, and patience have been my greatest comfort and motivation. Even when distance and time separated us, your love remained a constant source of warmth and courage. Our daily calls have always been the most relaxing moments of my day. We always find ourselves laughing together at the most unexpected little things. This journey would not have been the same without you, and I am endlessly grateful to have you by my side.

Dissertations of the Cerebrovascular Research Program

- Liselore Snaphaan. *Epidemiology of post stroke behavioral consequences.* Radboud University Nijmegen, 12 March 2010.
- Karlijn F. de Laat. *Motor performance in individuals with cerebral small vessel disease: an MRI study.* Radboud University Nijmegen, 29 November 2011
- Anouk G.W. van Norden. *Cognitive function in elderly individuals with cerebral small vessel disease: an MRI study.* Radboud University Nijmegen, 30 November 2011.
- Rob Gons. *Vascular risk factors in cerebral small vessel disease: a diffusion tensor imaging study.* Radboud University Nijmegen, 10 December 2012.
- Loes C.A. Rutten-Jacobs. *Long-term prognosis after stroke in young adults.* Radboud University Nijmegen, 14 April 2014.
- Noortje A.M.M. Maaijwee. *Long-term neuropsychological and social consequences after stroke in young adults.* Radboud University Nijmegen, 12 June 2015.
- Nathalie E. Synhaeve. *Determinants of long-term functional prognosis after stroke in young adults.* Radboud University Nijmegen, 28 September 2016.
- Anil M. Tuladhar. *The disconnected brain: mechanisms of clinical symptoms in small vessel disease.* Radboud University Nijmegen, 4 October 2016.Pauline Schaapsmeerders.
- *Long-term cognitive impairment after first-ever ischemic stroke in young adults: a neuroimaging study.* Radboud University Nijmegen, 24 January 2017.
- Ingeborg W.M. van Uden. *Behavioral consequences of cerebral small vessel disease: an MRI approach.* Radboud University Nijmegen, 14 February 2017.
- Renate M. Arntz. *The long-term risk of vascular disease and epilepsy after stroke in young adults.* Radboud University Nijmegen, 16 February 2017.
- Helena M. van der Holst. *Mind the step in cerebral small vessel disease: brain changes in motor performance.* Radboud University Nijmegen, 5 April 2017.
- Joyce Wilbers. *Long-term neurovascular complications in cancer patients.* Radboud University Nijmegen, 25 September 2017.
- Frank G. van Rooij. *Transient neurological attacks: neuroimaging, etiology, and cognitive consequences.* Radboud University Nijmegen, 14 June 2018.
- Tessa van Middelaar. *Memory under pressure: blood pressure management to prevent dementia.* Radboud University Nijmegen, 5 November 2018.
- Esther M.C. van Leijsen. *Unraveling the heterogeneity of cerebral small vessel disease: from local to remote effects.* Radboud University Nijmegen, 19 November 2018.
- Mayte E. van Alebeek. *Risk factors and prognosis of stroke in young adults: what to expect?* Radboud University Nijmegen, 18 October 2019.
- Selma Lugtmeijer. *Neurocognitive mechanisms of visual working memory and episodic memory in healthy aging and after stroke.* University of Amsterdam, 25 September 2020.

- Annemieke ter Telgte. *On the origin of cerebral small vessel disease: from in vivo to ex vivo to histopathology.* Radboud University Nijmegen, 9 June 2020.
- Kim Wiegertjes. *Ischemic and hemorrhagic MRI markers of cerebral small vessel disease: two sides of the same coin?* Radboud University Nijmegen, 16 September 2021.
- Marthe Smedinga. *Diseased without symptoms.* Radboud University Nijmegen, 5 October 2021.
- Mengfei Cai. *Temporal dynamics of cerebral small vessel disease: a motor perspective.* Radboud University Nijmegen, 19 April 2022.
- Thijs Landman. *Ischemic conditioning and exercise as treatment for cerebrovascular disease: squeeze the arm to protect the brain?* Radboud University Nijmegen, 28 June 2022.
- Ileana Camerino. *White matter tracts associated with executive aspects of language production in small vessel disease and stroke.* Radboud University Nijmegen, 27 September 2022.
- Merel Sanne Ekker. *Stroke in the young: from epidemiology to prognosis.* Radboud University Nijmegen, 27 September 2022.
- Hanna Abdulrahman. *Dementia risk factors and diagnostics.* Radboud University Nijmegen, 5 July 2023.
- Anna M. de Kort. *Cerebral amyloid angiopathy: novel insights on prevalence and fluid biomarkers.* Radboud University Nijmegen, 17 April 2024.
- Lotte Sondag. *Towards new acute treatments for spontaneous intracerebral hemorrhages: the role of surgery and perihematomal edema.* Radboud University Nijmegen, 30 September 2024.
- Mayra I. Bergkamp. *The clinical spectrum of cerebral small vessel disease.* Radboud University Nijmegen, 4 December 2024.
- Gemma S. Guardia. *Brain under pressure: association between hypertension and cerebral small vessel disease.* Radboud University Nijmegen, 7 March 2025.
- Jamie I. Verhoeven. *Unraveling stroke in the young.* Radboud University Nijmegen, 20 March 2025.
- Mina A. Jacob. *The course of cerebral small vessel disease.* Radboud University Nijmegen, 13 May 2025.
- Theresa Jozefina van Lith. *Unmasking COVID-19: Cerebral consequences from a neuroimaging perspective*, Radboud University Nijmegen, 25 June 2025.
- Esmée Verburgt, *A navigation of stroke in the young Exploring risk factors and prognosis*, Radboud University Nijmegen, 9 september 2025.

Donders Graduate School

For a successful research Institute, it is vital to train the next generation of scientists. To achieve this goal, the Donders Institute for Brain, Cognition and Behaviour established the Donders Graduate School in 2009. The mission of the Donders Graduate School is to guide our graduates to become skilled academics who are equipped for a wide range of professions. To achieve this, we do our utmost to ensure that our PhD candidates receive support and supervision of the highest quality.

Since 2009, the Donders Graduate School has grown into a vibrant community of highly talented national and international PhD candidates, with over 500 PhD candidates enrolled. Their backgrounds cover a wide range of disciplines, from physics to psychology, medicine to psycholinguistics, and biology to artificial intelligence. Similarly, their interdisciplinary research covers genetic, molecular, and cellular processes at one end and computational, system-level neuroscience with cognitive and behavioural analysis at the other end. We ask all PhD candidates within the Donders Graduate School to publish their PhD thesis in de Donders Thesis Series. This series currently includes over 750 PhD theses from our PhD graduates and thereby provides a comprehensive overview of the diverse types of research performed at the Donders Institute. A complete overview of the Donders Thesis Series can be found on our website: https://www.ru.nl/donders/donders-series

The Donders Graduate School tracks the careers of our PhD graduates carefully. In general, the PhD graduates end up at high-quality positions in different sectors, for a complete overview see https://www.ru.nl/donders/destination-our-former-phd. A large proportion of our PhD alumni continue in academia (>50%). Most of them first work as a postdoc before growing into more senior research positions. They work at top institutes worldwide, such as University of Oxford, University of Cambridge, Stanford University, Princeton University, UCL London, MPI Leipzig, Karolinska Institute, UC Berkeley, EPFL Lausanne, and many others. In addition, a large group of PhD graduates continue in clinical positions, sometimes combining it with academic research. Clinical positions can be divided into medical doctors, for instance, in genetics, geriatrics, psychiatry, or neurology, and in psychologists, for instance as healthcare psychologist, clinical neuropsychologist, or clinical psychologist. Furthermore, there are PhD graduates who continue to work as researchers outside academia, for instance at non-profit or government organizations, or in pharmaceutical companies. There are also PhD graduates who work in education, such as teachers in high school, or as lecturers in higher education. Others continue in a wide range of positions, such as policy advisors,

project managers, consultants, data scientists, web- or software developers, business owners, regulatory affairs specialists, engineers, managers, or IT architects. As such, the career paths of Donders PhD graduates span a broad range of sectors and professions, but the common factor is that they almost all have become successful professionals.

For more information on the Donders Graduate School, as well as past and upcoming defences please visit:

http://www.ru.nl/donders/graduate-school/phd/

9 789465 152073 >

2025

DONDERS INSTITUTE

Radboud University

Radboudumc